August 2019

DEVELOPMENT OF COLLOIDS-BASED FOOD DELIVERY SYSTEMS TO ENHANCE THE BENEFICIAL EFFECTS OF NUTRACEUTICALS FOR HUMAN HEALTH

zipei zhang

DEVELOPMENT OF COLLOIDS-BASED FOOD DELIVERY SYSTEMS TO ENHANCE THE BENEFICIAL EFFECTS OF NUTRACEUTICALS FOR HUMAN HEALTH

A Dissertation Presented

by

ZIPEI ZHANG

Submitted to the Graduate School of the
University of Massachusetts Amherst in partial fulfillment
of the requirements for the degree of

DOCTOR OF PHILOSOPHY

May 2019

The Department of Food Science

DEVELOPMENT OF COLLOIDS-BASED FOOD DELIVERY SYSTEMS TO ENHANCE THE BENEFICIAL EFFECTS OF NUTRACEUTICALS FOR HUMAN HEALTH

A Dissertation Presented

by

ZIPEI ZHANG

Approved as to style and content by:

_____
David Julian McClements, Chair

_____
Lili He, Member

_____
Matthew Moore, Member

_____
Sarah Perry, Member

_____
Eric A. Decker, Department Head
Department of Food Science

DEDICATION

To my parents, my adorable Chestnut and my wife

ACKNOWLEDGMENTS

Special mention goes to my enthusiastic supervisor, Dr. Julian McClements. My PhD has been an amazing experience and I want to thank Julian wholeheartedly, not only for his tremendous academic support, but also for giving me so many wonderful opportunities. His continuous support, his patience and motivation during the past five years strongly support me to complete this work. Also, I would like to thank my committee members, Dr. He, Dr. Moore, and Dr. Perry, for their kindly guidance.

Many thanks to all of my lab members, past and present: Long, Bingjing, Jorge, Shanshan, Tommy, Dora, Luping, Qian, and Dingkui for their help and friendship during the past five years. I would like to thank all of Food Science faculties, staffs and students, especially Jean, Fran, Deby, Stacy, Ruth and Mary.

I would like to thank all of my friends, especially Weicang, Zili, Yuanbiao, Liqiang, Dingkui, Peiyi, Yuxing, Gumin and for your continuous help and encouragement.

Nobody has been more important to me in the pursuit of this project than the members of my family. I would like to thank my parents, whose love and guidance are with me in whatever I pursue. They are the ultimate role models. I would also like to thank my adorable cat, Chestnut to bring me so much happiness. Most importantly, I wish to thank my loving and supportive wife, Ruojie, who provide unending inspiration.

ABSTRACT

DEVELOPMENT OF COLLOIDS-BASED FOOD DELIVERY SYSTEMS TO ENHANCE THE BENEFICIAL EFFECTS OF NUTRACEUTICALS FOR HUMAN HEALTH

MAY 2019

B.A., GANSU AGRICUTURE UNIVERSITY, CHINA

M.A., SOUTHWEST UNIVERSITY, CHINA

Ph.D., UNIVERSITY OF MASSACHUSETTS AMHERST, USA

Directed by: Professor David Julian McClements

Numerous bioactive agents within the food and pharmaceutical industries need to be encapsulated in delivery systems to overcome problems associated with poor water-solubility, chemical instability, and low oral bioavailability. Hydrogel particles are one kind of food-grade delivery system that offers considerable scope for tailored functionality, which can be used for encapsulation, protection, and controlled release of these bioactives. In current studies, hydrogel particles were formed by polysaccharides (i.e., alginate or pectin) and protein (i.e., casein or gelatin) through complex coacervation. Our results indicated that the encapsulation of protein or polyunsaturated lipid droplets nanoparticles within the hydrogel particles could improve their chemical or physical stability during storage. The lipid droplets encapsulated within the hydrogel particles could be released under simulated oral conditions, which was triggered by a pH or temperature change. The current study further fabricated the hydrogel particles (beads) using alginate or carrageenan based on an injection-gelation method. We found carrageenan beads had a relatively fragile structure that was easily disrupted in the GIT and released the encapsulated lipid droplets and curcumin. Conversely, alginate beads

had a robust structure that remained relatively intact throughout the GIT and retained the lipid droplets and curcumin. The incorporation of the β-carotene-loaded lipid droplets into hydrogel beads greatly improved its chemical stability during storage and digestion process. The current study further fabricated the hydrogel beads with self-regulating internal pH microclimates by encapsulating antacid agents (i.e., $Mg(OH)_2$ or $CaCO_3$) inside them. A quantitative fluorescence confocal laser scanning microscopy (CLSM) method was developed to map the local pH inside the hydrogel beads. Our results showed that the pH inside antacid-loaded beads remained close to neutral in the mouth and stomach, leading to retention the activity of acid sensitive agents (i.e., lactase, lipase, insulin and probiotics) in the small intestine. The current study further studied the effect of pH on the encapsulation, retention and release of whey proteins from alginate-based hydrogel beads. Our results indicated that the protein encapsulation efficiency and retention of the beads increased with decreasing fabrication pH, which was attributed to the fact that there was a strong electrostatic attraction between the cationic protein and anionic beads matrix (alginate molecules) at low pH conditions. We further found heat-denaturation of the protein prior to microgel formation led to the highest encapsulation efficiency and retention, which was attributed to the formation of a cold-set protein gel inside the beads. Simulated GIT studies indicated that protein encapsulation in the microgels retarded its digestion in the stomach, but not in the small intestine. Overall, our study suggest that hydrogel particles with different structures and compositions can be designed for encapsulation, protection, and delivery of hydrophilic or lipophilic bioactive agents, which is advantageous for the development of certain functional food products.

TABLE OF CONTENTS

Page

LIST OF TABLES

Table Page

LIST OF FIGURES

Figure Page

CHAPTER 1

INTRODUCTION

Many pharmaceuticals, nutraceuticals, and vitamins have to be encapsulated within delivery systems to overcome physicochemical or physiological challenges that normally limit their efficacy, such as poor water solubility, chemical or biochemical instability, and low or variable oral bioavailability [1]. Numerous types of delivery systems have been designed to control the retention, stability, and release of bioactive components within the gastrointestinal tract (GIT) [2]. In particular, there has been a strong emphasis on developing delivery systems that can target or control the release of bioactives at specific locations within the GIT (such as mouth, stomach, small intestine, or colon) because this may improve their efficacy, as well as reduce any undesirable side effects. Food grade delivery systems are one of the most suitable candidates for encapsulation and delivery of bioactives because they are relatively simple and inexpensive to fabricate [3].

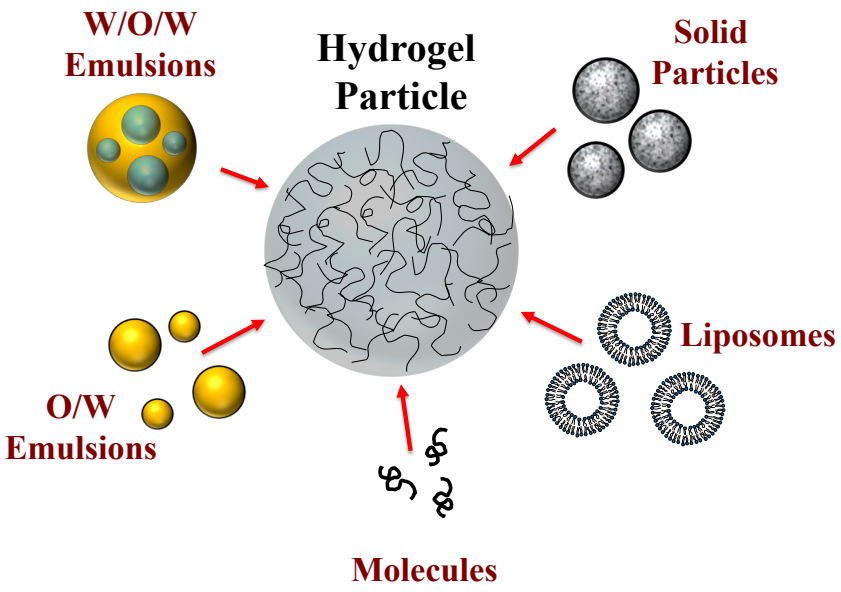

Figure 1. 1 A variety of bioactive molecules or particles can be trapped inside filled hydrogel particles to alter their physicochemical properties and delivery.

Hydrogel particles are one category of food grade delivery system that offers considerable scope for tailored functionality **(Figure 1.1)**. Hydrogel particles contain biopolymer networks with a three-dimensional structure that is capable of trapping relatively large quantities of water [4]. A filled hydrogel particle contains oil droplets trapped within the biopolymer network [5]. Typically, bioactives are first dissolved in an oil phase, and then an oil-in-water emulsion is formed by homogenizing this oil phase with an aqueous phase containing a suitable emulsifier. The resulting oil droplets are then trapped within the hydrogel particles during the preparation procedure. The ability to tune the composition, dimensions, shape, and internal structure of hydrogel particles has led to widespread interest in their utilization as delivery systems in the food, pharmaceutical, and personal care industries.

In my projects, I was working on the formation and design of food-grade hydrogel particles that can encapsulate bioactive agents suitable for use in the food industry, such as oil-soluble vitamins and nutraceuticals. In particular, My research focus on the application of hydrogel particles for controlled or targeted release of bioactive agents in the GIT.

CHAPTER 2

LITERATURE REVIEW

2.1 Hydrogel particle characteristics

The structural and physicochemical characteristics of hydrogel particles can be manipulated to tailor their functional attributes for specific applications. In this section, we therefore highlight some of the most important properties of hydrogel particles that can be controlled during the fabrication process, *e.g.,* particle composition, size, pore size, and cross-linking.

2.1.1 Composition

Hydrogel particles are typically fabricated from natural polymers (such as proteins and polysaccharides) due to their good biocompatibility and biodegradability. The nature of the biopolymers used to assemble hydrogel particles determines many of their functional attributes, such as stability, retention, and release properties. It is therefore crucial to have a good understanding of the molecular, physicochemical and physiological properties of the biopolymer molecules used to fabricate a hydrogel particle. Typically, biopolymers can be distinguished based on their conformations in solutions such as globular, random coil, or rod-like (**Figure 2.1**).

2.1.2 Polysaccharides

Polysaccharides are usually isolated from plant or microbial sources and may vary considerably in their molecular and physicochemical properties, such as molecular weight, branching, flexibility, charge, polarity and digestibility [6]. There are a large

number of different polysaccharides available to form hydrogels, and we only focus on a selected number that have been widely used. In general, there are three major mechanisms that can be used to prepare hydrogels from polysaccharides, *i.e.* ionotropic, cold-set, and heat-set gelation [7].

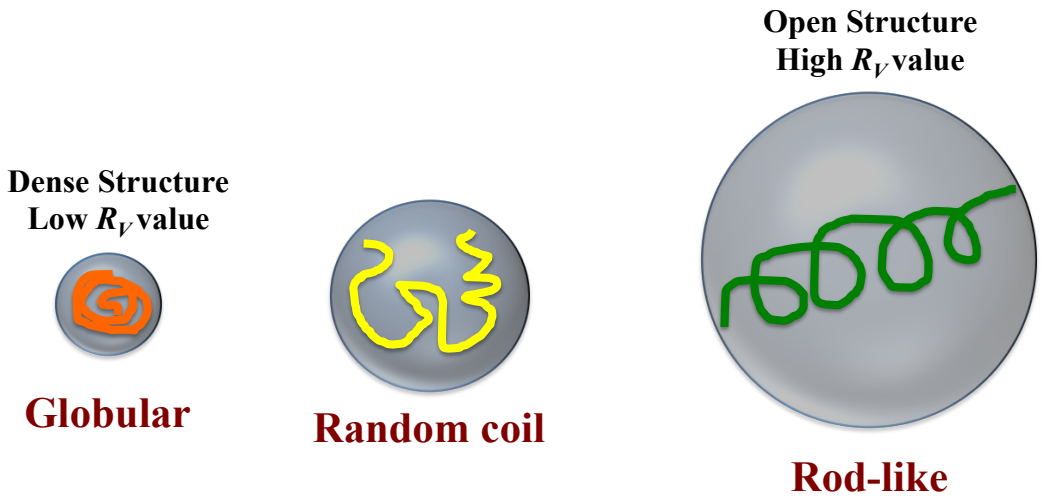

Figure 2. 1 Biopolymers may adopt different conformations in aqueous solutions, which influences their ability to form hydrogel particles with different effective volume fractions and volume ratios (R_v).

2.1.2.1 Pectin

Pectin can be considered to consist of a linear anionic backbone with neutral side chains protruding from certain regions, with an overall molecular weight of around 110 to 150 kDa [8]. The linear backbone is mainly comprised of α(1-4)-d-galacturonic acid residues that may be partly esterified with methyl groups. The degree of methyl esterification (DE) is an important factor determining the gel forming properties of pectin. Low methoxy (LM) pectin has DE < 50%, and is typically gelled *via* ionotropic gelation by adding divalent ions (*e.g.* calcium). High methoxy (HM) pectin has a DE > 50% and is typically gelled by adding high levels of soluble solids (such as sugar) under acidic

conditions [9]. Pectin is not digested by gastric or small intestinal enzymes, but is easily degraded by pectinases produced by the colonic microflora. LM pectin is more tolerant of pH variations and calcium levels, which could make it more suitable for colonic delivery systems formation [10]. Calcium pectinates have been widely used in different formulations for the lipophilic bioactive agents encapsulation and delivery [11-12]**.** The integrity of calcium pectinate beads can be reinforced by formation of polyelectrolyte coatings, *e.g.,* by electrostatic deposition of cationic biopolymers (such as chitosan) onto the anionic beads[13]. The charge characteristic of pectin can be selected to control lipid digestion and bioactive release, *e.g.,* decreasing DE reduced lipid digestion and bioactive bioavailability [14-16].

2.1.2.2 Alginate

Alginate is a linear anionic biopolymer that is widely used to form hydrogel particles to encapsulate lipophilic agents[17-19]. Alginate is a block copolymer composed of 1-4-linked residues of β-D-mannuronic acid (M) and α-L-guluronic (G) acid, with an overall molecular weight around 60 kDa to 700 kDa [20]. Alginate hydrogels are usually formed through an electrostatic cross-linking interaction between multivalent cations (typically Ca^{2+}) and anionic carboxyl groups ($-COO^-$) on G residues from different alginate chains[21]. The pore size of this type of hydrogel has been reported to be between 5 and 200 nm depending on alginate and calcium concentration [22]. Calcium alginate hydrogels shrink at low pH (gastric environment) due to the loss of negative charge on the alginate molecules when the carboxyl groups become protonated (-COOH, $pK_a \approx 3.5$). On the other hand, once transferred into higher pH solutions (intestinal phase), the alginate molecules become highly charged and the hydrogel network may swell [23]. This

pH dependent behavior can be exploited to fabricate targeted delivery systems for GIT applications. Alginate can be further cross-linked or mixed with other polymers such as neutral gums, chitosan or pectin to strengthen the structure and restrict the pore of the gel network [22]. Studies indicate that the guluronic acid content of the alginate molecules influences the release properties of alginate-based hydrogels: the amount of bioactive component that diffused out of alginate hydrogels decreased with increasing G-content [24].

2.1.2.3 Carrageenan

Carrageenan is another type of linear anionic polysaccharide that is commonly used to form hydrogels[25]. It consists of galactan monomers linked together by alternating (1→3)- and (1→4)-β-D-glycosidic bonds, and has a negative charge due to the presence of sulfate groups [26]. Carrageenan can form hydrogels through ionotropic gelation coupled with a cold-set mechanism. Three types of carrageenan (κ, ι and λ) are commonly used that have different molecular and gelation properties: κ- and γ- carrageenan can undergo coil-helix conformational transitions and form hydrogels upon cooling in the presence of appropriate salts. Gelation of κ-carrageenan is promoted by the presence of potassium ions, whereas γ-carrageenan gelation is promoted by the presence of calcium ions. The κ-type dissolves when heated and forms strong gels that tend to be rigid and brittle, whereas the γ-type is either hot or cold soluble and forms soft, elastic and cohesive gels. λ-carrageenan does not form gels, but it can be used to thicken solutions or as an anionic building block for structures held together by electrostatic interactions. These differences in functional performance can be attributed to differences in molecular structure, such as the linear density of sulfate groups and the preferred molecular conformation (helix *versus* ribbon) [20, 27]. After hydrogel formation, it is sometimes possible to modify

hydrogel properties and release characteristics by covalent cross-linking, *e.g.,* κ-carrageenan hydrogel particles have been cross-linked using genipin [28].

2.1.2.4 Agar

Agar is a linear neutral polysaccharide that is capable for forming hydrogels under appropriate conditions[29]. The agar molecule consists of alternating β-1,3-linked-D-galactose and α-1,4-linked 3,6-anhydro-L-galactose units, and has an overall molecular weight above about 100 kDa. The gelling properties of agar depend on its molecular weight and chemical characteristics [30]. Agar can be dissolved in water after heating, and forms a hydrogel when the solution is cooled due to a coil-helix transition and hydrogen bonding of helical regions of different molecules. It can therefore be used to form hydrogel particles by cooling agar microspheres formed by extrusion or biopolymer phase separation [31]. Agar hydrogels tend to be transparent, rigid, and brittle. The gelation temperature of agar ($T_g \approx 40$ °C) tends to be appreciably lower than the melting temperature ($T_m \approx 85$ °C), which can be useful for forming hydrogel particles that are stable over a range of temperatures. The melting and gelling temperatures of agar gels have been reported to decrease in the presence of ionic surfactants, whereas nonionic surfactants had the opposite effect [32]. Thus, it may be possible to control their thermal behavior by incorporating additives that modulate the melting and gelation temperatures.

2.1.2.5 Starch

Starch is a water-soluble polysaccharide mainly composed of two types of biopolymers: amylose and amylopectin. Amylose is a linear biopolymer consisting of α-D-glucopyranose units joined by (1 → 4) linkages, whereas amylopectin is a branched

biopolymer with a main chain similar to amylose, but with branches formed due to the presence of (1 → 6) linkages [33]. Certain types of starch ("digestible starch") are rapidly degraded in the mouth and stomach due to hydrolysis by α-amylase, whereas other types of starch ("resistant starches") are not hydrolyzed until they reach the colon. Hydrogel particles have been fabricated by thermal gelatinization of digestible starch and used for targeted delivery of oil-soluble flavors [34-36]. Native starches may be modified by various chemical, enzymatic, and physical methods to improve their functional properties, such as addition of attachment of hydrophobic, polar, or charge groups, as well as controlled hydrolysis or cross-linking [37]. Modified starches have been widely used to form different kinds of hydrogel particles for bioactive delivery. For example, chemically modified starches have been used for targeted delivery of curcumin [38].

2.1.2.6 Chitosan

Chitosan is one of the few examples of positively charged polysaccharides available to form hydrogels. It has a linear structure composed of randomly distributed β-(1-4)-linked D-glucosamine and N-acetyl-D-glucosamine units, with an overall average molecular weight around 3.8 to 20 kDa [39]. The presence of ionizable amino groups ($-NH_3^+$, $pK_a \approx 6.3$) is the origin of the cationic charge on chitosan and plays an important role in its ability to form hydrogels[40-41]. Chitosan hydrogels can be formed by complexation with anionic biopolymers or multivalent ions (such as tripolyphosphate)[42]. The hydrogel particles formed by chitosan tend to swell and dissolve at low pH (gastric environment) but be insoluble at higher pH ranges (intestinal phase) due to changes in the charge characteristics [43]. The mechanism of pH sensitive swelling involves the protonation of amine groups of chitosan under low pH conditions. This property means

that it is possible to use chitosan to fabricate targeted delivery systems for gastric applications. Chitosan-based hydrogel particles may also be a good candidate for delivery of lipophilic bioactive agents due to their mucoadhesive properties, which may prolong the contact time between the bioactive and absorption sites in the GIT [44].

2.1.2 Protein

Proteins are the other commonly used food biopolymer for the fabrication of hydrogel particles. Protein-based hydrogels can be formed by various strategies including heat-set, cold-set, and ion-set gelation. Hydrogel particles can be formed using a number of top-down and bottom-up fabrication methods (see Section 3). After particle fabrication, a chemical, physical, or enzymatic hardening step can be used to further cross-link the proteins and stabilize the particle structures formed [45-48]. It should be noted that many proteins have anti-oxidant properties, which makes them particularly suitable for encapsulation of lipophilic bioactive agents that are susceptible to oxidation, such as carotenoids and ω-3 oils.

2.1.2.1 Gelatin

Gelatin is usually obtained by acid or alkaline treatment of collagen extracted from animal or fish sources. Gelatin can form hydrogels through two different mechanisms leading to physical or chemical gels. Physical gels are the result of reversible (non-covalent) cross-links formed between different gelatin molecules, which are usually induced by cooling below the coil-to-helix transition temperature of gelatin chains [49]. Conversely, chemical gels are the result of the formation of covalent cross-links between different gelatin molecules by chemical or enzyme reactions. Previous studies have

shown that once gelatin is cross-linked by chemicals (*e.g.,* gluteraldehyde) or enzymes (*e.g.,* transglutaminase), it loses the ability to undergo thermally reversible coil-to-helix transitions [50]. Physical gelatin gels can melt slightly below the physiological temperature of humans. This "melt-in-the-mouth'' property can be used to develop gelatin-based delivery systems for targeted delivery of bioactive components in the mouth [34].

2.1.2.2 Whey protein

Whey proteins are isolated from the supernatant that remains after milk is treated to precipitate the casein proteins. Whey protein actually contains numerous different globular protein fractions, with the most abundant being β-lactoglobulin (β-Lg), α-lactoalbumin (α-La), bovine serum albumin (BSA), and immunoglobulins with molecular weights ranging from 14 kDa to 1,000 kDa [51]. Whey proteins can form heat-set and cold-set gels through different processing strategies. Heat-set gels are produced when globular proteins are heated above their thermal denaturation temperature under conditions that favor protein-protein interactions (*i.e.,* pH near pI and/or high ionic strength). Cold-set gels are formed using a two-step process. First, the globular proteins are heated above their thermal denaturation temperature under conditions that oppose protein-protein interactions (*i.e.,* pH far from pI and low ionic strength), which leads to the formation of unfolded proteins that assemble into thin filaments. Second, conditions are altered to favor protein-protein interactions (*i.e.,* pH near pI and/or high ionic strength), which promotes protein gelation due to aggregation of the filaments. Cold-set gels are particularly suitable for encapsulating lipophilic bioactive agents that are thermally unstable[52-53]. Whey proteins have an isoelectric point around pH 5, and so are positively charged below this value and negatively charged above it. They can therefore be used to

assemble structures based on electrostatic attraction, such as coacervates and multilayers. In addition, whey proteins are surface-active and can be used to form oil-in-water emulsions. However, whey protein-coated lipid droplets are particularly sensitive to pH, ionic strength, and temperature.

2.1.2.3 Casein

Caseins are a group of fairly flexible proteins isolated from milk by selective acid or enzyme precipitation. There are four major casein fractions in bovine milk that have somewhat different molecular structures and functional properties: α_{S1} (~ 44%), α_{S2} (~ 11%), β (~ 32%) and κ (~ 11%) [54]. Nevertheless, all types of caseins have relatively disordered and flexible structures, with a limited amount of secondary and tertiary structure. Certain caseins have regions along their backbones that are either highly non-polar or highly charged, which plays an important role in determining their ability to associate into hydrogels and other structures. In their native state, caseins usually exist as molecular clusters ("casein micelles") that are typically between about 50 and 250 nm in diameter and are partly held together by mineral ions (such as calcium phosphate). Casein micelles may be useful for the development of delivery systems because they can encapsulate lipophilic bioactives in their non-polar interiors, such as carotenoids, curcumin, and oil-soluble vitamins [55-58]. Caseins are amphiphilic molecules that have good surface-activity and can therefore be used as emulsifiers to stabilize lipid droplets. They have an isoelectric point around pH 4.6, and are positive at lower pH and negative at higher pH. Casein molecules, casein micelles or casein-coated oil droplets tend to aggregate strongly around their isoelectric point due to the reduction in electrostatic

repulsion at this pH [59]. Caseins are less sensitive to thermal treatments than globular proteins (such as whey protein) due to their disordered flexible structures.

2.2 Hydrogel particle fabrication methods

The properties of hydrogel particles can be tailored for specific applications by selecting the most appropriate fabrication method and operation conditions. A wide range of different techniques can be utilized to fabricate hydrogel particles, which have been reviewed in detail elsewhere [60]. Some of the most suitable methods for encapsulating lipophilic or hydrophilic bioactives are discussed below.

2.2.1 Coacervation-based gelation methods

Coacervation is a well-established technique for encapsulation of bioactive components, and it is already widely used in the food industry for fabricating hydrogel particles [61-62]. The bioactive is trapped within an electrostatic complex formed when two oppositely charged biopolymers associate with each other through electrostatic attraction, and then the resulting system is gelled to form a hydrogel particle[63-64]. The swelling/shrinking behavior of hydrogels based on complex coacervation depend on pH and ionic strength since these parameters influence the sign, magnitude, and range of electrostatic interactions. Changes in pH alter the electrical characteristics of proteins and ionic polysaccharides, which influences the formation, stability, and properties of coacervate-based hydrogels. For example, a protein and anionic polysaccharide associate at pH values around and below the isoelectric point of the protein due to electrostatic attraction (one anionic, one cationic), but they may dissociate at higher pH values due to electrostatic repulsion (both anionic). Addition of salt weakens electrostatic attraction,

which may also cause dissociation of coacervates. The type and amount of biopolymers used to assemble a coacervate also determines its properties. The ratio of two biopolymers required to form a hydrogel particle using coacervation depends on their charge densities [65]. The release characteristics of hydrogel particles can be controlled by manipulating their composition and fabrication *e.g.,* biopolymer type and concentration, order of mixing, stirring conditions, temperature, pH, and ionic strength [66-70]. The pH sensitivity of hydrogel particles can be improved by cross-linking the biopolymers molecules or by coating them with a layer of polyelectrolytes [71]. The main limitations of the coacervation method are that it is difficult to tightly control the particle dimensions and to avoid particle coalescence and phase separation over time. Previous studies have shown that hydrogel particles based on coacervation may vary widely in size, ranging from less than 100 nm to greater than 100 μm [34, 72].

Recently, filled hydrogel particles have been fabricated within our laboratory based on complex coacervation using various combinations of biopolymers, *e.g.* alginate-chitosan, pectin-casein, gelatin-starch, gelatin-pectin, and alginate-casein [62, 73-75]. The encapsulation of lipids within coacervate-based hydrogel particles has been shown to delay their digestion by pancreatic lipases, which may be useful to controlled delivery systems for gastrointestinal applications [76].

2.2.2 Thermal-denaturation gelation methods

Studies have shown that protein hydrogels can be formed by heating a solution of globular proteins above its thermal denaturation temperature under controlled solution conditions, *e.g.* protein concentration, pH, ionic strength, and holding temperature/time [77-78]. The proteins expose non-polar groups on their surfaces after they are denatured,

which increases the hydrophobic attractive between them. The protein molecules will tend to associate with each other and form nanoparticles when the hydrophobic attraction is strong enough to overcome any electrostatic repulsion, but not too strong to promote extensive aggregation. The size of the hydrogel particles formed can be controlled by altering the initial biopolymer concentration, holding time, holding temperature, pH and ionic strength [79]. Mixed biopolymer hydrogel particles have been formed by controlled thermal treatment of electrostatic complexes containing globular proteins and ionic polysaccharides. These particles were formed by heating a solution of globular proteins above their thermal denaturation temperature at a specific pH and then complexing with an ionic polysaccharide [70, 77, 80-81], or by directly heating a solution of protein–polysaccharide complexes above the protein's thermal denaturation temperature at a specific pH [82].

2.2.3 Emulsification-based gelation methods

Emulsification-based methods typically rely on the formation of a water-in-oil (W/O) emulsion or microemulsion containing biopolymer molecules dissolved in the internal aqueous phase, and then gelling the internal aqueous phase [83]. Typically, an aqueous phase containing the biopolymer and an oil phase containing a lipophilic surfactant are homogenized together to form a W/O emulsion. Any bioactive components are usually incorporated into the aqueous phase prior to homogenization. After the W/O emulsion has been formed the internal aqueous phase is gelled using a method that is appropriate for the biopolymer used. For example, a heat-set biopolymer could be gelled by heating, a cold-set biopolymer by cooling, or an ion-set biopolymer by adding an appropriate organic salt or acid to the oil phase. Once the internal aqueous

phase has gelled, the resulting hydrogel particles have to be isolated from the surrounding oil phase, which can be achieved by centrifugation, filtration, and washing with an organic solvent. Finally, the washed hydrogel particles can be dispersed into an aqueous solution. This method can also be used to form filled hydrogel particles by preparing an O/W/O emulsion, gelling the aqueous phase, and then isolating the filled hydrogel particles from the external oil phase. One of the major advantages of the emulsification-based methods is that relatively small hydrogel particles with well-defined sizes can be produced. Hydrogel nanoparticles (10 to 1000 nm) can be formed using W/O microemulsions as templates, whereas hydrogel microparticles (100 nm to 100 μm) can be formed using W/O emulsions.

2.2.4 Injection-based gelation methods

Injection or extrusion methods are commonly used to form hydrogel particles from food-grade biopolymers [84-86]. In this case, a biopolymer solution containing the bioactive agent is initially placed into an injection system, such as a syringe (**Figure 2.2**). The biopolymer solution is then injected into another "hardening" solution under conditions that promote gelation of the biopolymer molecules. The hardening solution used depends on the gelation mechanism of the biopolymers. A cold or hot hardening solution could be used to promote cold-set or heat-set gelation of biopolymers. A hardening solution containing calcium ions could be used to promote ion-gelation of anionic biopolymers, such as alginate, pectin, or carrageenan. Enzyme or chemical cross-linking agents could be included to promote hydrogel formation through covalent bonds. The size of the hydrogel particles formed can be manipulated by controlling the needle diameter, flow rate, and solution viscosity.

Calcium alginate beads are commonly formed using the injection method. For example, filled hydrogel particles have been formed by mixing lipid droplets with an alginate solution, and then injecting this mixture into a hardening solution containing calcium ions. An *in vitro* digestion study indicated that calcium alginate beads were particularly effective at retarding the digestion of the encapsulated lipids, with the extent of inhibition increasing with increasing bead size and decreasing pore size [76]. The functional properties of calcium alginate beads can be further modulated by coating them with another polyelectrolyte, such as chitosan [87-88].

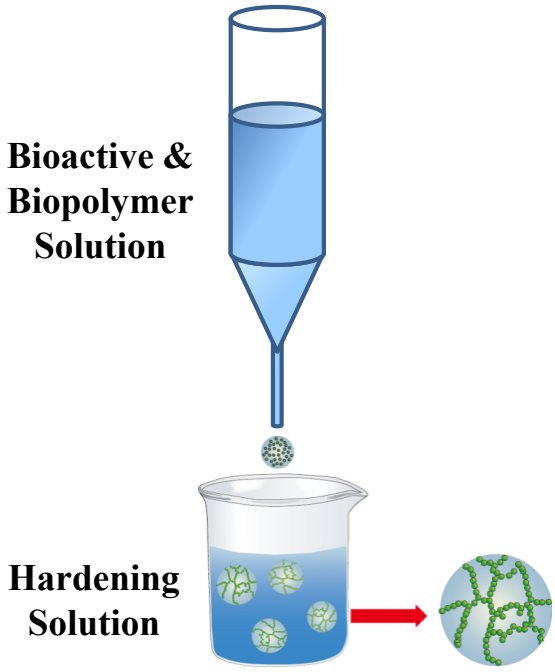

Figure 2. 2 Schematic representation of injection method used to produce hydrogel beads. A solution containing bioactive and biopolymer is injected into a hardening solution.

2.2.5 Shearing-based gelation methods

Fluid gels have been defined as suspensions of hydrogel particles formed by application of a flow field to a gelling biopolymer solution. Typically, the bioactive and biopolymer are dissolved within an aqueous solution, the system is stirred continuously,

and then gelation is induced using an appropriate method (*e.g.,* altering temperature, changing pH, or adding a gelling agent). The dimensions of the particles produced are typically around 4 to 100 μm, and depend on the shear rate relative to the gelation rate [89]. Studies of hydrogel particles formed using this method have shown that their size, shape, and strength can be controlled by varying biopolymer type and concentration, gelation mechanism, and shearing conditions *e.g.,* rate, duration, and type [90-91]. This creates an attractive opportunity to fabricate hydrogel particles with specific functional attributes [92]. For example, fluid gels have been designed to act as pourable viscoelastic fluids suitable for the oral delivery of bioactives to individuals with difficulties swallowing [92].

2.2.6 Spray drying and spray chilling-based methods

Hydrogel particles can also be formed using spray drying and spray chilling methods [20, 93]. In spray drying, an aqueous solution containing the bioactive component and the biopolymer is forced through a small nozzle into a hot chamber. The nozzle converts the biopolymer solution into small fluid drops that are rapidly converted into solid particles due to water evaporation caused by the hot air. The solid particles are then collected by filtration or centrifugal forces[94]. Typically, the solid particles formed have dimensions of around 10 to 100 μm, and have to be carefully designed to ensure good powder functionality (*e.g.,* flowability, dispersion, and dissolution). Hydrogel particles can be formed by dispersing the powder into an aqueous solution containing a suitable gelling agent. The size of the hydrogel particles formed depends on the relative rates of dissolution versus gelation [20]. Spray chilling can often be carried out using a similar apparatus as used for spray drying, however the chamber is usually cooled rather than heated [93]. In this case, the bioactive and a cold-set biopolymer are dissolved in an

aqueous solution held at a temperature above the gelation temperature. The biopolymer solution is then sprayed out of a nozzle into a cooled chamber, which promotes gelation of the biopolymers and leads to formation of hydrogel particles that can be collected by centrifugal forces or filtration.

2.2.7 Other methods

The fabrication methods discussed above are some of those that are most commonly used to form food-grade hydrogel particles suitable for encapsulation and delivery purposes. Nevertheless, there are also many other methods that might be utilized for specialist applications, such as molding, microfluidic, and electrospraying methods. A number of review articles have been published detailing the application of these methods for hydrogel particle fabrication [20, 31].

2.3 Body-particle interactions

Hydrogel particles can be designed to retain, protect, and deliver bioactive components to specific regions within the gastrointestinal tract [95]. For example, they might be used to release desirable flavor molecules within the mouth or to retain bitter bioactive molecules in the mouth but release them in the stomach. Alternatively, they may be designed to protect labile bioactive components from the harsh conditions in the stomach, but release them within the small intestine or colon. Knowledge of the different physicochemical and physiological conditions within the different regions of the GIT is required to design effective delivery systems that can retain and release bioactive components at specific sites (**Figures 2.3 and 2.4**).

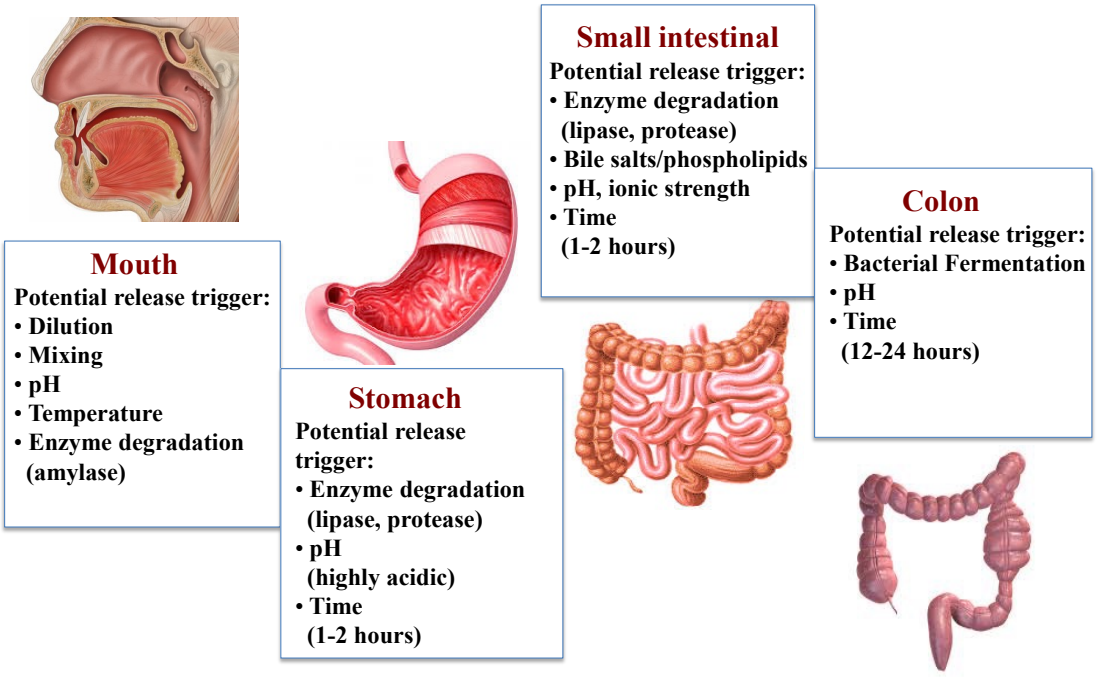

Figure 2. 3 Potential release trigger of bioactive released from hydrogel particles in mouth, stomach, small intestinal and colon.

2.3.1 Mouth

Numerous variables need to be taken into account when designing hydrogel particles to retain or release bioactive components in the mouth, including oral temperature, saliva composition and flow rate, pH and ionic strength, frictional forces, mixing conditions, duration, and enzyme activity [96-97]. Typically, fluid foods spend a shorter time in the mouth and are not subjected to intense mechanical forces during mastication, and are therefore often less susceptible to alterations induced by oral processing than solid foods [98]. The utilization of hydrogel particles to control the release of drugs within the mouth has been investigated by pharmaceutical researchers [99], and much of the information obtained from these studies is useful for food applications. Some food researchers have also examined the utilization of hydrogel particles to control the release of lipophilic bioactive food components in the mouth[100-101].

Malone and co-workers fabricated a range of different filled hydrogel particles to control the release of lipophilic flavors in the mouth through different mechanisms [34]. Calcium-alginate particles remained intact within the mouth during mastication and therefore released the flavors primarily through a diffusion-controlled mechanism. Agar particles broke down in the mouth due to fragmentation by mechanical forces and therefore released the particles primarily by a degradation-controlled mechanism. Gelatin particles and gelatin–gum complexes were susceptible to a combination of melting and fragmentation triggers, while starch particles were susceptible to a combination of α-amylase and fragmentation triggers. Factors such as hydrogel particle size, oil content, and partition coefficient affected the rate of flavor release [34]. Our laboratory has fabricated hydrogel particles based on complex coacervation of casein and alginate that dissociated and released encapsulated lipid droplets under simulated oral conditions due to a pH change [75].

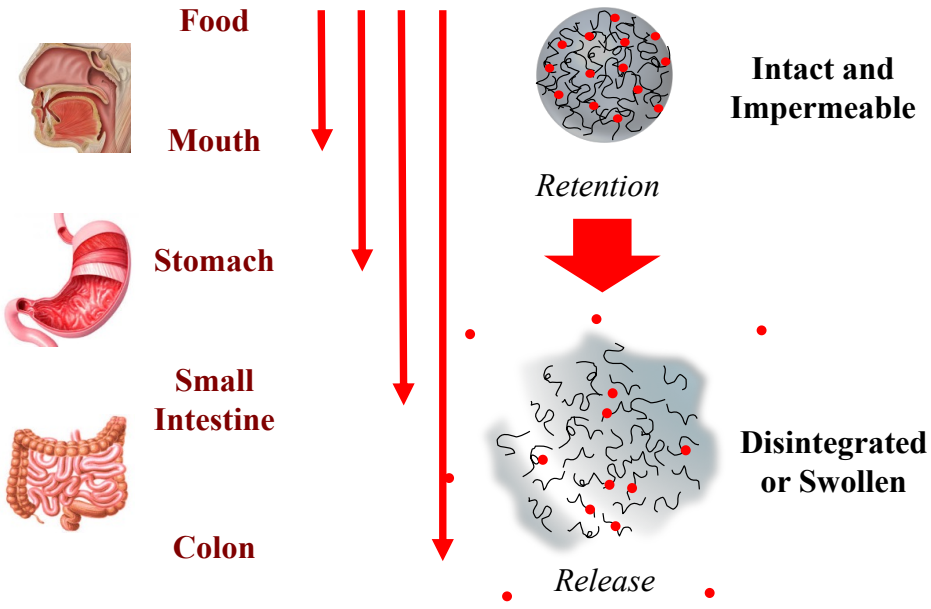

Figure 2. 4 Delivery systems may be designed to remain intact under one set of conditions, but breakdown under another set of conditions.

2.3.2 Stomach

In some cases it is desirable to have a delivery system that remains intact within the stomach so that it can protect an encapsulated bioactive component from degradation by acids or enzymes, whereas in other cases it is more desirable to release it in the stomach to enhance its bioactivity [102]. Hydrogel particles encounter a number of harsh physicochemical and physiological conditions within the dynamic stomach environment [103]. They are mixed with highly acidic gastric fluids (pH 1 to 3) that have a relatively high mineral content (*e.g.,* calcium, potassium, and sodium salts) and contain various types of digestive enzyme (*e.g.,* proteases, lipases, and amylases) and surface-active substances (*e.g.,* phospholipids and proteins). In addition, they are subjected to dynamic mechanical forces and fluid flows due to the motility of the gastric chamber [104-105].

Alginate gel bead was fabricated with the vegetable oil hold inside the hydrogel beads. In vitro digestion results indicated that release rate of drug from these hydrogel beads in artificial gastric juice was inversely related to the percentage of oil, which was due to the buoyancy characterization of the gel beads at presence of oil inside the gel particles [106]. Other study suggested that oil-entrapped calcium pectinate gel beads also showed a buoyancy characterization in stomach phase, which made them an excellent candidate of gastro-retention delivery system for lipophilic agents [107]. Calcium alginate beads have been shown to remain intact under stomach conditions, and are therefore capable of protecting bioactive components in the gastric environment [76]. On the other hand, various types of protein-based hydrogel particles have been shown to degrade under simulated gastric conditions, and may therefore be suitable for releasing bioactive components in the stomach [108-109].

2.3.3 Small intestine

After entering the duodenum, any hydrogel particles remaining in the chyme will be mixed with alkaline small intestinal fluids containing bile salts, phospholipids, digestive enzymes, and various salts. Pancreatic enzymes (a complex mixture of proteases, amylases, and lipases) and other digestive enzymes produced by the small intestine act in concert to degrade any digestible macronutrients in the hydrogels: proteins are converted to peptides and amino acids by proteases; starches are converted to oligosaccharides and glucose by amylases; triacylglycerols are converted to free fatty acids (FFA) and monoacylglycerols (MAG) by lipases [104]. It is often desirable to have bioactive components released from hydrogel particles in the small intestine so as to increase their bioavailability. This is particularly important for highly lipophilic bioactives (such as oil soluble vitamins, caroteonids, curcuminoids, and long chain fatty acids) that normally have low bioavailability because of their limited solubility in gastrointestinal fluids. These components need to be released from the hydrogel particles within the small intestine, and then solubilized within mixed micelles formed by bile salts, phospholipids, and lipid digestion products. The mixed micelles then transport the encapsulated bioactive components to the surfaces of the epithelium cells where they are absorbed [110].

Li and co-workers fabricated filled hydrogel particles by trapping protein-coated lipid droplets inside chitosan/calcium alginate hydrogel particles [76]. A simulated GIT model showed that the hydrogels could control the lipid digestion rate: relatively small hydrogel beads (d < 50 μm) caused a moderate delay in lipid digestion, while large hydrogel beads (d > 100 μm) delayed appreciably delayed digestion [76]. Mun and co-

workers showed that β-carotene bioaccessibility was increased after being encapsulated in starch-based filled hydrogels, which was attributed to the ability of the lipid droplets to form mixed micelles and the hydrogels to increase the surface area of lipid exposed to digestive enzymes by inhibiting droplet aggregation [111].

2.3.4 Colon

If they are designed for colonic delivery, then the bioactive components within hydrogel particles must pass through the mouth, stomach, and small intestinal without being released or absorbed. Most macronutrients (lipids, proteins, and starches) are digestible within the upper GIT and therefore they are largely unsuitable for the development of hydrogel particles suitable for use as colonic delivery systems. Conversely, dietary fibers are not digested within the upper GIT but are digested within the lower GIT due to enzymes secreted by colonic bacteria, and are therefore suitable building blocks for this type of delivery system [112]. Nevertheless, the delivery systems must still be carefully designed so that the bioactive agents remain retained and protected within the hydrogel particles throughout the upper GIT. This usually means that they should remain intact and impermeable within the mouth, stomach, and small intestine fluids. The ability of bioactive agents to be delivered to the colon by dietary fiber based hydrogels is due to the fact that the concentration of microbes present in the colon is much higher than that in other regions of the GIT [113]. Several dietary fibers had been investigated for colon-specific hydrogel particles such as pectin [114], alginate [115], dextran [116], guar gum [117] and chitosan [118] .

2.4 Conclusions

Structurally-designed hydrogel particles have been developed to encapsulate, protect, and release a wide range of bioactive components in the pharmaceutical industry. Hydrogel particles are now being explored for similar types of application in the food industry. In this case, food-grade biopolymers, such as proteins and polysaccharides, are used to fabricate the hydrogel particles rather than synthetic polymers or chemically-modified biopolymers. The biopolymers should be selected according to the characterization of encapsulated agents and the delivery target of the hydrogel matrix. For example, protein should be involved in the ω-3 fatty acids loaded hydrogels design. The dietary fiber is a good candidate used in the colon target hydrogel particles fabrication. In addition, the hydrogel particles must be fabricated utilizing processing operations that are inexpensive, robust, and scalable, which provides additional challenges. Hydrogel particles are being developed to protect bioactive components from degradation within foods and specific regions of the gastrointestinal tract, but then release them at an appropriate site of action.

CHAPTER 3

ENCAPSULATION, PROTECTION, AND RELEASE OF BIOACTIVE LIPIDS USING HYDROGEL PARTICLES

3.1 Encapsulation and protection of bioactives using hydrogel particles

3.1.1 Introduction

Epidemiological, clinical, and experimental studies indicate that fish oil, which contains n-3 polyunsaturated fatty acids (n-3 PUFA) such as eicosapentaenoic acid (EPA, 20:5 n-3) and docosahexaenoic acid (DHA, 22:6, n-3), can protect against the development of chronic diseases such as heart disease, brain disease, arthritis, and certain types of cancer (Riediger, Othman, Suh & Moghadasian, 2009, Ruxton, Reed, Simpson, Millington & Ruxton, 2007, Yashodhara, Umakanth, Pappachan, Bhat, Kamath & Choo, 2009). In the USA, where a western-style diet is predominant, the average fish intake is currently well below the recommended two to three servings per week [119]. There is therefore a concerted effort to enrich various food and beverage products with n-3 PUFA so as to improve their healthfulness. However, there are a number of challenges associated with incorporating these bioactive lipids into foods. Firstly, PUFAs are highly non-polar molecules with low water-solubility and therefore have to be encapsulated within emulsion-based delivery systems if they are going to be introduced into aqueous-based products [5, 120]. Second, PUFAs are highly susceptible to chemical degradation due to lipid oxidation, which leads to a reduction in product quality and acceptability, and therefore they have to be protected against this form of chemical degradation [121-125]. Third, it is important that PUFAs are fully absorbed within the upper gastrointestinal (GI)

tract after oral ingestion so that they can demonstrate their beneficial health effects [126]. Consequently, there is a need to develop effective food-grade delivery systems to encapsulate, protect, and release PUFAs.

There is growing interest in the utilization of proteins and peptides (referred to collectively as "polypeptides" for convenience) as functional ingredients in foods because of their beneficial health effects, such as antioxidant, antimicrobial, and anti-hypertension activities [127-130]. Typically, the activity of polypeptides depends on their three-dimensional structures and specific amino acid sequences [130]. Polypeptide activity may therefore be altered in food products during manufacture, storage, or transportation, due to changes in solution or environmental conditions that alter protein structure, such as pH, ionic strength, ingredient interactions, or temperature [131]. In addition, their activity may be altered after they are ingested and pass through the gastrointestinal tract (GIT) because they are exposed to digestive enzymes (proteases and peptidases) and environmental conditions (pH, ionic strength, and ingredient interactions) that may alter their structure [132]. Within the GIT, digestive enzymes and highly acidic gastric conditions may hydrolyze polypeptide chains at particular bond locations, thereby generating new peptides [133]. This process may be undesirable if it leads to loss of the bioactivity of an ingested polypeptide, or it may be desirable if it leads to the generation of new peptides with improved bioactivity. Consequently, it is often important to design food matrices that can control the gastrointestinal fate of polypeptides within foods and within the GIT so as to improve their bioactivity profiles [132, 134].

In the current study, we fabricated filled hydrogel particles containing n-3 PUFA droplets embedded within a dietary fiber matrix formed by complex coacervation. We

used low-methoxy (LM) amidated pectin as an anionic biopolymer and casein as a cationic biopolymer to form hydrogel particles. The casein was enzymatically cross-linked using transglutaminase to improve the stability of the biopolymer matrix. The effect of hydrogel particle encapsulation on the chemical stability of emulsified polyunsaturated lipids (fish oil) were investigated. Furthermore, we investigated the possibility of encapsulating protein nanoparticles within polysaccharide-based hydrogel particles, and studied the influence of solution and environmental conditions on their properties. Initially, protein nanoparticles were formed from a hydrophobic protein (zein) using an antisolvent precipitation method, and utilizing a protein-based emulsifier (whey protein) to stabilize them. These composite protein nanoparticles were then encapsulated within microgels formed by acidifying a polysaccharide/protein mixture (alginate/caseinate) to induce electrostatic complexation, leading to the formation of a hydrogel matrix that trapped the protein nanoparticles inside. The main focus of this study was to examine the influence of solution conditions (pH and ionic strength) on the stability and properties of the protein nanoparticle-loaded microgels. This information is useful for establishing their potential application in food products, and their potential behavior within the gastrointestinal tract

3.1.2 Materials and methods

3.1.2.1 Materials

Powdered sodium caseinate was obtained from the American Casein Company (MP Biomedicals LLC) and was used without further purification. As stated by the manufacturer, the protein and moisture content of the powder were 91.4% and 5.0%,

respectively. Zein (Lot# SLBD5665V) and sodium alginate (Lot 50K0180) were purchased from Sigma–Aldrich (St. Louis, MO, USA). Whey protein isolate (WPI) powder was obtained from Davisco Foods International Inc. (Le Sueur, MN, USA). Alginic acid (sodium salt) (Lot# 180947) was purchased from the Sigma Chemical Company (St. Louis, MO). Low methoxyl amidated pectin (Genu Pectin (Citrus), LM-104 AS-Z) was donated by CP Keloco (Lille Skensved, Denmark) and was used without further purification. The degree of esterification (DE) was approximately 27% as provided by the manufacturer. The protein cross-linking enzyme transglutaminase (Activa TI) was donated by Ajinomoto Food Ingredients (Chicago, Illinois). According to the manufacturer, the activity of this enzyme was 100 units per gram of powdered preparation. Fish oil was obtained from DSM Nutritional Products Ltd. (Basel, Switzerland). This oil contained 101 mg of EPA/g of oil, 148 mg of DHA/g oil, and a total ω-3 PUFA content of 312 mg/g of oil.

All chemicals used, including technical grade Nile red dye (CAS #7385-67-3) and fluorescein isothiocyanate isomer I, were purchased from Sigma-Aldrich (St. Louis, MO). Double distilled water was used to prepare all solutions and emulsions.

3.1.2.2 Conventional emulsion preparation

A 10% (w/w) oil-in-water (O/W) emulsion stabilized by sodium caseinate (NaC) was prepared as a stock emulsion. An emulsifier solution was prepared by dispersing 1% (w/w) NaC powder in 10 mM phosphate buffer (pH 7) with continuous stirring at 700 rpm for 2 hours (40 ^{o}C). A coarse emulsion was then prepared by blending fish oil (10% w/w) and emulsifier solution (90% w/w) using a high speed blender for 2 min (Tissue Tearor Model 985370-395, Biospec Products Inc., Bartles- ville, OK). The droplet size in

this coarse emulsion was further reduced by passing it three times through a high-pressure homogenizer (Microfluidics Microfluidizer M-110P, Newton, MA USA) at 12,000 psi.

3.1.2.3 Protein nanoparticles preparation

Protein nanoparticles were fabricated from zein using an antisolvent precipitation method. Initially, zein (26.4 mg/mL) was dissolved in ethanol solution (80% *v/v*). Then, 25 mL of aqueous ethanol solution was rapidly injected into 75 ml of whey protein solution (0.25% WPI, PBS, pH 6.5) that was continuously stirred at 1200 rpm using a magnetic stirrer (IKA R05, Werke, GmbH). The resulting colloidal dispersion was then stirred for another 30 min at the same speed. The ethanol remaining in the final colloidal dispersions was evaporated using a rotary evaporator (Rotavapor R110, Büchi Corp., Switzerland), and the same volume of pH 6.5 PBS was added to compensate for the lost ethanol.

3.1.2.4 Unfilled hydrogel particle preparation

The method used to form the hydrogel microspheres was adapted from Chung et al (2012) with some slight modifications. This method involves inducing thermodynamic incompatibility at a pH where the biopolymers have similar charges (*e.g.,* pH 7), and then adjusting the pH to a value where the biopolymers have opposite charges (*e.g.,* pH 4.5) to induce coacervation. This procedure promotes the formation of casein-rich microspheres surrounded by a pectin shell. Initially, 3% (w/w) NaC and 3% (w/w) pectin solutions were prepared by dissolving weighed amounts of biopolymers into phosphate buffer (pH 7). 2 M sodium hydroxide was used to adjust the biopolymer solution to pH 7. Equal

weights of the two stock solutions were then mixed together using stirring. The pH of this mixture was adjusted to 7 (if necessary) using 2 M sodium hydroxide. This mixture was then acidified to pH 4.5 using 1 M citric acid at a rate of 1 drop/10 s with continuous stirring at 500 rpm. The hydrogel particles were then cross-linked by adding a solution of transglutaminase (0.1 g/ml 10 mM PBS, pH 4.5) at a level of 10 units of enzyme activity/per gram of protein. The solution was then incubated at 40 ^{o}C for 2 hours with constant stirring at 500 rpm. At the end of the incubation period, the reaction was stopped by heating the samples in an 85 ^{o}C water bath for 5 minutes. Control (not cross-linked) particles were exposed to the same incubation and inactivation conditions as enzyme treated particles.

For the protein nanoparticles encapsulation, another hydrogel particles were prepared using caseinate and alginate. Firstly, 2 M sodium hydroxide was used to adjust caseinate (2%) and alginate (2%) solutions to pH 7. Then these two stock solutions and phosphate buffer were mixed together at different volume ratios under continuous stirring to form final compositions of 0.33% sodium caseinate/1.33% alginate (mass ratio 1:4). The mixtures were then acidified to pH 5 using 1 M citric acid at a rate of 1 drop/10 s with continuous stirring at 500 rpm to promote complex formation.

3.1.2.5 Filled hydrogel microsphere preparation

Stock solutions of 6% casein and 3% pectin were prepared separately in 10 mM phosphate buffer at pH 7 and stirred until fully dissolved. 2 M sodium hydroxide was used to adjust the dissolved biopolymer solution to pH 7. After pH adjustment, 10% (w/w) oil-in-water emulsion, 6% casein, and 10 mM phosphate buffer were mixed together to obtain a system containing 3% casein and 2% fat. Then equal volumes of droplet-

biopolymer mixture and pectin were mixed (500 rpm) and the solution was adjusted to pH 7.0 (if necessary). The obtained mixture was finally acidified to pH 4.5 using 1 M citric acid at a rate of 1drop/10 s with continuous string at 500 rpm to promote complex coacervation. The same procedure was also used as described in 2.2.1 to form cross-liked filled hydrogel microspheres.

2 M sodium hydroxide was used to adjust caseinate solutions, alginate solutions, and protein nanoparticle dispersions to pH 7. After pH adjustment, 6.6 mg/mL protein nanoparticle dispersion and 2% sodium caseinate solution were mixed together at a 1:1 volume ratio. Then, this system was mixed (500 rpm) with 2% alginate solution at a volume ratio of 1:2. Finally, the resulting mixture was acidified to pH 5 using 1 M citric acid with continuous stirring at 500 rpm to promote complex formation. The final composition of the resulting system was 1.1 mg/mL protein nanoparticles, 0.33% sodium caseinate, and 1.33% alginate.

3.1.2.6 Microstructure analysis

The microstructure of all systems was examined using optical and confocal scanning laser microscopy with a 60 × objective lens and 10 × eyepiece (Nikon D-Eclipse C1 80i, Nikon, Melville, NY, U.S.). A small aliquot of sample was placed on a microscope slide and covered with a cover slip prior to analysis. For the confocal microscopy, samples were dyed prior to particle formation. The oil phase in the filled hydrogel particles was dyed with Nile red solution (1 mg/mL ethanol) by adding 0.1 mL of Nile red solution to 2 mL of oil, covering, and stirring overnight. The dyed oil was then used to form an emulsion as described in Section 2.2.1. The NaC phase was dyed with fluorescein thiocyanate isomer I (FITC) solution (1 mg/mL dimethyl sulfoxide)

prior to measurements by adding 0.1 mL of FITC dye solution to 2 mL of sample. The excitation and emission spectrum for Nile red were 543 nm and 605 nm, respectively while for FITC they were 488 nm and 515 nm, respectively. The microstructure images for confocal microscopy were taken and analyzed using image analysis software (NIS-Elements, Nikon, Melville, NY).

3.1.2.7 Determination of lipid oxidation

The chemical stability of the filled hydrogel particles and non-encapsulated lipid droplets was evaluated by monitoring the formation of hydroperoxides over the course of 7 days storage. The hydroperoxides of different systems were extracted using chloroform/methanol solution: 1 ml of emulsion or filled hydrogel microsphere suspension was vigorously vortexed three times with 7.5 ml of chloroform: methanol (2:1 vol/vol) followed by centrifugation for 5 min at 1300g. Then 0.2 ml of the chloroform/methanol extract (lower layer) was carefully removed and mixed with 2.8 ml of methanol/1-butanol (2:1 vol/vol). Depending on the concentration of hydroperoxides, the chloroform/methanol extract was diluted with solvent such that the final absorbance of the reacted sample remained below 1.0 cm^{-1}. This mixture (3.0 ml) was then reacted with 15 μL of 3.94 M ammonium thiocyanate and 15 μL of ferrous iron solution (prepared by reacting 0.132 M barium chloride and 0.144 M ferrous sulphate). The mixture was vortexed and allowed to react for 20 min at room temperature in the dark before the absorbance of the sample was measured at 510 nm using a spectrophotometer. The concentration of hydroperoxides was determined based on a standard curve of cumene hydroperoxide (0–20 μM).

3.1.2.8 Stability of environmental conditions

The particle size and microstructure of the colloidal dispersions were determined after they were exposed to various environmental conditions.

Effect of pH: Freshly prepared colloidal dispersions were mixed with equal volumes of 10 mM phosphate buffer with pH values ranging from 3.0 to 7.0. The samples were then adjusted to the desired pH values with 1 mol/L NaOH or HCl.

Effect of salt: Protein nanoparticles were mixed with equal volumes of phosphate buffer at pH 6.5 containing sodium chloride (50–400 mM NaCl). While, nanoparticle-loaded microgels were mixed with equal volumes of phosphate buffer at pH 5.0 containing sodium chloride (0.5–2 M NaCl). If necessary, the samples were then adjusted to pH 6.5 or pH 5.0 with 1 mol/L NaOH or HCl.

3.1.2.9 Statistical analysis

All experiments were carried out on two or three freshly prepared samples. The results are expressed as means ± standard deviations (SD). Data were subjected to statistical analysis using SPSS software (version 18.0). Means were subject to Duncan's test and a *P*-value of <0.05 was considered statistically significant.

3.1.3 Results and discussion

3.1.3.1 Microstructure

The microstructure of the particles in the different delivery systems was measured using confocal scanning laser microscopy. The lipid droplets were dyed using Nile red (stained red) and the casein was dyed using FITC (stained green). The confocal images show that small lipid droplets were distributed throughout the casein-rich phase. In the

emulsion, the casein was distributed throughout the aqueous phase, indicating that it was not all adsorbed to the lipid droplet surfaces (**Figure 3.1 a**). In the unfilled hydrogel particles, casein-rich microspheres were distributed throughout a black background, indicating that most of the casein was present within the hydrogel particles. The location of pectin within the hydrogel particle suspensions could not be determined since it was not specifically dyed by a fluorochrome. However, based on the negative particle charge, we expect that some pectin molecules formed a coating around the casein-rich microspheres. In the presence of lipid droplets, the confocal images indicate that almost all of the lipid droplets (red) were embedded inside the casein-rich hydrogel microspheres (**Figure 3.1c**). Samples containing larger microspheres were prepared using moderate stirring conditions during fabrication of the filled hydrogel particles so as to better observe their internal structure. The images of these larger particles clearly indicate that lipid droplets (red) were encapsulated within casein-rich microspheres (green) (**Figure 3.1d**). This result is in agreement with the static light scatting data mentioned above. Both the filled and non-filled hydrogel microspheres had a uniform small diameter (around 3 to 5 μm). These filled hydrogel particles are smaller than those typically produced using conventional coacervation methods, which may an advantage for some commercial applications within the food industry.

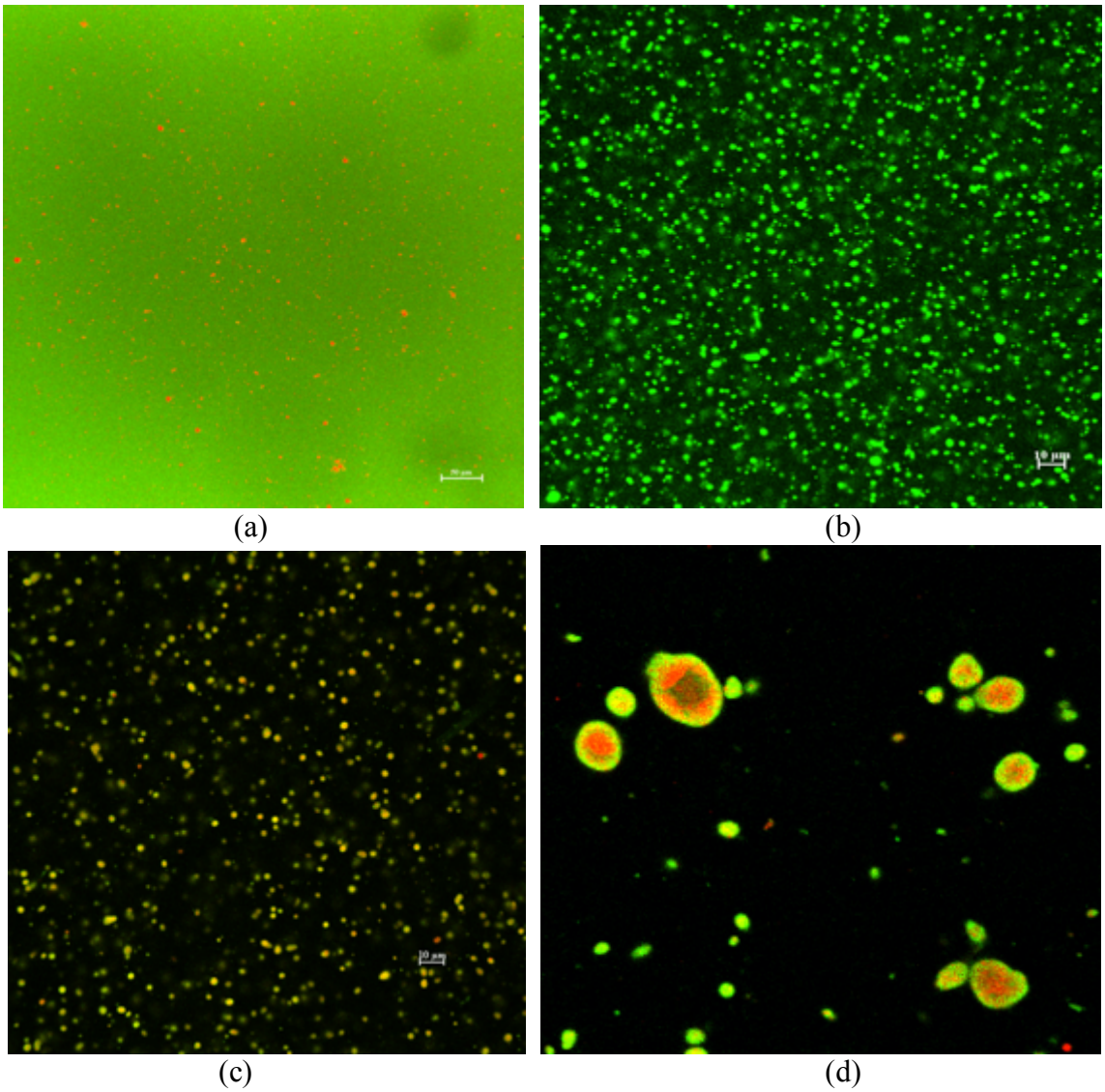

Figure 3. 1 Confocal micrographs (60× magnifications) of (a) 1% oil-in-water emulsion, (b) hydrogel particles fabricated without fat, (c) filled hydrogel particles and (d) filled hydrogel particles fabricated with moderate stirring. The oil phase (red) was stained with Nile red while the protein phase (green) was stained with FITC.

3.1.3.2 Lipid oxidation in filled hydrogel particles and emulsions

One of the major challenges associated with the fortification of foods with omega-3 fatty acids is their high susceptibility to lipid oxidation during storage [105, 122-123]. The rate and extent of lipid oxidation of emulsified lipids can often be overcome using well-

designed colloidal delivery systems. We therefore compared the oxidative stability of the lipid (fish oil) droplets in filled hydrogel microspheres and conventional emulsions (**Figure 3.2**). We measured the concentration of primary reaction products (hydroperoxides) in conventional emulsions and filled hydrogel microspheres during 7 days storage. The hydroperoxide concentration in the conventional emulsions increased sharply after 4 days storage and then remained high during further storage. On the other hand, the hydroperoxide concentration remained relatively low from 0 to 7 days storage for the lipid droplets encapsulated within filled hydrogel microspheres. These results were somewhat different from a previous study, which reported that filled casein-rich microspheres and casein-stabilized emulsions had fairly similar oxidation rates, but filled hydrogel microspheres had much better stability than Tween-stabilized emulsions [73]. These differences may be due to the different fabrication methods and materials used to form the filled hydrogel microspheres in both studies. Casein is known to have antioxidant properties due to its ability to scavenge free radicals and chelate pro-oxidant transition metals, such as iron or copper [135]. The confocal fluorescence images discussed earlier indicated that casein was concentrated within the hydrogel microspheres, and therefore there would be a high local concentration of this antioxidant protein in the vicinity of the lipid droplets. This casein-rich matrix may have been able to scavenge free radicals and bind transition metals thereby inhibiting their interaction with the lipid droplets inside the hydrogel microspheres. Overall, these results suggest that encapsulating fish oil droplets within a hydrogel matrix containing high concentrations of antioxidant proteins may be a more effective means of inhibiting lipid oxidation than simply having a thin layer of casein molecules around each lipid droplet.

3.1.3.3 Influence of pH on stability

Colloidal delivery systems utilized within foods and beverages may experience appreciably different pH environments depending on the nature of the product. In addition, they may be exposed to considerable variations in pH as they pass through the human gastrointestinal tract after ingestion. Consequently, it is useful to understand the influence of pH on the properties of any colloidal delivery system intended for use in commercial food and beverage products.

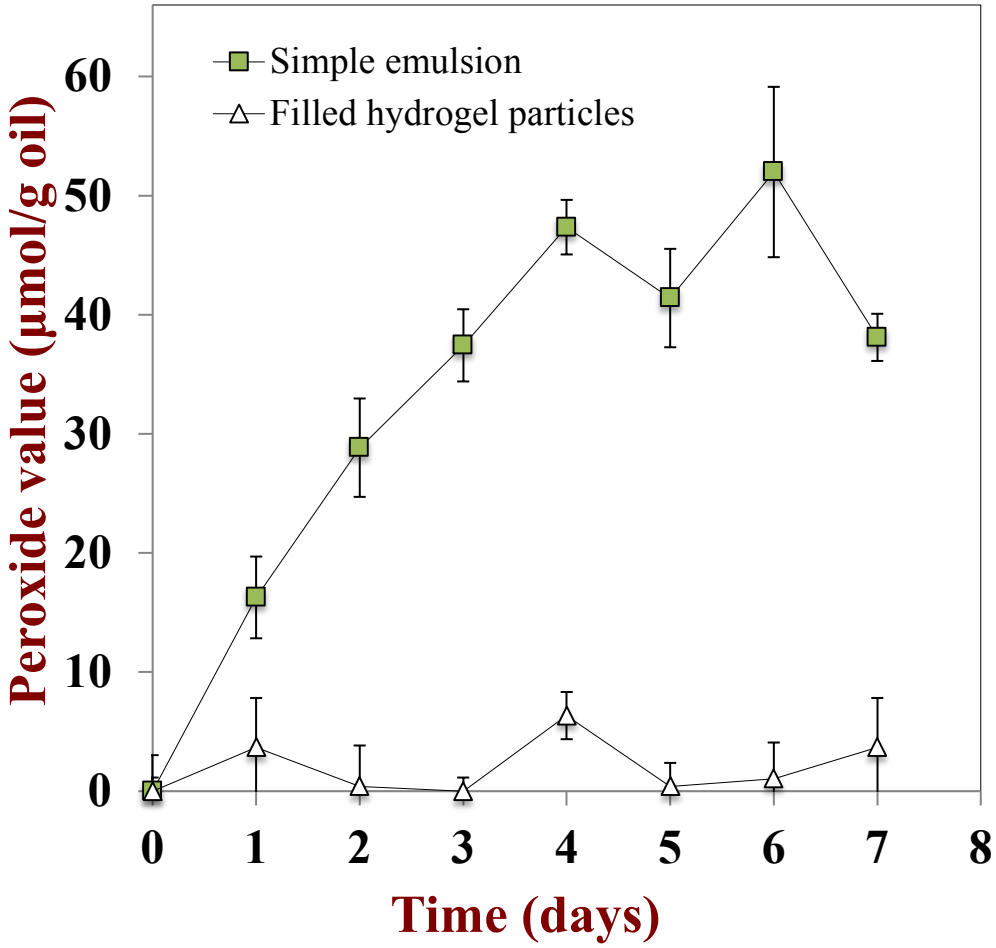

Figure 3. 2 Concentration of hydroperoxides formed from fish oil during 7 days storage in simple oil-in-water emulsions and in filled hydrogel particles

3.1.3.3 Influence of pH on stability

Colloidal delivery systems utilized within foods and beverages may experience appreciably different pH environments depending on the nature of the product. In addition, they may be exposed to considerable variations in pH as they pass through the human gastrointestinal tract after ingestion. Consequently, it is useful to understand the influence of pH on the properties of any colloidal delivery system intended for use in commercial food and beverage products.

3.1.3.3.1 Protein-nanoparticles

The tendency for aggregation to occur is highlighted in measurements of the influence of pH on the particle size and microstructure of the protein nanoparticle suspensions (**Figures 3.3 to 3.5**). At high pH values (6.5 to 7), the particles were relatively small (d_{32} < 1 μm), had a monomodal distribution, and were evenly distributed throughout the sample. At intermediate pH values (pH 5.5. to 4), the particle size was relatively big (d_{32} > 10 μm) and large irregular shaped aggregates were observed in the microscopy images. At low pH values (3 to 3.5), there was an appreciable increase in particle size detected by light scattering, and also evidence of some large aggregates in the microscopy images (**Figures 3.3 to 3.5**). It is possible that these aggregates formed as the suspensions were moved from high pH to low pH, and were not fully broken down under acidic conditions. The reason for the difference in appearance of the protein nanoparticle suspensions at low and high pH values also indicated that the nature of the

particles present had changed due to an alteration in the strength of the electrostatic interactions in the system.

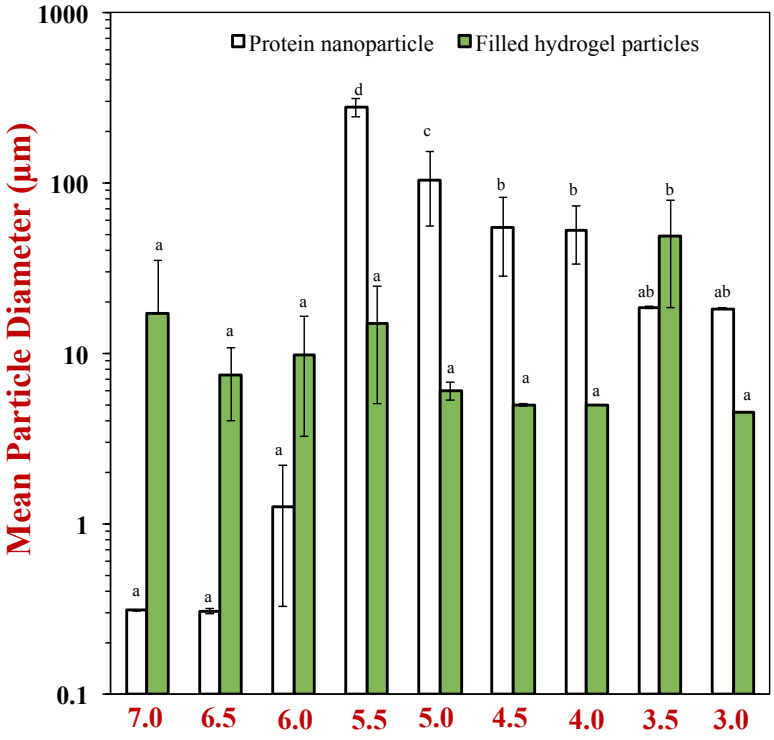

Figure 3. 3 Effect of pH on mean particle diameters (d_{32}) of protein nanoparticles and filled hydrogel particles. Different letters mean significant differences ($p < 0.05$) of the particle diameter at different pH values.

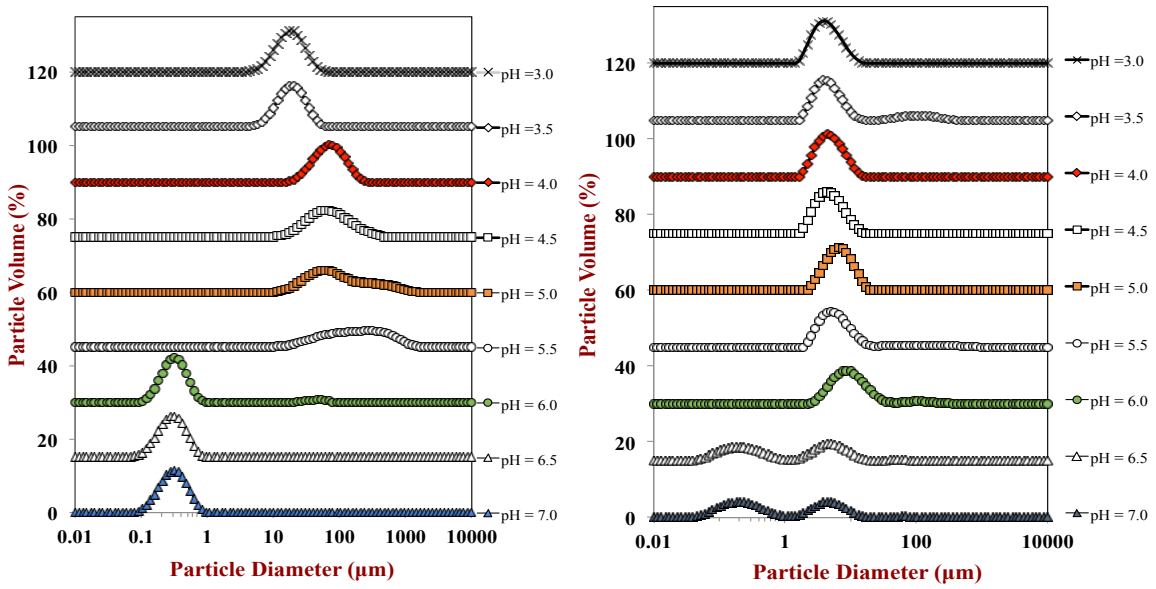

Figure 3. 4 The pH-dependence of the particle size distribution of (a) protein nanoparticles and (b) protein nanoparticle-filled hydrogel particles.

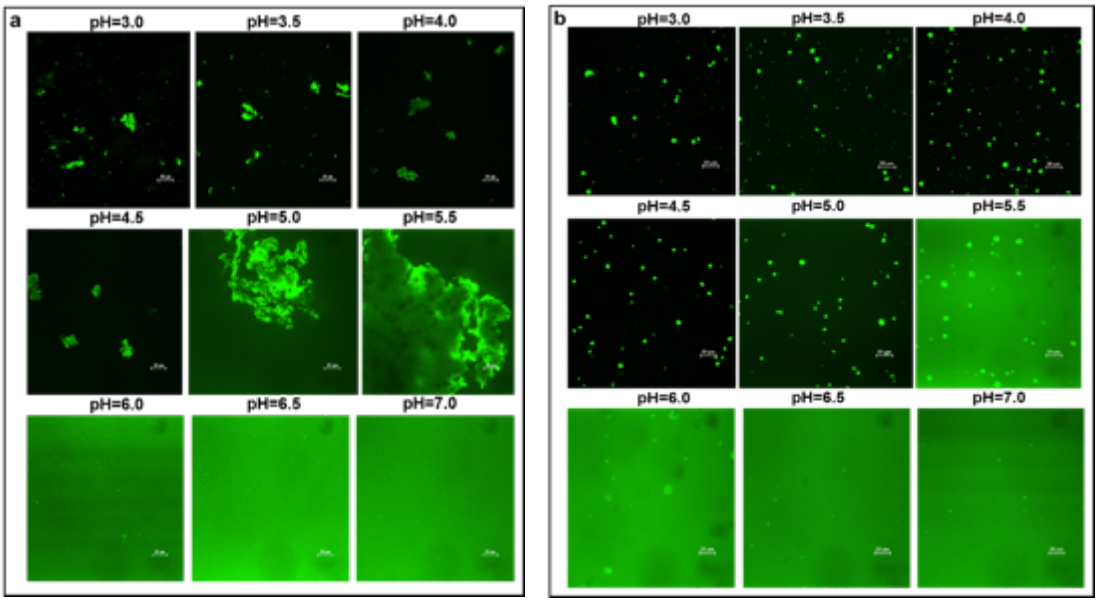

(a) (b)

Figure 3. 5 Confocal fluorescence micrographs of (a) protein nanoparticles and (b) protein nanoparticle-filled hydrogel particles after incubation at different pH values.

3.1.3.3.2 Filled microgels

We then examined the influence of pH on the properties of the protein-nanoparticle filled microgels. The light scattering measurements indicated that the dimensions of the microgels remained relatively constant from pH 3 to 6, with a monomodal particle size distribution (**Figures 3.3 and 3.4b**). However, the particle size distribution became bimodal at pH 6.5 and 7, with a population of particles around 180 nm and another population around 4 μm. We hypothesize that the microgels dissociated at these higher pH values because the alginate and caseinate molecules both had strong negative charges and so there was a strong electrostatic repulsion between them. Consequently, the microgels may have released the protein nanoparticles, which would account for the population of small particles observed in the particle size distributions at these pH values (**Figure 3.4b**). This observation was supported by the confocal microscopy images of the influence of pH on the microstructure of the system (**Figure 3.5b**). At pH 3 to 5, the microgels remained as discrete intact particles, *i.e.,* the images showed discrete regions of high fluorescence intensity (protein-rich particles) surrounded by a black (protein-free) background. At pH 5.5, there was evidence that some of the protein had leaked out of the microgels, *i.e.,* the images showed discrete regions of high fluorescence intensity (protein-rich particles) surrounded by a green (protein-rich) background. At pH 7, it appeared that the microgels had almost completely disintegrated and the protein was evenly distributed throughout the system. In these systems, we hypothesize that the protein nanoparticles had been released from the microgels and formed a stable colloidal dispersion. This hypothesis is based on the fact that a

population of small particles was observed in the light scattering data (**Figure 3.4b**), , and the protein was evenly spread throughout the samples.

3.1.4 Conclusion

This study has shown that protein nanoparticles and polyunsaturated lipid droplets can be successfully incorporated into biopolymer microgels formed from electrostatic complexation of casein and alginate. Incorporating polyunsaturated lipid droplets within the hydrogel microspheres effectively inhibited lipid oxidation, which may be important for stabilizing these healthy lipids in food and beverage products. In addition, we found The protein nanoparticles were retained within the microgels at low pH values (3 to 5.5) with no aggregation formed. Overall, our results suggest that encapsulation of protein or polyunsaturated lipid droplets nanoparticles within microgels may be a viable method of improving their chemical or physical stability, which have important implications for the development of food-grade delivery systems to fortify foods and beverages with bioactive protein and lipids.

3.2 Release of bioactives using hydrogel particles: pH-triggered release

3.2.1 Introduction

Various types of lipophilic active agents need to be incorporated into aqueous-based products, protected during storage, and then released in the mouth after ingestion, *e.g.,* certain oil-soluble drugs [136-137], antimicrobials for oral health [138-139], and food flavors [140]. Lipophilic actives usually have to be solubilized within an emulsified oil phase before they can be successfully incorporated into aqueous-based products. It is often important to be able to control the release profile of lipophilic components within the mouth after ingestion, *e.g.,* for controlled flavor release in the food industry [34, 101, 141]. In some situations, a rapid or burst release profile is required, but in other cases a prolonged or delayed release is preferred [142]. It is therefore important to develop delivery systems that can encapsulate lipophilic active agents, protect them within products, but then release them within the mouth. A number of studies have encapsulated lipophilic actives within solid particles produced by drying oil-in-water emulsions [143-146]. The resulting delivery systems are in a powdered form that is particularly suitable for application within low-moisture products. However, there is also a need for delivery systems that can be incorporated into high-moisture products (such as beverages, dressings, sauces, and desserts). For these applications it is possible to encapsulate lipophilic actives within hydrogel particles formed from food-grade biopolymers [34, 101]. These hydrogel particles may be specifically designed to control the release profile of lipophilic actives within the mouth.

Hydrogel particles can be formed using various fabrication methods, including extrusion, templating, molding, thermodynamic incompatibility, and coacervation, with

each method having certain advantages and disadvantages for particular applications [20, 79]. Complex coacervation is a relatively simple method that relies on the formation of electrostatic complexes between polymers that have opposite charges [147-148]. Coacervation refers to the phase separation of a liquid phase into a polymer-rich phase (coacervate) and a polymer-poor phase [149-152]. Coacervation is already widely used in the food and pharmaceutical industries to encapsulate active ingredients [145, 153-154]. Filled hydrogel microspheres based on complex coacervation can be used as aqueous-based delivery systems, and can be considered to be examples of $O/W_1/W_2$ type structured emulsions [79]. Lipid droplets are trapped within hydrogel microspheres (W_1), which themselves are suspended within a continuous aqueous phase (W_2). In recent studies, we have successfully fabricated fish oil loaded hydrogel particles based on complex coacervation of caseinate and LM-pectin [155]. Encapsulation of fish oil within filled hydrogel particles improved their stability to lipid oxidation compared to conventional emulsions.

The design of delivery systems that can control the release of encapsulated actives within the mouth relies on an understanding of their oral processing [156-158]. Aqueous-based delivery systems containing relatively small particles do not require chewing before swallowing. Nevertheless, they are still exposed to changes in environmental conditions within the mouth that may alter their release properties, such as changes in temperature, enzyme activity, dilution, pH, ionic strength, flow profiles, and interactions [159-161]. A number of these factors may be used as potential triggers to release encapsulated active components within the mouth.

In this work, we fabricated filled hydrogel particles by trapping emulsified lipids within complex coacervates formed from two food-grade biopolymers: alginate and casein. Casein is a milk protein with a flexible structure known to have strong antioxidant properties [155], and may therefore be used to stabilize encapsulated polyunsaturated lipids from oxidation during storage [155]. Alginate is an anionic linear polysaccharide that is commonly used as a building block in the formation of hydrogel particles [6]. The ability of hydrogel particles to control the release of encapsulated lipid droplets within the mouth was evaluated using simulated oral conditions. We hypothesized that lipid droplets could be retained within hydrogel particles during storage, but released under simulated oral conditions using pH as a trigger. The results of this study provide valuable information for the rational design and fabrication of delivery systems for lipophilic agents that need to be released in the mouth.

3.2.2 Materials and methods

3.2.2.1 Materials

Powdered sodium caseinate was obtained from the American Casein Company (MP Biomedicals LLC) and was used without further purification. As stated by the manufacturer, the protein and moisture content of the powder were 91.4% and 5.0%, respectively. Corn oil was purchased from a local supermarket and used without further purification. Alginic acid (sodium salt) (Lot# 180947, viscosity of 1% alginic acid in water is 15–20 cp) was purchased from Sigma–Aldrich (St. Louis, MO). All chemicals used were analytical grade and purchased from Sigma-Aldrich (St. Louis, MO). Double distilled water was used to make all solutions.

3.2.2.2 Conventional emulsion preparation

A 10% (w/w) oil-in-water (O/W) emulsion stabilized by sodium caseinate (NaC) was prepared as a stock emulsion. An emulsifier solution was prepared by dispersing 1% (w/w) NaC powder into 10 mM phosphate buffer (pH 7) with continuous stirring at 700 rpm for 2 hours (40 ^{o}C). A coarse emulsion was then prepared by blending corn oil (10% w/w) and emulsifier solution (90% w/w) together using a high-speed blender for 2 min (Tissue Tearor Model 985370-395, Biospec Products Inc., Bartles- ville, OK). The droplet size in this coarse emulsion was further reduced by passing it 3 times through a high-pressure homogenizer (Microfluidics Microfluidizer M-110P, Newton, MA USA) at 12,000 psi.

3.2.2.3 ζ-potential measurements

The electrical charge (ζ-potential) of caseinate and alginate at different pH values (2 to 7) was measured using a particle electrophoresis instrument (Zetasizer Nano ZA series, Malvern Instruments Ltd. Worcestershire, UK). Samples were diluted using 10 mM phosphate buffer (at the same pH as the sample) prior to analysis to keep the instrument attenuation value between 5 and 10. All measurements were made on at least two freshly prepared samples and each sample was measured in duplicate.

3.2.2.4 Turbidity measurements

The turbidities of dispersions containing caseinate and alginate were determined using a UV–visible spectrophotometer at 600 nm (Ultrospec 3000 pro, Biochrom Ltd., Cambridge, UK). The samples were contained within 1 cm path length optical cells, and

phosphate buffer was used as a control. Turbidity measurements were carried out on at least two freshly prepared samples.

3.2.2.4 Unfilled and filled hydrogel microsphere preparation

Initially, 1% (w/w) NaC and 2% (w/w) alginate solutions were prepared by dissolving weighed amounts of biopolymers into phosphate buffer (pH 7). 2 M sodium hydroxide was used to adjust the dissolved biopolymer solution to pH 7. Then these two stock solutions and phosphate buffer were mixed together at different volume ratios under continuous stirring to form final compositions of 0.33% casein/1.33% alginate (mass ratio 1：4) and 0.75% casein/0.25% alginate (mass ratio 3:1). The pH of the biopolymer mixtures was adjusted to 7.0 (if necessary) using 2 M sodium hydroxide. The mixtures were then acidified to pH 5 using 1 M citric acid at a rate of 1 drop/10 s with continuous stirring at 500 rpm. The influence of pH on the characteristics of the hydrogel particles formed was studied by adding different amounts of 1 M citric acid or sodium hydroxide.

Stock solutions of 2% casein and 2% alginate were prepared separately in 10 mM phosphate buffer at pH 7 and stirred until fully dissolved. 2 M sodium hydroxide was used to adjust the dissolved biopolymer solution to pH 7. After pH adjustment, 6% (w/w) oil-in-water emulsion and 2% casein were mixed together to obtain a system containing 1% casein and 3% fat. Then this droplet-biopolymer mixture was mixed (500 rpm) with 2% alginate solution at a volume ratio of 1:2. The obtained mixture was finally acidified to pH 5 using 1 M citric acid with continuous string at 500 rpm to promote complex coacervation. The final composition of the resulting system was 1% fat, 0.33% casein, and 1.33% alginate.

3.2.2.5 Particle size measurements

The particle size of hydrogel particles at different pH (2-7) was determined using static light scattering (Mastersizer 2000, Malvern Instruments, Worcestershire, United Kingdom). This instrument infers the size of the particles from measurements of their angular scattering pattern. All measurements were made on at least two freshly prepared samples. Samples were diluted in 10 mM phosphate buffer (pH 2-7) by adding small aliquots into a measurement chamber. A refractive index of 1.33 was used for the aqueous phase, 1.472 for the oil phase and hydrogel particle phase. Particle size measurements are reported as surface-weighted mean diameter (d_{32}).

3.2.2.5 Simulated Oral Conditions

Simulated saliva fluid (SSF), containing mucin and various salts, was prepared according to a previous study [162]. A 5 mL-aliquot of the filled hydrogel particle solution was mixed with 5 mL of SSF, so that the final mixture contained 0.5% (w/w) oil. The pH of the mixture was adjusted to 6.8 and it was incubated at 37 °C for 10 min with continuous agitation at 100 rpm. The particles size distribution and microstructure were measured immediately after incubation.

3.2.2.6 Microstructure analysis

The microstructure of all systems were examined using confocal scanning laser microscopy with a 60 × objective lens and 10 × eyepiece (Nikon D-Eclipse C1 80i, Nikon, Melville, NY, U.S.). A small aliquot of sample was placed on a microscope slide and covered with a cover slip prior to analysis. For the confocal microscopy, samples were dyed prior to particle formation. The oil phase in the filled hydrogel particles was

dyed with Nile red solution (1 mg/mL ethanol) by adding 0.1 mL of Nile red solution to 2 mL of oil, covering, and stirring overnight. The dyed oil was then used to form an emulsion as described in Section 2.2.1. The sodium caseinate phase was dyed with fluorescein thiocyanate isomer I (FITC) solution (1 mg/mL dimethyl sulfoxide) prior to measurements by adding 0.1 mL of FITC dye solution to 2 mL of sample. The excitation and emission spectrum for Nile red were 543 nm and 605 nm, respectively while for FITC they were 488 nm and 515 nm, respectively. The microstructure images for confocal microscopy were taken and analyzed using image analysis software (NIS-Elements, Nikon, Melville, NY).

3.2.2.7 Statistical analysis

All experiments were carried out in triplicate using freshly prepared samples. The mean and standard deviations were calculated from these values using SPASS.

3.2.3 Results and discussion

3.2.3.1 Electrical characteristics of biopolymer molecules

The formation of hydrogel particles by complex coacervation is an electrostatically driven process, and so it is important to measure the electrical characteristics of the biopolymers used. The pH dependence of the ζ-potential of the two biopolymers was therefore determined using an electrophoresis method *i.e.,* by measuring the direction and velocity of molecular movement in a well-defined electrical field. The charge on the caseinate molecules went from negative at pH 7.0 (≈ -27 mV) to positive at pH 2.0 (≈ +18 mV), with a point of zero charge around pH 4.6 (**Fig. 3.6**). The point of zero charge is in good agreement with the reported isoelectric point (pI) of caseinate

molecules [163]. The ζ-potential of alginate changed from strongly negative (≈ -68 mV) at pH 7 to slightly negative (≈ -9 mV) at pH 2 (**Fig. 3.6**). Thus, the magnitude of the negative charge on the alginate molecules was appreciably lower under acidic conditions than neutral conditions, which can be attributed to the fact that the anionic carboxylic ($-COO^-$) groups on the mannuronic and guluronic acid groups became partially protonated (–COOH) in this pH range (pK ≈ 3.5). Fig. 3.6 also shows the ζ-potential obtained for the mixed caseinate-alginate system at different pH values. The charge on the mixed system was between those of the individual caseinate and alginate values, which suggested that alginate was electrostatically bound to caseinate molecules over the pH range studied. Nevertheless, in mixed systems it is difficult to precisely determine whether the measured charge is from a complex or from individual molecules.

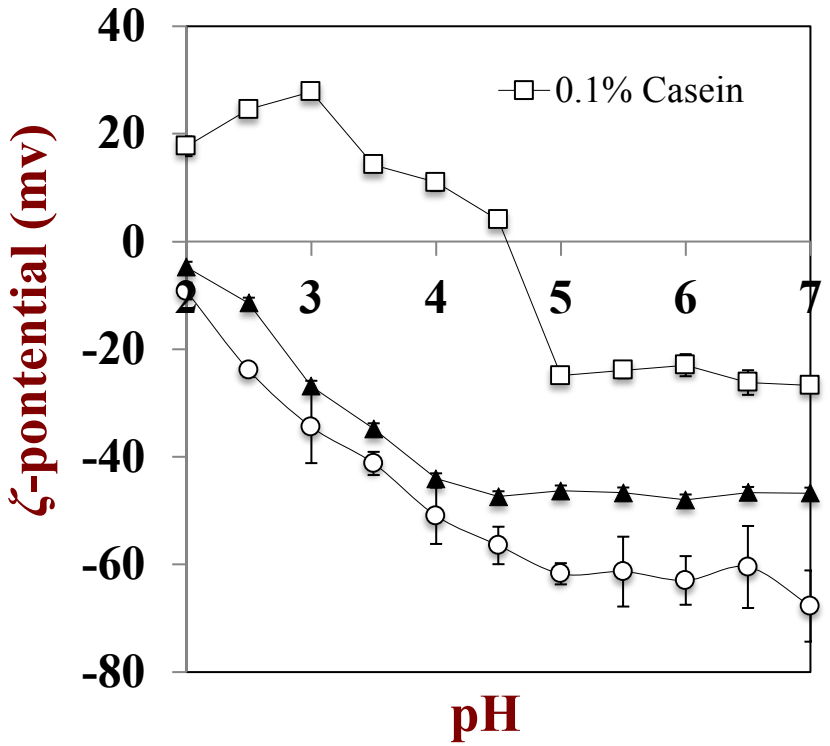

Figure 3. 6 Dependence of pH on the ζ-potential for 0.1 wt% caseinate and 0.1 wt% sodium alginate in 10 mM phosphate buffer.

In this study, hydrogel particles were assembled/dissembled by modulating solution conditions so as to induce complex coacervation of the two biopolymers. Based on the electrical characteristics of the two biopolymers we would expect them to associate with each other at low-to-intermediate pH values because they have opposite charges, but to dissociate at high pH values because they have similar charges (**Fig. 3.6**). Thus, we would anticipate that hydrogel particles could be assembled by complex coacervation in the pH regime where both biopolymers had opposite charge. Nevertheless, the characteristics of hydrogel particles formed under conditions where electrostatic attraction occurs is known to be highly dependent on interaction strength and stoichiometry [147]. We therefore used turbidity, light scattering, and microscopy measurements to obtain information about the influence of pH and biopolymer composition on the nature of the electrostatic complexes formed.

3.2.3.2 Aggregation characteristics of mixed biopolymer systems

Initially, the formation of protein-polysaccharide complexes was studied by measuring the change in turbidity as a function of pH at two different biopolymer mass ratios. Initially, we characterized the behavior of a biopolymer mixture where the protein was in excess, *i.e.,* caseinate-to-alginate mass ratio in the final mixture was 3:1 **(Fig. 3.7a)**. At pH 7, the turbidity of the mixed biopolymer solution was relatively low (≈0.016 cm^{-1}), which can be attributed to a relatively strong electrostatic repulsion between the anionic alginate and anionic caseinate under neutral pH conditions (**Fig. 3.7**). When the pH was decreased, there was initially a gradual increase in turbidity around pH 5.6, and then a much steeper increase around pH 3.7. The turbidity exhibited a maximum value at pH 3.1, and then decreased appreciably when the pH was adjusted to lower values.

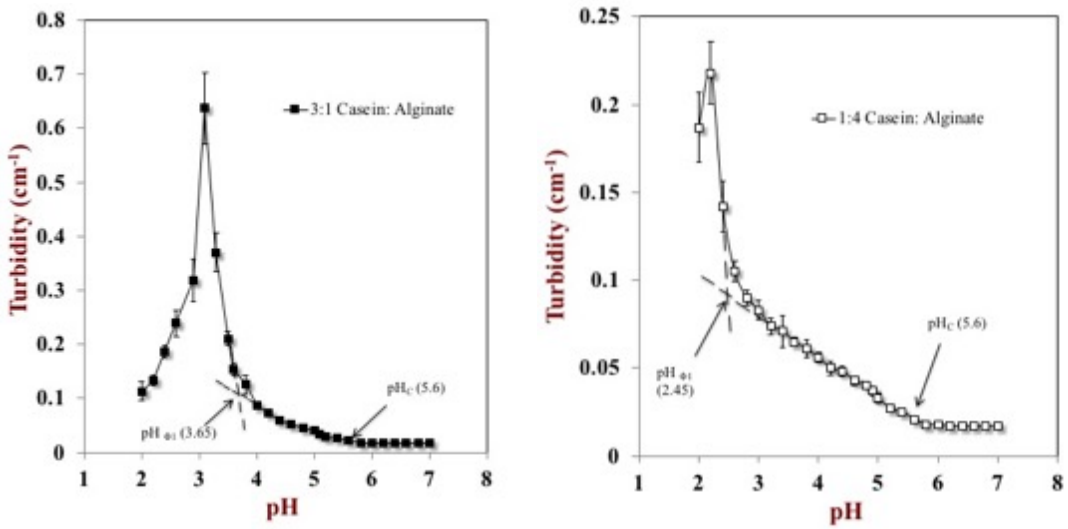

(a) (b)

Figure 3. 7 Turbidity at 600 nm as a function of pH for the system of caseinate/alginate at different biopolymers volume mixing ratios: (a) 0.1% sodium caseinate (NaC) and 0.1% sodium alginate (NaA), 3:1, (b) 0.1% casein and 0.2% alginate, 1:2.

Critical pH values corresponding to the formation of different structures for the caseinate-alginate mixtures are also given in **Fig. 3.7a**. In general, complex coacervation involves two main pH-induced structuring events associated with the formation of soluble and insoluble complexes [164]. The formation of soluble complexes ("coacervates") occurs at a pH (denoted "pH_C") corresponding to the first experimentally detectable increase in turbidity during a pH titration from a region where the biopolymers have similar charges and do not form complexes. This is followed by a second structure-forming event (denoted "$pH_{\Phi 1}$"), associated with the formation of insoluble complexes ("precipitates") and a large rise in turbidity. In our study, complex coacervation began around pH 5.6 (pH_C), and insoluble complex formation began around pH 3.65 ($pH_{\Phi 1}$) (**Fig.3.7a**). These results indicate that complex coacervation began under conditions (pH 5.6) where both the caseinate and alginate molecules had net negative charges (**Fig. 3.7**). Previous studies have also shown that coacervates can be formed under conditions where

a protein and anionic polysaccharide have similar net negative charges, due to electrostatic attraction between anionic groups on the polysaccharides and cationic patches on the protein surfaces [147, 165-166].

We also studied the aggregation behavior of a biopolymer mixture in which the polysaccharide was dominant, *i.e.,* a caseinate-to-alginate mass ratio of 1:4 **(Fig. 3.7b)**. Qualitatively, the behavior of this biopolymer mixture was similar to that where protein was dominant: as the pH was reduced, the turbidity initially remained low, then increased slightly, then increased steeply to a maximum value, and then fell. The two different casein-to-alginate mixing ratios used (3:1 and 1:4) gave similar pH_C values (pH ≈ 5.6), but the $pH_{\Phi 1}$ values shifted to lower pH values with decreasing mixing ratio (**Fig. 3.7b**). These results are in agreement with other studies that showed that the protein-to-polysaccharide mixing ratio had little effect on pH_C [167-168]. The turbidity measurements indicate that the protein and polysaccharide used in this study may form either soluble or insoluble complexes depending on the pH. In the following section, we examined the influence of biopolymer ratio on the microstructure of the complexes formed.

3.2.3.3 Microstructural characteristics of hydrogel particles

To identify suitable conditions for forming hydrogel particles, we measured the particle size distribution of biopolymer mixtures containing different ratios of casein and alginate (**Fig. 3.8**). These samples were prepared by adjusting the mixed biopolymer solutions from pH 7 to 5 to induce electrostatic complex formation. This final pH was selected based on the turbidity *versus* pH profiles of the biopolymer mixtures (**Fig. 3.7**), which showed that coacervates could be formed under these conditions, *i.e.,* $pH_I < pH < pH_C$. At a casein-to-alginate ratio of 3:1 very large hydrogel particles were detected by

static light scattering ($d \approx 700$ μm). Presumably, hydrogel particles formed under these conditions were highly prone to coalescence, and were therefore unsuitable for use as delivery systems. On the other hand, at a casein-to-alginate ratio of 1:4 small uniform hydrogel particles were detected ($d \approx 4$ μm). Caseinate solutions are highly prone to aggregation near their isoelectric point (pI ≈ 4.6), and therefore there may have been insufficient alginate present to prevent some protein aggregation from occurring in the mixed systems containing high protein levels (3:1). Conversely, in the mixed system containing high alginate levels (1:4) there may have been sufficient anionic polysaccharide molecules present to inhibit aggregation between protein molecules thereby forming more stable complexes. Another possible explanation is that the protein molecules were on the outside of the electrostatic complexes for the 3:1 system thereby promoting aggregation, but the alginate molecules were at the exterior for the 1:4 system thereby inhibiting aggregation. For this reason, we only used the 1:4 mass ratio of caseinate-to-alginate in the following experiments.

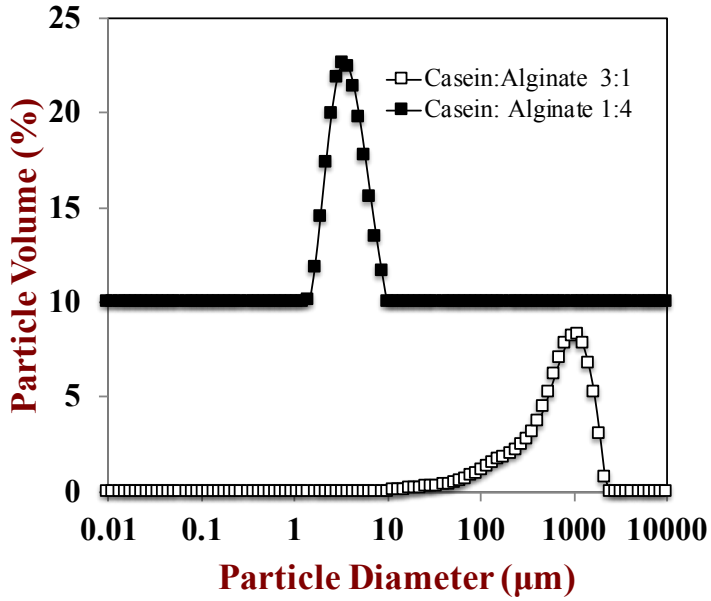

Figure 3. 8 Particle size distribution of hydrogel particles formed at pH 5 by different mixing ratios: 1% casein and 1% alginate at volume ratio of 3:1(concentration ratio: 3:1) and 1% casein and 2% alginate at volume ratio of 1:2 (concentration ratio: 1:4).

3.2.3.4 Influence of pH on hydrogel particle integrity

Hydrogel particles may be exposed to various pH conditions in food products and after ingestion when they pass through the various stages of the gastrointestinal tract [169-170]. Knowledge of the influence of pH on the properties of hydrogel particles is therefore important for their commercial application, and for creating delivery systems designed to release encapsulated lipids in response to a particular pH trigger (such as the oral environment). We therefore used confocal scanning laser microscopy and static light scattering to study the influence of pH on the microstructure and dimensions of the hydrogel particles.

Initially, hydrogel particles were formed by adjusting a 1:4 caseinate-to-alginate mixture from pH 7 to 5 to induce complex coacervation. The change in particle size and microstructure was then measured when this system was adjusted to lower or higher pH values. The observed changes can be divided into three distinct pH regions according to the structures formed. At pH 4 to 5, stable hydrogel particles were formed which had fairly uniform dimensions with diameters around 2 to 4 μm. Most of the particles had a spherical shape, which can be attributed to the presence of sufficient alginate to stabilize the casein molecules [171]. These hydrogel particles may be suitable for incorporation into commercial products that have aqueous phases in this intermediate pH range (such as yogurts). When the system was increased into the range pH 6 to 7 the hydrogel particles completely dissociated, as indicated by the confocal images, which showed that the continuous phase became a uniform green color suggesting that the caseinate molecules

were evenly distributed throughout the system rather than located within hydrogel particles (Fig. 3.9). The origin of this effect can be attributed to the change in the electrical characteristics of the two biopolymers. At high pH values, both the caseinate and alginate molecules have relatively high negative charges and therefore there will be a strong electrostatic repulsion between them. The increase in particle size measured by light scattering at high pH values suggests that there may have been some biopolymer aggregation, even though hydrogel particles were not formed. For example, there may have been some bridging of caseinate and alginate molecules through electrostatic attraction of cationic patches on the protein and anionic groups on the polysaccharide.

When the pH of the mixed biopolymer system was reduced from pH 5 to 3 there was a large increase in mean particle diameter determined by light scattering, and extensive protein aggregation observed by confocal microscopy (Fig. 3.9). This phenomenon can also be attributed to changes in the electrical characteristics of the two biopolymers. When the pH is reduced below the isoelectric point of the caseinate, the two biopolymers have opposite charges, which leads to a strong electrostatic attraction between them. Consequently, the biopolymers become more closely packed and larger aggregates are formed. Extensive protein aggregation also occurred at pH 2, but the size of the aggregates was smaller than those formed at pH 3 (Fig. 3.9), which probably occurred because the anionic groups on the alginate molecules became partially protonated causing a reduction in their negative charge and therefore weaker electrostatic attraction [172]. Insolubilization and/or precipitation of alginate would also be induced at pH value lower than the pKa of carboxyl groups. An understanding of the influence of pH on the properties of the hydrogel particles is useful for developing delivery systems

for oral applications. Our results indicate that the caseinate-alginate hydrogel particles should be stable at pH 4 to 5, but should dissociate at pH 7 thereby releasing any encapsulated components.

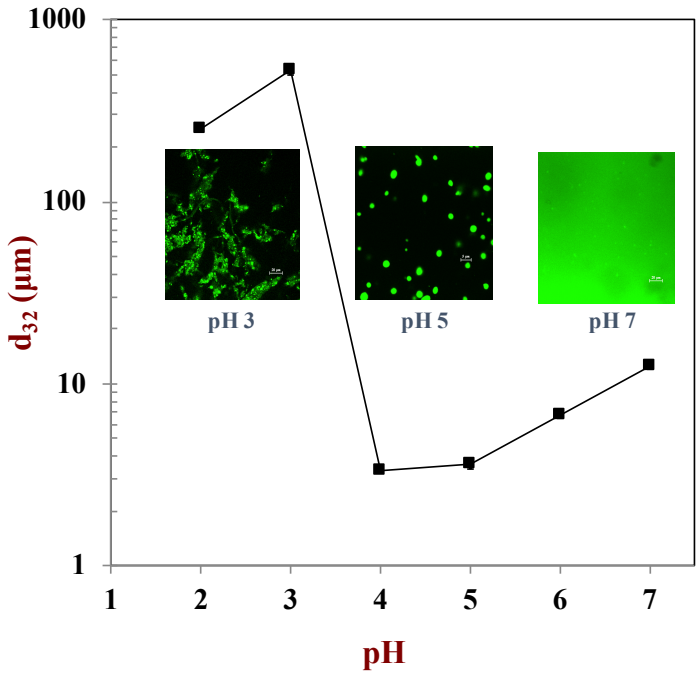

Figure 3. 9 Influence of pH (2-7) on the particle size (d_{32}) of hydrogel particles. (Confocal micrographs show the hydrogel particles at pH 3, 5, 7 respectively in the up right, protein phase in green was stained with FITC).

3.2.3.5 Influence of simulated oral conditions on lipid droplet release

For certain applications it is desirable to have filled hydrogel particles that remain intact within food products, but then release encapsulated lipid droplets within the mouth after ingestion. We therefore prepared hydrogel particles at pH 5 containing encapsulated lipid droplets, and then exposed them to simulated oral conditions (SSF, pH 6.8, 37 ºC). The particle size distribution and microstructure of the filled hydrogel particles before and after being exposure to oral conditions was determined by static light scattering and confocal microscopy (Figs. 3.10 and 3.11). In addition, the particle size distribution and

microstructure of the lipid droplets in the initial emulsion were also measured (Figs. 3.10and 3.11)

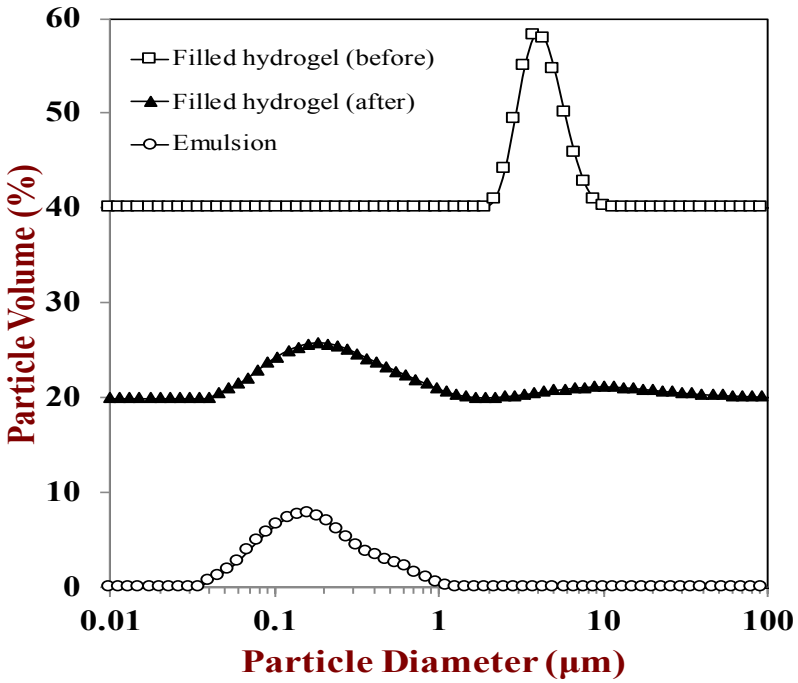

Figure 3. 10 Particle size distribution of filled hydrogel particles before and after mouth digestion.

The particle size distribution of the lipid droplets in the initial emulsion had a single broad peak at a particle diameter of about 0.2 µm (Fig. 3.10), and the droplets were evenly distributed throughout the system (Fig. 3.11). Thus, the initial protein-coated lipid droplets were relatively small and stable to aggregation. It should be noted that the aqueous phase surrounding the lipid droplets had a relatively strong green color, which suggests that there was an appreciable amount of non-adsorbed casein in the initial emulsions. Prior to exposure to oral conditions (pH 14), the particle size distribution of the filled hydrogel particles showed a single peak around 3 µm (Fig. 3.10), which was fairly similar to that observed in the absence of lipid droplets (Fig. 3.9). This suggests that incorporation of lipid droplets into the hydrogel particles did not cause a major

change in their overall dimensions. The confocal microscopy images indicated that all of the lipid droplets and casein molecules were initially trapped inside the hydrogel particles, *i.e.,* the red (lipid) and green (protein) fluorescence dyes were located together in spheroid shapes surrounded by black (Fig. 3.11). This finding is also supported by the light scattering data which indicated that there was no small peak corresponding to free lipid droplets in the particle size distribution of the filled hydrogel particles at pH 5 (Fig. 3.10). After exposure to the oral phase, the particle size distribution of the filled hydrogel particles and lipid droplets were fairly similar (Fig. 3.10), which suggested that the hydrogel particles had dissociated and released the lipid droplets. As mentioned earlier, the origin of this effect is likely to be the dissociation of the complex coacervates at neutral pH because of the strong electrostatic repulsion between the negatively charged protein and polysaccharide molecules [173].

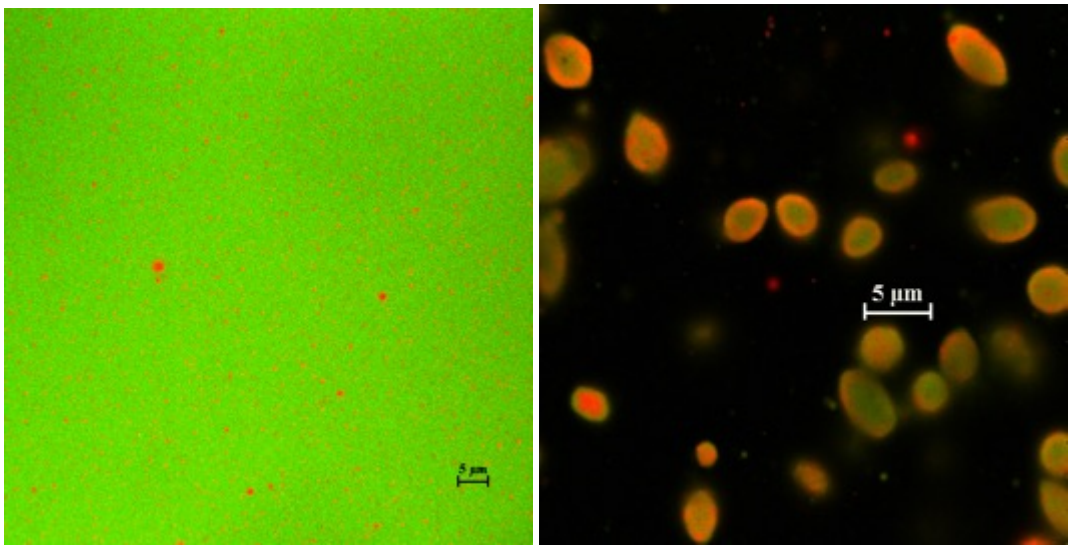

(a) (b)

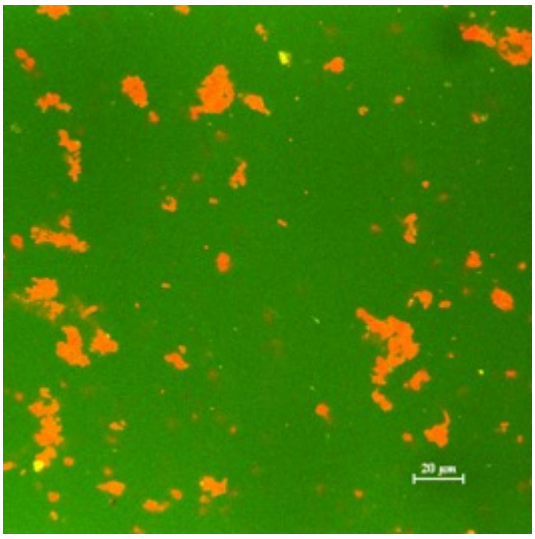

(c)

Figure 3. 11 Confocal micrographs of (a) oil emulsion, (b) filled hydrogel particles before digestion and (c) after mouth digestion. The oil phase (red) was stained with Nile red while the protein phase (green) was stained with FITC.

3.2.3 Conclusions

In this study, hydrogel particles containing encapsulated lipid droplets were fabricated based on complex coacervation of caseinate and alginate. Relatively small and stable hydrogel particles could be formed at pH values around the isoelectric point of the protein (pH 4 to 5), even under conditions where both biopolymers had net negative charges. This effect can be attributed to electrostatic attraction between anionic groups on the alginate and cationic groups on the caseinate molecules. The biopolymer mixing ratio was also an important factor in forming stable hydrogel particles. At a relatively high protein-to-polysaccharide ratio very large unstable aggregates were formed that were unsuitable as delivery systems, but at a high polysaccharide-to-protein ratio small stable hydrogel particles were formed. These hydrogel particles remained stable from pH 4 to 5, but aggregated at lower pH due to increased electrostatic attraction or insolubilization and/or precipitation of alginate, and dissociated at higher pH due to

increased electrostatic repulsion. Using simulated oral conditions, we showed that filled hydrogel particles could be made to release encapsulated lipid droplets within the mouth. These results have important implications for the development of food-grade delivery systems that may protect encapsulated lipophilic active agents in products, but release them in the mouth. One limitation of the delivery systems developed in this study, is that the hydrogel particles are only stable over a narrow range of pH conditions (pH 4 to 5), which would limit the number of food or beverage products they could be incorporated into. This problem could be overcome by using different combinations of biopolymers or different cross-linking approaches.

3.3 Release of bioactives using hydrogel particles: temperature-triggered release

3.3.1 Introduction

There is increasing interest within the food and biomedical industries to incorporate lipophilic bioactive agents into functional food and medical food products, *e.g.,* vitamins, nutraceuticals, pharmaceuticals, antimicrobials, flavors, and colors [174-177]. However, the poor water-solubility and chemical stability of many lipophilic bioactive agents makes them difficult to incorporate into food matrices. The low solubility of these bioactive agents in aqueous environments means they tend to phase separate, whereas their chemical instability means they may degrade within the product prior to consumption, thereby reducing their efficacy. It is therefore necessary to design food-grade delivery systems to improve the dispersibility and chemical stability of lipophilic bioactive agents in food matrices [178].

Flavor perception (taste and aroma) throughout the eating process is a key factor in determining the desirable sensory attributes of many food products [140, 179-180]. It is often important to control the release profile of lipophilic flavors within the mouth to provide the desired overall sensory experience [181]. Other types of lipophilic bioactive agents may also need to be released within the mouth after consumption of medical or functional foods. *e.g.,* some oil-soluble drugs [182-183], and antimicrobials for oral health [138-139]. It is therefore important to food-grade effective delivery systems that can: encapsulate efficacious levels of lipophilic bioactive agents; easily be incorporated into food or beverage matrices; protect the bioactive agents from chemical degradation during storage; release them within the mouth after ingestion (often at a controlled rate).

For many applications, delivery systems are needed that can be incorporated into high-moisture food matrices, such as those in beverages, yogurts, dressings, sauces, creams, soups, dips, and desserts. A variety of different emulsion-based delivery systems have been developed to encapsulate lipophilic bioactive agents, including emulsions, nanoemulsions, multiple emulsions, multilayer emulsions, filled hydrogel particles, and solid lipid nanoparticles [105, 184-189]. Each of these delivery systems has their own advantages and disadvantages in terms of cost, ease of preparation, in-product stability, product compatibility, ingredient utilization, and functional performance.

In this study, we focus on the utilization of filled hydrogel particles, which consist of lipid droplets trapped within hydrogel microspheres. Initially, the lipophilic bioactive agents are dissolved in an oil phase, and then an oil-in-water emulsion or nanoemulsion is formed using an appropriate homogenization method [190]. The hydrogel microspheres can be formed using a number of different fabrication methods depending on the final characteristics of the particles required, including extrusion, templating, molding, thermodynamic incompatibility, and complexation [79]. Electrostatic complexation is a relatively straightforward method that can easily be implemented commercially, since it simply relies on the formation of complexes between polymers in solution that have opposite charges [148, 191]. Filled hydrogel particles can be designed to control the protection and release of lipophilic bioactive agents by controlling the composition and structure of the hydrogel matrices. The properties of hydrogel particles formed using electrostatic complexation can be modulated by selecting biopolymers with different molecular characteristics (such as electrical properties, molecular weight, and structure) and by modulating preparation conditions (such as pH, salt, and stirring).

The design of delivery systems that can control the release of encapsulated bioactive agents within the mouth depends on an understanding of oral processing [156-158]. Numerous factors can potentially influence the behavior of delivery systems within the oral cavity, including: warming or cooling in the mouth; saliva composition, volume and flow rate; mixing, disruption and frictional forces; and pH changes. In a recent study, we fabricated hydrogel particles by trapping lipid droplets within electrostatic complexes formed by sodium caseinate and alginate at pH 5 [192]. We showed that these lipid droplets could be retained within hydrogel particles during storage, but released from the hydrogel matrix under conditions simulating oral processing. In that system, the main driving force for hydrogel disruption and droplet release was the pH change in the mouth. Under storage conditions (pH 5), the electrostatic complexes were stable due to electrostatic attraction between anionic pectin and cationic patches on the caseinate molecules. However, under oral conditions (pH 7), the complexes dissociated due to electrostatic repulsion between the anionic pectin and anionic caseinate molecules. These results suggested that filled hydrogel particles based on electrostatic complexation of two oppositely charged biopolymers might be useful for oral delivery of lipophilic bioactive agents.

The purpose of the current study was to develop filled hydrogel particles that would release encapsulated lipid droplets primarily through a temperature trigger. These hydrogel particles were prepared by incorporating lipid droplets into electrostatic complexes formed from two food-grade proteins: gelatin and sodium casein. The filled hydrogel particles formed can be considered to be an oil-in-water-in-water ($O/W_1/W_2$) emulsion that contains oil droplets (O) trapped within hydrogel microspheres (W_1), which

are themselves suspended within a continuous aqueous phase (W_2). A potential advantage of using caseinate to form the hydrogel particles is that it can stabilize encapsulated polyunsaturated lipids against oxidation, which has been attributed to its antioxidant capacity [193]. On the other hand, a potential advantage of using gelatin for fabricating oral delivery systems, is that it can form gels that melt in the mouth, *i.e.,* undergo a gel-to-sol transition around body temperature. The information obtained from this study could be useful for the rational design of emulsion-based delivery systems that release encapsulated lipophilic bioactive agents within the mouth.

3.3.2 Materials and methods

3.3.2.1 Materials

Corn oil was purchased from a local supermarket and used without further purification. Sodium caseinate powder was obtained from the American Casein Company (MP Biomedicals LLC). As stated by the manufacturer, this ingredient had a protein content of 91.4% and moisture content of 5.0%. Type A gelatin (100 bloom, extracted from pork skin) was kindly donated by GELITA American Company (Sergeant Bluff, IA). Double distilled water was used to prepare all solutions.

3.3.2.2 Methods

3.3.2.2.1 Emulsion preparation

An oil-in-water (O/W) emulsion stabilized by sodium caseinate (NaC) was prepared as a stock emulsion. Initially, an aqueous emulsifier solution was prepared by dispersing 1% (w/w) NaC powder into 10 mM phosphate buffer solution (pH 7) with

continuous stirring at 700 rpm for 2 hours (40 ^{o}C). A coarse emulsion was then prepared by blending corn oil (10% w/w) and emulsifier solution (90% w/w) together using a high-shear mixer for 2 min (Model 985370-395, Tissue Tearor, Biospec Products Inc., Bartlesville, OK). The size of the droplets in the resulting coarse emulsion was further reduced by passing it three times through a high-pressure homogenizer (Microfluidics Microfluidizer M-110P, Newton, MA USA) at 12,000 psi. The final emulsion was then diluted to 6% (w/w) for the further experiments.

3.3.2.2.2 ζ-potential measurements

The electrical characteristics (ζ-potential) of solutions of caseinate, gelatin, and their mixture were measured at different pH values (pH 5 to 10) using a particle electrophoresis instrument (Zetasizer Nano ZA series, Malvern Instruments Ltd. Worcestershire, UK). Samples were diluted using 10 mM phosphate buffer (at the same pH as the sample) prior to analysis so that the instrument attenuation value was within the optimum range (5 to 10). All measurements were made on at least two freshly prepared samples and each sample was measured in duplicate.

3.3.2.2.3 Turbidity measurements

The turbidities of dispersions containing caseinate and gelatin were determined using a UV–visible spectrophotometer at 600 nm (Ultrospec 3000 pro, Biochrom Ltd., Cambridge, UK). The samples were contained within 1 cm path length optical cells, and phosphate buffer was used as a control. Turbidity measurements were carried out on at least two freshly prepared samples. The turbidity of biopolymer solutions (pH 5.8) with increasing temperature was analyzed using an UV/visible spectrophotometer at 600 nm

(Ultraspec 3000 pro, Biochrom Ltd., Cambridge, UK). Temperature scanning was carried out from 20 to 60 °C at a heating rate of 1 °C per minute.

3.3.2.2.4 Unfilled and filled hydrogel microsphere preparation

Stock solutions of 2% sodium casein and 1% gelatin were prepared separately in 10 mM phosphate buffer at pH 7 and stirred until fully dissolved. 2 M sodium hydroxide was used to adjust the dissolved biopolymer solutions to pH 10. After pH adjustment, 6% (w/w) caseinate-stabilized oil-in-water emulsion (prepared in the section 2.2.1) and 2% caseinate solution were mixed together (1:1 volume ratio) with continuous stirring at 200 rpm to obtain a system containing 1% sodium casein and 3% oil. The resulting mixture of caseinate-coated lipid droplets and sodium casein was then mixed with a 1% gelatin solution (1:2 volume ratio) to form filled hydrogel particles. The final mixture was then acidified to pH 5.8 using 1 M citric acid with continuous string at 500 rpm to promote electrostatic complexation. The final composition of the resulting system was 1% fat, 0.33% sodium casein, and 0.67% gelatin.

3.3.2.2.5 Particle size measurements

The particle size of the various samples was determined using static light scattering (Mastersizer 2000, Malvern Instruments, Worcestershire, United Kingdom). This instrument infers the particle size distribution from measurements of the angular scattering pattern. Samples were diluted in 10 mM phosphate buffer by adding small aliquots into a measurement chamber. A refractive index of 1.33 was used for the continuous phase (water) and 1.472 for the disperse phase (oil or hydrogel). Particle size measurements are reported as the surface-weighted mean diameter (d_{32}).

3.3.2.2.6 Rheological measurements

A higher total biopolymer concentration was required to produce samples that were viscous enough to make reliable rheology measurements. Consequently, 3% (w/w) NaC and 3% (w/w) gelatin solutions were used to fabricate hydrogel particles using a similar approach to that described in Section 2.2.4. The rheology of the hydrogel particle suspensions was characterized using a dynamic shear rheometer with a cup-and-bob measurement cell (Kinexus, Malvern, Worcestershire, UK). The effect of thermal treatment on the apparent shear viscosity was determined by temperature scanning from 25 to 60 and then to 25 °C at a scan rate of 1 °C/min^{-1}. A constant shearing rate (10 s^{-1}) and test time (1 min) was used for all measurements.

3.3.2.2.7 Simulated Oral Conditions

Simulated saliva fluid (SSF), containing mucin and various salts, was prepared as described in an earlier study [162]. A 5 mL-aliquot of the filled hydrogel particle solution was mixed with 5 mL of SSF, so that the final mixture contained 0.5% (w/w) oil. The resulting mixture was then adjusted to pH 6.8 and incubated at 37 °C for 10 min with continuous agitation (100 rpm). This time is longer than the time a food would typically spend in the mouth, but was used to ensure consistent measurements between samples. The particle size distribution and microstructure were then measured immediately after incubation under these conditions.

3.3.2.2.8 Microstructure analysis

The microstructure of the samples was examined using confocal scanning fluorescent laser microscopy with a 60 × objective lens and 10 × eyepiece (Nikon D-

Eclipse C1 80i, Nikon, Melville, NY, U.S.). A small aliquot of sample was placed on a microscope slide and covered with a glass cover slip prior to analysis. Samples were stained with a fluorescent dye prior to particle formation. The oil phase in the filled hydrogel particles was dyed with Nile red by adding 0.1 mL of Nile red solution (1 mg/mL ethanol) to 2 mL of oil, covering, and stirring overnight. The dyed oil was then used to form an emulsion as described in Section 2.2.1. The sodium caseinate phase was dyed with fast green (0.4% w/v in deionised water) after one night cold storage at 5 °C. The excitation and emission spectrum for Nile red were 543 nm and 605 nm, respectively while for fast green they were 488 nm and 515 nm, respectively. The microstructure images were acquired and then analyzed using image analysis software (NIS-Elements, Nikon, Melville, NY).

3.3.2.2.9 Statistical analysis

All experiments were carried out in triplicate using freshly prepared samples. Means and standard deviations were calculated from a minimum of three measurements using SPSS (IBM, USA). Means were subjected to Duncan's test and a *P*-value of <0.05 was considered statistically significant.

3.3.3 Results and discussion

3.3.3.1 Electrical characteristics of single and mixed biopolymer solutions

The hydrogel particles used in this study were assembled by electrostatic complexation of gelatin and caseinate. Knowledge of the electrical characteristics of these biopolymers is therefore useful for the rational design and fabrication of the filled

hydrogel particles. For this reason we measured the pH dependence of the ζ-potential of the two biopolymers and their mixture using electrophoresis (**Figure 3.12**).

The charge on the solution containing individual gelatin molecules went from negative at pH 10.0 (≈ -5 mV) to positive at pH 5.0 (≈ +4 mV), with a point of zero charge around pH 6. This value was appreciably different from the isoelectric point of gelatin reported by the manufacturer (around pI ≈ 8-9), which we attributed to some binding of ions in the buffer solution to charged groups on the gelatin molecules. We therefore measured the pH dependence of the ζ-potential for gelatin dissolved in distilled water. The results indicated that the zero point charge of gelatin in water was indeed around pH 8 (data not shown). One possible explanation for this difference is that phosphate anions (PO_4^-) from the buffer solution adsorbed to cationic groups on the gelatin molecule, thereby altering its net charge characteristics. For the solution containing only caseinate, the charge was negative (-22 to -36 mV) over the entire pH range (pH 5 to 10), which can be attributed to the fact that the caseinate molecules were always above their isoelectric point (pI = 4.6). We also measured the ζ-potential of a biopolymer mixture (1:2 w/w caseinate:gelatin), since this biopolymer ratio was used to prepare the hydrogel particles (discussed later). The charge on the mixed system was between those of the individual caseinate and gelatin values, which suggested that the two biopolymers formed a complex over the entire pH range studied. It is likely that cationic groups on the gelatin molecules bound to anionic groups on the caseinate molecules (and vice versa).

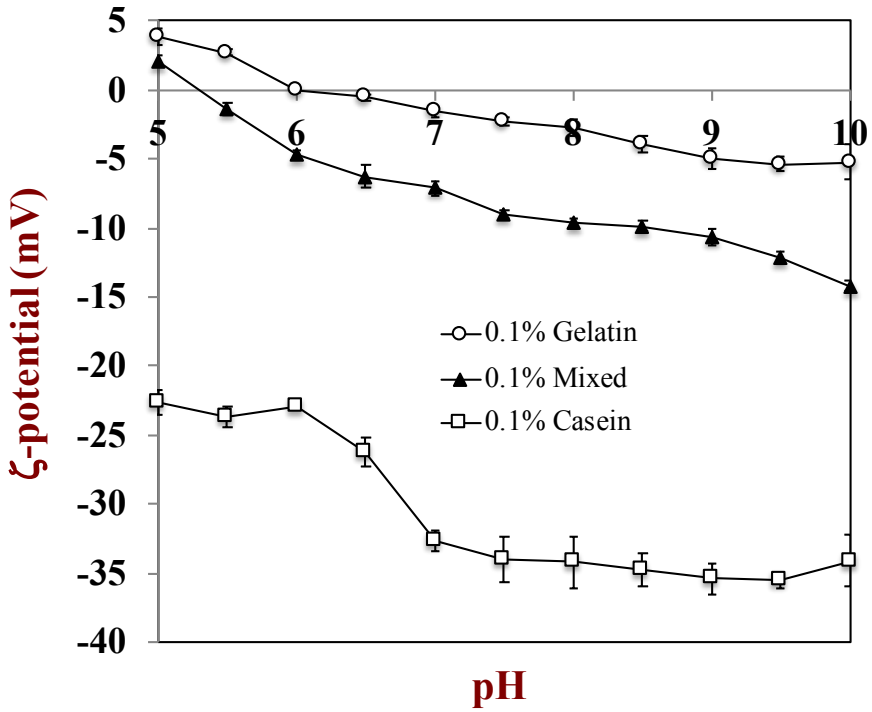

Figure 3. 12 The pH-dependence of the ζ-potential of 0.1 wt% caseinate, 0.1 wt% gelatin, 0.1% mixed biopolymers (0.033 wt% caseinate + 0.067 wt% gelatin) in 10 mM phosphate buffer and 0.1 wt% gelatin in water.

Though the net charge point of the mixture was shown around pH 5.4. In mixed biopolymer systems, it is difficult to precisely determine the electrical characteristics of the complexes themselves as the net particle charge determined by the electrophoresis instrument may be a result of the signal from individual biopolymer molecules as well as from the complexes. Turbidity measurements were therefore used to provide further information about the influence of pH on electrostatic complex formation.

3.3.3.2 Influence of pH on complex formation

The turbidity of a solution depends on the size and concentration of the complexes it contains [194]. Turbidity measurements therefore present a simple but powerful tool for monitoring the electrostatic complexation of biopolymers. Typically,

soluble complexes are formed when the electrostatic interactions are fairly weak and the net charge is relatively high, whereas coacervates are formed when the electrostatic interactions are stronger and the net charge is low [191, 195-196]. Turbidimetric titrations were therefore performed to obtain qualitative information about the interaction of the sodium casein and gelatin.

Transparent and homogeneous mixtures were obtained when the two biopolymers were mixed above pH 8, which suggests that no electrostatic complexes large enough to scatter light were formed (**Figure 3.13**). The electrophoresis measurements indicated that both biopolymers had negative charges in this pH range (**Figure 3.12**), which would have inhibited the formation of large hydrogel particles due to electrostatic repulsion. The first small increase in turbidity in the biopolymer mixtures was considered to be the critical pH (pH_c) where primary soluble complexes were formed, which was around pH 9 (**Figure 3.13**). This pH value is slightly above the reported isoelectric point of this type of gelatin. Consequently, the electrostatic complexes may have formed due to the binding of negative groups on the caseinate molecules to positive patches on the gelatin surfaces. A sharp rise in turbidity was detected when the pH was decreased below about 6, which is often designated as the critical coacervation pH *i.e.,* pH_ϕ [197]. There was a maximum in the turbidity around pH 4.8, after which the turbidity decreased steeply with further acidification. This decrease in turbidity is probably a result of dissociation of the electrostatic complexes. Below the isoelectric point of caseinate (pI ≈ 4.6), both proteins will have a net positive charge, and therefore there will be an electrostatic repulsion between them.

Based on these results, we used a pH of 5.8 to prepare the particles, since this led to the formation of electrostatic complexes that still had an appreciable negative charge (**Figure 3.12**), and were therefore more stable to aggregation and phase separation.

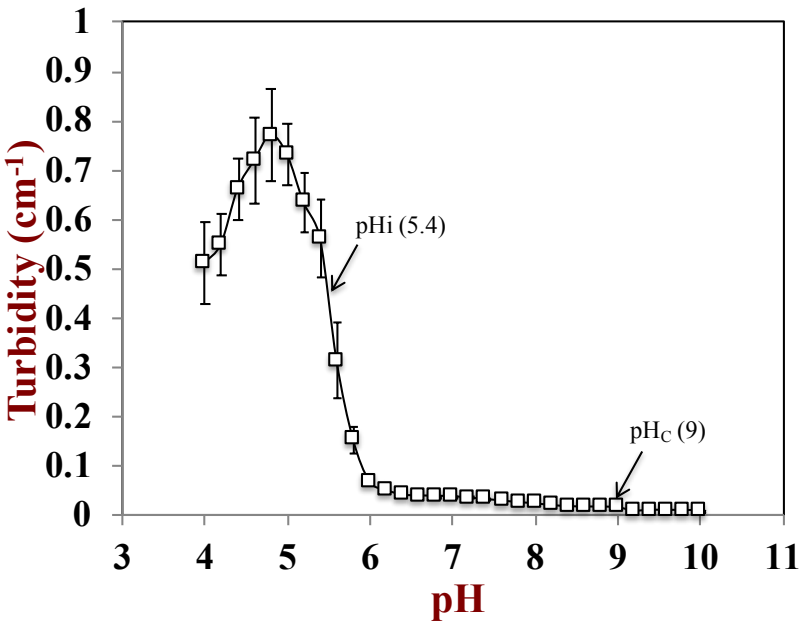

Figure 3. 13 The pH-dependence of the turbidity (600 nm) of mixed biopolymer solutions containing 0.333 % caseinate and 0.667% gelatin (biopolymer ratio = 1:2).

3.3.3.3 Influence of temperature on complex properties

Gelatin solutions undergo a sol-to-gel transition during heating due to changes in the molecular conformation of the gelatin molecules, *i.e.,* a helix-to-coil transition [198]. Hydrogel particles based on electrostatic complexation were fabricated by mixing a 1% sodium casein solution and a 1% gelatin solution at a volume ratio of 1:2 at pH 5.8 (final composition = 0.33% sodium casein and 0.67% gelatin). A range of different biopolymers ratios were tested in preliminary studies, and this ratio gave the most stable complex particles and was therefore used to prepare the hydrogel particles. The effect of

temperature scanning on the stability of the hydrogel complexes was determined by measuring their turbidity during heating from 25 to 60 °C, and then cooling back to 25 ºC (**Figure 3.14**). The initial turbidities of the caseinate-gelatin complex solutions at pH 5.8 and ambient temperature were high (around 0.82 cm^{-1}), which meant that hydrogel particles were relatively stable under these conditions. The turbidity of the hydrogel particles remained relatively constant from 25 to 31 °C, decreased steeply from 31 to 38 °C, and then reached a fairly constant value at higher temperatures. These results suggested that the structure of caseinate-gelatin complexes were appreciably altered by heating, which may be important for the development of temperature-triggered delivery systems. The dissolution of the caseinate-gelatin complexes appeared to be closely associated with the melting characteristics of the gelatin molecules. Indeed, previous researchers have reported that the gel-melting temperature of gelatin is just below body temperature, *i.e.,* < 35 °C [198].

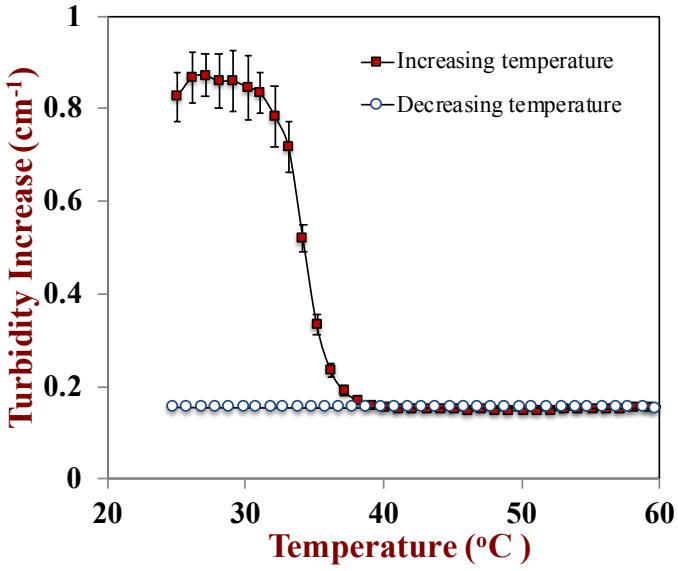

Figure 3. 14 Influence of temperature on turbidity of hydrogel particles (0.333% casein and 0.667% gelatin) during heating and cooling.

Heating-cooling scans were carried out to determine whether the complexes dissociation behavior was thermally reversible or irreversible. In these experiments the change in turbidity with temperature was recorded when the heated hydrogel particles were cooled back to 25 °C. The turbidity of the biopolymer mixture remained relatively low when the samples were cooled back to their initial temperature (25 °C), which may have occurred because of thermal hysteresis *i.e.,* the gelation temperature is appreciably lower than the melting temperature [198]. Whether the gelatin molecules remained attached to the caseinate molecules after cooling is currently unknown, and would be an interesting area for future studies.

3.3.3.4 Influence of temperature on rheology of hydrogel suspensions

The shear rheology of hydrogel particle suspensions was measured as a function of temperature, *i.e.* heating from 25 to 60 °C and then cooled to 25 °C (**Figure 3.15**). There was a slight decrease in the apparent shear viscosity of the samples after being heated from 25 to 33 °C, followed by a step decrease from 34 °C to the end of the measurements. These results suggested that heating the gelatin-hydrogel particles above a critical temperature led to network breakdown. This critical temperature was close to the hydrogel particle dissociation temperature determined using the turbidity measurements (**Figure 3.14**), and this phenomenon may again be due to melting of the gelatin around these temperatures. These results are in agreement with a previous study that reported that the viscosity of suspensions of chondroitin 6-sulfate and gelatin decreased with increasing temperature [199].

Heating-cooling scans showed that the viscosity of hydrogel particle suspensions increased slightly with decreasing temperature and did not return back to the initial value

after cooling back down to 25 °C. These results might again be attributed to the thermal hysteresis effect of gelatin mentioned earlier.

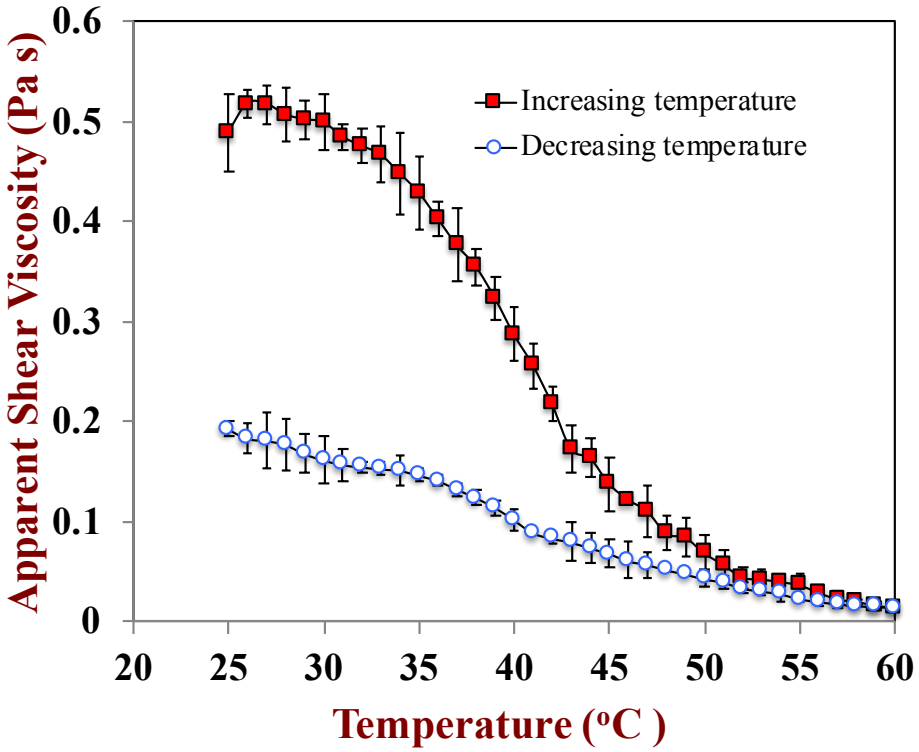

Figure 3. 15 Influence of temperature on the viscosity of hydrogel particles fabricated by mixing 3% casein and 3% gelatin solutions.

Taken together, the turbidity and viscosity results indicated that the caseinate-gelatin hydrogel particles were stable at room temperature, but dissociated above a particular temperature (close to body temperature). These hydrogel particles may therefore be suitable for developing food-grade delivery system for lipophilic bioactive agents that respond to a temperature-trigger in the oral cavity.

3.3.3.5 Influence of simulated oral conditions on lipid droplet release

For many applications it is desirable to have delivery systems that will remain intact within food products, but then release the encapsulated active agents in the mouth after ingestion. The melt-in-the-mouth behavior of gelatin hydrogels make them particularly suitable for this type of application [34]. We therefore fabricated gelatin-based hydrogel particles containing encapsulated lipid droplets, and then exposed them to simulated oral conditions (SSF, pH 6.8, 37 ºC). The particle size distribution and microstructure of the filled hydrogel particles before and after being exposure to simulated oral conditions was determined by static light scattering and confocal microscopy (**Figures 3.16 and 3.17**). In particular, fast green was used to stain caseinate so that they appeared green in the confocal images, while the gelatin remained black. In addition, the particle size distribution and microstructure of the lipid droplets in the initial emulsion were also measured as a control (**Figures 3.16 and 3.17**).

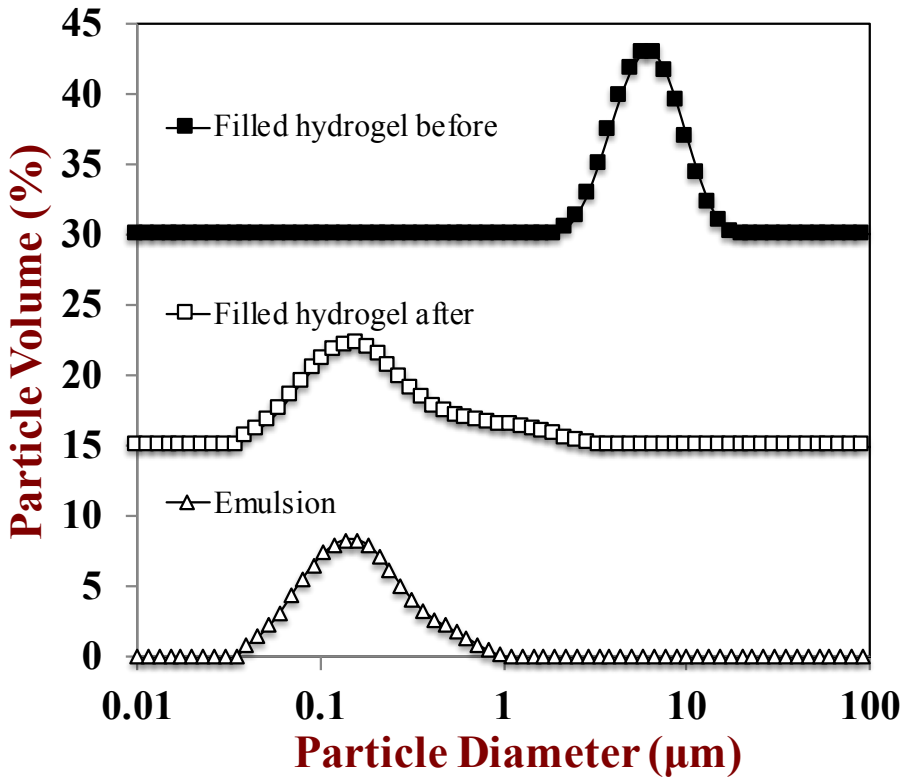

Figure 3. 16 Particle size distribution of filled hydrogel particles before and after mouth processing.

After the filled hydrogel particles were passed through the simulated mouth phase the particle size distribution became fairly similar to that of the initial emulsion, which suggests that the lipid droplets had been released from the dissociated hydrogel particles, but the emulsion remained stabilized by sodium caseinate. Control experiments were carried out keeping all conditions the same, except that room temperature was used rather than 37 ºC. The particle size distribution and microstructure results indicated that the lipid droplets remained within the hydrogel particles after exposing to the oral conditions at this lower temperature. These results suggested that the temperature change in the mouth was the major factor promoting hydrogel dissociation and the release of the lipid droplets.

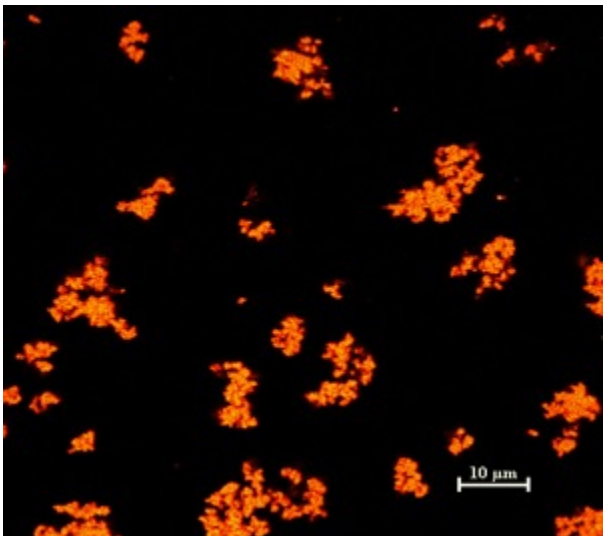

(a)

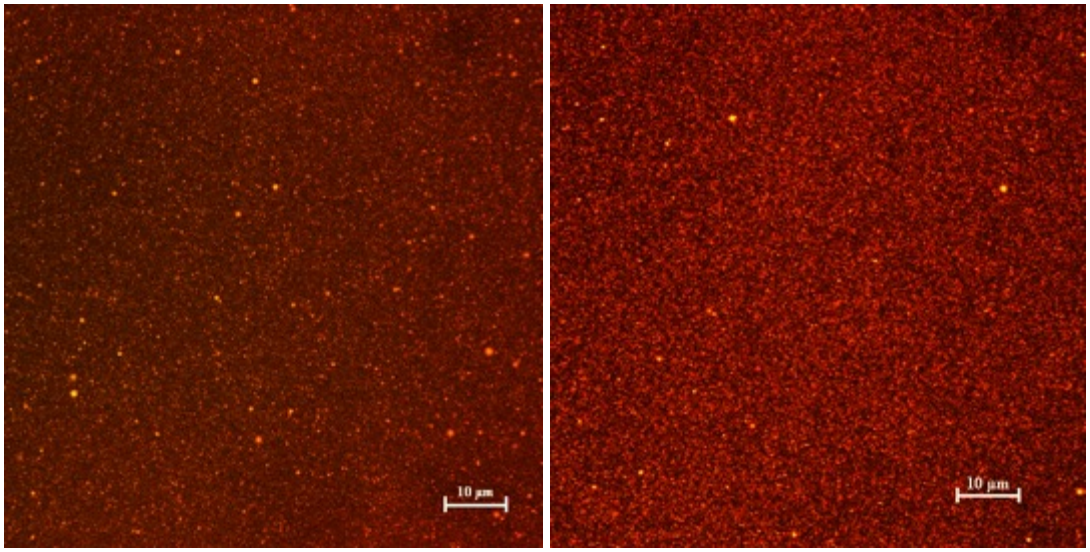

(b) (c)

Figure 3. 17 Confocal micrographs of (a) filled hydrogel particles before digestion and (b) after mouth processing and (c) oil emulsion. The oil phase (red) was stained with Nile red while the protein phase (green) was stained with fast green.

3.3.4 Conclusions

The objective of this study was to develop delivery systems for lipophilic bioactive agents based on electrostatic complexation of biopolymers that would release the bioactive agents due to a temperature-trigger under oral conditions. Gelatin and caseinate were used to fabricate the hydrogel particles. Relatively stable filled hydrogel

particles were formed at pH 5.8 with the majority of the lipid droplets being trapped inside the hydrogel phase. Optical and rheological measurements indicated that the structure of the hydrogel particles was disrupted when they were heated above a critical temperature (around body temperature), which was attributed to the melting properties of gelatin. After simulated oral processing, the lipid droplets were shown to be released from the hydrogel particles and dispersed into the surrounding continuous phase. The temperature change in the mouth was identified as the main trigger mechanism for hydrogel dissolution. These results have important implications for the development of food-grade delivery systems that may protect encapsulated lipophilic active agents in food products, but release them in the mouth.

CHAPTER 4

ENCAPSULATION, PROTECTION, AND RELEASE OF BIOACTIVE AGENTS USING HYDROGEL BEADS

4.1 Encapsulation of curcumin in polysaccharide-based hydrogel beads: Impact of bead type on lipid digestion and curcumin bioaccessibility

4.1.1 Introduction

Turmeric is a commonly used pigment, spice, and nutraceutical in foods due to its intense yellowish color, unique flavor profile, and biological activities [200-201]. Curcumin is the major bioactive agent in turmeric, and it consists of three closely related lipophilic molecules that have a number of phenolic groups and conjugated double bonds [201-202]. The potential pharmaceutical activity of curcumin has been established for numerous diseases, including multiple myeloma, rheumatoid arthritis, cystic fibrosis, inflammatory bowel disease, and colon cancer [201-203]. Previous research suggests that the health benefits of curcumin are associated with a number of biological activities, including anti-oxidative, anti-inflammatory, anti-microbial, anti-parasitic, anti-mutagenic, and anti-tumor activities [203-205]. Another benefit of curcumin is that it has a low toxicity even when ingested at relatively high doses. Consumer demand for health-promoting foods containing fewer synthetic additives has made curcumin of particular interest as a natural nutraceutical ingredient [206].

However, there are a number of physicochemical characteristics of curcumin that currently limit its incorporation into many functional food products, such as its intense color, strong flavor, low water-solubility, and chemical instability [207]. Moreover,

curcumin is rapidly metabolized within the gastrointestinal tract (GIT), which limits its potential beneficial biological effects [206, 208]. Some of these limitations can be overcome by appropriate food product selection, *e.g.,* appearance and flavor problems can be overcome by incorporating curcumin into highly colored and spicy products. Other limitations can be overcome by encapsulating curcumin within food-grade colloidal delivery systems or by mixing it with colloidal excipient systems [209-215]. A colloidal delivery system consists of small particles (typically comprised of lipids, phospholipids, surfactants, and/or biopolymers) that contain the curcumin [134]. On the other hand, a colloidal excipient system consists of small particles that are mixed with another food containing curcumin [216]. These small particles are specifically designed to boost the bioavailability of curcumin. Colloidal delivery systems can be designed to facilitate the incorporation of curcumin into commercial food products, while both colloidal delivery and excipient systems can be designed to improve curcumin's chemical/biochemical stability and to control its fate within the GIT.

Previous studies have demonstrated the potential of improving the bioavailability of curcumin using colloidal delivery systems [217-222] or colloidal excipient systems [215-216, 223]. Emulsion-based systems are particularly useful for this purpose because their composition and structures can be designed to alter the bioaccessibility, absorption, and transformation of lipophilic bioactives [177]. In particular, the lipid phase in emulsions can be designed to rapidly digest within the small intestine and form mixed micelles capable of solubilizing and transporting lipophilic bioactives [224-225]. In addition, emulsions are already integral parts of many commercial food and beverage products [226], and so emulsion-based delivery or excipient systems can easily be incorporated into a wide

range of foods and beverages. One of the main limitations of conventional oil-in-water emulsions for this purpose is that they only have limited scope for controlling the stability and release of any encapsulated bioactive agents because the lipid droplets are only coated by a thin layer of emulsifier molecules. This limitation can be overcome by trapping the lipid droplets inside hydrogel beads ("microgels").

Hydrogel beads suitable for utilization in the food industry are usually fabricated from food-grade biopolymers, such as proteins and/or polysaccharides [227-229]. These beads can be fabricated using numerous approaches, including injection, coacervation, thermodynamic incompatibility, antisolvent precipitation, templating, and molding methods [79]. The injection-gelation method is one of the simplest and most widely used approaches for the encapsulation, protection, and delivery of food-grade bioactive components such as nutrients, nutraceuticals, and vitamins. In this method, a biopolymer solution containing the bioactive component is injected into another ''hardening'' solution under conditions that promote the gelation of the injected biopolymer. This procedure results in the formation of a hydrogel bead with the bioactive components trapped inside. The nature of the hydrogel matrix surrounding the bioactive can be designed to improve its physical and chemical stability, as well as to control its GIT fate.

In the present study, curcumin was initially solubilized within the lipid phase of an oil-in-water nanoemulsion. The curcumin-loaded lipid droplets were then used as delivery systems themselves, or they were incorporated into hydrogel beads fabricated from either carrageenan or alginate. The filled hydrogel beads were formed by mixing the lipid droplets with a polysaccharide solution (alginate or κ-carrageenan), and then injecting the resulting mixture into a solution of positively charged ions (Ca^{2+} or K^{+},

respectively). The cations act as salt bridges to promote gelation of the anionic polysaccharides molecules. Carrageenan and alginate were used to form the hydrogel beads because they are already widely utilized as food-grade ingredients. Furthermore, these two polysaccharides were used because they are expected to form hydrogel beads with different functional attributes. Alginate is a block copolymer composed of 1–4-linked residues of β-d-mannuronic acid (M) and α-l-guluronic (G) acid. Carrageenan consists of galactan monomers linked together by alternating (1 → 3)- and (1 → 4)-β-d-glycosidic bonds with a negative charge due to the presence of sulfate groups within the molecules. The hydrogel beads formed by the polysaccharides with these different structures may show different gastrointestinal fate of the encapsulated curcumin during digestion. The potential gastrointestinal fate of the different curcumin delivery systems was studied using a simulated GIT (mouth, stomach, and small intestine). In particular, the influence of the different hydrogel beads on the bioaccessibility of encapsulated curcumin was compared. The information obtained in this study may facilitate the rational design of hydrogel beads to modulate the bioavailability of encapsulated lipophilic nutraceuticals.

4.1.2 Materials and methods

4.1.2.1 Materials

Corn oil was purchased from a local supermarket and used without further purification. The following chemicals were purchased from the Sigma Chemical Company (St. Louis, MO): alginic acid (sodium salt) (Lot# 180947, viscosity of 1% alginic acid in water is 15–20 cp); curcumin (C1386-10G, purity ≥ 65%); mucin from

porcine stomach (M2378-100G); pepsin from porcine gastric mucosa (P7000-25G); lipase from porcine pancreas pancreatin (L3126-100G); porcine bile extract (B8631-100G); Tween 80 (P1754-1L); and Nile Red (N3013-100MG). Carrageenan was kindly donated by FMC Biopolymer (Viscarin SD 389, Philadelphia, PA). All chemicals used were analytical grade. Double distilled water was used to make all solutions.

4.1.2.2 Preparation of oil-in-water emulsions

Initially, an aqueous phase was prepared by mixing 1% (w/w) Tween 80 with a buffer solution (5 mM phosphate buffer saline (PBS), pH 6.5) and stirring for at least 2 h. The emulsifier solution were then stored overnighted at 4 °C to ensure complete dissolution. Excipient emulsions stabilized by Tween 80 were prepared by homogenizing 10% (w/w) corn oil with 90% (w/w) aqueous emulsifier solution using a high-speed blender for 2 min (M133/1281-0, Biospec Products, Inc., ESGC, Switzer- land). The droplet size in this coarse emulsion was reduced by passing it through a high-pressure homogenizer (Microfluidizer, M110Y, Microfluidics, Newton, MA) with a 75 μm interaction chamber (F20Y) at an operational pressure of 12,000 psi for 3 passes. The resulting excipient emulsions were stored in a refrigerator at 4 °C before use.

4.1.2.3 Preparation of curcumin-loaded emulsion

The curcumin was solubilized within the lipid phase of the emulsions using a method described previously [223]. Curcumin (9 mg) was weighed into a beaker and then excipient emulsion (10% oil, 30 mL) was added, and then held at 100 °C for 10 min. This amount of emulsion was utilized because it has the ability to completely dissolve the curcumin based on the measured equilibrium solubility of curcumin reported in corn oil

at ambient temperature ≈ 3.2 ± 0.1 mg/mL [217]. The resulting curcumin-loaded emulsion was stored in the refrigerator (4°C) prior to hydrogel bead fabrication.

4.1.2.4 Preparation of curcumin-loaded emulsion

Aqueous κ-carrageenan and alginate (2.5% w/w) solutions were prepared by dissolving powdered polysaccharide ingredients in distilled water and then stirring continuously at 60 °C for an hour, and then reducing the temperature to 35 °C. Polysaccharide solutions and curcumin-loaded emulsions were then mixed together (1:4, mass ratio**)** for 2 h with continuous stirring to form a solution that contained 8% emulsion (w/w) and 0.5 % polysaccharide (w/w). Curcumin-loaded carrageenan hydrogel beads were prepared using a syringe to drip curcumin-loaded emulsion/κ-carrageenan mixtures into 10 mL 5% potassium chloride solution with continuous stirring. Similarly, curcumin-loaded alginate hydrogel beads were formed by dripping curcumin-loaded emulsion/alginate mixtures into 5% calcium chloride solution. The hydrogel beads formed were incubated with the cations (K^+ or Ca^{2+}) for a 1 h at ambient temperature to promote cross-linking. The beads were then collected by filtration and subsequently washed with distilled water and phosphate buffer to remove any excess ions from their surfaces.

4.1.2.5 Gastrointestinal tract model

Curcumin delivery systems with the same total lipid concentration (5%) and total volume (15 mL) were prepared by diluting the original systems with buffer solution (5 mM PBS, pH 6.5). The samples were then passed through a static GIT model that simulated the mouth, stomach, and small intestine phases. This method has been described in detail in our previous study [230], and so is only briefly summarized below.

Initial System: 15 mL of the initial systems were placed into a glass beaker in an incubator shaker at a rotation speed of 100 rpm for 15 min at 37 °C for preheating (Innova Incubator Shaker, Model 4080, New Brunswick Scientific, Edison, NJ). Three different initial curcumin-loaded delivery systems were tested: (i) lipid droplets, (ii) filled alginate beads, and, (iii) carrageenan beads.

Mouth phase: 15 mL of simulated saliva fluid (SSF) containing 0.03 g/mL mucin was preheated to 37 °C and then mixed with the initial samples. After being adjusted to pH 6.8, the mixture was incubated in an incubator shaker for 10 min at 37 °C to mimic agitation in the mouth.

Stomach phase: 30 mL of the "bolus" sample resulting from the mouth phase was mixed with 30 mL of simulated gastric fluid containing 0.0032 g/mL pepsin preheated to 37 °C and then the pH was adjusted to 2.5. This mixture was incubated in the incubator shaker for 2 h at 37 °C to mimic stomach conditions.

Small intestine phase: 60 mL of "chyme" sample from the stomach phase was placed into a 150 mL glass beaker that was placed into a water bath at 37 °C and then adjusted to pH 7.00. 3 mL of simulated intestinal fluid was added to the reaction vessel, followed by 7 mL of bile salt solution with constant stirring. The pH of the reaction system was adjusted back to 7.00. 5 mL of lipase solution was then added to the sample and an automatic titration unit (Metrohm, USA Inc.) was used to monitor the pH and maintain it at pH 7.0 by titrating 0.25 mM NaOH solution into the reaction vessel for 2 h at 37 °C. The amount of free fatty acids released was calculated from the titration curves as described previously [231].

4.1.2.6 Determination of particle characterization

The particle size distribution of the samples was measured using a static light scattering device (Mastersizer 2000, Malvern Instruments Ltd., Malvern, Worcestershire, UK). Initial, mouth, and small intestine samples were diluted with phosphate buffer (5 mM, pH 7.0) and stomach samples were diluted with acidified water (pH 2.5) to avoid multiple scattering effects. The refractive index of the oil phase used in the calculations

was 1.472. The average particle sizes are reported as the surface-weighted mean diameter (d_{32}). The hydrogel beads could not be analyzed by static light scattering because they were too large and rapidly sedimented or creamed inside the measurement chamber. We therefore used image analysis software (Image J, version 1.49) to characterize the particle size distribution of the hydrogel beads based on images of the samples. The images of the beads after each digestion stage were obtained using a regular camera at the fixed height, and at least 20 samples were selected to determine the particle size characterization of the hydrogel beads.

4.1.2.7 Microstructure analysis

The microstructure of samples after passing each digestion process was studied in this section. The microstructure of the all the samples were examined using confocal scanning laser microscopy with a 60 × objective lens (Nikon D-Eclipse C1 80i, Nikon, Melville, NY, U.S.). For the confocal microscopy, each sample was dyed prior to confocal microscopy observation. The corn oil was dyed with Nile red solution (1 mg/mL ethanol) by adding 0.1 mL of Nile red dye solution to 2 mL of sample and storage at 5 °C overnight. The excitation and emission spectrum for Nile red were 543 nm and 605 nm, respectively. The microstructure images for confocal microscopy were taken and analyzed using image analysis software (NIS-Elements, Nikon, Melville, NY).

4.1.2.8 Determination of curcumin concentration, bioaccessibility, and transformation

After the samples had passed through the simulated GIT, 25 g of digesta from the small intestine phase was collected and centrifuged (18,000 rpm, Thermo Scientific,

Waltham, MA) at 25 °C for 30 min. The clear supernatant was collected and assumed to be the "micelle fraction" in which the curcumin was solubilized. Aliquots of 3 mL of micelle fraction were mixed with 3 mL of chloroform, vortexed, and centrifuged at 1,750 rpm for 10 min at ambient temperature. The bottom layer containing the solubilized curcumin was collected, while the top layer was mixed with an additional 3 mL of chloroform and the same procedure was repeated. The two collected chloroform layers were mixed together and then diluted to an appreciate concentration to be analyzed by a UV-visible spectrophotometer at 419 nm. The concentration of curcumin was calculated from the absorbance using a standard curve.

The *bioaccessibility* of curcumin (*i.e.,* the fraction in the small intestine that was solubilized in the mixed micelle phase) was calculated from this data: $B^* = 100 \times C_{Micelle}/C_{Digesta}$, where $C_{Micelle}$ and $C_{Digesta}$ are the curcumin concentrations in the micelle faction and in the total digesta collected after the small intestine phase, respectively. The *transformation* of curcumin (*i.e.,* the fraction remaining in a non-transformed state in the small intestine) was calculated: $T^* = 100 \times C_{Digesta}/C_{Initial}$, where $C_{Initial}$ is the curcumin concentration in the small intestine phase calculated based on the initial amount added, which was calculated based on the curcumin concentration in initial sample before digestion and the theoretical dilution process during the digestion. The *effective bioavailability* (*i.e.,* the fraction of ingested curcumin present in the mixed micelle phase) was also calculated: $BA = 100 \times C_{Micelle}/C_{Initial.}$ The bioaccessibility and transformation of curcumin in the filled hydrogel beads could not be calculated because it was not possible to extract all of the curcumin from the hydrogel beads, so $C_{Digesta}$ could not be measured.

4.1.2.9 Statistical analysis

All experiments were performed on at least two freshly prepared samples. The results are reported as averages and standard deviations, and the differences among

treatments were calculated based on an analysis of variance (ANOVA) and a post-hoc Duncan test with a confidence level of 95 %. These analyses were carried out using statistical analysis software (SPSS, IBM Corporation, Armonk, NY, USA).

4.1.3 Results and discussion

4.1.3.1 Preparation of the curcumin-loaded emulsions and filled hydrogel beads

In this study, three different curcumin delivery systems were prepared: lipid droplets; filled alginate beads; and filled carrageenan beads (Fig. 4.1). The filled hydrogel beads were formed by injection of a mixture of the lipid droplets and anionic biopolymer into a crosslinking cationic mineral solution. In general, several parameters may influence the physicochemical and structural properties (*e.g.,* size, shape, porosity, and hardness) of hydrogel beads fabricated by the injection method, including biopolymer concentration, cation concentration, needle diameter, injection flow rate, and hardening time. After some preliminary experiments to optimize the preparation conditions, we fabricated the hydrogel beads by injecting a 0.5 % polysaccharide solution (alginate or carrageenan) into a 5% cationic mineral solution (Ca^{2+} or K^{+}) using a syringe with a needle diameter of 0.5 mm at a rate of one drop per 2 s. After injection, the hydrogel beads were incubated in the cationic mineral solutions for an hour at ambient temperature to promote polysaccharide cross-linking. The alginate beads fabricated using this method had a spherical shape with a smooth surface, and had diameters ranging from about 2 to 3 mm (Fig. 4.1 and Table 4.1). Conversely, the carrageenan beads formed using the same method had an irregular shape and had rough surfaces with a larger mean particle diameter (around 3 to 4 mm). The difference in the properties of the hydrogel beads can be attributed to differences in the gelation mechanisms of the two different polysaccharides. The hydrogel matrix within the alginate beads is formed by calcium ion crosslinking of guluronic acid blocks within the alginate chains [232], whereas that in the carrageenan beads is formed by potassium ion crosslinking of sulfate groups along the carrageenan chains [233]. The fact that the alginate beads had a more spherical and smoother structure suggests that the crosslinking of the alginate molecules by calcium ions occurred more rapidly than the crosslinking of the carrageenan molecules by

potassium ions. Thus, the initial spherical shape of the polysaccharide solution injected into the cation solution was maintained more readily for the fast-gelling alginate system. This may have been because the multivalent calcium ions were more efficient at crosslinking that the monovalent potassium ions. We hypothesized that the difference in initial structure and properties of the hydrogel beads formed by the two different polysaccharides would alter their behavior within the simulated GIT, *e.g.,* their susceptibility to enzyme penetration, and their stability to mechanical forces or pH changes.

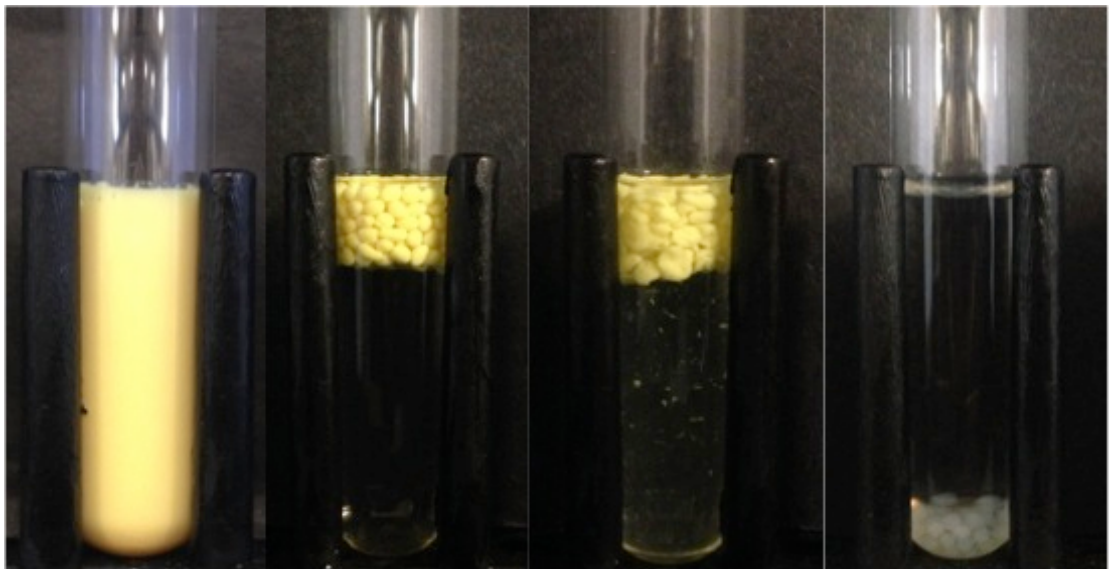

Figure 4. 1 Appearance of different curcumin-delivery systems prepared in buffer solution (5 mM PBS, pH 6.5), from left to right: lipid droplets; Filled alginate beads, and Filled carrageenan beads. Unfilled alginate beads (far right) are shown as a reference.

It is interesting to note that unfilled alginate and carrageenan beads sedimented to the bottom of the test tubes, whereas the filled beads creamed to the top (Fig. 4.1). This difference in behavior can be attributed to the influence of lipid droplets on the effective density of the hydrogel beads [173]: unfilled beads are denser than water, whereas filled beads are less dense than water. This effect occurs because lipids have a lower density than water, whereas biopolymers have a higher density. The buoyancy characteristics of filled hydrogel beads makes them good candidates for stomach targeting delivery systems as they may spend a longer time within the gastric cavity [106].

4.1.3.2 Influence of GIT conditions on particle size and microstructure

The particle size distribution (Fig. 4.2), general appearance (Fig.4.3), and microstructure (Fig. 4.4) of the curcumin-loaded lipid droplets and filled hydrogel beads were measured during passing through the simulated GIT.

Table 4. 1 The mean particle diameters of three curcumin delivery systems after each digestion stage in a simulated GIT: Lipid droplets; Filled alginate beads; and, Filled carrageenan beads.

	Mean Particle Diameter (μm)			
Sample	**Initial**	**Mouth**	**Stomach**	**Intestine**
Lipid Droplets	0.13 ± 0.01	0.14 ± 0.01	0.15 ± 0.01	0.22 ± 0.01
Filled alginate beads	2604 ± 75	2857 ± 166	2555 ± 204	1796 ± 58
Filled carrageenan beads	3107 ± 159	824 ± 640	372 ± 344	848 ± 184

Curcumin-loaded lipid droplets. The mean particle diameters (d_{32}) of the curcumin-loaded lipid droplets were fairly similar for the initial samples (0.13 μm) and the samples that had been exposed to the mouth (0.14 μm) and stomach (0.15 μm) phases (Table 4.1). In addition, the particle size distributions of the initial, mouth, and stomach samples were also fairly similar (Fig. 4.2). These results suggest that the lipid droplets were stable to coalescence in the simulated saliva and gastric fluids, which can be attributed to the fact that they were coated with a non-ionic surfactant (Tween 80) that inhibits droplet coalescence through steric repulsion. Other studies have also reported the good coalescence stability of lipid droplets coated by non-ionic surfactants under simulated mouth and stomach conditions [234-235]. Despite the fact little droplet coalescence was observed by light scattering, the confocal microscopy images indicated that there was some aggregation of the lipid droplets within the mouth and stomach phases (Fig. 4.4),

which may have been due to depletion flocculation caused by the presence of non-adsorbed mucin molecules in the simulated saliva [236]. These non-adsorbed mucin molecules generate an osmotic attraction between the lipid droplets that forces them together. These large particles were not seen in the particle size distributions because the samples had to be diluted for the light scattering measurements, which would have caused dissociation of any flocs held together by depletion forces. After passing through the small intestine phase, the particle size distribution of the samples initially containing curcumin-loaded lipid droplets became bimodal (Fig. 4.2a). This suggests that there was a wide range of different-sized colloidal particles present in the digesta after exposure to small intestinal fluids containing lipase and bile salts. These colloidal particles may have been mixed micelles (micelles and vesicles), undigested lipid droplets, and/or insoluble calcium salts.

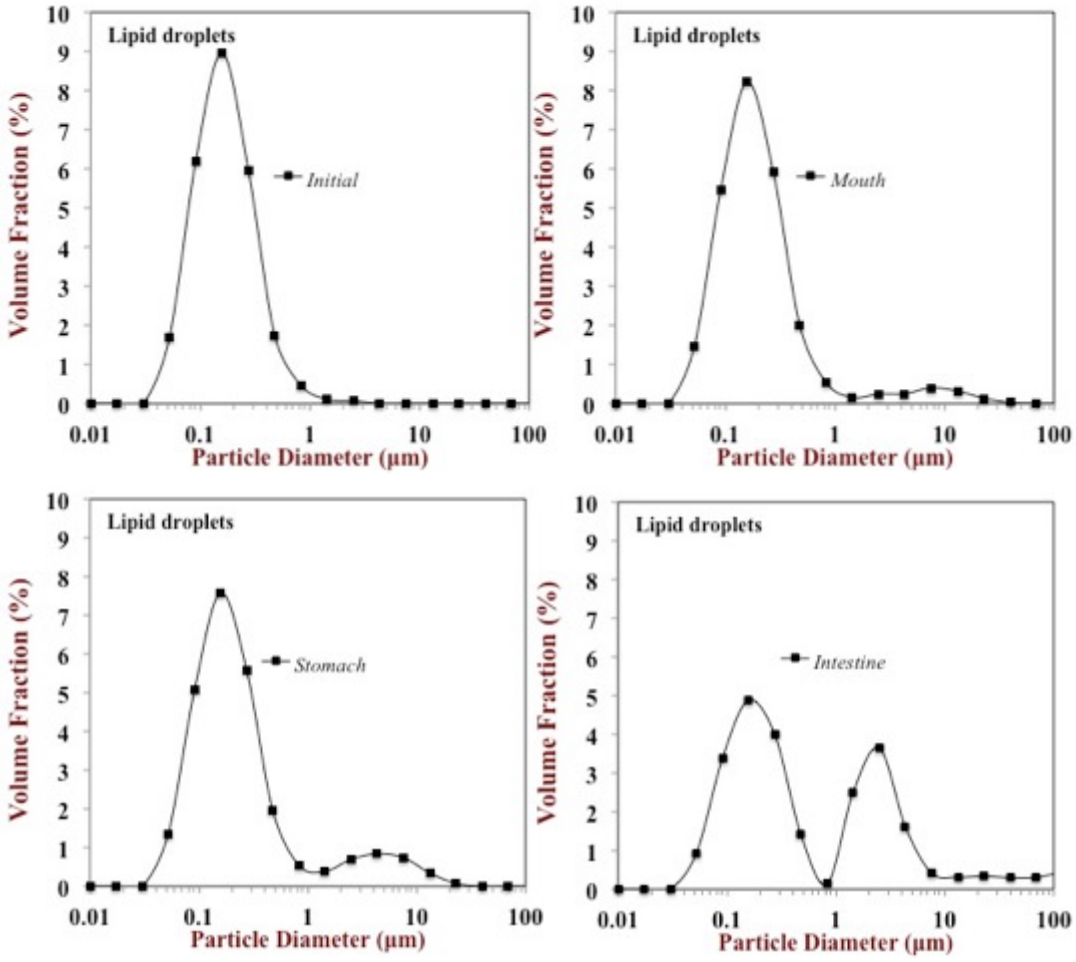

(a)

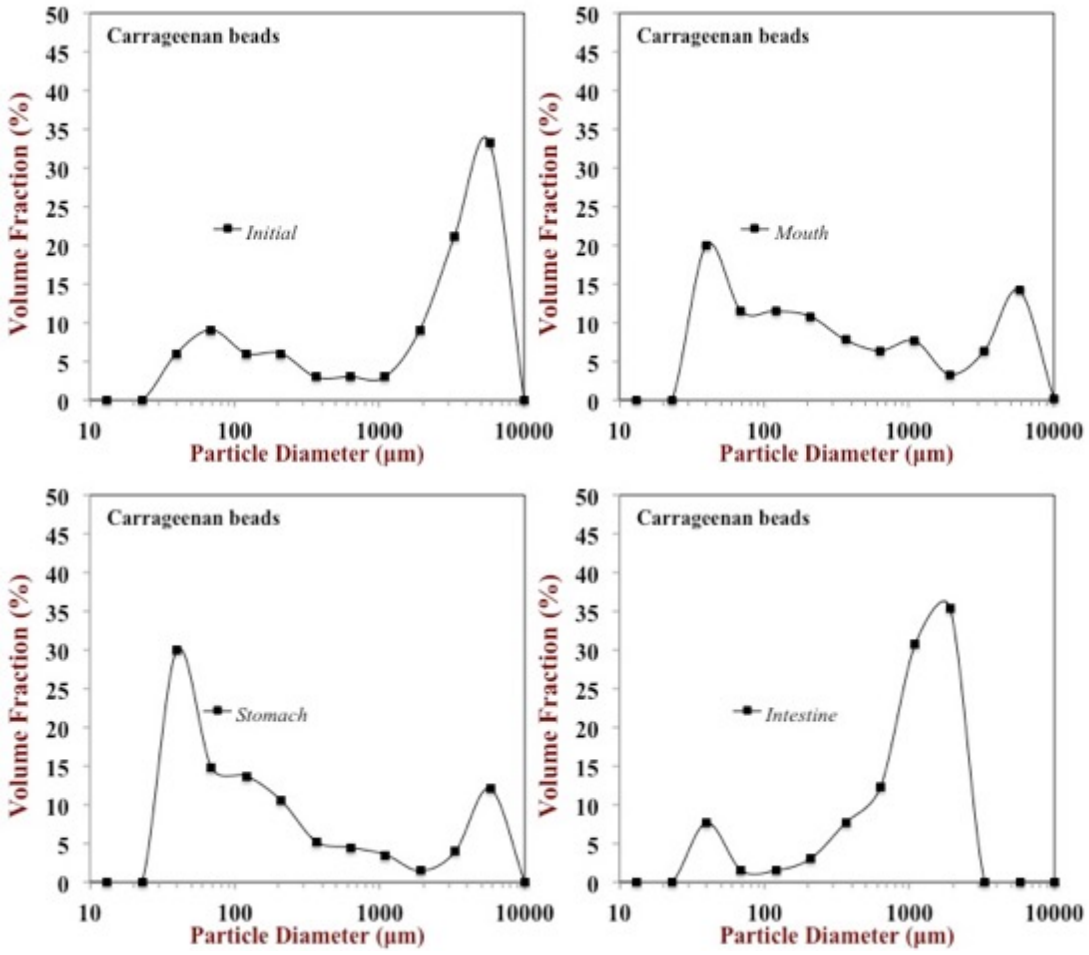
Carrageenan beads
Initial
Mouth
Stomach
Intestine
Volume Fraction (%)
Particle Diameter (µm)
0
5
10
15
20
25
30
35
40
45
50
10
100
1000
10000

(b)

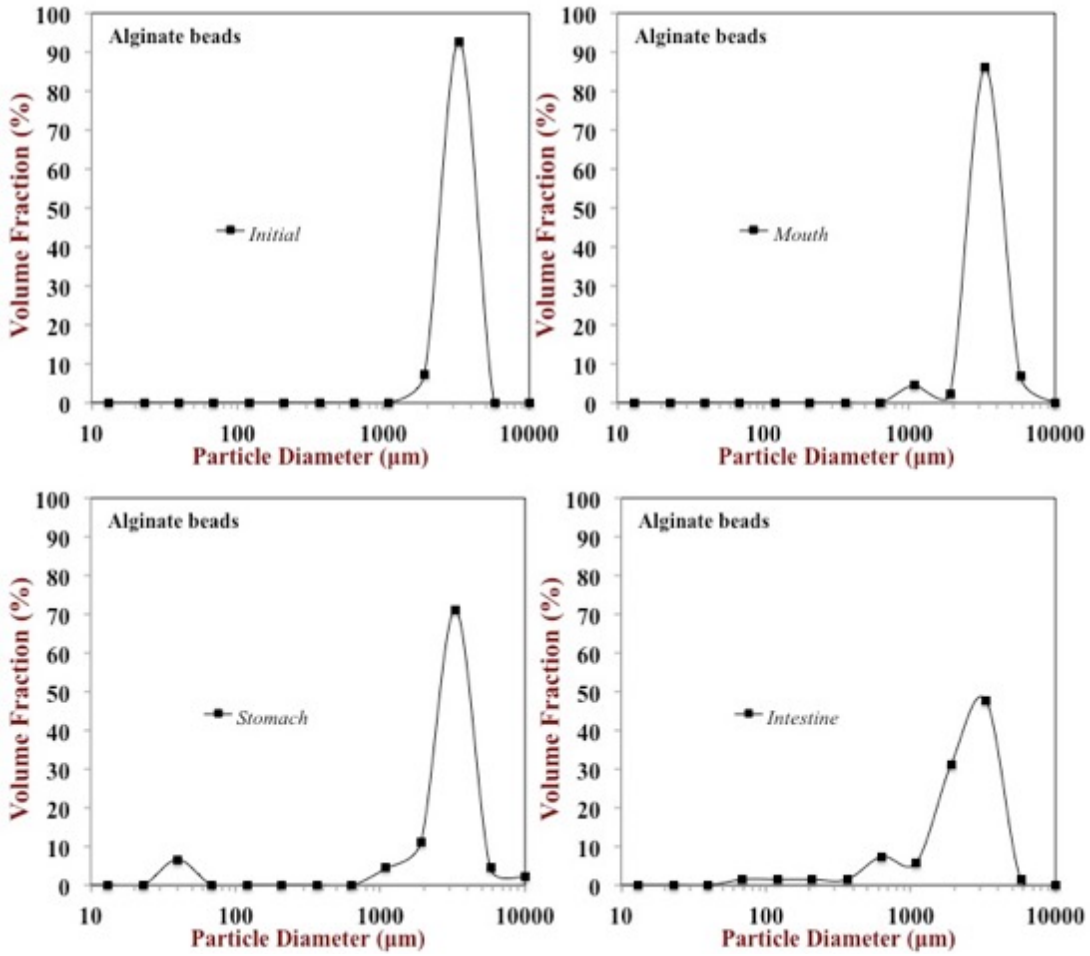

(c)

Figure 4. 2 Particle size distribution of different samples: (a) Lipid droplets, (b) Filled carrageenan beads, and (c) Filled alginate beads after each digestion stage.

Filled hydrogel beads. The particle size and microstructure of the filled hydrogel beads in the different regions of the GIT depended on the type of polysaccharide used (Figs. 4.2 to 4.4). For the alginate beads, the general shape of the particle size distribution remained fairly similar from initial-to-mouth-to-stomach, exhibiting a major population of large particles with diameters around 2,500 μm (Table 4.1, Fig. 4.2c). In addition, observation of the general appearance of the alginate beads indicated that they remained intact after exposure to the different GIT phases (Fig. 4.3). There was an appreciable decrease in the mean particle diameter of the alginate beads when they were moved from the simulated stomach to small intestine (Table 4.1). Previous studies have also reported that calcium alginate beads shrink under highly acidic gastric conditions [76, 237], which can

be attributed to a reduction in the electrostatic repulsion between the alginate molecules below the pK_a value of the carboxyl groups. The closer packing of the biopolymer molecules within the hydrogel beads under stomach conditions may be useful for protecting encapsulated components from the harsh gastric environment. Interestingly, there appeared to be an increase in the turbidity of the aqueous solution surrounding the hydrogel beads in the small intestine (Fig. 4.3b), which suggests that there were colloidal particles present large enough to scatter light. These particles may have been undigested lipid droplets or mixed micelles released from the hydrogel beads. Indeed, confocal microscopy images of the aqueous phase collected from outside of the hydrogel beads indicated that they contained some lipid-rich particles (data not shown).

4.1.3.3 Influence of delivery system type on lipid digestion

An automatic titration (pH stat) method was used to evaluate the effect of delivery system type on the rate and extent of lipid digestion. The fraction of free fatty acids (FFAs) released from the samples during the small intestine phase was calculated from measurements of the volume of NaOH that had to be titrated into the reaction chamber to maintain a constant pH (7.0). The nature of the delivery system clearly had a pronounced impact on the rate and extent of lipid digestion (Fig. 4.5). The free lipid droplets were rapidly digested during the first 10 minutes with over 60% of the FFAs being released, followed by a more gradual digestion for the remainder of the incubation time. Conversely, the rate of FFAs released was much slower for the filled hydrogel beads, and depended on polysaccharide type. For the filled alginate beads, no lipid digestion occurred during the first 30 minutes, then there was a relatively slow rate of lipid digestion at longer times, with only 33% of the FFAs being released by the end of the 2 hour digestion period. For the filled carrageenan beads, lipid digestion started immediately and occurred throughout the incubation period, but it was relatively slow compared to the free lipid droplets, with only 46% of FFAs released by the end of the small intestine phase. These results indicate that encapsulation of the lipid droplets within the hydrogel beads retarded lipid digestion, with the degree of lipase inhibition depending on hydrogel type. Similar results have been reported in earlier studies of lipid digestion in hydrogel beads [76].

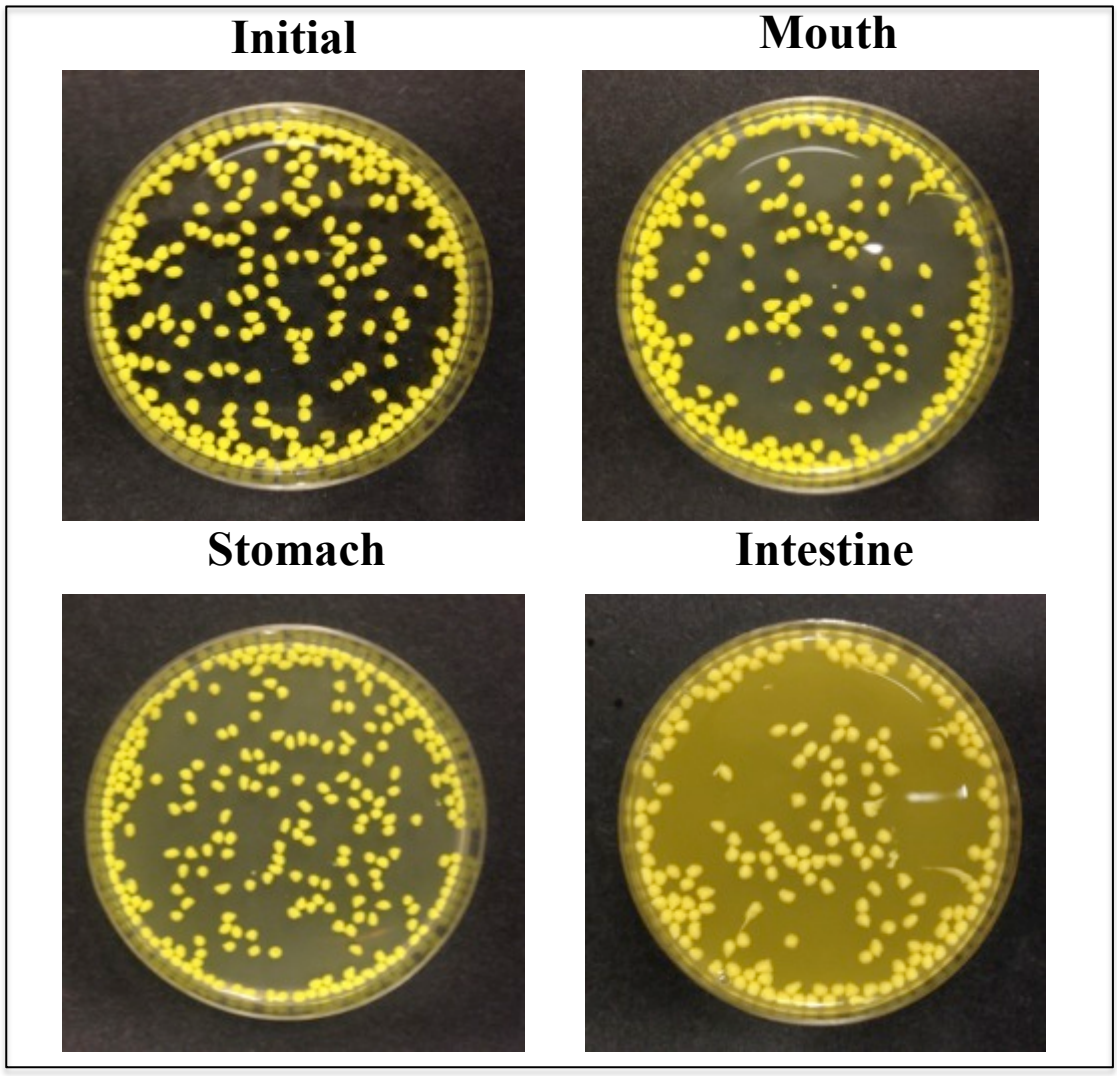

(a)

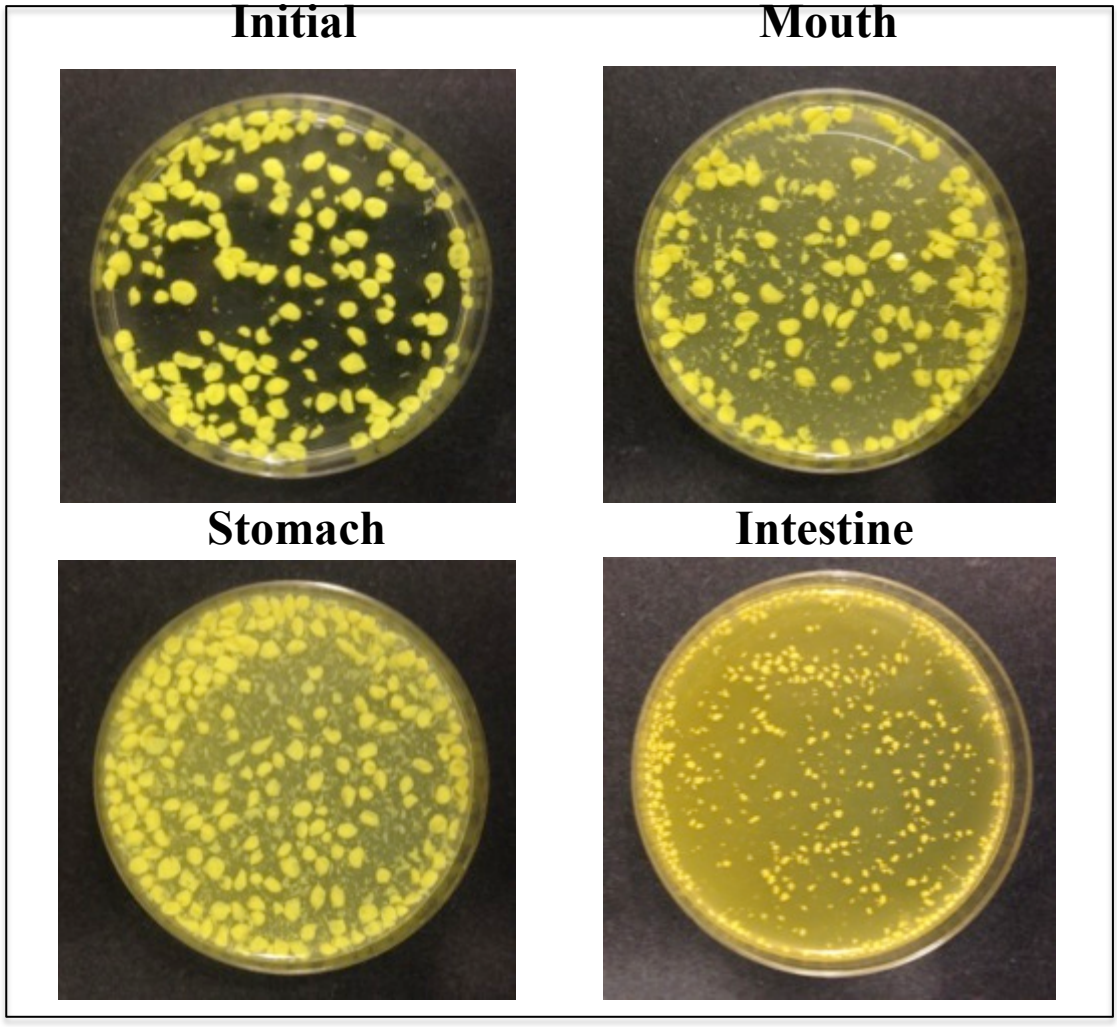

(b)

Figure 4. 3 Images of different curcumin-loaded beads after each digestion stage: (a) Filled alginate beads, and (b) Filled carrageenan beads.

There are a number of reasons that encapsulation may have inhibited lipid digestion. Firstly, lipid digestion can only occur if pancreatic lipase is able to adsorb to the surfaces of the lipid droplets and come into close proximity with its substrate, *i.e.,* triacylglycerol and diacylglycerol molecules [238]. For the free lipid droplets, the pancreatic lipase is able to rapidly move from the aqueous phase to the lipid droplet surfaces and initiate lipolysis. For the filled hydrogel beads, lipase and the other GIT components required for digestion (such as co-lipase and calcium) have to penetrate into the beads and diffuse through the hydrogel matrix before they can reach the lipid droplet surfaces. In particular, these components must diffuse through the network of cross-linked biopolymer molecules that

makes up the interior of the hydrogel beads [76]. The time taken for lipase molecules to reach the lipid droplets within the interior of the beads increases as the pore size of the hydrogel matrix decreases, the diameter of the beads increases, or the surface area of the beads decreases [76, 239]. The lag time observed before any lipid digestion occurred for the alginate beads may have been because the hydrogel matrix shrank under gastric conditions thereby decreasing the bead pore size and inhibiting penetration of lipase. However, the pore size expanded once the beads were placed into the small intestinal fluids, thereby allowing the lipase molecules to penetrate. This hypothesis is supported by the fact that the mean diameter of the alginate beads was smaller in the gastric fluids than in the intestinal fluids (Table 4.1). After the lag phase, the relatively slow rate of lipid digestion observed in the alginate beads, may have been because they were larger than the carrageenan beads. As mentioned earlier, the alginate beads maintained their general structure throughout the GIT, whereas the carrageenan beads were largely disrupted by the small intestine phase. The slow rate of digestion for the alginate beads may also have been because they had a smaller pore size than the carrageenan beads, which would inhibit lipase diffusion. A second potential reason for retarded lipid digestion in the filled hydrogel beads is that the long chain FFAs generated at the surfaces of the lipid droplets have to be removed otherwise the lipolysis reaction will be retarded [240-241]. Typically, FFAs are removed from the droplet surfaces by being incorporated into mixed micelles with bile salts and phospholipids, or by forming insoluble salts with calcium ions [242]. The removal of FFAs away from the lipid droplet surfaces may therefore be limited because bile salts, phospholipids, and calcium cannot easily penetrate through the cross-linked biopolymer network inside the hydrogel beads. In addition, the diffusion of the FFAs themselves out of the hydrogel beads may also be inhibited by the presence of the biopolymer network. These results clearly show that encapsulating lipid droplets in hydrogel beads can modulate the rate and extent of their digestion.

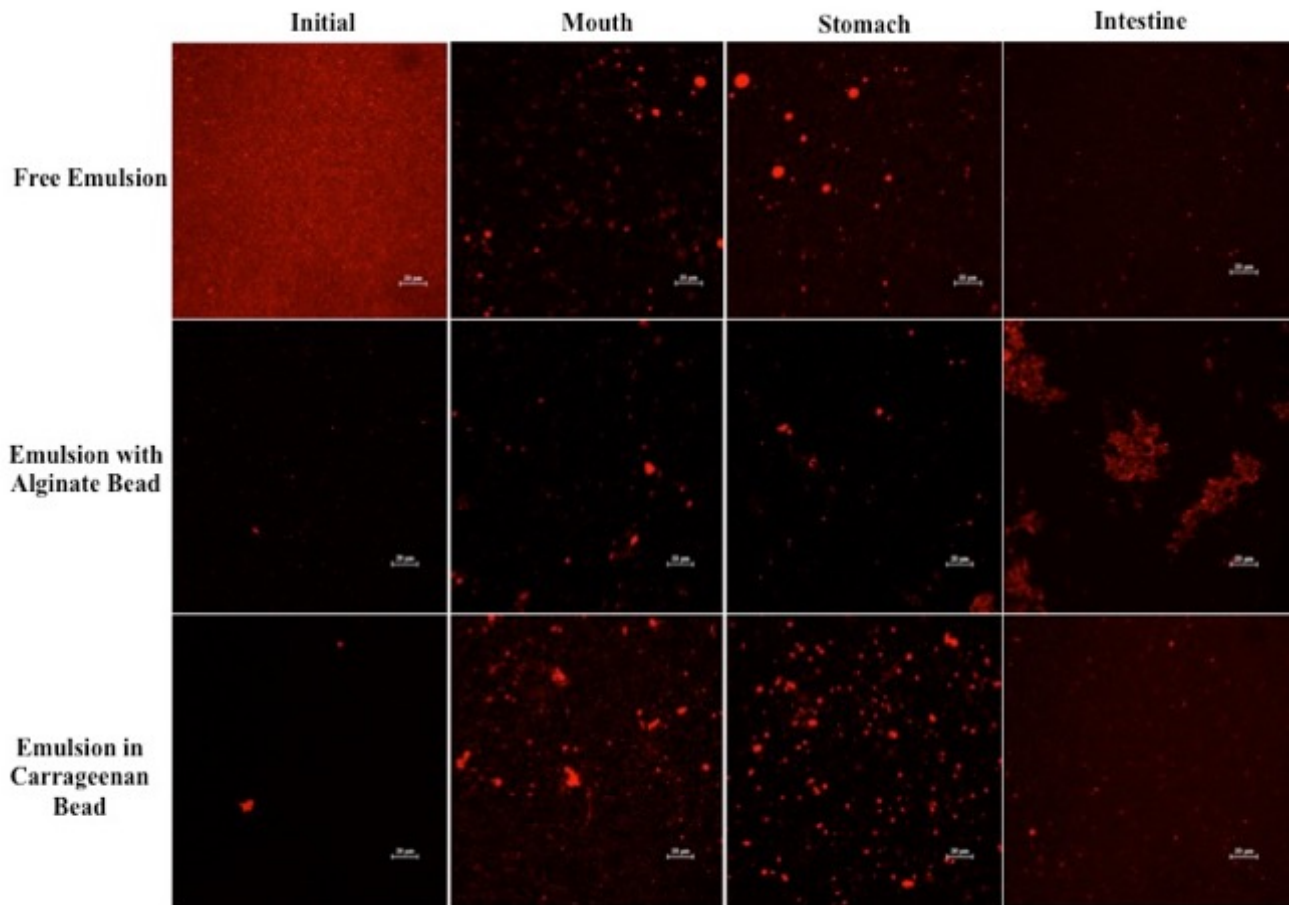

Figure 4. 4 Microstructures of three samples including free emulsion, emulsion in alginate beads and emulsion in carrageenan beads exposed to different regions of a simulated GIT. Scale bar is 20 μm.

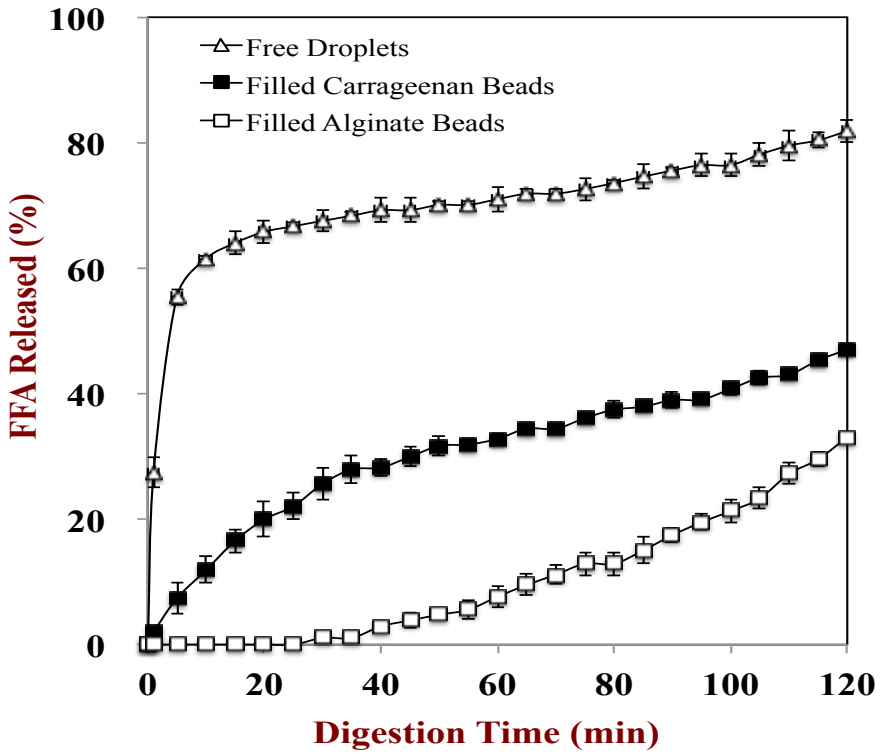

Figure 4. 5 Amount of fatty acids released from three samples including free emulsion, emulsion in alginate beads and emulsion in carrageenan beads measured in a pH-stat *in vitro* digestion model.

4.1.3.4 Influence of delivery system type on curcumin release

The amount of curcumin released into the mixed micelle phase clearly depended on the nature of the delivery system used to encapsulate it: free droplets > filled carrageenan beads > filled alginate beads (Fig. 4.6). For the free oil droplets, it was possible to calculate the bioaccessibility (73%), transformation (78%), and effective bioavailability (57%) from the initial, digesta, and micelle curcumin concentrations (Section 2.7). The effective bioavailability of the curcumin in the filled alginate beads (12%) and carrageenan beads (15%) was also determined. Pure curcumin typically has a very low bioavailability because of its poor chemical stability and low solubility in gastrointestinal fluids [202, 206]. Our results suggest that encapsulation of curcumin within free lipid droplets led to a relatively high effective bioaccessibility. This enhanced bioavailability can be attributed to two main physicochemical factors. First, when curcumin is present within the interior of the lipid droplets it is protected from chemical degradation induced by

aqueous phase components, which leads to a relatively high amount remaining in an active form in the small intestine (high T*). Second, the digestion of the lipid droplets leads to the formation of mixed micelles that can solubilize the hydrophobic curcumin molecules (high B*). Previous studies in our laboratory have also reported that nanoemulsions can increase curcumin bioaccessibility and transformation through these mechanisms when used as either delivery systems [217] or excipient systems [216, 223].

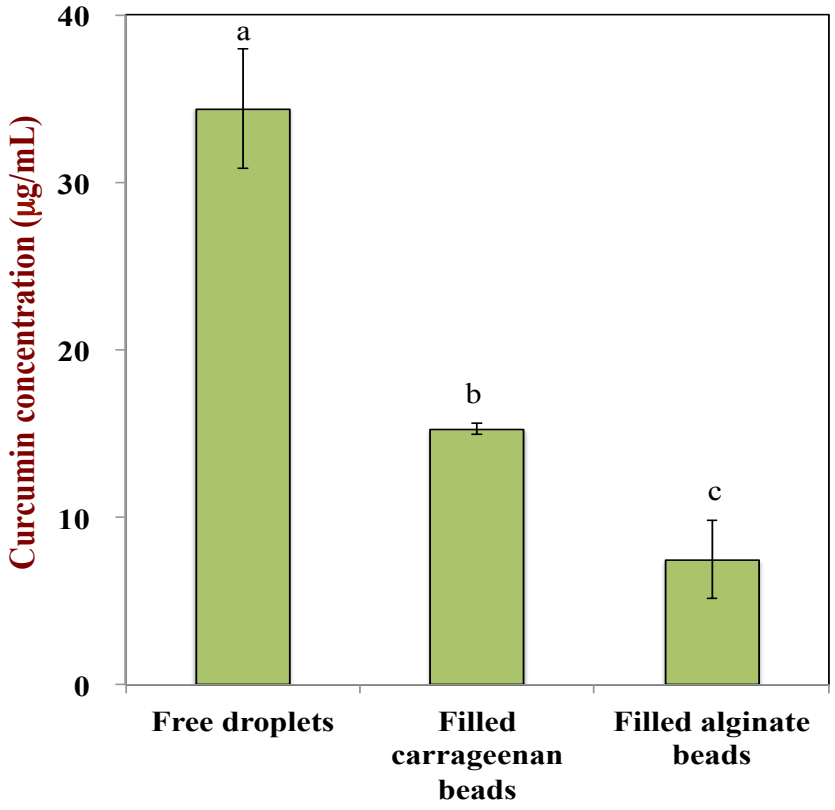

Figure 4. 6 Bioaccessibility (%) of curcumin in three samples including lipid droplets, filled alginate beads, and filled carrageenan beads after *in vitro* digestion.

The relatively low effective bioavailability of the curcumin in the filled hydrogel beads can largely be attributed to the fact that not all of the lipid phase was digested for these systems. Consequently, some of the curcumin remained within the undigested lipid droplets trapped inside the hydrogel beads and was therefore not released. In addition, there will have been less mixed micelles available in the aqueous phase to solubilize any curcumin molecules released: (i) because of the relatively low extent of lipid digestion; and, (ii) because the diffusion of any FFAs and monoacylglycerols formed within the

beads may have been hindered by the hydrogel matrix. There appeared to be a good correlation between the extent of lipid digestion at the end of the small intestine phase and curcumin release, *i.e.,* they followed the same trend: free droplets > filled carrageenan beads > filled alginate beads.

Overall, these results have a number of important practical implications. First, it is important to ensure that any hydrogel beads used to encapsulate and protect curcumin within food products do not inhibit its release within the GIT. Otherwise, any potential health benefits associated with consuming curcumin may not be fully realized. Second, it may be possible to control the release of curcumin in different regions of the GIT by encapsulating it within hydrogel beads. For example, if it was important to release curcumin in the colon then it could be encapsulated within hydrogel beads that retained it in the mouth, stomach, and small intestine, but released it in the colon. Alternatively, if one wanted to mask the taste of curcumin, but still ensure that it was absorbed in the upper intestine, it could be incorporated into hydrogel beads that retained it in the mouth, but released it in the stomach or small intestine.

4.1.4 Conclusions

In the present study a simulated GIT was used to study the influence of different types of delivery systems on lipid digestion and curcumin release: free lipid droplets; filled carrageenan beads; and, filled alginate beads. In all systems, the crystal form of curcumin was first dissolved in a digestible lipid phase, which was then converted into an oil-in-water nanoemulsion. In the case of the filled hydrogel beads, the curcumin-loaded lipid droplets were then trapped within a hydrogel matrix using an injection-gelation method. The alginate beads had a uniform spherical shape with diameters ranging from 2 to 3 mm, whereas the carrageenan beads had irregular shapes and diameters around 3 to 4 mm. Differences in hydrogel bead morphology were attributed to differences in the initial rate of biopolymer gelation during the injection process. Simulated GIT studies indicated that free lipid droplets were digested more rapidly and fully than those encapsulated within hydrogel beads. In addition, they showed that the rate and extent of lipid digestion in filled hydrogel beads depended on polysaccharide type, which was partly attributed to

differences in their integrity within the GIT. Alginate beads remained relatively intact throughout the GIT, while the carrageenan beads partly disintegrated. The extent of curcumin release into the mixed micelle phase in different samples followed the following order: free droplets > filled carrageenan beads > filled alginate beads. Our results have important implications for designing hydrogel beads to increase the oral bioavailability of lipophilic bioactives.

4.2 The physicochemical stability and in vitro bioaccessibility of β-carotene in alginate-based hydrogel beads

4.2.1 Introduction

Carotenoids are naturally occurring groups of pigments widely present in various fruits and vegetables to play essential roles in photosynthesis and photo-protection reactions. β-Carotene, one of the major carotenoids, is regarded as a natural carotenoid precursor of vitamin A. Because of its antioxidant and non-antioxidant activities, β-carotene have showed biological activities to reduce the risk of certain chronic diseases including cardiovascular disease, cataracts, age-related macular degeneration and cancers when ingestion of sufficient levels. Growing concern on healthy diet has encouraged many food companies to fortify their products with this bioactive ingredient. However, the pure hydrogen-carbon skeleton structure and high unsaturation degree of β-carotene greatly restrict its incorporation into many commercial foods and beverages. β-carotene has been reported to have low water-solubility, high melting point, and poor chemical instability [243-244]. Moreover, β-Carotene can be rapidly metabolized like most of lipophilic bioactive agents within the gastrointestinal tract (GIT), which limits its potential beneficial biological effects.

Colloidal delivery systems are one of the most convenient methods for incorporating lipophilic bioactive ingredients into food products. They usually consist of small particles (typically comprised of lipids, phospholipids, surfactants, and/or biopolymers) that contain the lipophilic bioactive agents. These small particles can be designed to facilitate the incorporation of bioactive agents into commercial food products, improve chemical/biochemical stability and control their fate within the GIT. A typical bioactive-loaded colloidal system can be simply prepared by solubilizing the lipophilic bioactive components within an oil phase and then homogenising it with an aqueous phase containing an emulsifier to form the oil-in-water emulsions. Previous studies have reported that emulsion-based systems were particularly suitable for encapsulation and delivery of carotenoids such as lutein [245], lycopene [246] and β-Carotene [247-248]. The bioavailability of carotenoids was greatly increased after encapsulation in emulsion-based systems [249]. One of the major limitations of conventional oil-in-water emulsions is that

they have limited scope for controlling the stability of lipophilic bioactives because the bioactives-loaded lipid droplets are coated only with a thin layer of emulsifier molecules, which hardly guarantee the encapsulated bioactives suffer from the harsh environment conditions. In particular, carotenoids have a conjugated polyunsaturated hydrocarbon chain, which makes them highly prone to degradation due to autoxidation promoted by light, heat, singlet oxygen, transition metals, free radicals and highly acidic condition [247]. This limitation can be overcome by trapping the lipid droplets inside hydrogel beads ("microgels"). Carotenoids may have a more stable environment after encapsulation in a polymer matrix, which creating a single compartment and thus protecting them from degradation.

Hydrogel beads are usually fabricated from food-grade biopolymers such as proteins and/or polysaccharides. These beads can be fabricated from numerous approaches such as injection, coacervation, thermodynamic incompatibility, antisolvent precipitation, templating, and molding methods [79]. The injection-gelation method is one of the simplest and most widely used approaches for the encapsulation, protection, and delivery of food-grade bioactive components. In this method, a biopolymer solution containing the bioactive component is injected into another ''hardening'' solution under conditions that promote the gelation of the injected biopolymer. This procedure results in the formation of a hydrogel bead with the bioactive components trapped inside. The nature of the hydrogel matrix surrounding the bioactive can be designed to improve its physical and chemical stability, as well as to control its GIT fate. In general, hydrogel beads with a particle size greater than 1.0 mm in diameter are prepared using a syringe with a needle or a pipette. Smaller size beads (less than 1 mm in diameter) could be fabricated using an extrusion device (Encapsulator). The beads with relatively small size may have several advantages over the traditional large ones on appearance, rheology and mouthfeel. The sizes of these beads can be further adjusted by several factors including the polymers and ion concentration, instrument parameters and hardening time.

In the present study, a high-pressure homogenisation method was used to prepare nanoemulsions containing β-carotene. The β-carotene-loaded lipid droplets were then used as delivery systems themselves, or they were incorporated into hydrogel beads

fabricated from alginate. The filled hydrogel beads were fabricated by mixing the lipid droplets with an alginate solution, and then injecting the resulting mixture into an ion solution (Ca^{2+}) with the extrusion device (Encapsulator). Two different alginate concentrations (0.5% and 1%) were used because they are expected to form hydrogel beads with different physical and functional attributes. The stability of β-carotene encapsulated within oil-in-water nanoemulsions and filled hydrogel beads was studied during the storage. In particular, the influence of the different delivery systems (nanoemulsion and filled hydrogel beads) encapsulation on the bioaccessibility of encapsulated β-carotene was compared using a gastrointestinal (GI) model that simulates the mouth, stomach and small intestine. The information obtained from this study should be useful for the development of bead-based functional food products fortified with lipophilic bioactive ingredients that may improve human health and wellness.

4.2.2 Materials and methods

4.2.2.1 Materials

Whey protein isolate (WPI) was kindly provided by Davisco Foods International Inc. (Le Sueur MN). The WPI was reported to contain 97.9 wt.% protein, 0.2 wt.% fat. Corn oil was purchased from a local supermarket and used without further purification. The following chemicals were purchased from the Sigma Chemical Company (St. Louis, MO): β-carotene; alginic acid (sodium salt); mucin from porcine stomach; pepsin from porcine gastric mucosa; lipase from porcine pancreas pancreatin; porcine bile extract; and Nile Red. All chemicals used were analytical grade. Double distilled water was used to make all solutions.

4.2.2.2 Preparation of β-carotene-loaded emulsions

Initially, an aqueous phase was prepared by mixing 1% (w/w) WPI with a buffer solution (5 mM phosphate buffer saline (PBS), pH 7) and stirring for at least 2 h. The emulsifier solution was stored overnighted at 4 °C and filtered before use to ensure the complete dissolution of any large particles. The β-carotene-loaded lipid droplets were prepared by dispersing β-carotene (0.1%, w/w) in corn oil by heating (55°C, 10 min) and

then ultrasonic processing (2min). This procedure was repeated several times to ensure the complete dissolution of β-carotene in the oil phase. The coarse emulsion was prepared by homogenizing 10% (w/w) corn oil with 90% (w/w) aqueous emulsifier solution using a high-speed blender for 2 min (M133/1281-0, Biospec Products, Inc., ESGC, Switzerland). The droplet size in this coarse emulsion was further reduced by passing it through a high-pressure homogenizer (Microfluidizer, M110Y, Microfluidics, Newton, MA) with a 75 μm interaction chamber (F20Y) at an operational pressure of 12,000 psi for 3 passes. The resulting β-carotene-loaded emulsions were stored in a refrigerator at 4 °C before use.

4.2.2.3 Encapsulation of β-carotene in alginate beads

Different concentration of aqueous alginate solutions were prepared by dissolving powdered alginic acid (1% and 2%, w/w) in distilled water and stirring continuously at 60 °C for an hour, and then reducing the temperature to 35 °C. Alginate solutions and β-carotene-loaded emulsions were then mixed together (1:1, mass ratio) for 2 h with continuous stirring to form a solution that contained 5% emulsion (w/w) and polysaccharide (0.5% and 1%). The β-carotene-loaded hydrogel beads were prepared using a commercial encapsulation unit (Encapsulator B-390, BUCHI, Switzerland) with a 120μm nozzle to inject the β-carotene/alginate solution into 10% calcium chloride solution. The formed hydrogel beads were incubated with the Ca^{2+} for 1 h at ambient temperature to promote cross-linking. The beads were then collected by filtration and subsequently washed with distilled water and phosphate buffer to remove any excess ions from their surfaces. The formed beads were then storage in refrigerator to dehydration and then the total weight was determined to facilitate the further measurements.

4.2.2.4 Measurement of β-carotene stability

The physicochemical stability of β-carotene encapsulated in the free emulsion and filled hydrogel particles were tested: 4 ml 5% emulsion samples and filled hydrogel beads (5% oil) were transferred into glass tubes and stored in the dark at 55°C for 12 days (pH 7). The β-carotene was isolated from a nanoemulsion and hydrogel beads using solvent extraction methods: each sample was extracted by the chloroform and alcohol

(volume fraction 1:1) solution at least two times. For the filled hydrogel beads, saturated ethylene diamine tetraacetic acid (EDTA) solution was used to dissolve the beads and release the encapsulated β-carotene. The transparent lower organic phase containing the β-carotene was collected and transferred to a cuvette, and then its absorbance was measured at 450 nm using a UV–visible spectrometer. A pure chloroform and alcohol solution was used as a blank. A corn oil nanoemulsion containing no added β-carotene was also analyzed as a control. The β-carotene content was determined using a standard curve created from solutions with varying amounts of known β-carotene. All measurements were repeated three times.

4.2.2.5 Gastrointestinal tract model

β-carotene delivery systems (free emulsion and filled hydrogel beads) with the same total lipid concentration (2%) and total volume (7.5 mL) were prepared by diluting the original systems with buffer solution (5 mM PBS, pH 7). The samples were then passed through a static GIT model that simulated the mouth, stomach, and small intestine phases. This method has been described in detail in our previous study [230], and so is only briefly summarized below.

Initial System: 7.5 mL of the initial systems were placed into a glass beaker in an incubator shaker at a rotation speed of 100 rpm for 15 min at 37 °C for preheating (Innova Incubator Shaker, Model 4080, New Brunswick Scientific, Edison, NJ). Three different initial β-carotene-loaded delivery systems were tested: (i) lipid droplets, (ii) filled alginate beads (0.5 % alginate) (iii) filled alginate beads (1 % alginate).

Mouth phase: 7.5 mL of simulated saliva fluid (SSF) containing 0.03 g/mL mucin was preheated to 37 °C and then mixed with the initial samples. After being adjusted to pH 6.8, the mixture was incubated in an incubator shaker for 10 min at 37 °C to mimic agitation in the mouth.

Stomach phase: 15 mL of the "bolus" sample resulting from the mouth phase was mixed with 15 mL of simulated gastric fluid containing 0.0032 g/mL pepsin preheated to 37 °C and then the pH was adjusted to 2.5. This mixture was incubated in the incubator shaker for 2 h at 37 °C to mimic stomach conditions.

Small intestine phase: 30 mL of "chyme" sample from the stomach phase was placed into a 150 mL glass beaker that was placed into a water bath at 37 °C and then adjusted to pH 7.00. 1.5 mL of simulated intestinal fluid was added to the reaction vessel, followed by 3.5 mL of bile salt solution with constant stirring. The pH of the reaction system was adjusted back to 7.00. 2.5 mL of lipase solution was then added to the sample and an automatic titration unit (Metrohm, USA Inc.) was used to monitor the pH and maintain it at pH 7.0 by titrating 0.25 mM NaOH solution into the reaction vessel for 2 h at 37 °C. The amount of free fatty acids released was calculated from the titration curves as described previously [231].

4.2.2.6 Determination of particle characterization

The particle size distribution of the samples after passing each digestion process was measured using a static light scattering device (Mastersizer 2000, Malvern Instruments Ltd., Malvern, Worcestershire, UK). Initial, mouth, and small intestine samples were diluted with phosphate buffer (5 mM, pH 7.0) and stomach samples were diluted with acidified water (pH 2.5) to avoid multiple scattering effects. The refractive index of the oil phase used in the calculations was 1.472. The average particle sizes are reported as the surface-weighted mean diameter (d_{32}) for emulsion samples and volume-weighted mean diameter (d_{43}) for beads.

4.2.2.7 ζ-potential measurements

The electrical charge (ζ-potential) of the samples after passing each digestion process was measured using a particle electrophoresis instrument (Zetasizer Nano ZA series, Malvern Instruments Ltd. Worcestershire, UK). Initial, mouth, and small intestine samples were diluted with phosphate buffer (5 mM, pH 7.0) and stomach samples were diluted with acidified water (pH 2.5) prior to analysis to keep the instrument attenuation value between 5 and 10. All measurements were made on at least two freshly prepared samples and each sample was measured in duplicate.

4.2.2.8 Microstructure analysis

The microstructure of samples after passing each digestion process was studied in this section. The microstructure of the all the samples were examined using confocal scanning laser microscopy with a 20 × objective lens (Nikon D-Eclipse C1 80i, Nikon, Melville, NY, U.S.). For the confocal microscopy, each sample was dyed prior to confocal microscopy observation. The corn oil was dyed with Nile red solution (1 mg/mL ethanol) by adding 0.1 mL of Nile red dye solution to 2 mL of sample and storage at 5 °C overnight. The excitation and emission spectrum for Nile red were 543 nm and 605 nm, respectively. The microstructure images for confocal microscopy were taken and analyzed using image analysis software (NIS-Elements, Nikon, Melville, NY).

4.2.2.9 Determination of β-carotene concentration, bioaccessibility, and transformation

After the samples had passed through the simulated GIT, 20 g of digesta from the small intestine phase was collected and centrifuged (18,000 rpm, Thermo Scientific, Waltham, MA) at 4 °C for 30 min. The β-carotene in digesta and micelle phase was extracted based on the methods described in section 2.4. The EDTA solution was used to dissolve the hydrogel beads and release the encapsulated β-carotene. The clear supernatant after extraction was collected and assumed to be the "micelle fraction" in which the β-carotene was solubilized. Aliquots of 2 mL of micelle fraction were mixed with 2 mL of chloroform and 2 mL of alcohol, vortexed several times, and centrifuged at 3500 rpm for 5 min at ambient temperature. The collected chloroform layers were diluted to an appreciate concentration to be analyzed by a UV-visible spectrophotometer at 450 nm. The concentration of β-carotene was calculated from the absorbance using a standard curve.

The *bioaccessibility* of β-carotene (*i.e.,* the fraction in the small intestine that was solubilized in the mixed micelle phase) was calculated from this data: $B^* = 100 \times C_{Micelle}/C_{Digesta}$, where $C_{Micelle}$ and $C_{Digesta}$ are the β-carotene concentrations in the micelle faction and in the total digesta collected after the small intestine phase, respectively. The *transformation* of β-carotene (*i.e.,* the fraction remaining in a non-transformed state in the

small intestine) was calculated: $T^* = 100 \times C_{Digesta}/C_{Initial}$, where $C_{Initial}$ is the β-carotene concentration in the small intestine phase calculated based on the initial amount added. The *effective bioavailability* (*i.e.,* the fraction of ingested β-carotene present in the mixed micelle phase) was also calculated: $BA = 100 \times C_{Micelle}/C_{Initial}$.

4.2.2.10 Statistical analysis

All experiments were performed on at least two freshly prepared samples. The results are reported as averages and standard deviations, and the differences among treatments were calculated based on an analysis of variance (ANOVA) and a post-hoc Duncan test with a confidence level of 95 %. These analyses were carried out using statistical analysis software (SPSS, IBM Corporation, Armonk, NY, USA).

4.2.3 Results and discussion

4.2.3.1 filled hydrogel beads formation and β-carotene stability

In current study, β-carotene was loaded into two delivery systems including nanoemulsion and filled alginate beads. The filled hydrogel beads were formed by injection of mixture of the emulsion and alginate solution into Ca^{2+} solution using an extrusion device (Encapsulator). Base on preliminary experiments, the size of these beads could be determined by several parameters including the biopolymer and cation concentration, infusing gas pressure, vibrational frequency, electrode voltage, nozzle size and the distance between the nozzle and the surface of the crosslinking solution. Two different alginate concentrations (0.5% and 1%) were chosen to fabricate the hydrogel beads using the same operating conditions (frequency 800 Hz, electrode 800 V, pressure 450 mbar). As shown in Fig. 4.7 and Table 4.2, the beads formed with different alginate concentration showed significant different size and appearance characterization: the 0.5% alginate-based beads with diameters around 285 μm creamed to the top of the test tube, whereas the 1% alginate-based beads with diameters around 660 μm sedimented to the bottom. These beads formed with different concentration of alginate may have different physical structure and properties. It can be expected that the difference in initial structure

and properties of the beads would alter the stability and in vitro digestion fate of encapsulated β-carotene.

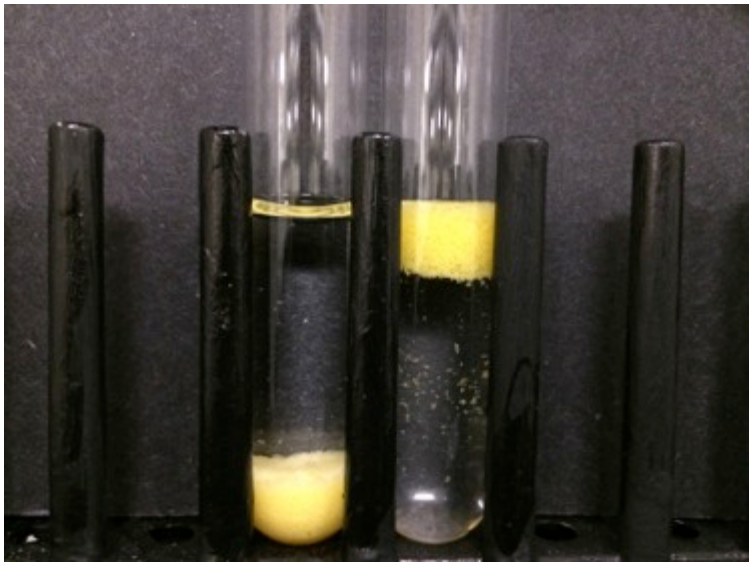

Figure 4. 7 The appearance of the β-carotene loaded emulsion in different alginate-based beads. Left to right: 1% alginate based beads and 0.5% beads

Table 4. 2 The mean particle diameter of three samples including free emulsion, emulsion in 0.5% alginate beads and emulsion in 1% alginate beads after each digestion stage.

Mean particle Diameter (μm)	Initial	Mouth	Stomach	Intestine
Free emulsion	0.15±0.01	0.29±0.02	33.3±3.2	6.6±1.1
0.5% bead	284.8±5.2	469.7±27.5	364.1±18.1	405±8.6
1% bead	660.6±26.4	879.7±33.5	718.4±22.8	837.3±31.5

β-carotene was widely reported to be sensitive to thermal and oxidative degradation during storage because of its highly unsaturated structure [250-251]. The effect of filled hydrogel beads encapsulation on the stability of β-carotene was thus examined in this

section. Fig.4.8 shows the relative β-carotene content in the different delivery systems including nanoemulsion, hydrogel beads formed by 0.5% alginate (0.5% beads) and hydrogel beads formed by 1% alginate (1% beads) during storage. The relative β-carotene content fell from an initial value of 100% after preparation to 0.2%, 37.6% and 55% for nanoemulsion, 1% beads and 0.5% beads respectively, after storage at 55 °C for 12 days. These results indicated that the β-carotene in nanoemulsions was highly unstable to chemical degradation stored at elevated temperatures, and hydrogel beads encapsulation could significantly improve its stability. There may be two reasons attributed to the hydrogel beads protection effect: firstly, the assembled size of the emulsion droplets was larger in hydrogel beads than those in the free emulsions, which meant a smaller surface area for chemical reaction of β-carotene degradation. The other reason is that beads encapsulation provides a physical barrier of wall polymers for the β-carotene, which limits the diffusion of oxygen, pro-oxidant or free radicals into the particle core to interact with β-carotene. It is interesting to note that the retention rate of β-carotene in 0.5% beads was higher than that in 1% beads. This is presumably due that these beads fabricated by 0.5% alginate have relatively smaller particle and also pore size, which provide the encapsulated β-carotene more protection by inhibiting less diffusion of oxygen, pro-oxidant and free radicals. The visual appearance of different samples before and after storage was also measured and shown in Fig. 4.9. It can be observed that β-carotene normally had an intense orange-yellow colour, but this colour completely faded to white when it underwent chemical degradation in nanoemulsion. The alginate-based beads encapsulation showed a good retention of the yellow colour of β-carotene after storage. These results suggested that alginate-based hydrogel beads encapsulation could improve the stability of β-carotene.

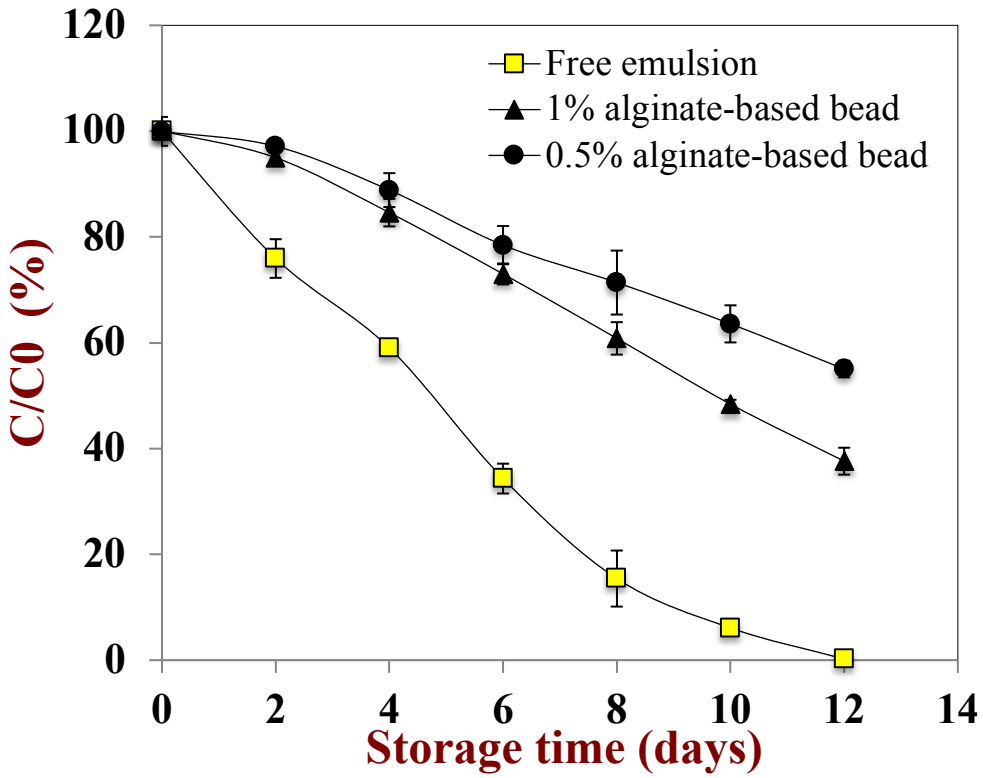

Figure 4. 8 Degradation rates of β-carotene loaded in different delivery systems (nanoemulsion and hydrogel beads) during storage at 55 °C.

4.2.3.2 Influence of GIT conditions on particle charge

In this section, changes in the charge characteristics of the samples were determined as they passed through the different stages of the GIT model to provide information about alterations in interfacial properties.

The ζ-potential of the initial samples of free emulsion, 0.5% beads and 1% beads were -47.6, -9 and -9.5, respectively (Fig. 4.10). The strong negative charge on the free emulsion can be due to the presence of the whey protein isolate (WPI) molecules at the droplet surfaces. WPI is above its isoelectric point (pI = 5.1) at the initial solution conditions (pH 7), and therefore shows a negative charge. The beads were negatively charged for both alginate concentrations, which attributed to the anionic carboxylic ($-COO^-$) groups on the mannuronic and guluronic acid groups of alginate molecules. The concentration of alginate showed little influence on the magnitudes of the electric charges. These results were also in accordance with the previous study [252].

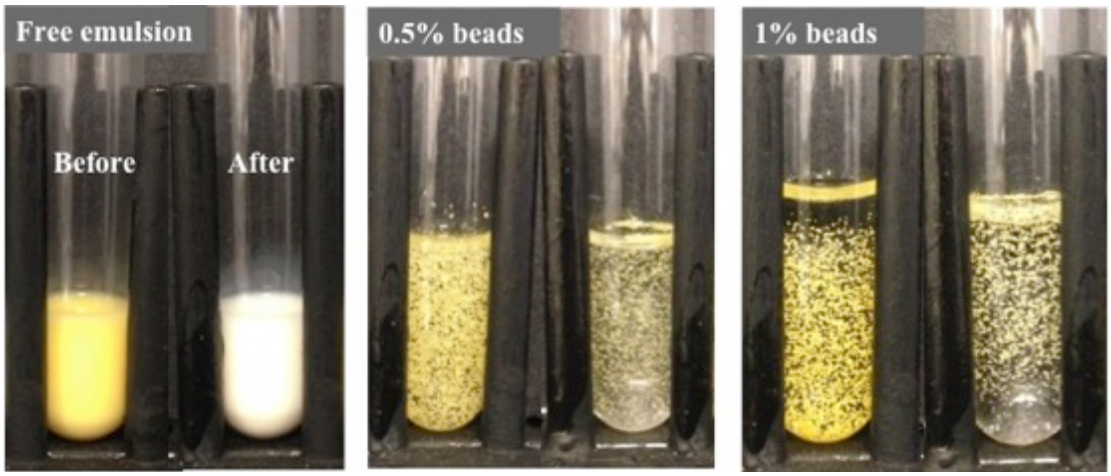

Figure 4. 9 The appearance of the β-carotene loaded in different delivery systems (nanoemulsion and hydrogel beads) before and after stability measurements. Left to right: the β-Carotene-loaded samples before and after storage.

After subjecting to simulated mouth conditions, there was a gently decrease in the magnitude of the negative charge on free emulsion (-40.9), while a slightly increase on these alginate-based beads (-11.2 for 0.5% beads, -15.6 for 1% beads). These changes were presumably due to electrostatic screening by mineral ions present within the simulated saliva, or it may have been due to interactions of the mucin molecules with the samples surfaces (WPI and alginate). There was an appreciable decrease in the magnitude of the electrical charge when all the samples were passing through stomach phase. It might be attributed to the low pH and high ionic strength in stomach phase, which resulted in the electrostatic screening effect on the electrical charge of the samples. It could be observed that free emulsion droplets were slightly negatively under gastric conditions, suggesting that they were not only coated by emulsifier whey proteins. Presumably some of the proteins was digested and displaced, and that some of the mucin molecules from the simulated saliva could also adsorb to the emulsion droplet surfaces [253]. The relative small magnitude of negative charge of alginate beads could be attributed to a loss of negative charge on the carboxyl groups at pH values around their pK_a value (≈3.5). The anionic carboxylic ($–COO^–$) groups of alginate molecules became partially protonated (–COOH) in the stomach phase (pH around 2.5). After small intestine digestion, all the samples showed relatively high negative charges (around -23). Previous

study has attributed that to the presence of various types of anionic particles in the digestion mixture phase such as micelles, vesicles, calcium salts and undigested lipids and proteins [253]. These anionic species may have come from the original emulsions (e.g., peptides, free fatty acids, or phospholipids) or from the gastrointestinal fluids (e.g., bile salts and phospholipids).

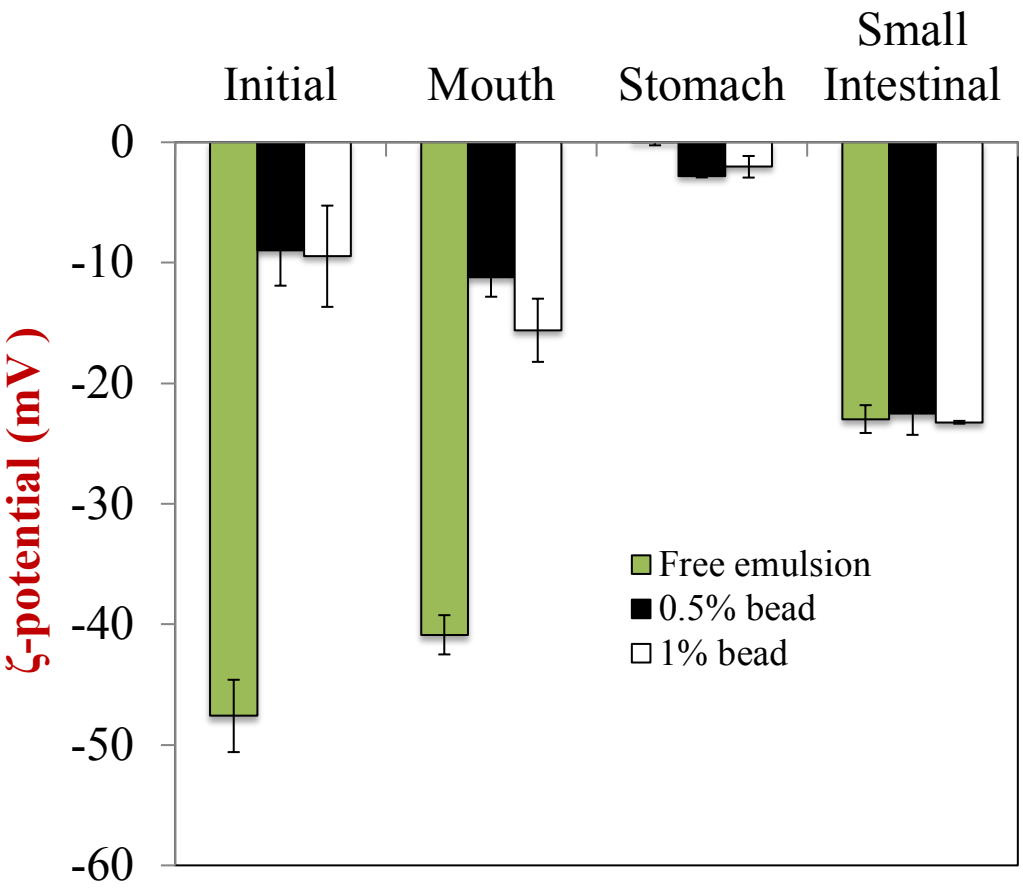

Figure 4. 10 The charge characterization of different samples including free emulsion, emulsion in 0.5% alginate beads, and emulsion in 1% alginate beads after each digestion stage**.**

4.2.3.3 Influence of GIT conditions on particle size and microstructure

β-carotene-loaded emulsion droplets. The particle size distribution of the lipid droplets in the initial emulsion had a single broad peak with a diameter around 0.15μm (Table 4.2, Fig. 4.11), and the droplets were evenly distributed throughout the system as shown from the confocal microscope images (Fig. 4.12). It can be deduced that the WPI-

coated lipid droplets were relatively small and stable to aggregation in the initial condition. After passing through the mouth phase, the particle size distributions of these emulsions became bimodal, with a slight increase in mean particle diameter ($d_{32}\approx$ 0.29μm). The confocal microscopy images indicated that extensive droplet aggregation occurred in mouth phase. It could be attributed either bridging or depletion flocculation induced by the presence of mucin in the simulated saliva, which is also in agreement with our previous study [254]. Bridging flocculation occurs because of the binding of mucin molecules to the surfaces of oil droplets, whereas depletion flocculation occurs due to the increase in the osmotic attractive forces between the droplets generated by non-adsorbed mucin molecules [253]. After exposure to the stomach phase, these emulsions showed an appreciable increase in mean particle diameter ($d_{32}\approx$ 33.31μm), and a further droplet aggregation could be observed from the confocal microscopy measurements (Fig.4.12). It has been reported that protein-stabilized emulsions was prone to aggregation under gastric conditions because of hydrolysis of adsorbed proteins, weakening of electrostatic repulsion, and depletion or bridging flocculation induced by mucin [230]. After passing through the small intestinal stage, the emulsions still contained relatively large size droplets ($d_{32}\approx$ 6.58μm) as detected by both light scattering and confocal microscopy methods. Presumably, there were many colloidal particles present in the digesta including undigested lipid droplets, undigested protein aggregates, micelles, vesicles, and insoluble calcium salts.

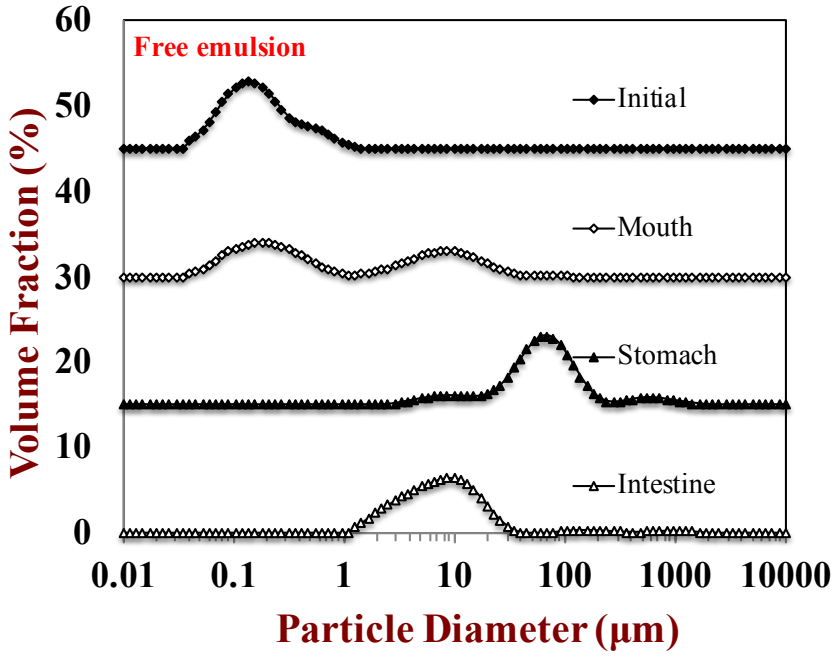
Free emulsion
Initial
Mouth
Stomach
Intestine
Volume Fraction (%)
0
10
20
30
40
50
60
0.01
0.1
1
10
100
1000
10000
Particle Diameter (µm)

(a)

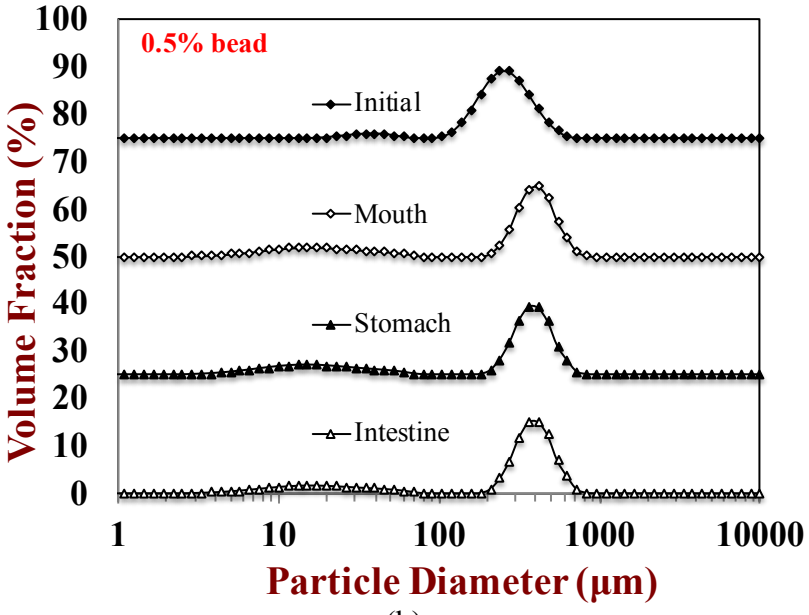
0.5% bead
Initial
Mouth
Stomach
Intestine
Volume Fraction (%)
0
10
20
30
40
50
60
70
80
90
100
1
10
100
1000
10000
Particle Diameter (µm)

(b)

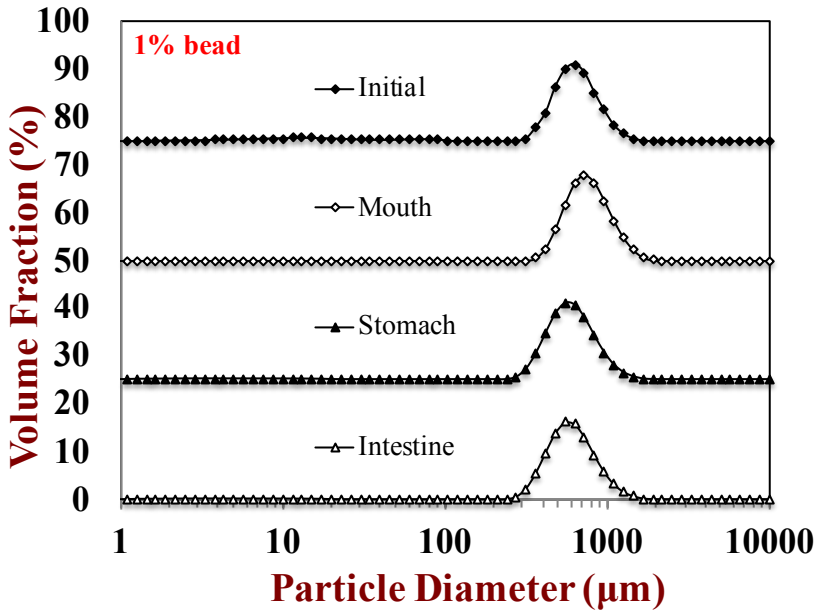

(c)

Figure 4. 11 Particle size distribution of different samples (a) Free emulsion, (b) Emulsion in 0.5% alginate beads, and (c) Emulsion in 1% alginate beads after each digestion stage.

Filled hydrogel beads. The particle size and microstructure of the filled hydrogel beads depended on the alginate concentration used for the beads formation. Initially, these beads fabricated with higher concentration of alginate showed larger size, which has been mentioned in the previous section. The reason could be attributed to the alginate property and the beads formation mechanism used by the instrument (Encapsulator). The alginate solution could form polymer flows when being pumped through the nozzle of the Encapsulator. After obtaining the electrical charge from the equipment, the polymer flows could be separated with each other due to the electrical repulsion, and then form small size droplets injected into cross-link agent solution (Ca^{2+}). High concentration of alginate tends to form high viscous polymer solution, which is hardly separated by electrical repulsion force and form small size droplets. High concentration polymers therefore can potentially form larger size beads using the Encapsulator methods.

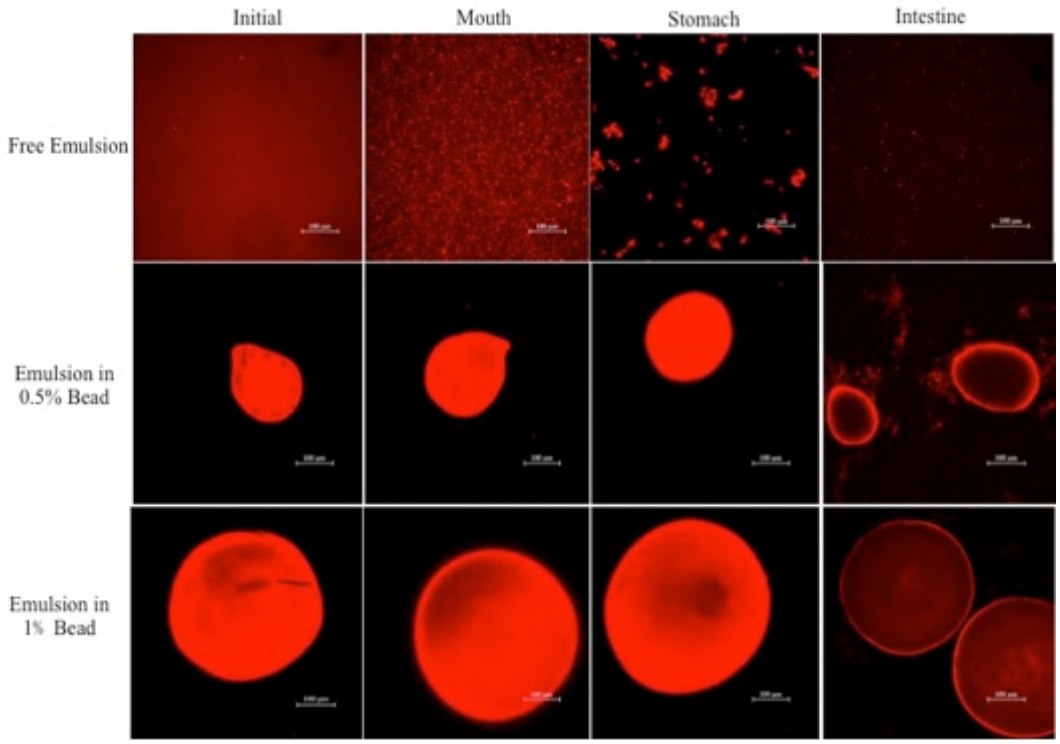

Figure 4. 12 Microstructures of different samples including free emulsion, emulsion in 0.5% alginate beads, and emulsion in 1% alginate beads after exposing to different regions of a simulated GIT model (Scale bar is 20 μm).

For both concentrations of the alginate beads, the general shape of the particle size distribution remained relatively similar during the whole digestion process. In addition, the confocal microscope images showed the similar structure (e.g., shape) of the beads after each digestion steps, indicating that they remained intact after exposure to the different GIT phases. There was an appreciable increase and then decrease in the mean particle diameter of the alginate beads when they were moved from the initial to mouth, and then from mouth to stomach phase. Presumably, it could be attributed to increase in the electrostatic repulsion between the alginate molecules in the mouth phase, and a reduction in the electrostatic repulsion below the pK_a value of the carboxyl groups in the stomach phase. Previous studies have also reported that calcium alginate beads tend to swell when placed in higher pH solutions, while shrink under highly acidic gastric conditions [255-256]. We can expect that the closer packing of the β-carotene within the alginate-based beads under stomach conditions may be useful for protecting encapsulated β-carotene from the harsh gastric environment. After intestinal digestion, the inner red

fluorescence dye of hydrogel beads faded to black, and there were aggregated particles surrounding the hydrogel beads observed from the confocal microscope images (Fig.4.12). These results suggested that lipids digestion occurred in intestine phase and colloidal particles were released from the beads after digestion. These particles may have been undigested lipid droplets or mixed micelles. It is therefore interesting to study the dynamic digestion process (e.g., the diffusion of lipase and digestion products) of filled hydrogel beads in the future studies.

4.2.3.4 Influence of delivery system type on lipid digestion

The effect of different delivery system encapsulation on the rate and extent of lipid digestion was evaluated using an automatic titration (pH stat) method. The fraction of free fatty acids (FFAs) released from the samples during the digestion process was calculated from measurements of the volume of NaOH that had to be titrated into the reaction chamber to maintain a constant pH (7.0) as shown in Fig. 4.13. The free emulsion was rapidly digested during the first 5 minutes with over 76% of the FFAs being released, followed by a more gradual digestion until a relatively constant final value (95.8%) was attained for the remainder of the incubation time. Conversely, the FFAs release rate was much slower for the filled hydrogel beads, which also depended on the alginate concentration. Around 22.2% and 36.7% FFA were released within first 5 min of digestion, and around 56.2% and 82.5% FFA had been release after 120min digestion for the 1% and 0.5% beads respectively. These results indicate that encapsulation of the lipid droplets within the hydrogel beads was highly effective at retarding lipid digestion. There are a number of physicochemical phenomena might account for the decreased digestion rate for the encapsulated oil droplets. Firstly, lipid digestion only occurs when pancreatic lipase can adsorb to the surfaces of the lipid droplets and come into proximity with its substrate such as triacylglycerol and diacylglycerol molecules [238]. For the free emulsion, the pancreatic lipase is able to rapidly move from the aqueous phase to the lipid droplets surfaces and thus initiate lipolysis. Whereas for the filled hydrogel beads, lipase (and the other GIT components) has to penetrate into the beads and diffuse through the hydrogel network before they can reach the lipid droplet surfaces. The diffusion rate to the interior of the beads increases as

the pore size of the hydrogel matrix decreases and also the diameter of the beads increases. The 0.5% beads with a smaller beads diameter therefore showed a higher digestion rate and extent compared with 1% beads. A second possible reason is that long chain FFAs generated in the digestion process must be removed otherwise the lipolysis reaction will be retarded [76]. These FFAs can be typically removed by being incorporated into mixed micelles with bile salts and phospholipids, or by forming insoluble salts with calcium ions [242]. For these hydrogel beads, the removal of FFAs away from the lipid droplet surfaces may be limited because bile salts, phospholipids, and calcium have to penetrate into the biopolymer matrix of the hydrogel beads. Furthermore, the diffusion of the FFAs themselves out of the beads may also be inhibited by the presence of the biopolymer network. Our results indicated that the in vitro digestion fate of lipid droplets could be modulated by encapsulating them in different hydrogel beads.

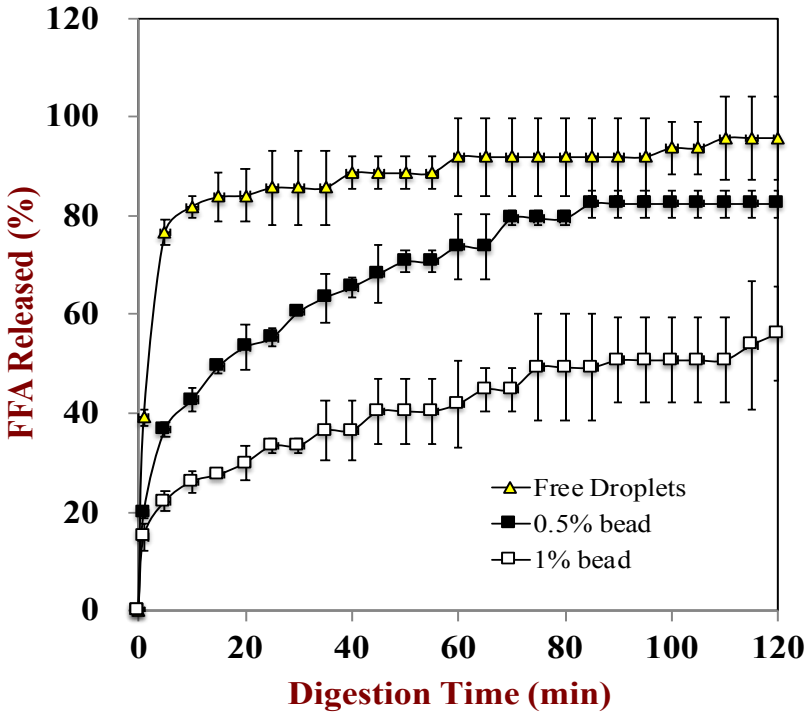

Figure 4. 13 Amount of fatty acids released from different samples including free emulsion, emulsion in 0.5% alginate beads, and emulsion in 1% alginate beads measured in a pH-stat *in vitro* digestion model.

4.2.3.5 Influence of delivery system type on β-carotene release

It has been mentioned earlier that pure β-carotene typically has a very low bioavailability because of its poor chemical stability and low solubility in gastrointestinal fluids. The concentration of β-carotene in the mixed micelle phase, total digesta and initial phase were thus determined to provide a measure of the amount of β-carotene that was solubilized and the amount that was not chemically degraded. The bioaccessibility, transformation, and effective bioavailability of β-carotene were also calculated from the equations described in section 2.9. It is indicated from the Fig.4.13 that free emulsion samples had higher bioaccessibility (B*) and effective bioavailability (BA) of encapsulated β-carotene compared with the hydrogel beads. It can be expected that the digestion of the lipid droplets lead to the formation of mixed micelles that can solubilize the high amount of β-carotene molecules (high B* and BA). Previous studies in our laboratory had also reported that emulsion systems (e.g., emulsion-based delivery systems and emulsion-based excipient systems) could increase lipophilic bioactive ingredients bioaccessibility through these mechanisms [257-259]. The relatively low B* and BA of the β-carotene in the filled hydrogel beads in current study can be attributed to several reasons. Firstly, some of the β-carotene remained within the undigested lipid droplets inside the hydrogel beads and was not released and solubilized in micelle. The second reason is that there was less mixed micelles available in the aqueous phase to solubilize any β-carotene molecules released from the hydrogel beads (Fig. 4.13). Both of these reasons could be attributed to the low β-carotene concentration in micelle. The transformation (T*) of β-carotene was also calculated to determine the extent of any chemical changes during digestion (Fig. 4.15). It was indicated that β-carotene encapsulated in free emulsion samples showed slightly lower transformation ($C_{\text{Digesta}}/C_{\text{Initial}}$) than hydrogel beads. We can expect that alginate-based hydrogel beads encapsulation can protect the β-carotene from degradation during digestion. Based on our preliminary experiments, the slight degradation of β-carotene majorly occurred after stomach digestion phase, and the reason could be attributed to the protonization of the methine carbon of β-carotene in high acid stomach phase. There appeared to be a good correlation between the β-carotene transformation and extent of β-carotene degradation during evaluated temperature storage, *i.e.,* they followed the completely opposite trend:

0.5% beads > 1% beads > Free emulsions. These results suggest that β-carotene showed higher stability after encapsulation in hydrogel beads.

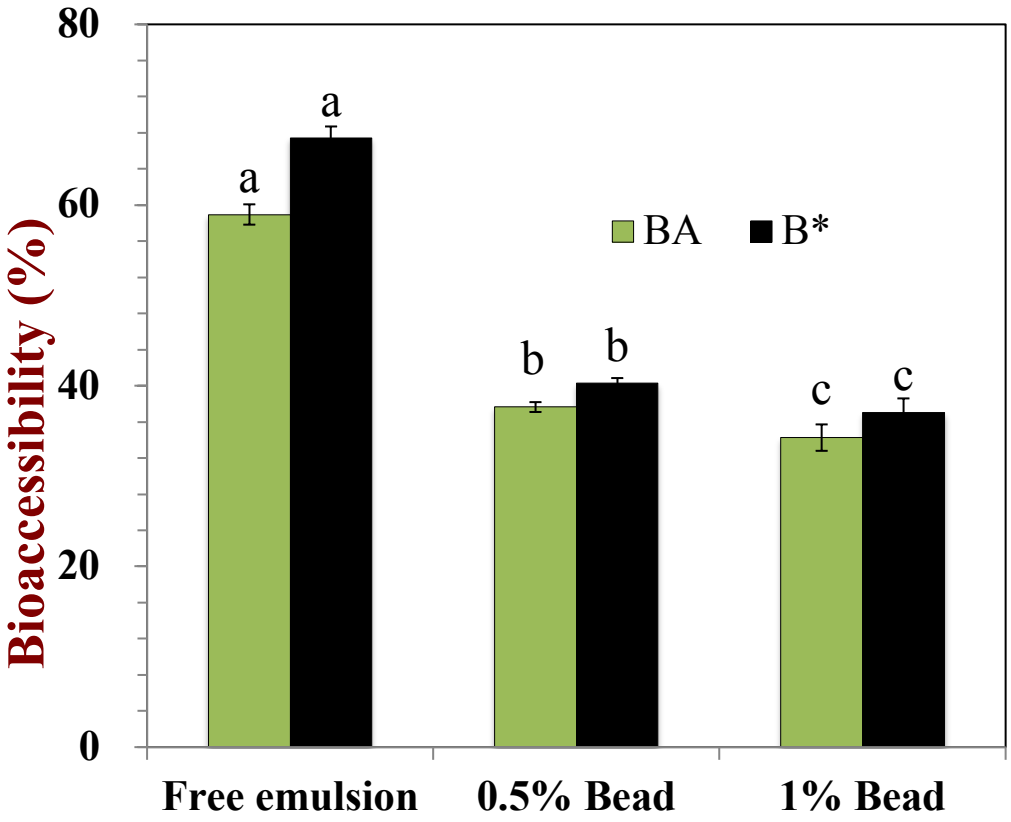

Figure 4. 14 Bioaccessibility (B*) and effective bioavailability (BA) of β-carotene in different delivery systems including free emulsion, emulsion in 0.5% alginate beads, and emulsion in 1% alginate beads measured in a pH-stat *in vitro* digestion model.

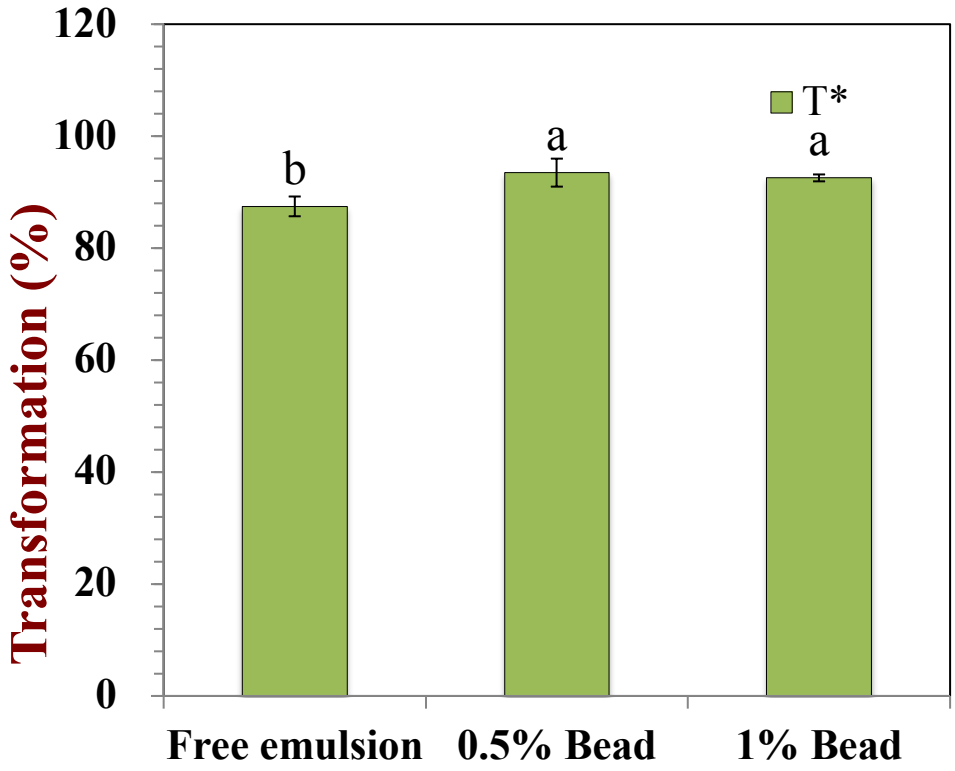

Figure 4. 15 Transformation (%) of β-carotene in in different delivery systems including free emulsion, emulsion in 0.5% alginate beads, and emulsion in 1% alginate beads after full digestion (mouth, stomach and intestine) process.

4.2.4 Conclusions

The influence of types of delivery systems encapsulation on physicochemical stability and in vitro bioaccessibility of β-carotene was studied in this present study. Three different delivery systems were prepared including free emulsion, filled hydrogel beads formed by 0.5% alginate and filled hydrogel beads formed by 1% alginate. The hydrogel beads formed with different concentration of alginate showed different physical structure and properties: the 0.5% beads (creamed to the top of the buffer phase) had much smaller diameter than 1% beads (sedimented to the bottom). The stability studies indicated that hydrogel beads encapsulation could protect the β-carotene from degradation. The retention rate of β-carotene in 0.5% beads was higher than that in 1% beads. In vitro digestion studies indicated that free lipid droplets were digested more

rapidly and fully than those encapsulated within hydrogel beads. The rate and extent of lipid digestion in filled hydrogel beads depended on alginate concentration: the 0.5% beads showed a higher digestion rate and extent compared with 1% beads. Free emulsion samples showed higher bioaccessibility and effective bioavailability of encapsulated β-carotene than that in the hydrogel beads. While the β-carotene transformation in different delivery systems followed the following order: 0.5% beads > 1% beads > Free emulsions. Our results may have important implications for designing hydrogel beads to increase the stability and oral bioavailability of β-carotene

CHAPTER 5

ENCAPSULATION, PROTECTION, AND RELEASE OF BIOACTIVE AGENTS USING HYDROGEL BEADS WITH SELF-REGULATING MICROCLIMATE PH PROPERTIES

5.1 Confocal fluorescence mapping of pH profile inside hydrogel beads (microgels) with controllable internal pH values

5.1.1 Introduction

There is growing interest in the design and fabrication of particle-based delivery systems to load, protect and release bioactive agents in the food, supplement, and pharmaceutical industries (Badruddoza, Godfrin, Myerson, Trout, & Doyle, 2016; Janes, Calvo, & Alonso, 2001). A diverse range of bioactive agents with differing molecular, physicochemical and biological properties need to be encapsulated, including proteins, peptides, probiotics, prebiotics, vitamins, minerals, nutraceuticals, triacylglycerol oils, flavors, colors, antimicrobials, and preservatives (Cook, Tzortzis, Charalampopoulos, & Khutoryanskiy, 2012; Zhu, Mallery, & Schwendeman, 2000). For example, many bioactive proteins and peptides need to be encapsulated because of their propensity to cause bitterness or astringency in the mouth, or their susceptibility to denaturation or degradation in the stomach and small intestine (Liu & Schwendeman, 2012). Similarly, probiotic bacteria often need to be encapsulated to maintain their viability when exposed to highly acidic gastric conditions, but then released in the colon where they exhibit their beneficial actions on colonic microflora (Li, et al., 2017). Many hydrophobic bioactive agents (such as carotenoids, curcumin and polyphenols) need to be encapsulated to prevent their chemical degradation within foods and the gastrointestinal tract (GIT) (Altunbas, Lee, Rajasekaran, Schneider, & Pochan, 2011; Zhang, Zhang, & McClements, 2016).

Numerous studies have shown that particle-based delivery systems can be designed to improve the handling, dispersibility, stability, and bioavailability of certain bioactive agents (Keen, Slater, & Routh, 2012; McClements, 2016). However, to be effective these

delivery systems must be carefully designed based on the molecular and physicochemical properties of the bioactives, the processing and storage conditions they are exposed to (such as pH, ionic strength, and temperature), and the desired quality attributes of the final products (such as optical, rheological, organoleptic, and stability properties). For certain applications, hydrogel beads are particularly suitable for encapsulation and delivery of bioactive agents (McClements, 2016). These hydrogel beads are typically spherical particles whose interiors are comprised of a porous network of cross-linked hydrophilic polymers. Hydrogel beads are often formed from natural polymers (such as polysaccharides and proteins) using relatively mild preparation conditions, and so they usually have little adverse affects on the properties of the encapsulated bioactives (Kim, Bae, & Okano, 1992; Zhang, Zhang, Zou, & McClements, 2016).

Many bioactive agents are highly susceptible to physical, chemical, or biological degradation over a certain pH range, but stable at other pH values. For example, some natural colors fade rapidly under highly acidic pH conditions, but slowly under neutral conditions (Castañeda-Ovando, Pacheco-Hernández, Páez-Hernández, Rodríguez, & Galán-Vidal, 2009). Similarly, many probiotics are rapidly inactivated under highly acidic conditions, but viable under neutral conditions (Anselmo, McHugh, Webster, Langer, & Jaklenec, 2016; Li, et al., 2016). A major drawback associated with the utilization of conventional hydrogel beads for encapsulation of pH-labile bioactives is that they are highly porous (Zhang, Zhang, Chen, Tong, & McClements, 2015), and so small acidic or basic ions (such as H^+ or OH^-) can easily diffuse in or out of them, thereby causing the internal pH to be fairly similar to the external pH. Consequently, pH-labile substances may be rapidly degraded when they are encapsulated in hydrogel beads that are exposed to destabilizing pH conditions. The pH sensitivity of conventional hydrogel beads therefore limits their utilization for certain applications in the food, supplement, and pharmaceutical industries. Attempts have been made to improve the pH-stability of bioactive agents in hydrogel beads by delaying the diffusion of acidic or basic ions into them, *e.g.,* by reducing the pore size of the internal core or the outer shell (Mei, et al., 2014). Nevertheless, these approaches have had limited success because the pH-determining ions involved are so small (< 1 nm) that they can rapidly diffuse through even small pores.

In the current study, hydrogel beads were fabricated with self-regulating internal pH microclimates. This was achieved by trapping a basic buffer (magnesium hydroxide) that was insoluble under neutral conditions but soluble under acidic conditions inside the beads. Initially, the hydrogel beads are formed under neutral conditions so that the buffer remains in an insoluble form. However, when the beads are submerged in an acidic environment some of the magnesium hydroxide dissolves, which releases OH^- ions that can neutralize the H^+ ions, thereby maintaining a neutral internal pH (until all the buffer has dissolved). A quantitative fluorescent method was developed to map the local pH inside the hydrogel beads when they were exposed to different pH conditions. This method involved encapsulating a pH-sensitive fluorescent probe inside of the hydrogel beads. The probe used has two functional groups, one that is pH sensitive and one that is pH insensitive, so that the pH can be determined quantitatively from the ratio of the fluorescence intensity of these two groups. Moreover, the probe is attached to a high molecular weight polymer (dextran) so that it can be successfully trapped within the biopolymer (alginate) network that makes up the interior of the hydrogel beads.

5.1.2 Materials and methods

5.1.2.1 Materials

Fluorescein tetramethylrhodamine dextran (FRD, average M_r 70,000) was purchased from Molecular Probes (Eugene, OR). Alginic acid (sodium salt), calcium chloride, and magnesium hydrate were purchased from the Sigma Chemical Company (St. Louis, MO). Sodium phosphate was purchased from Fisher Chemical Company (Pittsburgh, PA). All chemicals used were analytical grade. Double distilled water was used to make all solutions.

5.1.2.2 Hydrogel beads preparation

Aqueous alginate solutions were prepared by dispersing powdered alginic acid (0.8%, w/w) into phosphate buffer solution (5 mM, pH 7.0) and then continuously stirring at 60 °C for an hour. The temperature was then reduced to 35 °C and the samples were continually stirred until the solution became clear indicating that the alginate had fully

dissolved. 10 mg/mL FRD in phosphate buffer (5 mM, pH 7.0) was then added to the alginate solution (at a volume ratio of 1:200) with or without 0.3% $Mg(OH)_2$. After ensuring the sample was homogeneous by stirring, the mixture was injected into a 10% w/w calcium chloride solution using a commercial encapsulation unit (Encapsulator B-390, BUCHI, Switzerland) with a 120 μm vibrating nozzle to prepare the hydrogel beads. The encapsulation device was operated under fixed conditions: frequency = 800 Hz; electrode potential = 800 V; and operating pressure = 500 mbar. The alginate beads formed were kept in the Ca^{2+} solution for 1 h at ambient temperature to promote cross-linking and bead hardening.

5.1.2.3 Simulated gastric conditions

The impact of exposure of the hydrogel beads to simulated gastric fluid (SGF) on their internal pH was determined using a method described previously (Zhang, Zhang, Zhang, Decker, & McClements, 2015). Hydrogel beads (with or without encapsulated $Mg(OH)_2$) were added at a ratio of 1:4 (w/w) to SGF that had been preheated to 37 °C and adjusted to pH 2.5. This mixture was then incubated in an incubated shaker for 2 h at 37 °C to mimic stomach conditions.

5.1.2.4 Confocal Laser Scanning Microscopy

Images were obtained using confocal laser scanning microscopy with a 20× objective lens (Nikon D-Eclipse C1 80i, Nikon, Melville, NY, USA). The images of the ratiometric fluorescence dye were obtained using excitation wavelengths of 543 and 488 nm, and detection wavelengths/bandwidths of 650 nm/LP and 590 nm/50 nm, respectively. All samples were imaged using an exposure time of 0.5 s and a 12.5% excitation power level for both channels. The complete images of each sample were typically acquired in less than 2 min with at least eight measurements. The microstructural images for confocal microscopy were analyzed using image analysis software (NIS-Elements, Nikon, Melville, NY, USA).

5.1.2.5 Standard curve preparation

A stock FRD solution (10 mg/mL) was prepared by dissolving the powdered FRD dye in phosphate buffer (5 mM, pH 7) solution. 5 μL/ml FRD stock solution at pH 2.5–7 (adjusted by hydrochloric acid) was imaged using confocal microscopy to determine the linear range of the pH response. Solutions containing different concentrations of FRD (2.5, 5 and 10 μL/ml) were also used to prepare a standard curve using a SpectraMax spectrophotometer (Molecular Devices, Sunnyvale, CA) to assess the impact of dye concentration on the fluorescence intensity ratio used to calculate the local pH.

5.1.2.6 Image processing for pH measurement

The images were analyzed using Image J Software (1.50I, imagej.nih.gov). The ratio of pixel intensities of two images obtained from two wavelengths (488 and 543 nm) were calculated and correlated with the pH obtained from the standard curve. The average intensity was calculated from at least eight measurements. The pH gradient within the beads was determined by dividing their circular images into a series of same-pixel thickness concentric rings, and the mean pixel intensity was calculated for each ring from the number of pixels and individual pixel intensities in the ring.

5.1.3 Results and discussion

5.1.3.1 Development of pH standard curve

In this study, relatively small hydrogel beads (around 200 μm) were fabricated using a specialized extrusion device (Encapsulator) with a vibrating nozzle (**Figure 5.1**). The small dimensions and viscoelastic nature of these beads meant that it was not possible to measure their internal pH using traditional methods, such as pH electrodes. It was therefore necessary to develop an alternative method to measure the pH within the beads so as to confirm the potential of the encapsulated $Mg(OH)_2$ to control their internal pH profile. A fluorescent probe method was therefore developed to determine the local pH profile inside the beads. A dextran conjugated fluorescent probe, Fluorescein and Tetramethylrhodamine (FRD), was used as the pH indicator. This probe was selected

because it has a relatively high molecular weight (around 70 kDa), which ensures that it remains trapped inside the porous biopolymer network that makes up the bead interior. Moreover, this probe is a ratiometric dye that has both pH-dependent (FITC) and pH-independent (TMR) fluorescence groups. For this type of dye, the pH-independent channel can be used as an internal standard for quantitative pH evaluation (Chen & Arriaga, 2006; Deriy, et al., 2009). This ratiometric method also eliminates problems associated with photo-bleaching, variable bead thickness, and non-uniform dye distribution within the bead (Cope, Hibberd, Whetstone, MacRae, & Melia, 2002; Li & Schwendeman, 2005).

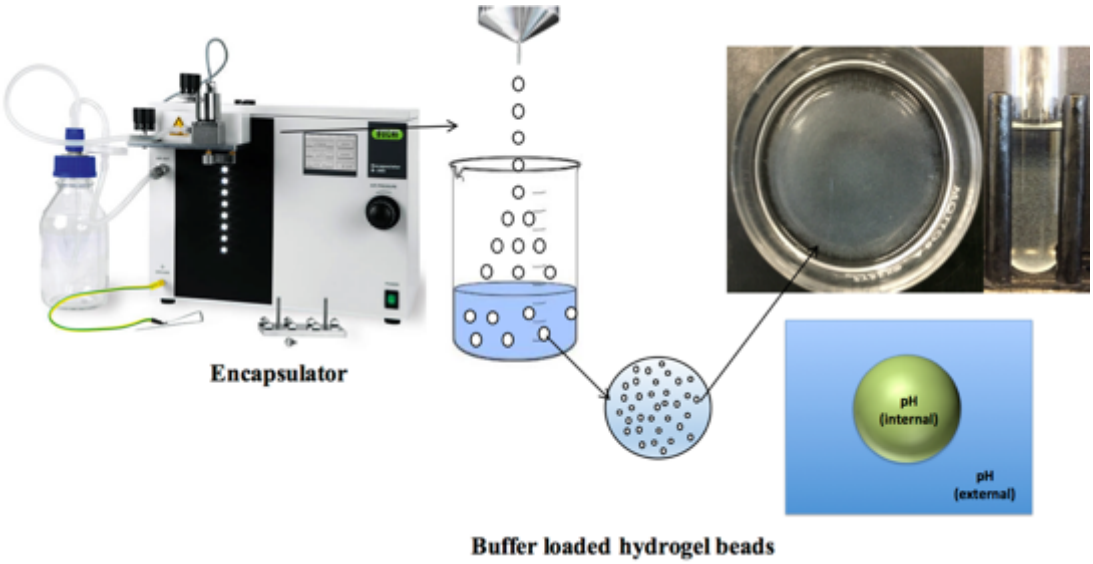

Figure 5. 1 Schematic diagram showing the fabrication of self-adjusting microclimate pH hydrogel beads. The beads are formed by injecting alginate and insoluble buffer into a cross-linking calcium ion solution.

In preliminary confocal microscopy studies, it was observed that the fluorescence emission intensity was pH-independent when an excitation wavelength of 543 nm was used, but pH-dependent when an excitation wavelength of 488 nm was used. The pH of a sample could therefore be obtained independent of dye concentration by taking the ratio of the emission intensities at these two excitation wavelengths (543 nm/ 488 nm). Standard curves of fluorescence intensity ratio versus pH were determined using a series of buffer solutions (pH 2.5-7.0) with dye concentrations of 2.5, 5 and 10 µL/ml of stock

solution (10 mg/mL). The fluorescence intensity ratio was exponentially related to pH from pH 2.5 to 7.0 when determined from the confocal microscopy images (**Fig. 5.2a**), but linearly related when measured using a microplate reader (**Fig. 5.2b**). Moreover, the fluorescence intensity ratio (TMR/FITC) was largely independent of overall dye concentration across the entire pH range as determined using the microplate reader. These results suggest that the pH inside the beads can be successfully mapped even though there may be some local variations in dye concentration within the beads *e.g.,* due to diffusion of dye outwards. The major advantage of the confocal microscopy approach is that the local pH can be obtained from the images, whereas only the overall pH of a sample can be obtained using the microplate reader.

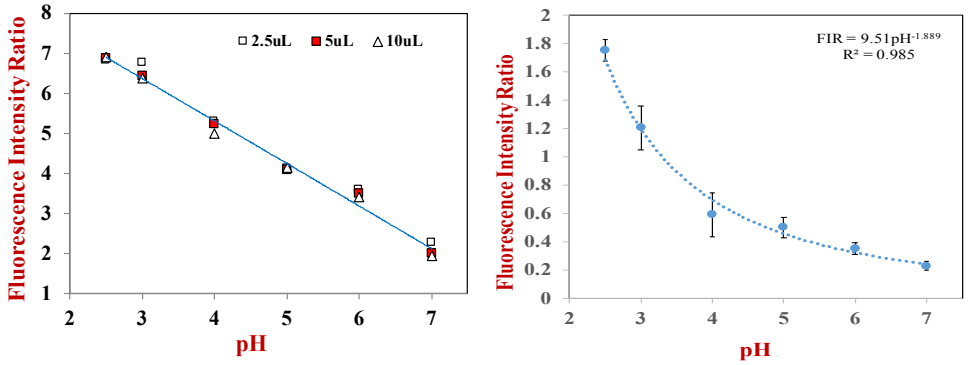

(a) (b)

Figure 5. 2 Standard curve of pH versus fluorescence intensity ratio (TMR/FITC) taken by (a) microplate at concentrations of 2.5, 5 and 10 µL/ml stock solution (10 mg/mL) and (b) confocal microscopy at 5 µL/ml stock solution (10 mg/mL).

5.1.3.2 Mapping the pH inside the beads

The highly acidic pH of human gastric juices causes an unwanted reduction in the activity of many orally delivered bioactive agents, such as many enzymes, probiotics, and nutraceuticals. Consequently, an antacid buffering agent ($Mg(OH)_2$) was encapsulated inside the hydrogel beads to create an internal pH that was considerably higher than the external pH, thereby protecting any co-encapsulated acid-sensitive bioactives. Under neutral pH conditions, $Mg(OH)_2$ forms insoluble solid particles that are retained within the hydrogel beads. However, when the beads are exposed to acid conditions some of the

$Mg(OH)_2$ particles will dissolve, thereby releasing OH^- ions that will neutralize any H^+ ions that diffuse into the hydrogel interior, thereby helping to maintain a high internal pH.

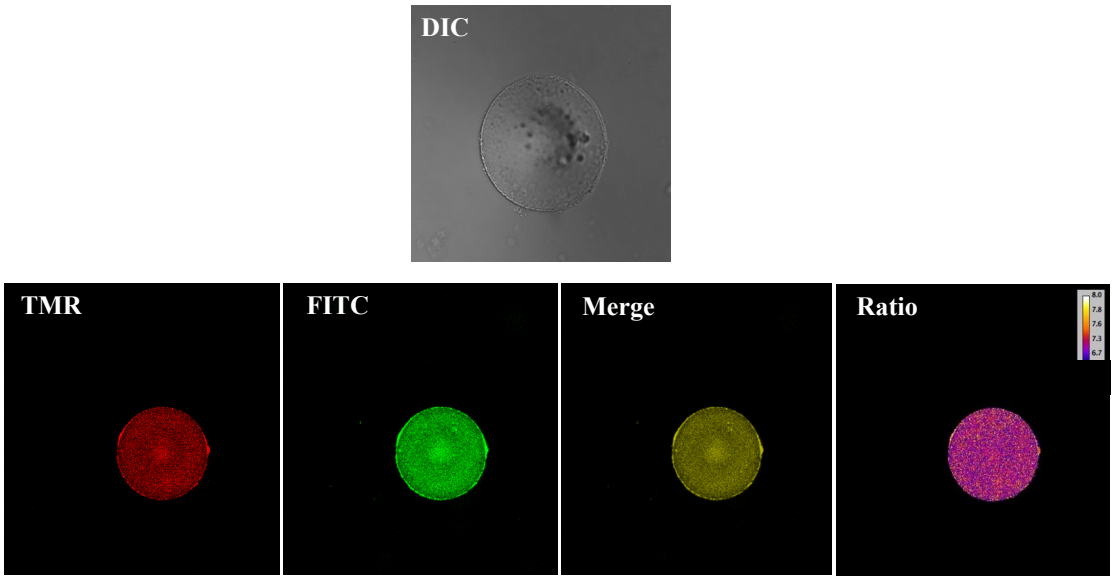

(a)

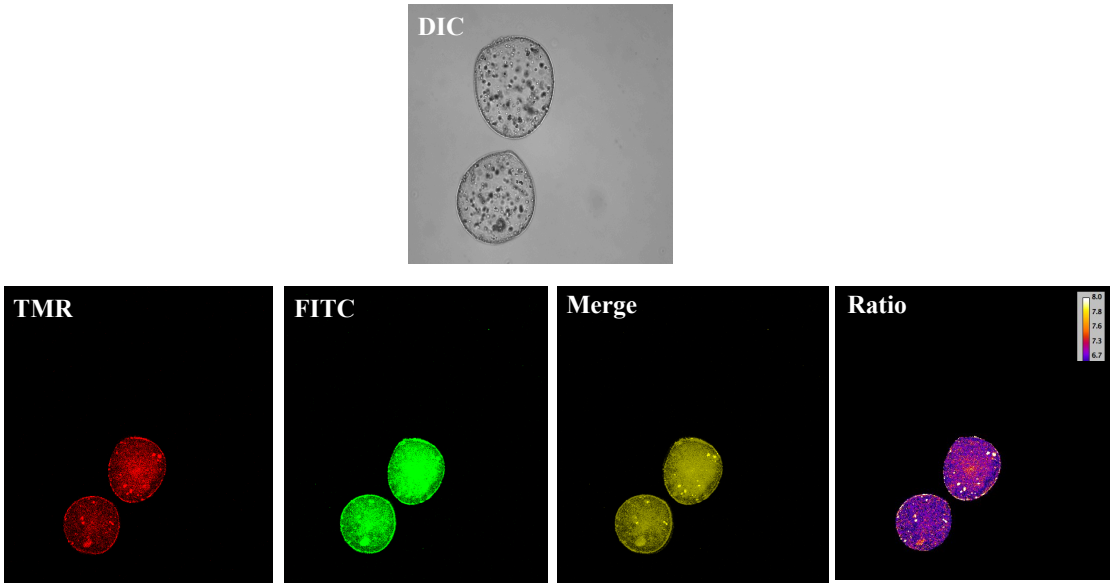

(b)

Figure 5. 3 Differential interference contrast (DIC) and fluorescent microscopy images of (a) hydrogel beads without $Mg(OH)_2$ encapsulation and (b) with 0.3% $Mg(OH)_2$ encapsulation. These images were taken after the beads were prepared. The images of the ratio channel were generated using Image J software (imagej.nih.gov) and the color strip shown on the top right represents the pseudocolor change with pH (intensity of TMR signal was enhanced using Image J to improve contrast).

Hydrogel beads were formed by injecting a solution containing gelling agent (alginate) and fluorescence dye (FRD) in the absence or presence of insoluble buffer particles (magnesium oxide) into another solution containing a cross-linking agent (calcium chloride). The initial beads formed by this method had mean diameters of around 200 μm as determined by confocal fluorescence and optical microscopy (**Fig. 5.3 and 5.4)**. Initially, the average internal pH values of the hydrogel beads determined from the CLSM images were around pH 6.5 for buffer-free beads and around pH 7.5 for buffer-loaded beads. The presence of $Mg(OH)_2$ slightly increased the internal pH of the buffer-loaded hydrogel beads, which can be attributed to the fact that it is a weak base and some dissolution may have occurred. The confocal images also indicated that the pH values inside the beads were not uniformly distributed after $Mg(OH)_2$ encapsulation (**Fig. 5.3b**). There appeared to be microenvironments around the insoluble $Mg(OH)_2$ particles that had a higher pH that the surrounding solution. The pH gradient distribution analysis indicated that the pH was relatively uniform throughout the buffer-free hydrogel beads, being in the range from pH 6.8-7 (**Fig. 5.4c**). Conversely, the pH was slightly lower at the edge of the buffer-loaded hydrogel beads than in their interiors, with the local pH values increasing from around pH 7.2 at the edge to pH 7.6 at the center (**Fig. 5.5c**). Presumably, most of the insoluble buffer particles were located in the center rather than at the edge of the hydrogel beads.

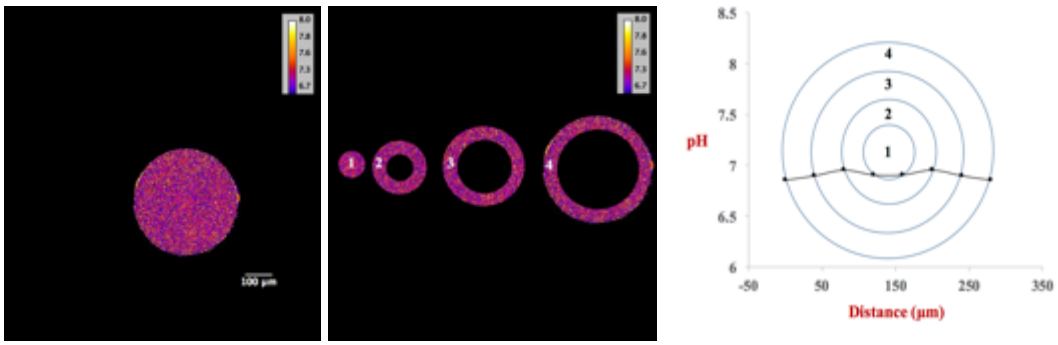

(a) (b) (c)

Figure 5. 4 An illustration of the image processing approach used to generate the pH gradient profile within buffer-free hydrogel beads. (a) The fluorescence intensity ratio image with pseudocolor color; (b) concentric rings of similar pixel thickness obtained from the images of the beads; and (c) the average pH value within each ring as a function of distance from the bead edge.

5.1.3.3 Monitoring pH changes after exposure to gastric conditions

Many types of bioactive agents are degraded when exposed to the highly acidic conditions found in the human stomach, and therefore it would be valuable to have delivery systems that protected them within the gastric fluids. In this section, we therefore applied the confocal fluorescence pH mapping method to monitor changes in the internal pH of the hydrogel beads in the absence and presence of encapsulated magnesium hydroxide. After incubation in simulated gastric fluids (SGF), the fluorescence intensity inside the buffer-free hydrogel beads rapidly decreased to around pH 3 (**Figs. 5.6 and 5.7**). Presumably, the small H^+ ions rapidly diffused through the porous alginate network within the hydrogel beads driven by the concentration gradient between the inside and outside of the beads. Consequently, the internal pH of the buffer-free beads was fairly similar to that of the external pH of the SGF after 2 h incubation in the gastric phase. Conversely, the pH value within the $Mg(OH)_2$-loaded hydrogel beads remained fairly similar to that of the original value (≈pH 7.5) after 2 hours of incubation in the acidic SGF (**Figs. 5.6 and 5.7**). This result suggests that these antacid hydrogel beads could be used to protect acid-sensitive bioactives during passage though the stomach. The confocal fluorescence images suggest that the pH was higher in the center of the beads than at their edges (**Fig. 5.6**). This effect is probably because the insoluble $Mg(OH)_2$ particles in the exterior regions of the beads dissolve first as hydrogen ions from the SGF diffuse into the beads. To verify this dissolution process, DIC optical images of the $Mg(OH)_2$-loaded hydrogel beads were taken throughout the simulated stomach phase (**Fig. 5.8**). These images clearly indicated that $Mg(OH)_2$ particles slowly dissolved during the stomach phase incubation, which can be attributed to their neutralization reaction with hydrogen ions arising from the gastric fluids.

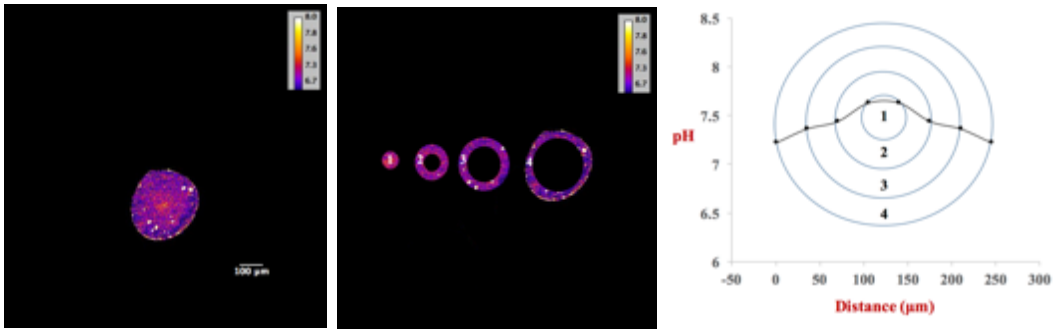

(a) (b) (c)

Figure 5. 5 An illustration of the image processing approach used to generate the pH gradient profile within $Mg(OH)_2$-loaded hydrogel beads. (a) The fluorescence intensity ratio image with pseudocolor color; (b) concentric rings of similar pixel thickness obtained from the images of the beads; and (c) the average pH value within each ring as a function of distance from the bead edge.

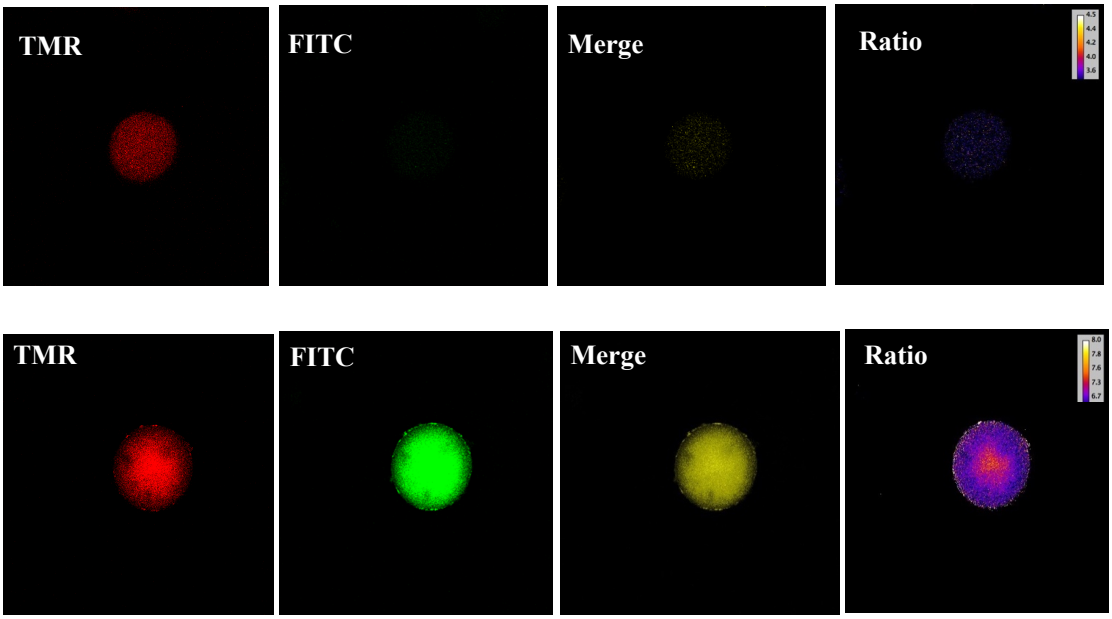

Figure 5. 6 Confocal fluorescence microscopy images of hydrogel beads without $Mg(OH)_2$ encapsulation (top) and with 0.3% $Mg(OH)_2$ encapsulation (bottom) after passage through the stomach phase. The images of the ratio channel were generated using Image J software and the color strip (top right of images) represents the pseudo-color change with pH. The intensity of the TMR signal was enhanced using Image J to improve the contrast.

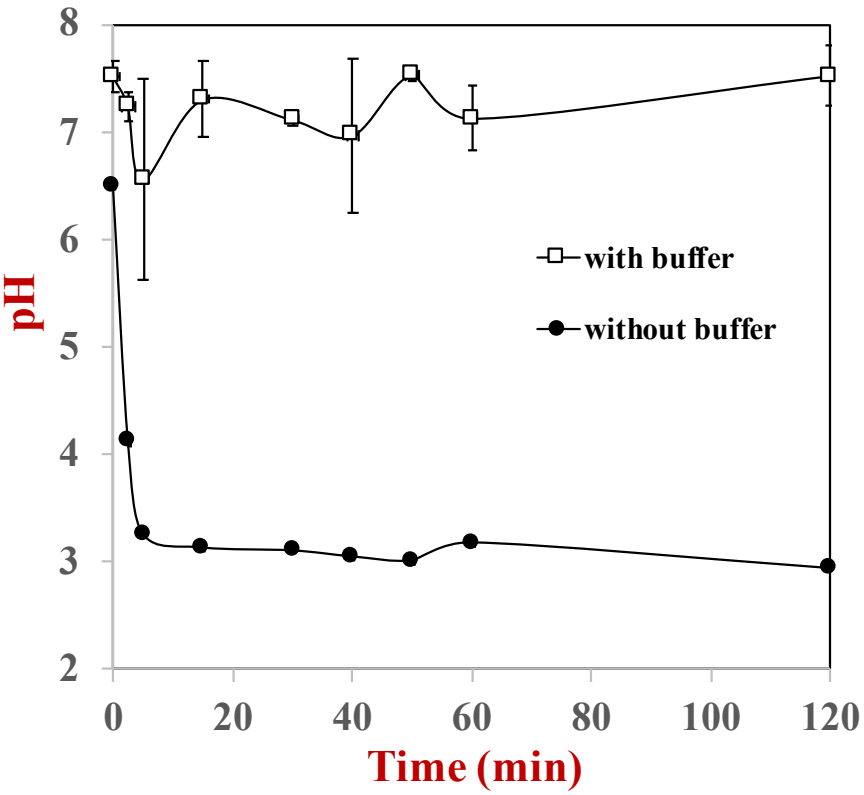

Figure 5. 7 The pH value of hydrogel beads without and with $Mg(OH)_2$ encapsulation during 2h stomach digestion process.

5.1.3.4 Dynamic pH change during incubation

The acid degradation of many bioactives is a rapid process, and so it is important to determine how long the hydrogel beads can maintain their high internal pH values after exposure to gastric fluids. Therefore, the internal pH of buffer-free and buffer-loaded hydrogel beads was periodically determined throughout the stomach phase (**Fig. 5.8**). In the presence of buffer, the average pH inside the beads remained fairly constant (pH 6.6 to 7.5) throughout the entire 2 hour incubation period within the SGF (**Fig. 5.7**). This result suggested that the amount of $Mg(OH)_2$ inside the beads was sufficient to act as a local antacid throughout the duration of the gastric phase. On the contrary, the pH value inside the buffer-free hydrogel beads fell sharply from pH 6.5 to 3.3 within the first 5 minutes, followed by a more gradual decrease at longer incubation times. As mentioned earlier, small H^+ ions can rapidly diffuse into highly porous hydrogel beads, thereby causing the pH inside the beads to be fairly similar to that outside.

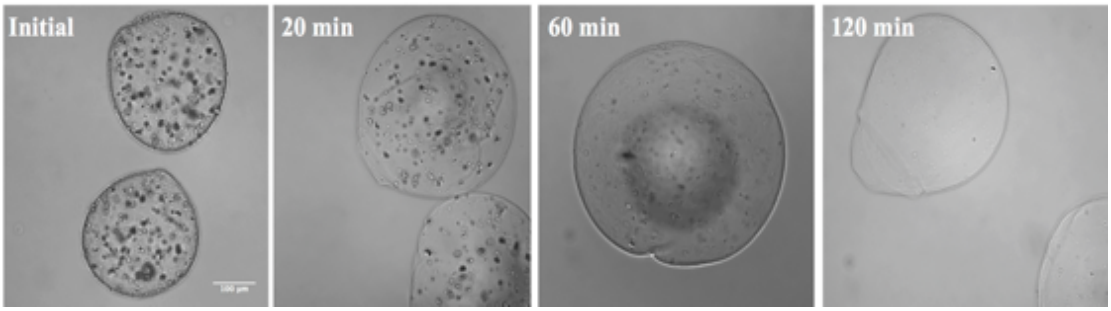

Figure 5. 8 Differential interference contrast (DIC) images of hydrogel beads containing encapsulated $Mg(OH)_2$ taken during incubation in the simulated stomach phase.

The amount of time required for hydrogen ions to diffuse into the hydrogel beads can be estimated from the following expression (Crank, 1975):

$$\Phi = \frac{M(t)}{M(\infty)} = 1 - \frac{6}{\pi^2}\sum_{n=1}^{\infty}\frac{1}{n^2}\exp\left(-\frac{D_{gel}n^2\pi^2 t}{a^2}\right) \quad (1)$$

Here, Φ is the fraction of hydrogen ions that have diffused into the hydrogel beads at time t, $M(t)$ and $M(\infty)$ are the hydrogen ion concentrations within the hydrogel beads at time t and at equilibrium, n is an integer, a is the radius of the hydrogel beads, and D_{gel} is the diffusion coefficient of the hydrogen ions through the biopolymer network inside the beads, which can be estimated using the following expression (Chan & Neufeld, 2009):

$$D_{gel} = D_w \exp\left(-\pi\left(\frac{r_H - r_f}{\xi + 2r_f}\right)\right) \quad (2)$$

Here, D_w is the diffusion coefficient of the hydrogen ions through pure water, r_H is the hydrodynamic radius of the hydrogen ions, r_f is the cross-sectional radius of the biopolymer chains (alginate) in the hydrogel network, and ζ is the mesh pore diameter of the hydrogel network. The following structural parameters have been reported for alginate hydrogels: pore diameter (ζ) = 4 to 400 nm; alginate chain radius (r_f) = 0.83 nm (Chan, et al., 2009). The radius of hydration (r_H) of the hydrogen ion (actually H_3O^+) has been estimated to be 0.1 nm (Marcus, 2012). The diffusion coefficient of hydrogen ions in water can be estimated from the expression: $D_w = k_B T/6\pi\eta r_H$, where k_B is Boltzmann's constant, T is absolute temperature, and η is the viscosity of the solvent. The above

equations were used to estimate the time-dependence of the fraction of hydrogen ions diffusing into hydrogel beads with different pore sizes after submerging in a more acidic environment (**Figure 5.9**). For these calculations, it was assumed that the pore diameter (ζ) of the alginate beads was 10 nm. Even assuming this relatively small pore size, the theoretical predictions suggest that the hydrogen ions would rapidly diffuse into the hydrogel beads in a few seconds, which supports our experimental results. These predictions suggest that any acid-sensitive bioactives encapsulated within the hydrogels beads would be rapidly exposed to highly acid conditions in the stomach in the absence of a co-encapsulated insoluble buffering agent.

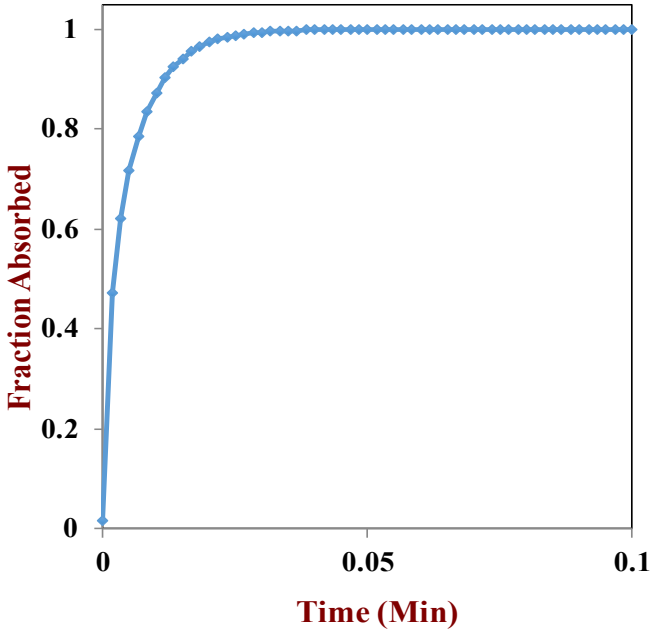

Figure 5. 9 Predicted time dependence of the fraction of hydrogen ions (H_3O^+) absorbed by alginate beads with a diameter of 200 μm and a pore size of 10 nm after submersion in an acidic environment.

5.1.4. Conclusions

Certain types of bioactive agents are degraded when exposed to highly acidic conditions, such as probiotics, enzymes, and some nutraceuticals. The development of microparticle-based delivery systems that are able to control the pH in the immediate vicinity of these bioactive agents may therefore be useful for improving their stability. In this study, edible hydrogel beads were fabricated using a simple injection method that

were able to maintain an internal pH that was appreciably higher than the pH of the surrounding solution. A fluorescence method to map the pH profile inside the hydrogel beads was also developed based on ratiometric imaging with a confocal laser scanning microscopy. This method showed that the average internal pH of the buffer-free hydrogel beads was around 6.5, while that of the buffer-loaded beads was around 7.5. In addition, the method showed that there were some local variations in pH inside the hydrogel beads. After exposure to simulated gastric fluids, the average pH inside the buffer-loaded beads remained fairly constant (around pH 6.6 to 7.5), whereas that in the buffer-free beads fell sharply within the first few minutes (from pH 6.5 to 3.3). The confocal microscopy method also indicated that the pH was higher in the center of the buffer-loaded beads than at their edges. These results show that the encapsulated $Mg(OH)_2$ particles acted as effective buffering agents that inhibited excessive acidification within the beads during the gastric phase. Overall, the novel hydrogel beads developed in this study may be suitable for encapsulation and delivery of acid-sensitive bioactives, which may be advantageous for certain food, supplement, and pharmaceutical applications.

5.2 Encapsulation of pancreatic lipase in hydrogel beads with self-regulating internal pH microenvironments: Retention of lipase activity after exposure to gastric conditions

5.2.1 Introduction

Exocrine pancreatic insufficiency (EPI) is a serious condition occurring accompanied with a several diseases (e.g., chronic pancreatitis and pancreatic cancer, etc.) [260-261]. EPI happens due to the pancreas of the patients fails to produce and/or secrete sufficient amounts of digestive enzymes to support digestion of intraluminal nutrients such as fats, proteins and carbohydrates, which results in the nutritional deficiencies of the patients [262]. The digestive enzymes normally refer to the trypsin, chymotrypsin, amylase and lipase. Lipase is one of the most important digestive enzymes derived from the pancreas and it plays a leading role in the digestion of fat, which provide the majority of calories for human body [263]. Enzyme supplementation is an important therapy for pancreatic insufficiency [264]. However, the supplementation of lipase by direct oral intake is unpractical because this enzyme is extremely susceptible to acidic degeneration during stomach incubation process. In healthy people, it was reported that just 1% of the lipase activity can survive through intestinal transit [265]. Thus the entrapment strategies are required for the lipase encapsulation and delivery.

Encapsulation of enzymes within porous polymer matrices have been widely utilized for many years to improve the stability and recovery of enzymes [6, 266]. In this techniques, the enzymes can be trapped within a porous matrix, which provide the enzyme with physical isolation from the surrounding medium. Several entrapment methods can be included for enzymes encapsulation such as physical entrapment, physical bonding, and/or chemical covalent bonding [267-268]. The physical approaches may have potential advantages over chemical methods because no chemical modification of the enzyme is required to form a covalent linkage with the hydrogel network. These physical approaches normally enable the enzymes to interact with the substrate molecules without causing pronounced changes in enzyme structure and activity, and thus are regarded as the best strategy for enzyme encapsulation. Hydrogel beads fabricated from biopolymers are particularly suitable for the enzyme encapsulation, because they often involve mild

preparation conditions to physical entrap the enzyme without altering their properties [269]. Moreover, the bead matrices can be prepared from food-grade ingredients (e.g., polysaccharides and/or proteins), which are more acceptable by majority of people [229]. The hydrogel beads are commonly fabricated using extrusion-gelation method. In this approach, a biopolymer solution containing the bioactive agents (e.g., enzyme) is injected into another "harden" solution to promote the biopolymer gelation, and the hydrogel beads can be formed during this procedure with bioactives trapped inside the biopolymer matrix [270]. One major drawback associated with the use of conventional hydrogel beads for lipase encapsulation and intestine target delivery is that the polymer matrix of these beads are highly porous, which allow the acid ions (H^+) easily diffuse in and out the beads network, thereby may hardly inhibit the encapsulated lipase from acid deactivation during stomach digestion process. Researches have been carried out to modify the properties of hydrogel beads to improve the pH-stability of encapsulated enzyme, such as by crosslinking the hydrogel matrix using specific enzymes or by coating the beads with one or more layers of biopolymers through electrostatic deposition [271-272]. The mechanism of these approaches are based on delaying the diffusion of pH determining ions (H^+ or OH^-) through the bead matrix [273]. However, there are several other limitations associated with these modifications, the most important one is that the function of encapsulated enzyme can be negatively interfered; because the diffusion of the enzyme and substrate can also be retarded at the desired site of action, which limit their mutual contaction and further hydrolysis reaction.

In this study, we fabricated a novel hydrogel beads with an internal pH self-regulating property. Specially, $Mg(OH)_2$ as the buffer agent was co-encapsulated with lipase into the hydrogel beads formed by alginate crosslinking with calcium chloride. $Mg(OH)_2$ was used because it was typical insoluble salts at neutral pH condition, which make it possible to be trapped inside the beads during storage; while it can be dissolved at acid condition and thus can be used as an antacid agent at low pH conditions. Moreover, $Mg(OH)_2$ has been regarded as the safe ingredient and widely used as an acid neutralize agent in food and pharmaceutical industries [274]. Alginate was used for hydrogel beads formation because it is a food-grade ingredient already widely utilized for bioactive agent

encapsulation. The mild cross-linking conditions of alginate gel are especially suitable for the enzyme entrapment and encapsulation. Furthermore, the acid insolubility of alginate gels makes them a good candidate for bioactives encapsulation and target delivery in harsh acid condition (e.g., the stomach) with improved stability. The digestion characteristic of lipid by the lipase loaded in the hydrogel beads with/without $Mg(OH)_2$ co-encapsulation was compared. An in vitro model developed in our lab was used to simulate the digestion conditions in mouth, stomach and small intestine. The microclimate pH change of the hydrogel beads after going through different digestion steps was also estimated using a quantitative ratiometric method based on confocal laser scanning microscopy (CLSM). The results obtained from this study may provide valuable information for lipase encapsulation and target delivery.

5.2.2 Materials and methods

5.2.2.1 Materials

Fluorescein tetramethylrhodamine dextran (FRD, average M_r 70,000) was obtained from Molecular Probes (Eugene, OR). Alginic acid (sodium salt), calcium chloride, and magnesium hydrate were purchased from Sigma Chemical Company (St. Louis, MO). Lipase was purchased from Sigma-Aldrich (Sigma Chemical Co., St. Louis, MO) and as reported by the manufacturer the activity was 100-400 units/mg. Mucin from porcine stomach, porcine bile extract, sodium chloride, monobasic phosphate and dibasic phosphate, Nile red and fluorescein thiocyanate isomer I (FITC) were obtained from either Sigma-Aldrich (Sigma Chemical Co., St. Louis, MO) or Fisher Scientific (Pittsburgh, PA). All chemicals used were analytical grade. Double distilled water was used to make all solutions.

5.2.2.2 Hydrogel beads preparation

The alginate aqueous solution was prepared by dissolving powdered alginic acid (1.6%, w/w) in phosphate buffer and continuously stirring at 60 °C for an hour, then reducing the temperature to 35 °C with continuously stirring until totally dissolved. The alginate solution was then mixed with lipase solution to obtain a concentration of 0.8%

alginate and 2.7% lipase mixture with or without 0.15% $Mg(OH)_2$. For the pH mapping, 10 mg/mL FRD in phosphate buffer was added to the 0.8% alginate solution (at a volume ratio of 1:200) with or without 0.15% $Mg(OH)_2$. After continuously stirring, the mixtures were injected into 10% calcium chloride solution using a commercial encapsulation unit (Encapsulator B-390, BUCHI, Switzerland) with a 120 mm vibrating nozzle to prepare the hydrogel beads. The encapsulation device was operated under fixed conditions: frequency 800 Hz; electrode 800 V; and pressure 500 mbar. The formed beads were held in the Ca^{2+} solution for 30 min at ambient temperature to promote cross-linking.

5.2.2.3 In vitro digestion model

The lipase-loaded hydrogel beads with or without buffer (0.15% $Mg(OH)_2$) co-encapsulation were passed through a gastrointestinal tract (GIT) model that simulated the mouth, stomach and small intestine, which was slightly modified from the one developed in our lab [230]. The free lipase without beads encapsulation was also studied as the control sample passing through the same digestion model.

Initial system: 7.5 g of the initial systems were placed into a glass beaker in an incubator shaker at a rotation speed of 100 rpm for 15 min at 37 °C for preheating. Two different initial lipase-loaded delivery systems were tested: with or without buffer co-encapsulation.

Mouth phase: 7.5 g of simulated saliva fluid (SSF) containing 0.03 g/mL mucin was preheated to 37 °C and then adjusted to pH 6.8. After being mixed with the initial samples, the mixture was incubated in an incubator shaker for 2 min at 37 °C to mimic agitation in the mouth.

Stomach phase: 15 g of simulated gastric fluid preheated to 37 °C, and the pH was adjusted to 2.1. After being mixed with 15 g of the “bolus” sample resulting from the mouth phase, the initial pH of the mixture was about 2.5 and incubated in the incubator shaker for 2 h at 37 °C to mimic stomach conditions.

Small intestine phase: 30 g of "chyme" sample from the stomach phase was placed into a 100 mL glass beaker that was placed into a water bath at 37 °C and then adjusted to pH 7.00. 1.5 g of simulated intestinal fluid was added to the reaction vessel, followed by 3.5 g of bile salt solution with constant stirring. The pH of the reaction system was adjusted back to 7.00. 2.5 g of 6% (w/w) corn oil-loaded emulsions was then added to the sample and an automatic titration unit (Metrohm, USA Inc.) was used to monitor the pH and maintain it at pH 7.0 by titrating 0.1 N NaOH solution into the reaction vessel for 2 h at 37 °C. The amount of free fatty acids released was calculated from the titration curves as described previously using the following formula:

$$\%FFA = 100 \times \left(\frac{V_{NaOH} \times m_{NaOH} \times M_{Lipid}}{W_{Lipid} \times 2}\right) \quad \ldots\ldots\ldots\

were taken and analyzed using image analysis software (NIS- Elements, Nikon, Melville, NY, USA).

5.2.2.2.5 Standard curve preparation

The stock FRD solution (10 mg/mL) was prepared by dissolving the powdered FRD dye in phosphate buffer (5mM, pH 7) solution. 5 µL/ml FRD stock solution at pH 4–7 (adjusted by hydrochloric acid) was imaged using confocal microscope to determine the linear range of pH response.

5.2.2.2.6 Image processing for pH measurement

The images were analyzed using the Image J software (1.50I). The ratio of pixel intensities of two images obtained from two wavelengths (488 nm, 543 nm) were calculated and correlated with pH from the obtained standard curve. The images were processed by repeated scan with frame averaging from at least eight measurements.

5.2.2.2.7 Determination of droplet size

The particle size distribution of the hydrogel beads with/without $Mg(OH)_2$ co-encapsulation initially and after stomach digestion was determined using a laser diffraction device (Mastersizer 2000, Malvern Instruments Ltd., Malvern, Worcestershire, UK), which utilizes measurements of the angular scattering pattern of emulsions. Samples were diluted in aqueous solutions to avoid multiple scattering effects, and then stirred (1200 rpm) to ensure homogeneity. Phosphate buffer (5 mM, pH 7.0) was used to dilute the initial samples, while pH 2.5 adjusted distilled water was used to dilute stomach samples. The average particle sizes are reported as the volume-weighted mean diameter (d_{43}).

5.2.2.2.8 Statistical analysis

All experiments were performed on at least three freshly prepared samples. The results are reported as averages and standard deviations. These analyses were carried out using Excel (Microsoft, Redmond, VA, USA) and a statistical software package (SPSS).

5.2.3 Results and discussion

5.2.3.1 Development of the standard curve

In this study, mapping the pH values inside the beads is critical for the verification of antacid effect of our hydrogel beads during the digestion process. Therefore, a quantitative ratiometric method based on CLSM methods was developed to quantitatively measure the microclimate pH in the hydrogel bead matrix. Fluorescein and Tetramethylrhodamine (FRD), as the pH indicator dye, was used to estimate the pH change inside the beads during the whole digestion process. This fluorescent dye was selected because it has both pH-dependent (FITC) and pH-independent (TMR) fluorescence groups within its molecule structure, which enable the quantitatively measure the pH value based on the fluorescence intensity ratio with the elimination of the dye concentration effect [275-276]. Furthermore, these two fluorescence groups are conjugated to the dextran with relatively large molecule weight (around 70,000 Da), which ensures the entrapment of dye inside the beads during the measurement process. The ratiometric method has also been used for the pH measurements inside the pellets or microspheres by other studies, it was reported that this ratiometric method can eliminates the problems associated with variable microsphere or pellet matrix thickness, and non-uniform indicator distribution within the microsphere or pellet because of loading efficiency variations [277-279].

It was indicated based on the preliminary studies that the emission intensity obtained from the FITC channel was correspondingly increased for the dye incubated in higher pH buffer, while the emission intensity of TMR channel remains at a constant value irrespective of change of stock buffer with different pH values (data not shown). The corresponding pH can therefore be obtained independent of dye concentration by taking the ratio of the emission intensities at these two channels (FITC/TMR). In this study, the standard curve of pH vs. intensity ratio was determined using standard pH buffer solutions of pH 4-7 (**Fig. 5.10**). Based on our previous studies, the TMR/FITC value was almost independent of the dye concentrations across the pH range of 2.5-7. Therefore, it can be estimated that the pH value inside the beads could still be quantitatively measured even though the leakage of the dye occurs during the fabrication and incubation.

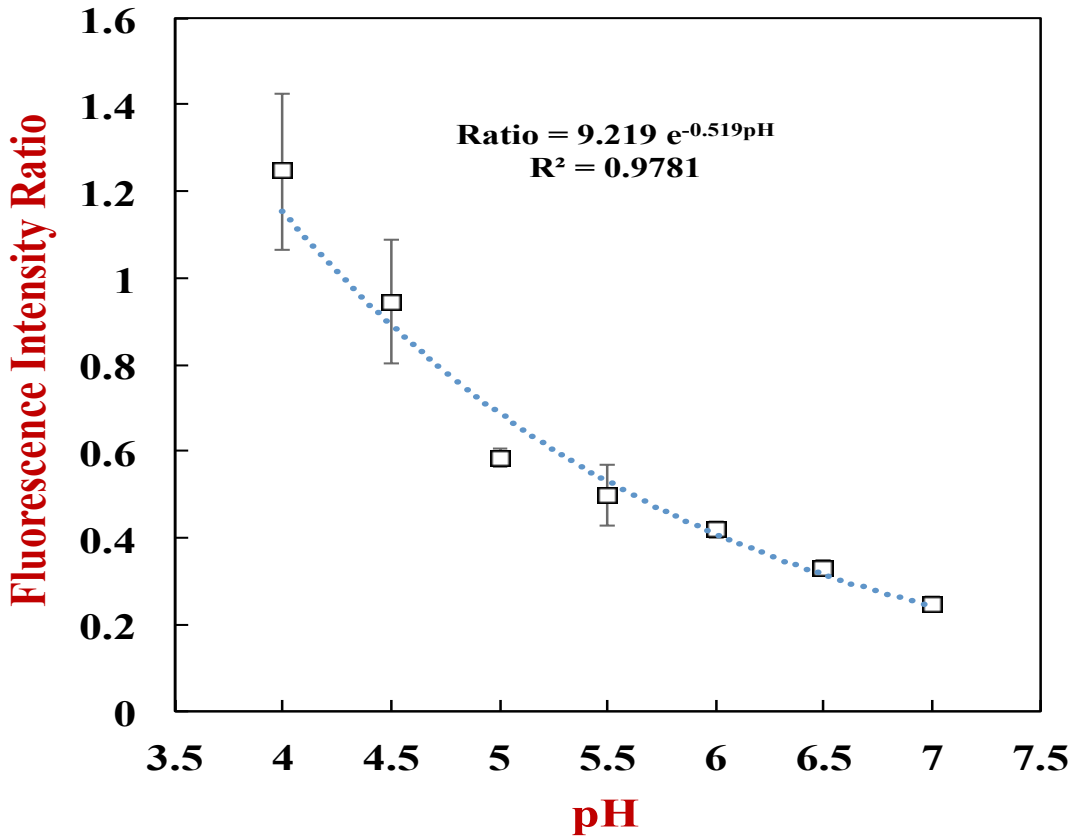

Figure 5. 10 Standard curve of pH vs. intensity ratio taken by 5 µL/ml stock solution (10mg/mL).

5.2.3.2 Mapping the pH inside the beads during digestion

An antacid buffer agent ($Mg(OH)_2$) was encapsulated within the hydrogel beads to adjust the internal pH inside the beads during the simulated digestion process. It was estimated that $Mg(OH)_2$ can be retained within the hydrogel beads with its intrinsic solid state at neutral condition, while partly dissolved and ionized the hydroxide ion (OH^-) when incubated at low pH conditions. Hydrogel beads fabricated at the same conditions without $Mg(OH)_2$ encapsulation were also studied as the control samples, and the pH value inside the beads with or without $Mg(OH)_2$ encapsulation during different steps of digestion process (i.e., mouth stomach and intestine) was measured based on the developed standard curve described in previous section.

It was indicated that the pH value inside the hydrogel beads remained fairly constant for the initial samples and the samples after incubation in mouth phase irrespective of

$Mg(OH)_2$ encapsulation (**Fig. 5.11, Fig. 5.12**). This result can be attribute to the reason that pH value in the initial phase and mouth phase was relatively similar with each other (pH around 7 for initial phase and 6.8 for mouth phase). The averaged internal pH of the hydrogel beads before and after mouth digestion was evaluated to be around pH 6.74 to 6.29 for buffer-free beads and pH 7.25 to 7.33 for buffer-loaded beads (**Table 5.1**). The encapsulated $Mg(OH)_2$ slightly increased the microclimate pH of the hydrogel beads, which can be attributed to the weak base characteristic of encapsulated $Mg(OH)_2$. The confocal fluorescent images also showed that the pseudo-color was constantly distributed within the buffer-free hydrogel beads, which indicated that the pH value was relatively uniform within these beads matrix (**Fig. 5.11**). For the $Mg(OH)_2$ encapsulated beads, the pseudo-color inside the beads was not evenly distributed. The insoluble $Mg(OH)_2$ particles showed higher pH value compared with surrounding solution based on the color strip (**Fig. 5.12**). These results again verify the weak base characteristic of encapsulated $Mg(OH)_2$. After incubation in simulated gastric fluids, the fluorescence intensity sharply decreased for the hydrogel beads without $Mg(OH)_2$ encapsulation. The pH was estimated to be acid value (lower than 4) based on the standard curve calculation. This result can be attributed that the hydrogen ions can diffuse through the pores of the hydrogel beads to balance the concentration between inside and outside the beads, thus equilibrium state was finally achieved after 2h stomach digestion process with a low pH value. On the contrary, it was showed that the pH value inside the buffer-loaded beads still remain relatively constant compared with initial value (around pH 7.39) after stomach digestion. It can be expected that $Mg(OH)_2$ particles slowly ionized and neutralized the hydrogen ions arising from the gastric fluids, which maintain the pH value inside the beads constant above 7.

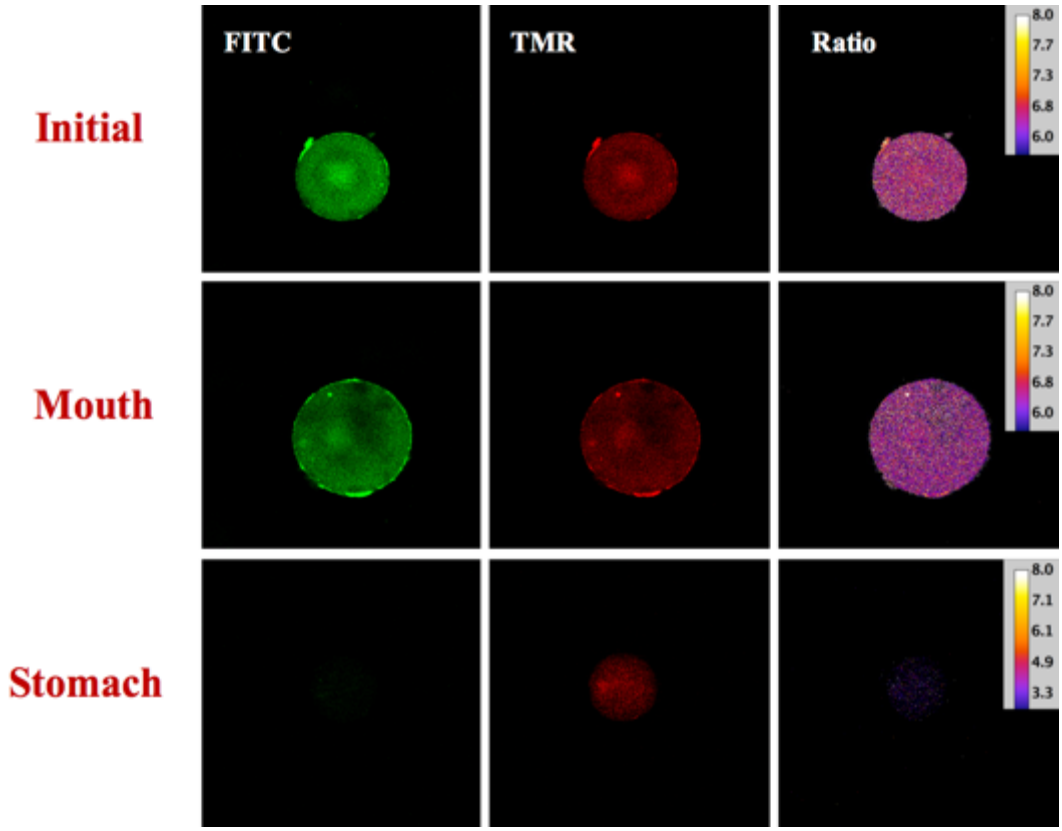

Figure 5. 11 Fluorescent images of hydrogel beads without buffer encapsulation during the digestion process (intensity of TMR signal was enhanced using Image J to improve contrast). The images of the TMR channel and FITC channel were emitted at 543 and 488 nm, detected at 650/LP and 590/50 nm respectively.

Table 5. 1 The measured pH value inside beads with/ without buffer co-encapsulation during digestion process

	Initial	**Mouth**	**Stomach**
Without buffer (pH)	6.74 ± 0.08	6.29 ± 0.104	pH < 4.0
With buffer (pH)	7.25 ± 0.106	7.33 ± 0.182	7.39 ± 0.15

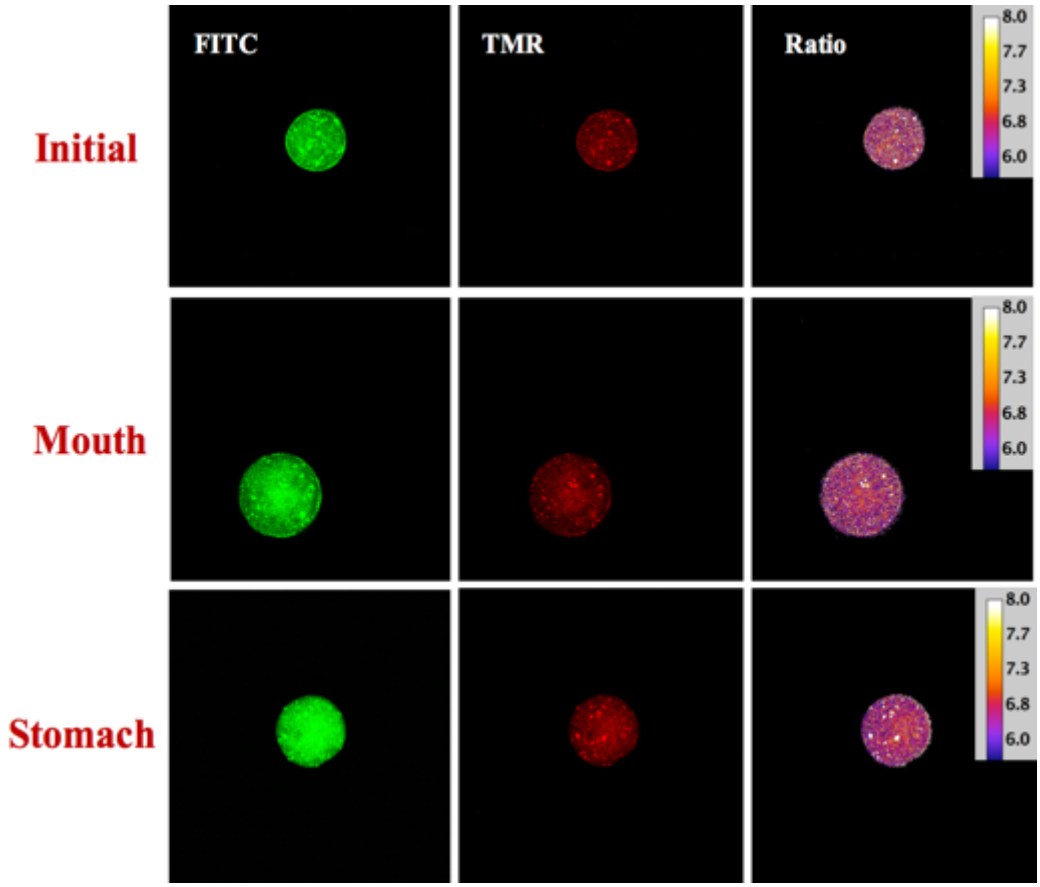

Figure 5. 12 Fluorescent images of hydrogel beads with buffer encapsulation during the digestion process (intensity of TMR signal was enhanced using Image J to improve contrast). The images of the TMR channel and FITC channel were emitted at 543 and 488 nm, detected at 650/LP and 590/50 nm respectively.

5.2.3.3 Influence of different beads encapsulation on lipid digestion

In this section, the influence of different beads encapsulation on lipid digestion was studied using an automatic titration ("pH-stat") method. Specifically, the lipase-loaded beads with or without $Mg(OH)_2$ co-encapsulation after the mouth and stomach digestion were incubated with oil in the simulated intestine phase. The amount of free fatty acids released over time was then calculated from the volume of NaOH titrated into the samples to maintain a constant pH value (7.0).

For the buffer free beads and free lipase samples, there is almost no free fatty acids released during the whole digestion process, which indicated that lipase has been already deactivated during the stomach digestion process even though encapsulated in the

hydrogel matrix (**Fig. 5.13**). The poor lipases activity at low pH has been attributed to the titration of the active site histidine or to the weakening of the coordination of stabilizing calcium ions [280]. It has been noted that the acid ions (H^+) can easily diffuse in the beads matrix and get access to the active site of lipase during stomach incubation. The lipid digestion profile of lipase-load beads with $Mg(OH)_2$ co-encapsulation is significantly different from buffer free one: a rapid increase in free fatty acids (FFAs) release can be detected within the first 45 min, and then followed by a more gradual increase until a relatively constant final value was attained. These results indicated the preservation of lipase activity when the $Mg(OH)_2$ was co-encapsulated into the beads.

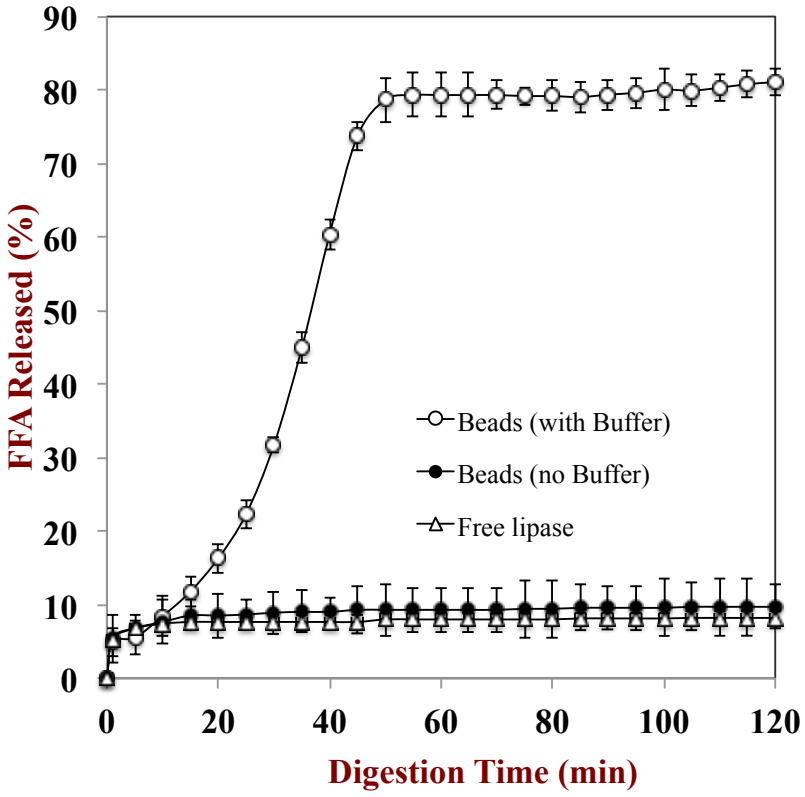

Figure 5. 13 Amount of free fatty acids released from the systems (free lipase and hydrogel beads with or without buffer co-encapsulation) using a pH-stat in vitro digestion model.

To visually testify the digestion process in the lipase-loaded beads, lipase was dyed to green and oil was dyed to red using FITC and Nile red respectively. The confocal microscopy images indicated that most of lipase molecules were trapped inside the hydrogel beads, *i.e.*, the green (lipase) fluorescence dyes were mostly located together in

the spheroid shape beads matrix (**Fig. 5.14)**. It suggested that large amount of lipase can be successfully delivered to intestine phase using hydrogel beads entrapment. The green fluorescence intensity can also be detected outside the beads in the surrounding intestine phase, which suggested that the lipase can partly release from the beads after intestine digestion. The alginate beads have been reported to swell when placed in higher pH solutions such as in intestine phase, because the alginate molecules become highly charged (carboxylate group) and repel with each other causing the hydrogel network to expand, thus the encapsulated lipase can partly release from the beads during intestine digestion process [23]. Furthermore, compared to the system without buffer, there was a decrease in the red fluorescence intensity of the surrounding aqueous phase in system with buffer, which is indicative of a reduction in the amount of lipids present the surrounding aqueous phase. It can be estimated based on the digestion profiles that the lipid droplets had been digested by lipase molecules with reserved activity released from buffer-loaded hydrogel beads. These results also indicated that co-encapsulation of $Mg(OH)_2$ within the lipase-loaded hydrogel beads can protect the lipase from deactivation during digestion process.

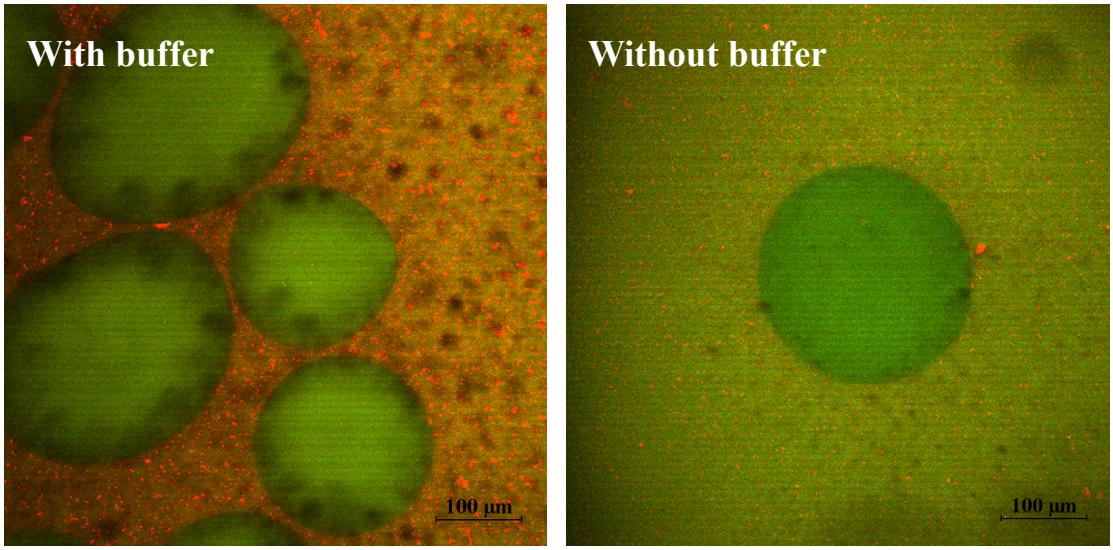

Figure 5. 14 Confocal microscope of lipase-loaded beads with and without buffer encapsulation after exposure to the small intestine phase for 2 hours. Lipase was dyed with FITC to show green fluorescence, while the lipid phase was dyed by Nile Red to show red fluorescence.

5.2.3.4 The particle size characteristic of beads during digestion

Alginate beads are regarded as a good polymer based acid indicator due to its pH dependent behavior. Calcium alginate matrix tend to shrink at acid condition because of the loss of negative charge on the alginate molecules when the carboxyl groups become protonated (–COOH, pK_a=3.5). Conversely, they will swell when incubated in higher pH solutions because of charge retrieve which has been discussed in the previous section. It is thus interesting to study the size characteristic of hydrogel beads with/without buffer co-encapsulation during the digestion process.

Based on the static light scattering measurements, it was indicated that the general shape of the particle size distribution was relatively similar from initial-to-stomach for the buffer-loaded bead, exhibiting a major population of large particles with diameters around 250μm (**Fig. 5.15**). The mean particle diameter of these beads was slightly decreased during this process (initial-to-stomach), i.e., from 264.2 to 244.5μm (**Fig. 5.16**). For the beads without buffer encapsulation, an obvious size reduction can be detected from the particle size distribution after stomach digestion, and the mean particle diameter of alginate beads sharply decreased from 273.5 to 208.5μm. These results indicated that the alginate beads can undergo swell to shrink transformation when the incubation pH reduced from neutral to acid (initial-to-stomach). Moreover, the buffer-loaded hydrogel beads could maintain the pH relatively constant during this digestion process, which restrained the shrink of hydrogel beads in acid stomach phase.

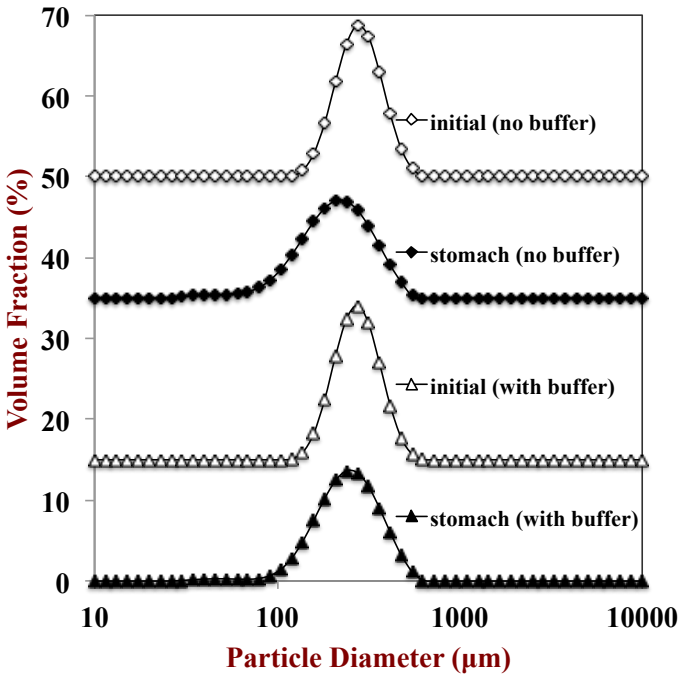

Figure 5. 15 Particle size distributions of different samples initially and after the stomach digestion process.

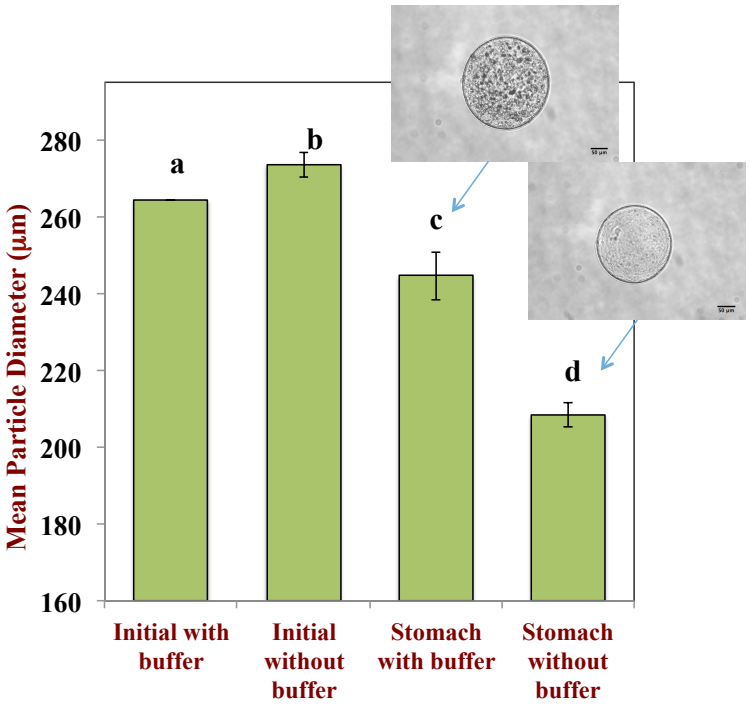

Figure 5. 16 Mean particle diameter (d_{43}) of different samples initially and after the stomach digestion process.

5.2.4 Conclusions

It is an important challenge to stabilize lipase inside any carriers during the digestion process. In this study, alginate based hydrogel beads were fabricated based on injection-gelation method to encapsulate the lipase, the buffer agent ($Mg(OH)_2$) was also co-encapsulated in these beads to adjust the microclimate pH inside beads during the simulated digestion process. The fluorescence pH measurements based on laser scanning confocal microscope indicated that the pH value inside the buffer free beads was sharped decreased to acid condition after stomach digestion. For the buffer-loaded beads, the pH value was measured to be fairly constant from initial-to-stomach. The lipase-loaded beads with buffer co-encapsulation clearly had a pronounced impact on the rate and extent of lipid digestion. Conversely, for the lipase-loaded alginate beads without buffer encapsulation, no lipid digestion occurred by the end of the 2 h digestion period. The particle size of buffer free beads was greatly reduced during the digestion process (initial-to-stomach), while the size remains relatively similar for the buffer-loaded beads. These results indicated that $Mg(OH)_2$ can work as an effective buffer agent against acidification in stomach phase, the lipase-loaded hydrogel beads with $Mg(OH)_2$ co-encapsulation can reserve the activity of lipase during the digestion.

5.3 Lactase (β-galactosidase) encapsulation in hydrogel beads with controlled internal pH microenvironments: Impact of bead characteristics on enzyme activity

5.3.1 Introduction

Lactose intolerance is a common disease in humans that is associated with the deficiency of a specific enzyme (β-galactosidase) produced within the brush border of the small intestine [281-282]. Individuals with lactose intolerance have a limited ability to digest and absorb lactose in the small intestine. As a result, this disaccharide enters the colon in an undigested form where it can promote health problems, such as gut distension, stomach pain, flatulence, diarrhea, and nausea [283]. Individuals who suffer from lactose intolerance often avoid consuming milk and other dairy products so as to avoid exhibiting these undesirable symptoms. Several other approaches have also been developed to aid individuals with lactose intolerance, including creating lactose-free foods and the co-ingestion of lactase supplements with lactose-containing foods [284]. Enzyme supplement treatments are particularly promising because they do not cause undesirable changes in food quality or nutritional profile. Typically, a tablet or capsule containing lactase is taken at the same time as a lactose-containing food, which promotes lactose hydrolysis within the gastrointestinal tract (GIT). β-galactosidase (β-gal) is the most common form of lactase used in enzyme supplements, but it cannot simply be delivered in its free form because it is highly susceptible to denaturation and deactivation under GIT conditions [285]. In particular, lactase is usually deactivated when exposed to the highly acidic gastric fluids present within the human stomach [286].

The encapsulation of enzymes within porous matrices can improve their stability by creating a protective microenvironment or by acting as a physical barrier to the external environment [287-288]. At the same time, the porous matrices can be designed to allow small molecules (such as co-factors, substrates, and products) to easily diffuse into them and reach the catalytic site of the encapsulated enzyme, which enables the enzyme to maintain its activity even after encapsulation [6, 289]. Enzymes can be encapsulated within

porous matrices using physical entrapment, physical interactions, or chemical bonding [267-268]. The encapsulation of enzymes in hydrogels is particularly attractive for application in the food industry because these semi-solid materials can be fabricated from food-grade ingredients using simple processing operations [270]. Enzymes are physically entrapped in the hydrogel network during the sol-gel transition, which is a relatively mild process that tends to preserve the structural integrity and activity of the enzymes. After fabrication, the enzymes can be retained within the hydrogel matrix by ensuring that its pore size is appreciably smaller than the enzyme dimensions, or by ensuring that there is a sufficiently strong attraction between the enzymes and the hydrogel matrix.

For many applications it is desirable to utilize hydrogel beads, rather than bulk hydrogels to encapsulate and deliver bioactive substances [6]. Hydrogel beads consist of small particles (typically from 100 nm to 1000 μm) that can easily be dispersed in aqueous solutions. These beads can be fabricated from food-grade biopolymers (typically polysaccharides and/or proteins) using simple processing operations, such as the injection-gelation method [229, 269, 290-291]. Typically, the formation of hydrogel beads requires two-steps that may occur consecutively or simultaneously: particle-formation and particle-gelation. For the injection-gelation method, particle-formation is performed by injecting an aqueous solution containing a biopolymer (gelling agent) and a bioactive agent (enzyme) into a gas or immiscible liquid, and then particle-gelation is performed by exposing the particles formed to solution or environmental conditions that promote biopolymer gelation. This process leads to the formation of hydrogel beads with bioactives trapped inside a biopolymer matrix [76]. A serious limitation of this approach for the encapsulation of acid-sensitive enzymes (such as lactase) is that small hydrogen ions (H^+) can easily diffuse through the biopolymer network inside the hydrogel beads, thereby inducing enzyme deactivation. For this reason, a number of research groups have tried to improve the acid-resistant characteristics of hydrogel beads, *e.g.,* by reducing the pore size of the biopolymer network or by coating the beads with biopolymer layers [271-272]. However, these approaches are often unsuccessful because the hydrogen ions are so small that they can still easily penetrate through the biopolymer networks that make up the hydrogel core or shell.

In the present study, an alternative approach was used to create hydrogel beads that would protect enzymes from acid-induced deactivation when exposed to gastric conditions. The enzyme (lactase) was co-encapsulated with magnesium hydroxide (a basic buffer) inside the hydrogel beads. $Mg(OH)_2$ was selected as a buffering agent because it is a widely used food-grade antacid, which is insoluble in water at neutral and basic pH values, but soluble at acidic pH values [274]. When these buffer-loaded hydrogel beads are dispersed in an acidic solution, the pH inside them remains close to neutral for an extended period. This phenomenon occurs because as hydrogen ions (H^+) from the surrounding aqueous phase diffuse into the hydrogel beads they cause some of the $Mg(OH)_2$ to dissociate, which generates hydroxyl ions (OH^-) that neutralize any pH changes. Moreover, it has been widely proven that the presence of Mg^{2+} can also increase the activity of lactase (Juers, et al., 2009), which should be another advantage of co-encapsulation with lactase. The hydrogel beads were fabricated by an injection-gelation method using an anionic polysaccharide (κ-carrageenan) as the gelling agent and a cationic mineral ion (potassium) as a cross-linking agent. This polysaccharide was selected because it was previously shown that relatively high encapsulation efficiency (around 63%) can be achieved by the carrageenan beads. In addition, β-gal encapsulated within potassium-carrageenan beads had a higher activity than the free enzyme due to the stabilization effects of K^+ ions on enzyme structure [266]. The ability of the buffer-loaded hydrogel beads to protect lactase from acid-induced deactivation was demonstrated by exposing them to simulated gastric conditions. A quantitative ratiometric fluorescence method based on confocal laser scanning microscopy (CLSM) was also used to map the pH inside the beads before and after exposure to gastric conditions. This study provides information that can be used to facilitate the fabrication of hydrogel beads designed to encapsulate and deliver acid-labile enzymes and other bioactive agents.

5.3.2 Materials and methods

5.3.2.1 Materials

Fluorescein tetramethylrhodamine dextran (FRD) with an average molecule weight of around 70 kDa was purchased from Molecular Probes (Eugene, OR). Lactase (β-

galactosidase) with a specific activity of around 2600 U/g was obtained from Sigma Chemical Co (St. Louis, MO, USA). Carrageenan was kindly donated by FMC Biopolymer (Viscarin SD 389, Philadelphia, PA). The reagents o-nitrophenol (o-NP) and o-nitrophenyl-b-d-galactosidase (o-NPG) were obtained from the Sigma Chemical Co. (St. Louis, MO, USA). All chemicals used were analytical grade. Double distilled water was used to prepare all solutions.

5.3.2.2 Hydrogel beads preparation

An aqueous κ-carrageenan (2% w/v) solution was prepared by dissolving the powdered ingredient in distilled water by stirring at 50 °C for an hour, and then reducing the temperature to room temperature with continuous stirring until fully dissolved. The κ-carrageenan solution was then mixed with β-gal solution to obtain a concentration of 1% κ-carrageenan and 130 U β-gal mixture with or without different amount of $Mg(OH)_2$ co-encapsulation. After continuously stirring, the mixtures were injected into 10% potassium chloride solution using a syringe or a commercial encapsulation unit (Encapsulator B-390, BUCHI, Switzerland) with a 150 μm vibrating nozzle to prepare the hydrogel beads. The encapsulation device was operated under the following conditions: frequency 800 Hz; electrode 750 V; and pressure 450 mbar. The formed beads were held in the K^+ solution for 30 min at ambient temperature to promote bead hardening.

5.3.2.3 Simulated gastric conditions

A simulated stomach model was used to investigate the influence of exposure to acidic gastric fluids on the internal pH and lactase activity of the hydrogel beads as described previously [230]. Hydrogel beads (with or without $Mg(OH)_2$) were added to preheated simulated gastric fluids (pH 2.5, 37 °C) at a ratio of 1:4 (w/w). This mixture was then incubated in an incubated shaker for 2 h at 37 °C to mimic stomach conditions.

5.3.2.4 Local pH determination by confocal laser scanning microscopy

The fluorescence images were obtained using confocal laser scanning microscopy with a 20 × objective lens (Nikon D-Eclipse C1 80i, Nikon, Melville, NY, USA). The

images of the fluorescence probe (FRD) were obtained using emission wavelengths of 543 and 488 nm, and detection wavelengths/bandwidths of 650 nm/LP and 590 nm/50 nm, respectively. All samples were imaged using an exposure time of 0.5 s and a 12.5% excitation power level. The complete images of each sample were typically acquired in less than 2 min with at least eight measurements. The microstructural images for confocal microscopy were acquired using image specialized software (NIS-Elements, Nikon, Melville, NY, USA).

A stock FRD solution (10 mg/mL) was prepared by dissolving powdered FRD dye in phosphate buffer (5mM, pH 7) solution. 5 μL/ml of FRD stock solution was dissolved in a series of phosphate buffer solutions with different pH values and imaged using confocal microscopy to determine the linear range of pH response.

The confocal microscopy images were analyzed using Image J software (1.50I, imagej.nih.gov). The ratio of pixel intensities of images taken using two wavelength channels (488 nm, 543 nm) was calculated and correlated to the pH using the standard curve. Each pH value was estimated from at least eight measurements.

5.3.2.5 Measurement of lactase activity

The relative activity of β-gal encapsulated in hydrogel beads that was retained after different incubation times in simulated gastric fluids was assayed using a colorimetric test with o-NPG as a substrate. Filtered beads were added to 2 mL of o-NPG in phosphate buffer (0.3 mg/ml) to reach a final alginate to o-NPG ratio of 1:40 (v/v). The formation rate of free o-NP was recorded by measuring the absorbance (λ = 420 nm) of solutions contained in a 1-cm path length cuvette using a UV-visible spectrophotometer. The relative activity of encapsulated lactase was calculated based on the conversion rate of the substrate (o-NPG) into the reaction products (o-NP) initially and after stomach phase incubation. At least three freshly prepared samples were used for the activity measurements.

5.3.2.6 Measurement of bead dimensions

The particle size distribution of the small beads was measured using laser diffraction (Mastersizer 2000, Malvern Instruments Ltd., Malvern, Worcestershire, UK), which is based on analysis of the angular scattering pattern of particulate suspensions. Samples were diluted in aqueous buffer solutions to avoid multiple scattering effects, and then stirred (1200 rpm) to ensure homogeneity. The diameter of the large beads was measured using a digital micrometer (0–300 mm, EC10, High Precision Digital Caliper, Tresna Instruments, Guilin, China). The bead diameter of at least 5 individual beads was measured, and the mean and standard deviation were calculated from at least three measurements.

5.3.2.7 Statistical analysis

All experiments were performed on at least three freshly prepared samples. The results are reported as means and standard deviations. These analyses were carried out using Excel (Microsoft, Redmond, VA, USA) and a statistical software package (SPSS).

5.3.3. Results and discussion

5.3.2.1 pH Mapping inside the beads

Knowledge of the local pH inside the hydrogel beads is required to better understand the ability of buffer-loaded beads to protect lactase from acid-induced deactivation in simulated gastric fluids. A pH-sensitive fluorescence probe (FRD) was therefore used to estimate the internal pH of the beads using a ratiometric fluorescence method. FRD has both pH-dependent (FITC) and pH-independent (TMR) fluorescence groups within its molecular structure [275-276]. Consequently, the local pH can be determined by calculating the ratio of fluorescence intensities arising from the FITC and TMR groups. In this study, the FRD was conjugated to a large molecular weight dextran (70 kDa) to ensure that the fluorescence dye remained trapped inside the hydrogel beads.

The confocal fluorescence microscopy measurements indicated that the emission intensity from the FITC channel (488 nm) decreased when the fluorescent dye was

incubated in lower pH buffers, while the emission intensity from the TMR channel (543 nm) remained relatively constant (**Fig. 5.16**). A standard curve of fluorescence intensity ratio *versus* pH (from pH 4 to 7) was then obtained by taking the ratio of the emission intensities for the FITC/TMR channels (data not shown). The pH value inside the hydrogel beads could then be determined from the confocal fluorescence microscopy images using this calibration curve.

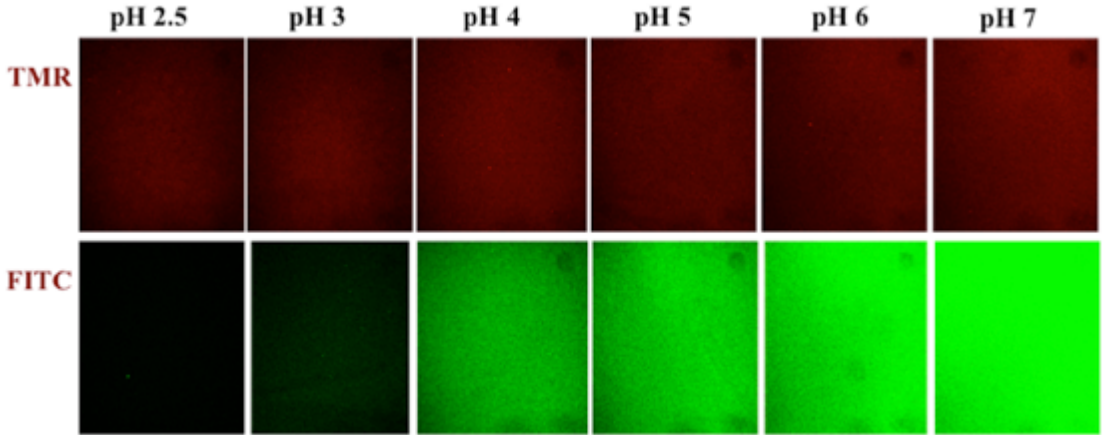

Figure 5. 17 Fluorescent images of fluorescence probe dispersed in phosphate buffer solutions with different pH values. The images in the top row (TMR channel) and bottom row (FITC channel) were represent the fluorescence intensity using emulsion wavelengths of 543 and 488 nm, and detection wavelengths of 650 and 590 nm, respectively**.**

Confocal microscopy images of the hydrogel beads were taken before and after exposure to simulated gastric fluids (**Figs. 5.17** and **5.18**). For the buffer-free beads, the fluorescence intensity of the FITC channel (pH-dependent) changed from relatively strong before exposure to very weak after exposure, which is indicative of a substantial reduction in the internal pH of the beads based on the calibration curve (**Fig. 5.17**). The interior of the buffer-free beads was calculated to be around pH 6.9 before exposure, and below the limit of detection (pH < 4) after exposure. These results suggest that the hydrogen ions (H^+) from the acidic gastric fluids rapidly diffused into the hydrogel beads and decreased their internal pH. Conversely, for the buffer-loaded beads, the fluorescence intensity of the FITC channel only decreased slightly after incubation in simulated gastric fluids (**Fig. 5.18**). Indeed, the interior of the buffer-loaded beads changed from around pH 7.2 before exposure to around pH 6.6 after exposure. As mentioned earlier, this effect can be attributed to the fact that the encapsulated $Mg(OH)_2$ is insoluble under neutral

conditions, but dissolves under acidic conditions. Consequently, when hydrogen ions from the gastric fluids diffuse into the hydrogel beads, some of the $Mg(OH)_2$ dissolves, which generates OH^- ions that neutralize the H^+ ions, thereby maintaining a neutral pH inside the beads. Presumably, there was sufficient magnesium hydroxide initially present within the hydrogel beads to counteract all the hydrogen ions arising from the gastric fluids.

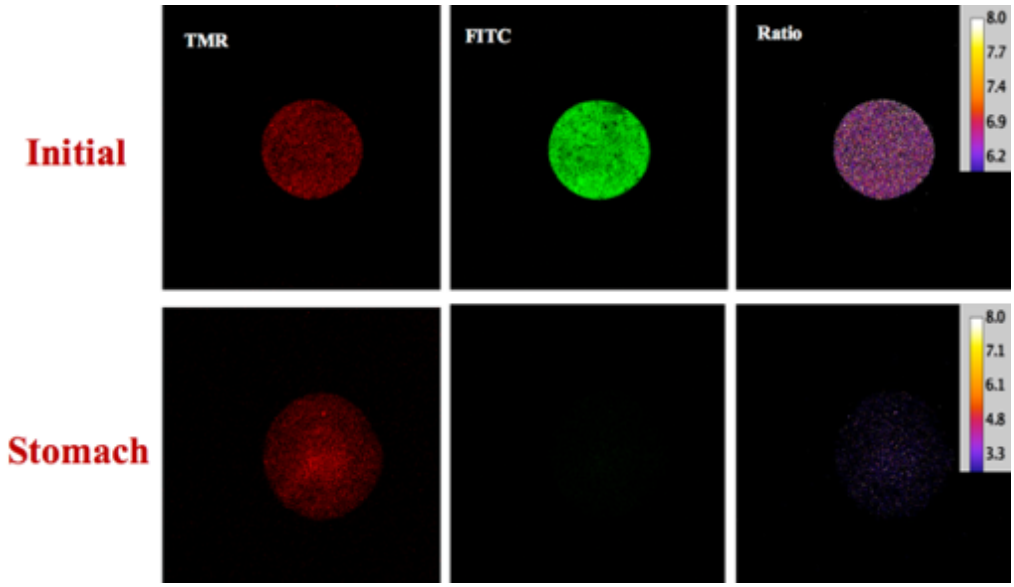

Figure 5. 18 Fluorescent microscopy images of hydrogel beads without $Mg(OH)_2$ encapsulation before and after stomach digestion. The images of the ratio channel were generated using Image J software (imagej.nih.gov) and the color strip shown on the top right represents the pseudocolor change with pH (intensity of TMR signal was enhanced using Image J to improve contrast).

5.3.2.2 Influence of encapsulation on enzyme activity: Spectrophotometric assay

The local pH that lactase experiences within the stomach phase influences its molecular conformation and enzyme activity. For this reason, the activity of lactase encapsulated in hydrogel beads containing different amounts of co-encapsulated $Mg(OH)_2$ was measured after incubation in simulated gastric fluids. The impact of bead dimensions on enzyme activity were determined by fabricating large and small hydrogel beads using either a simple syringe or a dedicated encapsulation unit, respectively. The hydrogel beads were then incubated in simulated gastric fluids for different times, and the enzyme activity was measured using a spectrophotometric method.

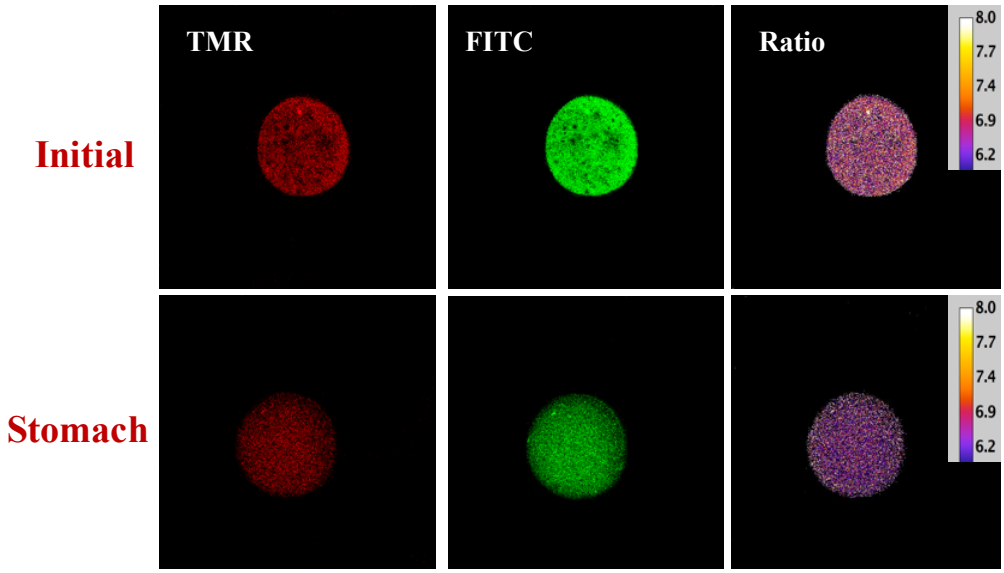

Figure 5. 19 Fluorescent microscopy images of hydrogel beads containing 0.6% $Mg(OH)_2$ before and after stomach digestion. The images of the ratio channel were generated using Image J software (imagej.nih.gov) and the color strip shown on the top right represents the pseudocolor change with pH (intensity of TMR signal was enhanced using Image J to improve contrast).

For both sizes of buffer-free beads, lactase activity was completely lost after 5 min incubation in simulated gastric fluids (**Figs. 5.20** and **5.21**). Presumably, this type of hydrogel bead was unable to prevent acid-induced loss of lactase activity because small H^+ ions easily diffuse through the pores in the biopolymer matrix and rapidly reduced the internal pH [292]. Conversely, for the buffer-loaded beads, the activity of the encapsulated enzyme depended on both the level of $Mg(OH)_2$ present and the bead dimensions (**Figs. 5.20** and **5.21**). Lactase activity decreased steeply after 5 minutes incubation for large buffer-loaded beads containing only 0.06% or 0.1% $Mg(OH)_2$, with a complete loss of enzyme activity after 25 min incubation (**Fig. 5.20**). These results suggest that there was insufficient buffer present inside the beads to completely neutralize all the hydrogen ions (H^+) that diffused into them. At 0.15% and 0.3% $Mg(OH)_2$, the enzyme activity within the large buffer-loaded beads remained > 60% after 120 min incubation (**Fig. 5.22**), which indicated that these systems were effective at preventing the acid-denaturation of lactase. This effect can be attributed to their ability to maintain a relatively high pH inside the hydrogel beads. For the small buffer-loaded beads, a higher amount (0.6 or 0.8%) of

$Mg(OH)_2$ was needed to maintain a reasonable level of enzyme activity at the end of the gastric phase (26 or 42% respectively) (**Figs. 5.21 and 5.22**). The observed impact of hydrogel bead dimensions on the activity of the enzyme can be attributed to the shorter distance that the H^+ ions have to diffuse into smaller beads (see later).

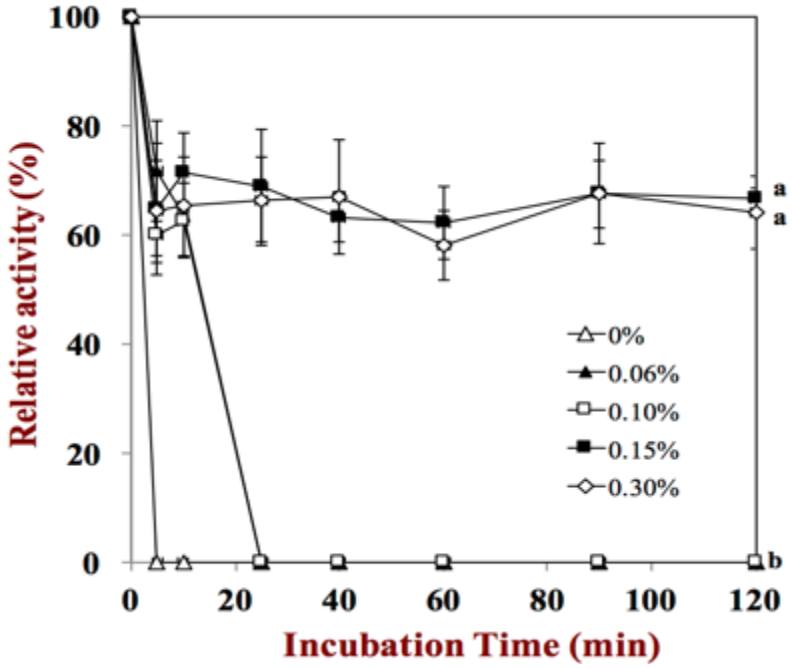

Figure 5. 20 The relative activity of β-galactosidase encapsulated in large hydrogel beads after incubation in simulated gastric fluids for different times. The enzyme was encapsulated in hydrogel beads containing different amounts of $Mg(OH)_2$ (0 to 0.30%). Samples designated with different capital letters (a, b) were significantly different (Duncan, $p < 0.05$) when compared between different delivery systems for the final point (120 min).

5.3.2.3 Influence of encapsulation on enzyme activity: Visual appearance

Additional insights into the impact of encapsulation on the stability of lactase was obtained by measuring changes in the appearance of hydrogel bead suspensions incubated at pH 2.5 (gastric) and pH 7.0 (intestinal) in the presence of a lactase substrate (o-NPG). Photographic images of the samples were taken periodically to indicate color changes during incubation: an increase in the intensity of the yellow color of the samples is an indication of a higher conversion of o-NPG to galactose o-NP by lactase.

For the buffer-free beads, the yellow color was evenly distributed within the o-NPG solution during incubation at pH 7 (**Fig. 5.23a**), which suggests a high enzyme activity under these conditions. Conversely, when buffer-free beads were incubated in the o-NPG solution at pH 2.5, no color change was observed indicating that the enzyme was completely deactivated under these acidic conditions (**Fig. 5.23b**). For the buffer-loaded beads incubated at pH 2.5, the yellowish color first appeared in the hydrogel beads located at the bottom of the tube, then the external o-NPG solution became yellowish at longer incubation times (**Fig. 5.23c**). Presumably, the substrate (o-NPG) initially diffused into the hydrogel beads where it was hydrolyzed by the encapsulated lactase. At longer times, some of the reaction products diffused out of the hydrogel beads and into the surrounding aqueous phase, thereby turning the whole solution yellow. A schematic diagram of the proposed reactions taking place in these systems is shown in **Figure 5.24**.

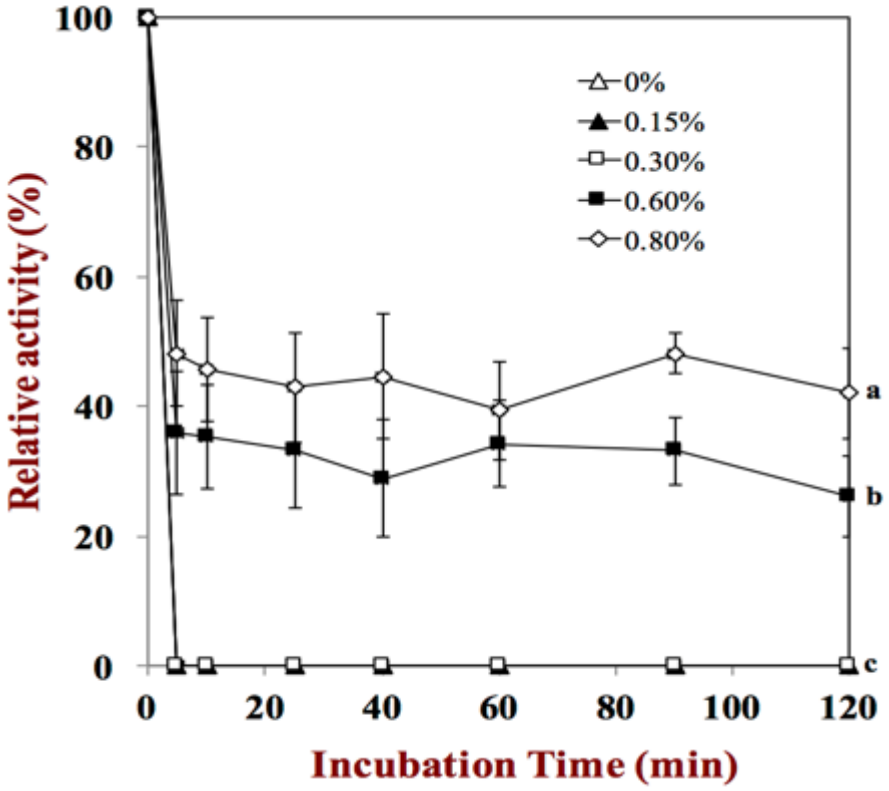

Figure 5. 21 The relative activity of β-galactosidase encapsulated in small hydrogel beads after incubation in simulated gastric fluids for different times. The enzyme was encapsulated in hydrogel beads combined with different amounts of $Mg(OH)_2$ (0 to 0.80%). Samples designated with different capital letters (a, b, c) were significantly different (Duncan, $p < 0.05$) when compared between different delivery systems for the final point (120 min).

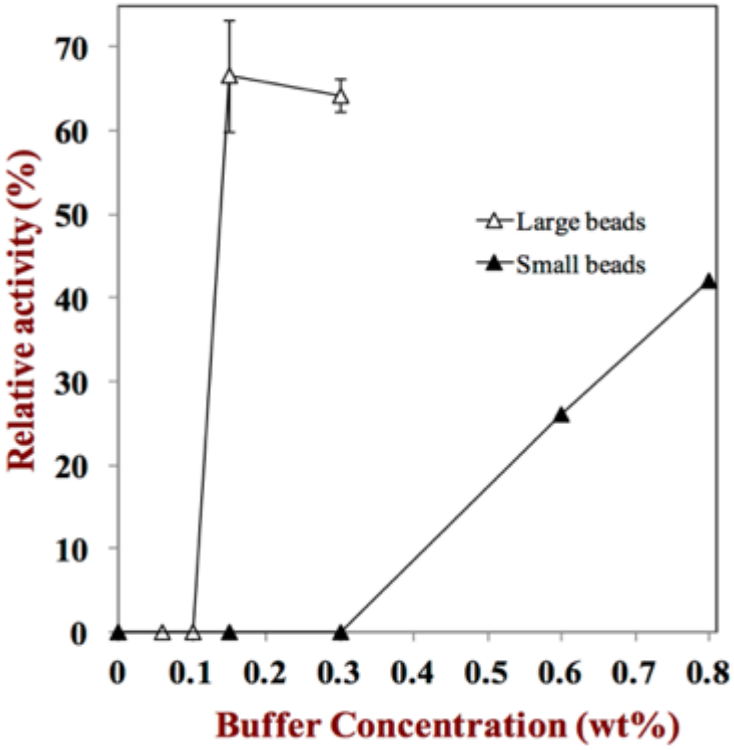

Figure 5. 22 The relative activity of β-galactosidase encapsulated in hydrogel beads after 120 minutes incubation in simulated gastric fluids. The enzyme was encapsulated in hydrogel beads containing different amounts of $Mg(OH)_2$.

5.3.2.4 Impact of bead dimensions on H^+ ion diffusion

The experimental studies indicated that the hydrogel bead dimensions had a major impact on the stability of the encapsulated lactase to acidic environments, which was attributed to the impact of particle size on the kinetics of H^+ ion diffusion into the beads. In this section, the impact of bead dimensions on hydrogen ion diffusion were therefore investigated using a mathematical model.

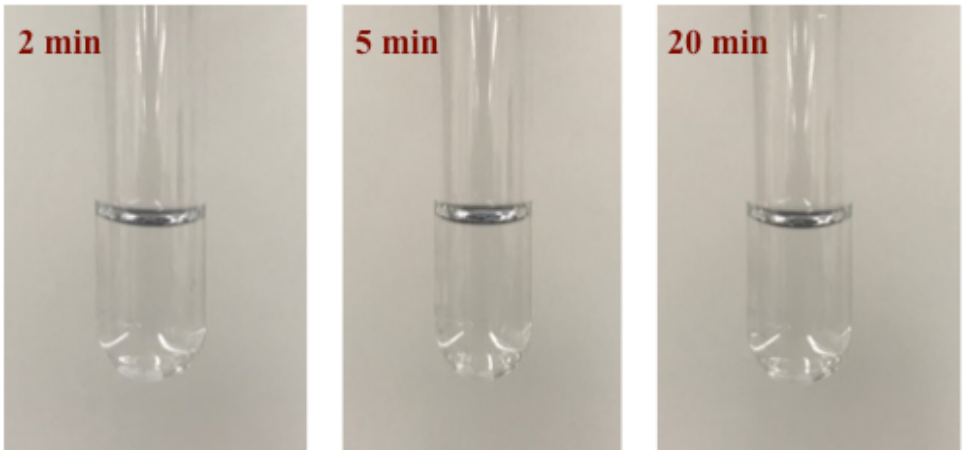

(a)

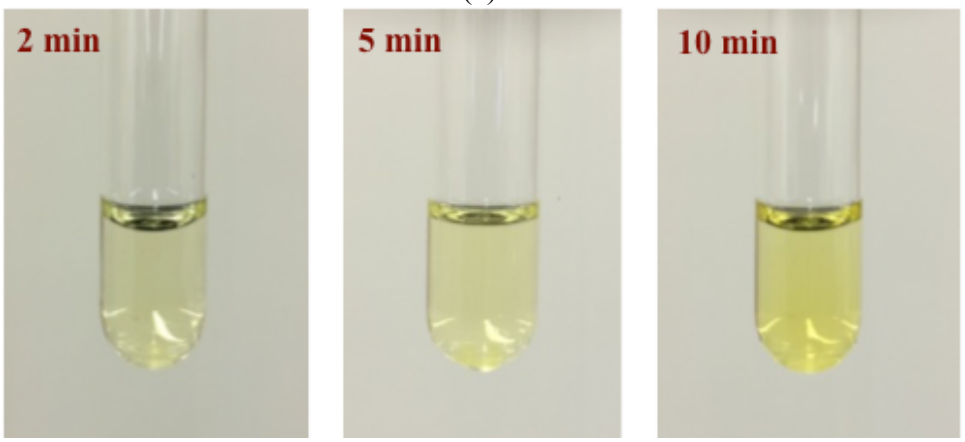

(b)

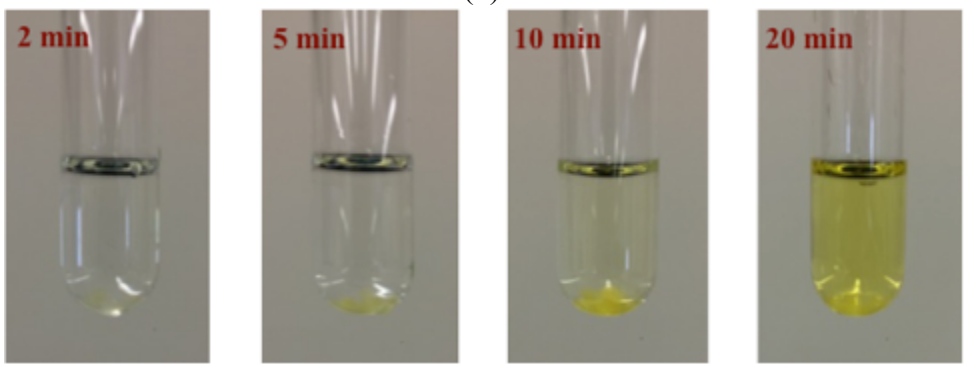

(c)

Figure 5. 23 Visual appearance of the color change of lactase-loaded large beads incubated in (a) the o-NPG solution at pH 7 without buffer co-encapsulation, (b) the o-NPG solution at pH 2.5 without buffer co-encapsulation, and (c) the o-NPG solution at pH 2.5 with 0.3% $Mg(OH)_2$ co-encapsulation.

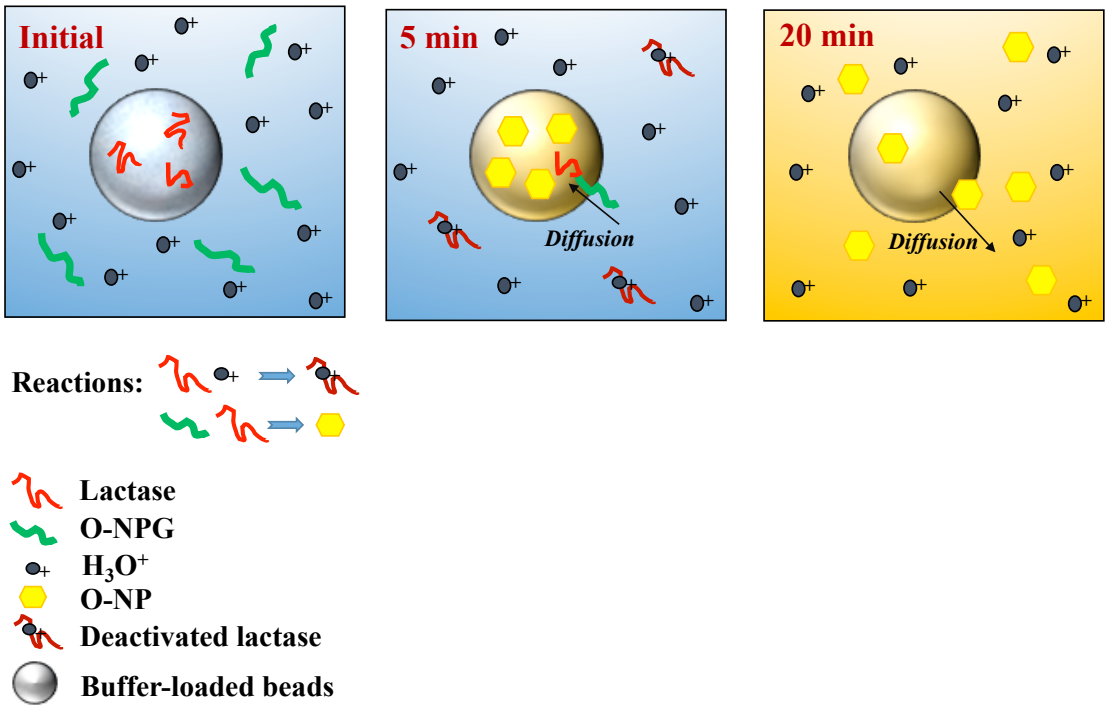

Figure 5. 24 Schematic representation of physicochemical processes occurring in the lactase-loaded beads incubated in o-NPG solution at pH 2.5 with $Mg(OH)_2$ co-encapsulation.

The particle size distributions of suspensions of both small and large hydrogel beads contained a single peak (**Fig. 5.25a**). Digital photographs of the samples showed that they contained fairly uniform size particles that were evenly distributed throughout the system (**Fig. 5.25b**). The mean particle diameters of the small and large beads were around 255 and 2610 μm, respectively.

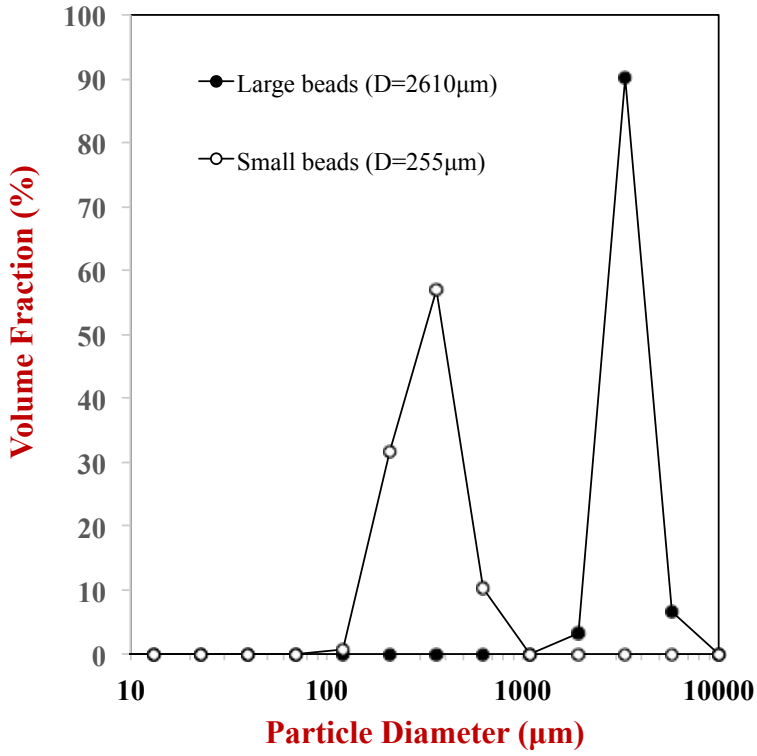

(a)

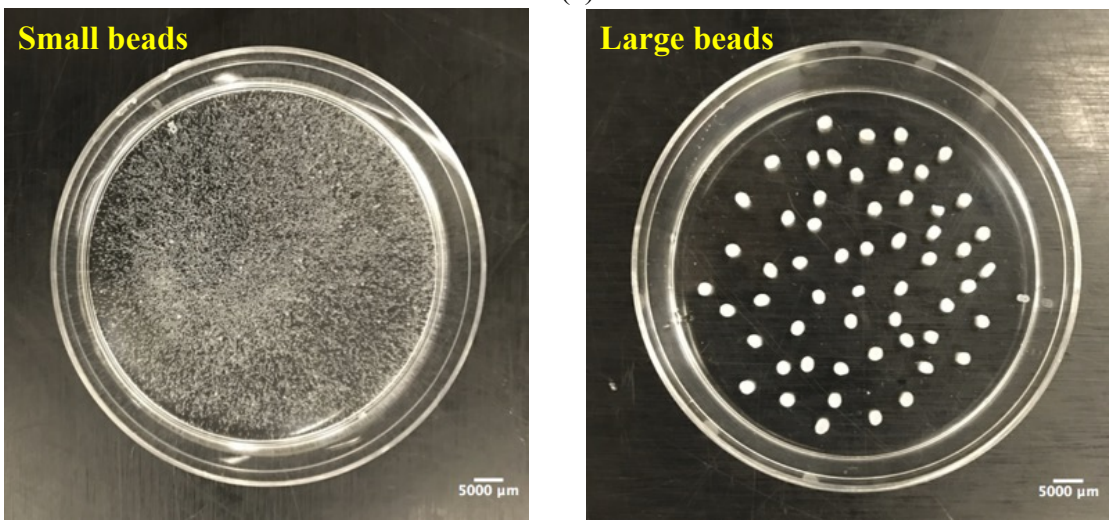

(b)

Figure 5. 25 (a) Particle size distributions and (b) visual appearances of carrageenan beads fabricated by syringe (large beads) and Encapsulator (small beads).

The diffusion of hydrogen ions into hydrogel beads with different dimensions can be predicted using the following equation [293]:

$$\Phi = \frac{M(t)}{M(\infty)} = 1 - \frac{6}{\pi^2}\sum_{n=1}^{\infty}\frac{1}{n^2}\exp\left(-\frac{D_{gel}n^2\pi^2 t}{a^2}\right) \quad (1)$$

Here, Φ refers to the fraction of H^+ ions that have diffused into the hydrogel beads at time t, $M(t)$ and $M(\infty)$ are the concentrations of H^+ ions inside the hydrogel beads at time t and at equilibrium, n is an integer, a is the hydrogel bead radius, and D_{gel} is the diffusion coefficient of the H^+ ions through the hydrogel bead matrix, which can be estimated based on the following expression [239]:

$$D_{gel} = D_w \exp\left(-\pi\left(\frac{r_H + r_f}{\xi + 2r_f}\right)\right) \quad (2)$$

Here, D_w is the diffusion coefficient of the H^+ ions through pure water, r_H is the hydrodynamic radius of the H^+ ions, r_f is the cross-sectional radius of the biopolymer chains (κ-carrageenan) in the hydrogel network, and ζ is the mesh pore diameter of the hydrogel network. The radius (r_f) of the carrageenan chain has been reported to be around 0.50 nm [294]. Typical pore sizes of biopolymer hydrogels are reported to be in the range 5 to 500 nm [270], and a value of 15 nm was assumed for the purpose of this study. The hydration (r_H) radius of the H^+ ions (actually H_3O^+ ions) has been estimated to be around 0.1 nm [295]. The diffusion coefficient of H^+ ions in water can be obtained from: $D_w = k_B T/6\pi\eta r_H$, where k_B is Boltzmann's constant, T is absolute temperature, and η is the viscosity of the solvent. These equations can be used to estimate the time-dependence of the fraction of H^+ ions diffusing into hydrogel beads with different sizes after incubation in the stomach phase (**Fig. 5.26**).

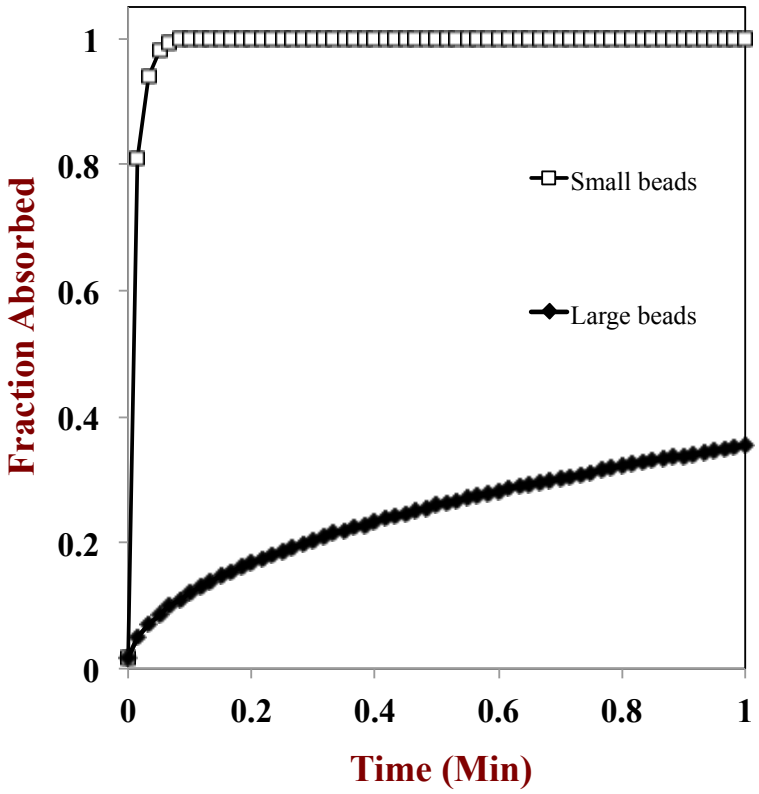

Figure 5. 26 Predicted time dependence of the fraction of hydrogen ions (H_3O^+) absorbed by carrageenan beads with a diameter of 255 μm (small size beads) and 2609 μm (larger size beads) with a pore size of 15 nm after submersion in an acidic environment.

The calculations highlight the importance of hydrogel bead dimensions on the diffusion rate of H^+ ions into the beads. The predictions show that H^+ ions can diffuse into the small beads much quicker (in a few seconds) than into the large ones, which would account for the fact that a higher amount of $Mg(OH)_2$ has to be loaded into the smaller beads to maintain a neutral internal pH. These calculations partly account for the reason that the smaller beads are less effective at protecting the lactase from acidic conditions than the larger beads

In practice, smaller hydrogel beads are often preferred for applications in the food industry because they give products with more desirable optical, rheological, stability, and mouthfeel characteristics. This study has shown that smaller beads can still be used to protect lactase from acid-induced degradation, but that a higher level of $Mg(OH)_2$ must be incorporated into the beads. In addition, it may be possible to further enhance enzyme

activity by using different types and amounts of biopolymers or cross-linking agents to control the hydrogel pore size and physical interactions.

5.3.4. Conclusion

In this study, lactase was encapsulated within potassium carrageenan-based hydrogel beads using the injection-gelation method. The acid-stability of the enzyme could be improved by co-encapsulating it with a basic buffering agent: $Mg(OH)_2$. This buffer is insoluble under neutral conditions, but dissolves when hydrogen ions diffuse into the hydrogel beads, thereby ensuring a neutral internal pH (as long as some buffer remains). A quantitative ratiometric fluorescence method proved to be highly effective at determining the local pH inside the beads before and after exposure to simulated gastric conditions. The interior of the buffer-free beads rapidly decreased from pH 6.9 to < 4 when exposed to the stomach phase, which led to rapid deactivation of the encapsulated lactase. Conversely, the interior of the buffer-loaded beads remained relatively close to neutral (pH 6.6) even after 2 hours exposure to simulated gastric fluids, which helped to retain lactase activity. A higher amount of $Mg(OH)_2$ was required to protect lactase encapsulated in small beads than in large beads, which was attributed to faster diffusion of H^+ ions into the smaller bead interiors. This study suggests that buffer-loaded hydrogel beads may be suitable food-grade delivery systems for acid-sensitive enzymes, such as lactase. However, *in vivo* animal and human studies are stilled needed to confirm that buffer-loaded beads can maintain lactase activity under real life conditions.

5.4 Protection of insulin from gastric conditions by encapsulation in antacid-loaded biopolymer microgels

5.4.1 Introduction

It has been estimated that there were around 382 million people in the world with diabetes in 2013, and that this number will increase to around 592 million by 2035 [296]. Consequently, diabetes is a global health concern, which reduces the quality of life of numerous people, and is a major economic burden on society due to increased health costs and lost economic activity [297-298]. Individuals with Type 1 diabetes, as well as those with advanced Type 2 diabetes, have a chronic health condition in which their pancreases cannot produce sufficient insulin to properly regulate their blood sugar levels [299-300]. Insulin is a peptide-based hormone that normally regulates the uptake of glucose into cells where it can be used as an energy source, and so individuals with diabetes need to receive regular doses of insulin to remain healthy [301]. At present, regular subcutaneous injections are the most common means of administering insulin, which is associated with local discomfort and the possibility of infection [299, 302-303]. Delivery of insulin through the oral route would be much more preferable, as it would be more convenient and less painful than injections [304-305].

However, there are a number of challenges that currently hold back the development of successful oral insulin delivery systems. First, insulin is highly susceptible to degradation in the stomach due to the high proteolytic activity and acidity of the gastric fluids [306-307]. Second, the fraction of ingested insulin, which is a hydrophilic peptide, that is actually absorbed by the epithelium cells is relatively low [308]. In the current study, we focus on the first of these challenges – improving the gastric stability of insulin. One of the most promising strategies for increasing the stability of insulin within the stomach is to encapsulate it inside colloidal particles, such as nanoparticles or microparticles [16, 305, 309-310]. These colloidal delivery systems may be assembled from synthetic polymers, natural polymers, lipids, surfactants, or phospholipids suitable for oral ingestion, using various types of particle preparation methods. In this study, we examined the possibility of encapsulating insulin within biopolymer microgels assembled from calcium alginate. These microgels can be

fabricated using a mild preparation method, simple injection at ambient temperature, which is important to minimize any loss of insulin activity during the loading procedure [311].

A number of researchers have examined the efficacy of calcium alginate microgels for encapsulating, protecting, and delivering insulin. Insulin has been encapsulated within calcium alginate microgels fabricated using an emulsification/gelation method, but this system was unable to protect the insulin from degradation under simulated gastrointestinal conditions [304], presumably because these simple microgels have relatively large pores and are therefore unable to protect insulin from the acids and pepsin in the gastric juices. Structural design principles have therefore been employed to improve the encapsulation and protection properties of alginate microgels. For instance, the anionic alginate microgels have been coated with cationic biopolymers such as poly-L-lysine [312] or chitosan [313-314] to form a protective coating around them. Alternatively, alginate has been used in combination with other biopolymers to form a mixed hydrogel matrix inside the microgels, such as cellulose derivatives, pectin, and chitosan [315-317]. These studies showed that the insulin could be successfully entrapped and retained within the microgels, but that it was still susceptible to degradation under simulated gastrointestinal conditions. Again, the reason for this is because the pores in biopolymer microgel cores or coatings are still relatively large compared to the size of small ions (H^+) or digestive enzymes (pepsin) in the gastric fluids. Consequently, these molecular species can easily diffuse into the interior of the microgels and promote insulin degradation.

In the current study, a different approach was adopted to create alginate microgels that could protect insulin from acid and pepsin-induced deactivation when exposed to gastric conditions. In this approach, insulin was co-encapsulated with magnesium hydroxide inside the microgels. $Mg(OH)_2$ is a widely used food-grade antacid, which is soluble in water at acidic pH, but insoluble at neutral and basic pH [274]. Consequently, the pH inside antacid-loaded microgels stays close to neutral for an extended time when dispersed in simulated gastric fluids, because some of the antacid dissolves and releases hydroxyl ions (OH^-) when hydrogen ions (H^+) diffuse into them [318-319]. It has been reported that pepsin loses most of its enzyme activity at neutral pH [320]. Consequently,

any gastric pepsin that diffuses into the neutral interior of antacid-loaded microgels may lose its activity, and therefore be unable to hydrolyze the encapsulated insulin. We therefore postulated that these antacid-loaded biopolymer microgels could protect insulin from both acid- and protease-degradation in gastric fluids. For this reason, we carried out a series of experiments to determine the effectiveness of the antacid-loaded microgels for the encapsulation, retention, protection, and release of insulin under simulated gastrointestinal conditions.

5.4.2 Materials and methods

5.4.2.1 Materials

The pH-sensitive fluorescence probe, fluorescein tetramethylrhodamine dextran (FRD, average M_Γ 70,000), was purchased from Molecular Probes (Eugene, OR). L6 cells were from American Type Culture Collection (Manassas, VA). α-minimum Eagle's medium (α-MEM) was from Invitrogen (Carlsbad, CA). RIPA buffer, phosphatase inhibitor and protease inhibitor cocktail were from Thermo Scientific, Rockford, IL). Protein (or insulin) concentrations were determined with a protein DC assay kit (Bio-Rad Co., Hercules, CA). Immobilin P membrane was from Millipore (Bedford, MA). Primary rabbit antibodies including protein kinase B (AKT), phospho-AKT Thr308, phosphor-Akt Ser473, β-actin and horseradish peroxidase conjugated goat anti-rabbit IgG were obtained from Cell Signaling Technology (Danvers, MA). Enhanced chemi-luminescence detection kit (Bio-Rad Co., Hercules, CA). The following chemicals were purchased from the Sigma Chemical Company (St. Louis, MO): fetal bovine serum; Penicillin; Streptomycin; alginic acid (sodium salt); pepsin from porcine gastric mucosa; fluorescein isothiocynate (FITC) isomer I; calcium chloride dehydrate; and magnesium hydrate. Sodium phosphate and calcium chloride were purchased from Fisher Chemical Company (Pittsburgh, PA). All chemicals used were analytical grade. Double distilled water was used to make all solutions.

5.4.2.2 Microgels preparation

The microgels were prepared using an injection-gelation method as described previously [318-319], with some slight modifications. Aqueous alginate solutions were prepared by dispersing powdered sodium alginate (1%, w/w) into phosphate buffer solution (5 mM, pH 7.0), and then stirring at 60 °C for 60 min. The temperature was then reduced to 35 °C with continuous stirring until the alginate was fully dissolved. The alginate solution was then mixed with powdered 1 mg/mL insulin and either 0% (antacid-free) or 0.15% (antacid-loaded) $Mg(OH)_2$, and then stirred until the system was homogeneous. Microgels were then prepared by injecting these mixtures through a 120 μm vibrating nozzle into a 5% w/w calcium chloride solution using a dedicated encapsulation device (Encapsulator B-390, BUCHI, Switzerland). The operating conditions used for the encapsulation device were as follows: frequency = 800 Hz; electrode potential = 650 V; and operating pressure = 300 mbar. The biopolymer microgels formed were held in the Ca^{2+} solution for 20 min at ambient temperature to promote hardening before being removed. They were then filtered and washed with buffer solution to remove any residual hardening solution.

5.4.2.3 Simulated gastrointestinal conditions

The impact of incubation of the microgels in simulated gastric fluid (SGF) on their internal pH and on insulin activity was determined using a method described previously [319], with some slight modifications. Specifically, microgels (with or without $Mg(OH)_2$) were added at a ratio of 1:4 (w/w) to SGF (containing 0.0032 g/mL pepsin) that had been preheated to 37 °C and adjusted to pH 2.5. The resulting mixture was then incubated within a shaking device for 2 h at 37 °C to mimic stomach conditions.

After exposure to stomach phase, the microgels were then exposed to simulated small intestinal conditions by mixing them with phosphate buffer solution (pH 7.0, 37 °C) at a fixed mass ratio of 1:4, and then the mixture was adjusted to pH 7.0. For the release experiments, the microgels were incubated in this simulated small intestinal phase for 2 h at 37 °C.

5.4.2.4 Confocal laser scanning microscopy

The microstructural analysis of the biopolymer microgels was carried out using a confocal scanning laser fluorescence microscope with a 20 × objective lens (Nikon D-Eclipse C1 80i, Nikon, Melville, NY, U.S.). The insulin was dyed using FITC solution and then stored at 5 °C overnight. The excitation and emission wavelength used for detection of the FITC-labeled insulin were 488 nm and 515 nm, respectively.

The pH inside the biopolymer microgels was measured using a fluorescence intensity method described previously [321]. A known amount of the pH-sensitive dye (10 mg/mL FRD) was dissolved in phosphate buffer (5 mM, pH 7.0), and then mixed with alginate solution (1:200 v/v) with or without 0.15% $Mg(OH)_2$. Microgels were then fabricated using the encapsulation device described in Section 2.2. Images of the microgels were acquired using the confocal laser scanning fluorescence microscope with a 20×objective lens. Images of the pH-sensitive dye were obtained using excitation wavelengths of 543 and 488 nm, and detection wavelengths/bandwidths of 650 nm/LP and 590 nm/50 nm, respectively [322-323]. All samples were imaged using an exposure time of 0.5 s and a 12.5% excitation power level for both channels. Full images of each sample were typically acquired in less than 2 min and then stored on the computer using the microscope's software (NIS-Elements, Nikon, Melville, NY, USA). The images were then analyzed using Image J software (1.50I, imagej.nih.gov). The ratio of pixel intensities of the two images obtained at two different wavelengths (488 and 543 nm) were calculated and correlated with the pH obtained using a standard curve, as described previously [321]. The average intensity ratio was calculated from at least eight measurements.

5.4.2.5 Particle size characterization

Particle size distributions were carried out using a static light scattering instrument (Mastersizer 2000, Malvern Instruments Ltd., Malvern, Worcestershire, UK). Phosphate buffer (5 mM, pH 7.0) was used for the dilution of the initial samples and acidified distilled water (pH 2.5) was used to dilute the gastric samples to avoid multiple scattering effects.

5.4.2.6 Insulin activity assay with L6 myotubes and immunoblotting

The activity of insulin was assayed by determining its ability to stimulate Akt phosphorylation in L6 myotubes. L6 cells were maintained in α-MEM with 10% fetal bovine serum, 100 μg/ml streptomycin, and 100 U/ml penicillin at 37 °C in a humidified 5% CO_2 atmosphere. Cells were differentiated into myotubes for 6 days as has been reported previously [324]. Prior to analysis the microgels were dissociated by mixing them with a calcium chelating agent (EDTA). Filtered microgels were dissolved in 2 mL of 10% EDTA solution and then immediately diluted with α-minimum Eagle's medium by 100 times before treating myotubes for 10 minutes. Cells were lysed with RIPA buffer supplemented with phosphatase inhibitor and protease inhibitor cocktail. Protein concentrations were measured using a protein DC assay kit. Cell lysates containing 50 μg of protein were separated with 10 % SDS-polyacrylamide gel and transferred to Immobilin P membrane and incubated with primary antibodies overnight at 4 ° C and then secondary antibodies for 1 hour. Detections were performed with an enhanced chemi-luminescence detection kit. The images acquired were quantified using the Image J software described earlier.

5.4.2.7 Statistical analysis

All experiments were performed on at least three freshly prepared samples, and the results reported as averages and standard deviations calculated using Excel (Microsoft, Redmond, VA, USA).

5.4.3 Results and discussion

5.4.3.1 Preparation and characterization of insulin-loaded microgels

The ability of the biopolymer microgels to encapsulate insulin and then retain it within the stomach phase was determined using confocal fluorescence microscopy (**Fig. 5.27)**. Prior to exposure to simulated gastric conditions, the insulin (stained green) was distributed evenly throughout the interior of the microgels indicating that it had been successfully encapsulated. After exposure, the interior of the microgels was still stained

green, indicating that the insulin was retained within the microgels. However, there was a significant decrease in the fluorescence intensity of the insulin after exposure to the stomach phase. This effect can mainly be attributed to the fact that the intensity of the fluorescence probe used to stain the insulin (FITC) decreases under acidic conditions [321]. It should be noted that the fluorescence measurements only indicate the location of the insulin within the system, rather than its biological activity, and so this was measured using another method (described later).

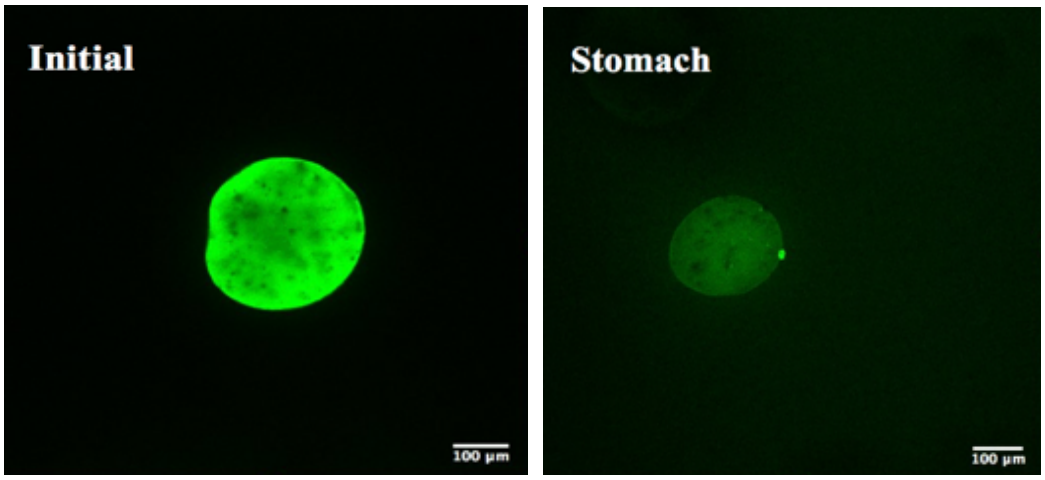

(a) (b)

Figure 5. 27 Confocal microscopy images of antacid-loaded microgels (a) before and (b) after exposure to simulated gastric conditions.

The confocal microscopy images indicated that the microgels had a roughly spherical shape, and remained intact after exposure to the simulated gastric conditions, which is in agreement with earlier studies [318-319]. The light scattering measurements indicated that the microgels had a monomodal particle size distribution both before and after exposure (**Fig. 5.28**). In addition, they indicated that there was a slight shrinkage of the microgels after they were incubated in the gastric fluids, with the mean particle diameter decreasing from around 280 µm before exposure to 265 µm after exposure. Microgel shrinkage under highly acidic conditions can be attributed to a decrease in the electrostatic repulsion between the alginate chains when the carboxyl groups become more protonated: $-COO^- + H^+ \leftrightarrow -COOH$, $pK_a = 3.5$ [319]. This phenomenon is advantageous for the retention of the insulin within the microgels in the stomach, since a cross-linked biopolymer network with smaller pores will trap the insulin molecules more effectively.

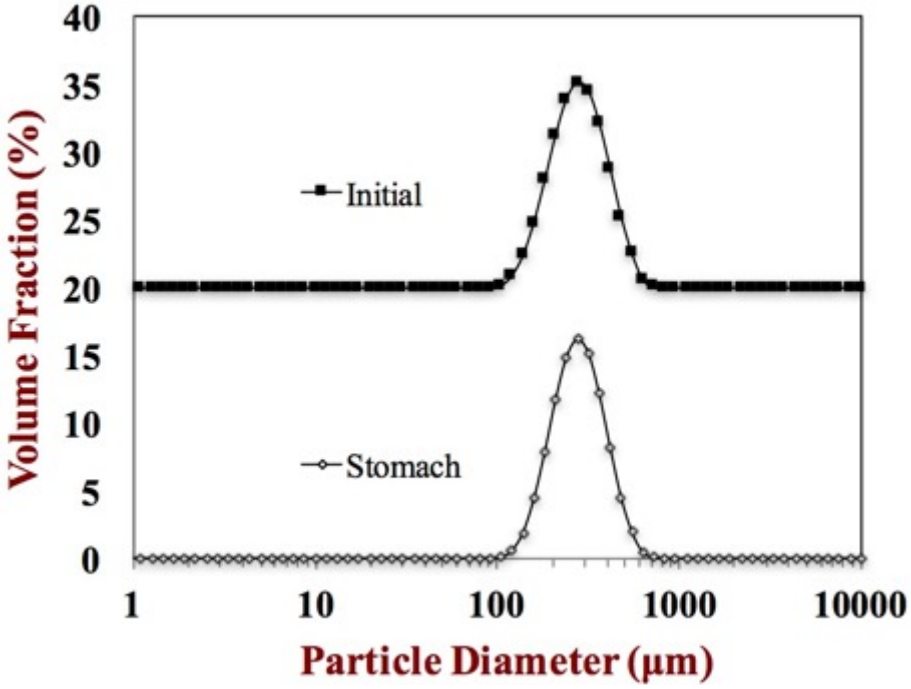

Figure 5. 28 The particle size distribution of antacid-loaded microgels before and after exposure to simulated gastric conditions.

5.4.3.2 Mapping the pH inside the microgels

As mentioned earlier, one of the main hurdles to the oral administration of insulin is its tendency to degrade in the stomach due to the high acidity and protease activity of the gastric fluids [307, 325]. Protection against these effects is therefore an important strategy for the development of effective oral delivery systems for insulin [326-327]. We hypothesized that antacid-loaded microgels would protect insulin from both acid- and protease-degradation by maintaining a neutral pH inside them. Insulin is known to degrade under acidic conditions [325], and therefore keeping the local environment neutral should protect it from this type of degradation. Moreover, the optimum activity of pepsin has been reported to be around pH 2 to 3 [328], and it is known to be deactivated around pH 7 [320]. Consequently, maintaining a neutral environment inside the microgels may also protect the insulin from protease-induced degradation by reducing the local pepsin activity.

In this study, an insoluble antacid ($Mg(OH)_2$) was co-encapsulated with the insulin to control the internal pH of the microgels under gastric conditions. The local pH inside the microgels was measured using a pH-sensitive fluorescence probe (FRD) based on a fluorescence intensity ratio method described earlier [321]. The FRD probe has both pH-dependent (FITC) and pH-independent (TMR) fluorescence groups, and so the pH can be determined by measuring the FITC-to-TMR fluorescence intensity ratio. In addition, the FRD probe selected for this study had a polymer chain (dextran) attached to inhibit its release from the biopolymers microgels.

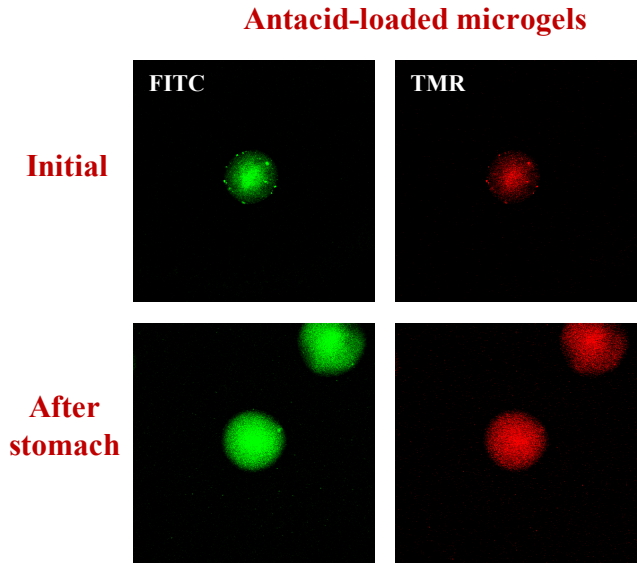

(a)

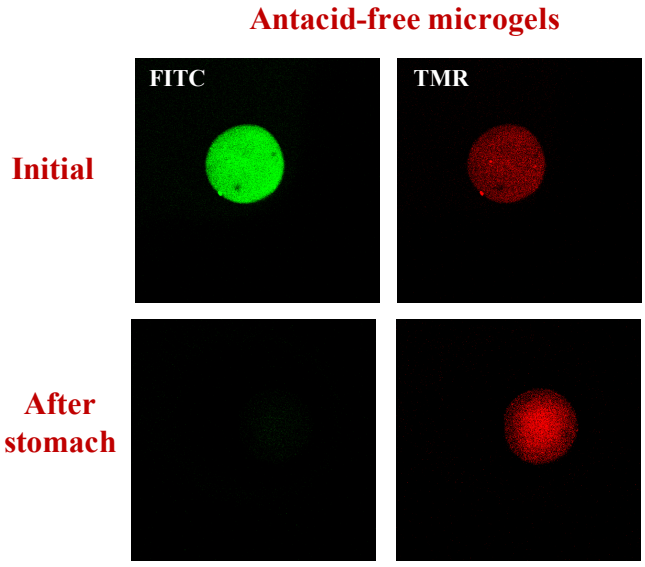

(b)

Figure 5. 29 Fluorescent microscopy images of microgels (a) with or (b) without 0.15% $Mg(OH)_2$ before and after exposure to simulated gastric conditions. The intensity of the TMR signal was enhanced using Image J to improve contrast.

Confocal fluorescence microscopy images of the FRD probe within the microgels was acquired before and after exposure to simulated gastric fluids (**Fig. 5.29**). For the antacid-loaded microgels, the fluorescence intensity of the FITC channel (pH-dependent) was relatively strong both before and after incubation in the stomach phase. Conversely, for the antacid-free microgels, the fluorescence intensity of the FITC channel changed from relatively strong before incubation to very weak after incubation. The average internal pH value was determined to be around pH 7.4 for the antacid-loaded microgels after exposure to the simulated gastric fluids, but below the limit of detection (pH < 4) for the antacid-free microgels. These results indicate that the co-encapsulated magnesium hydroxide was able to maintain a neutral pH inside the microgels, which is in agreement with our previous studies with lipase- and lactase-loaded alginate microgels [318-319]. This effect has been attributed to the ability of the $Mg(OH)_2$ particles to partially dissolve when hydrogen ions diffuse into the microgels, thereby releasing OH^- ions that neutralize the H^+ ions and maintain a neutral pH.

5.4.3.3 Influence of encapsulation on insulin activity

In this series of experiments, a biological model was used to test the activity of insulin after it had been exposed to simulated gastric conditions. In its active form, insulin is known to stimulate Akt phosphorylation in L6 myotubes [324], and so this assay was used to determine the activity of free and encapsulated insulin. Insulin was encapsulated in both antacid-free and antacid-loaded microgels to ascertain the impact of the antacid on its stability under gastric conditions.

The Akt phosphorylation at both Thr308 and Ser473 was significantly higher for insulin encapsulated in the antacid-loaded microgels, than for free insulin or for insulin encapsulated in antacid-free microgels (**Figs. 5.30** and **5.31**). This result suggests that the microgels containing the antacid protected the insulin under gastric conditions, which can be attributed to its ability to maintain a neutral pH inside the microgels, thereby inhibiting both acid- and pepsin-induced degradation.

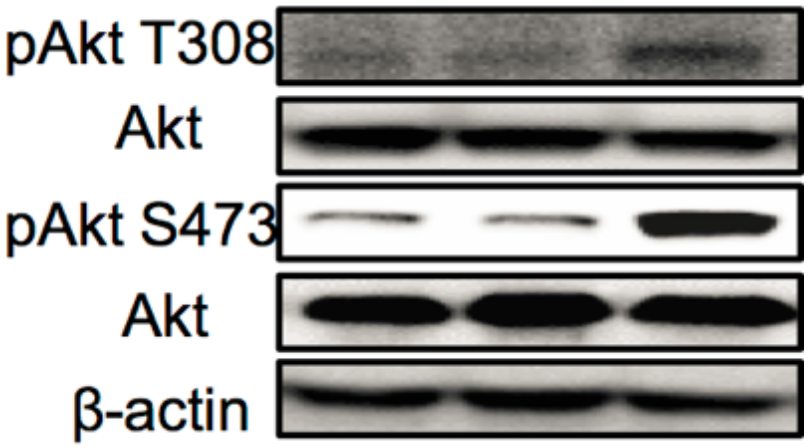

Figure 5. 30 Effects of diluted digestion solution with insulin (beads free, encapsulated in beads and encapsulated in microgels with antacid) on Akt phosphorylation in L6 myotubes. (The diluted digestion solution was obtained by diluting orginal digestion solution by 100 times with DMEM medium. Protein expression levels were determined after treatment with or without diluted digestion solution (100 nM) for 15 min).

A number of previous researchers have focused on the impact of encapsulation of insulin on its activity under gastric conditions. Studies have shown that insulin can be encapsulated in biopolymer nanoparticles fabricated from alginate and dextran sulfate, and that its biological activity was retained after encapsulation [329]. However, the activity of the insulin in this study was only tested by injecting insulin-loaded nanoparticles subcutaneously into diabetic rats. Hence, it is unclear whether the insulin would still remain active if insulin-loaded nanoparticles were orally administered to the rats. Insulin has also been successfully loaded into poly(lactic-co-glycolic acid) nanoparticles, which were shown to protect it from gastric degradation, and to maintain its activity after oral administration to diabetic rats [330]. Alginate-chitosan microgels have also been shown to be effective at encapsulating insulin, protecting it from degradation under gastrointestinal conditions, and maintaining its activity after oral administration to diabetic rats [331]. Thus, various types of polymer-based microgels seem to have promise as oral delivery systems for insulin [332]. Each system has its own advantages and disadvantages in terms of the commercial viability of the ingredients and fabrication processes used to prepare them, and their functional attributes.

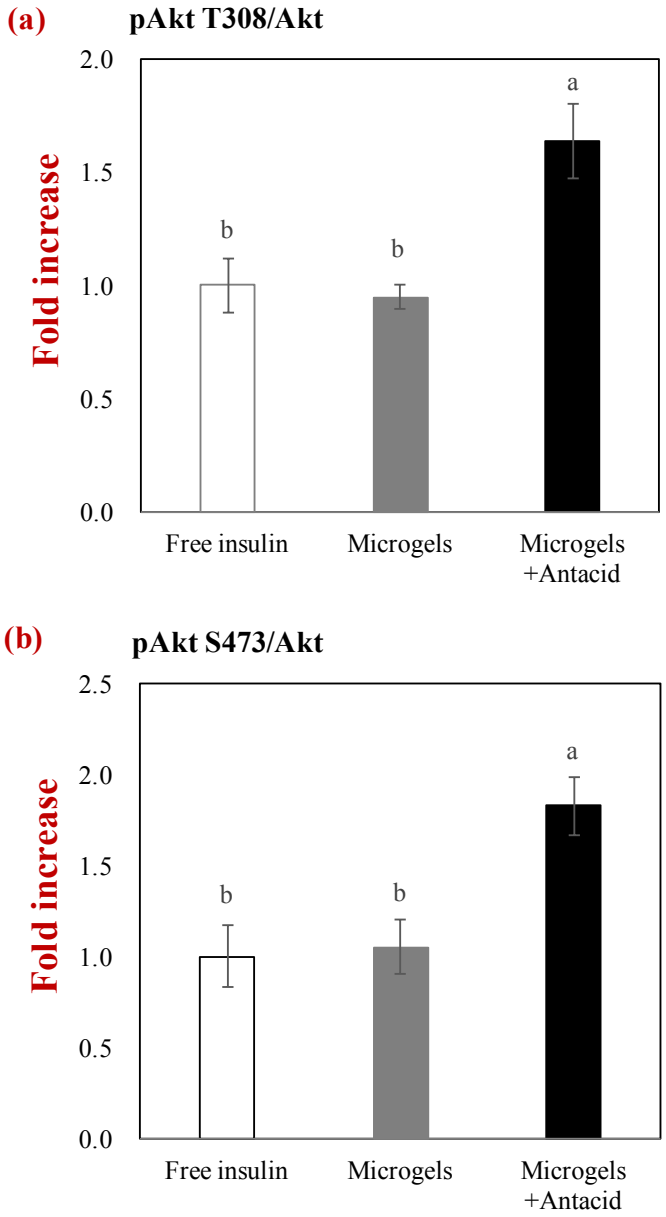

Figure 5. 31 The ratio of (a) pAkt/T308 and (b) pAkt/Akt S473, representing the phosphorylation of Akt, which is due to insulin stimulation in muscle cells. The higher ratio of beads + antacid group suggests that insulin was better protected under gastric conditions than the other groups.

5.4.3.4 Release of insulin in a simulated small intestine phase

Insulin that survives intact after passage through the stomach has to be absorbed by the epithelium cells after reaching the small intestine so that it can enter the systemic

circulation. It has been reported that free insulin can be absorbed by intestinal enterocytes through various internalization mechanisms [333-334]. It is therefore important to understand the release properties of the insulin from the microgels in the small intestine.

In this section, we determined the release profile of insulin from the antacid-loaded microgels during incubation in simulated small intestinal fluids for two hours (**Fig. 5.32**). Around 21% of the insulin was released fairly rapidly during the first 30 minutes and then another 10% was released more gradually over the next 90 minutes. Presumably, the remainder of the insulin would also be released gradually at longer incubation times, which may be useful for sustained release applications. The release of insulin from the biopolymer microgels in the small intestine phase can be attributed to changes in the electrical properties of the alginate and insulin molecules, as well as alternations in the structure of the alginate microgels. The insulin and alginate molecules are both negatively charged in the small intestine phase (pH 7) and so they will electrostatically repel each other, which promotes insulin release [335]. Moreover, alginate microgels swell when they are moved from acidic to neutral conditions because of the increase in electrostatic repulsion between the anionic alginate chains [291]. This leads to an increase in hydrogel pore size, which can increase the release of any encapsulated substances [336]. Overall, these results suggest that insulin could be successfully released from the microgels in the small intestine phase, which would facilitate their subsequent absorption. Nevertheless, it is also possible that the insulin would still be degraded in the small intestinal fluids prior to adsorption due to the presence of digestive enzymes, such as proteases. In addition, it will be important to determine the fraction of insulin that is actually absorbed and enters the systemic circulation where it can have its beneficial effects. In future studies, it will therefore be important to test the efficacy of these antacid-loaded microgels using animal feeding studies, *e.g.,* with diabetic rats.

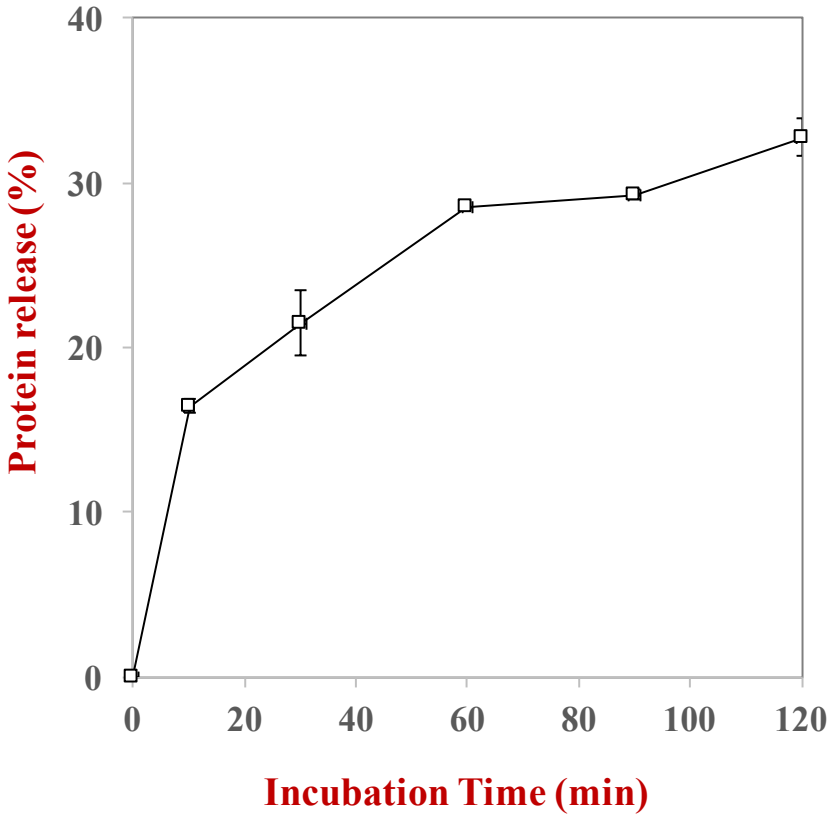

Figure 5. 32 The release profile of insulin from antacid-loaded biopolymer microgels during incubation in a simulated small intestine phase.

5.4.4 Conclusion

In this study, insulin was encapsulated within calcium alginate microgels using an injection-gelation method. The stability of insulin after exposure to simulated gastric conditions was improved by co-encapsulating it with a basic antacid: $Mg(OH)_2$. This antacid is insoluble under neutral conditions, but dissolves when hydrogen ions diffuse into the microgels, thereby ensuring that a neutral internal pH is maintained (as long as some antacid remains). Gastric pepsin is rapidly inactivated under neutral pH conditions, and so encapsulation of insulin in antacid-loaded microgels protects it from both acid- and protease-degradation. This study suggests that antacid-loaded microgels may be a suitable food-grade delivery system for acid and/or pepsin-sensitive bioactive proteins and peptides. However, *in vivo* animal and human studies are needed to confirm that these microgels can maintain their insulin activity under real life conditions. In addition,

it will be important to establish that the microgels can be fabricated economically on a sufficiently large scale for commercial applications, and that they can be successfully incorporated into formulations intended for oral administration.

CHAPTER 6

CONTROL THE DIGESTION AND RELEASE OF BIOACTIVE PROTEIN USING HYDROGEL BEADS

6.1 Protein encapsulation in alginate hydrogel beads: Effect of pH on microgel stability, protein retention and protein release

6.1.1 Introduction

Colloidal delivery systems are finding increasing application for the encapsulation, protection, and release of bioactive agents in the pharmaceutical, supplement, and food industries [337-339]. Each type of bioactive agent has its own unique molecular and physicochemical properties, which means that delivery systems typically have to be specifically designed for each application. Proteins and peptides are commonly used as bioactive agents because they exhibit a range of biological activities, including nutritional, antimicrobial, antioxidant, flavor, anti-hypertension, anti-diabetic, and anticancer [128, 130, 227, 340]. Nevertheless, the incorporation of these bioactive proteins into food products is often challenging because of their sensitivity to chemical or biochemical degradation, their susceptibility to aggregation, and their potential for causing off-flavors (such as bitterness or astringency). For this reason, there has been considerable interest in encapsulating proteins within polymer particles to protect and release them in different environments [341-344]. Studies have shown that proteins encapsulated within polymer matrices may be protected from unfolding and aggregation [345]. Moreover, these protein-loaded polymer particles can be designed to carry bioactive proteins to specific locations within the gastrointestinal tract (GIT) and release them at a controlled rate or in response to a particular trigger [227]. Consequently, the functional attributes and biological activity of proteins can be enhanced by encapsulating them within microgels [291, 341].

Many different approaches have been developed to fabricate hydrogel beads suitable for protein encapsulation, including extrusion, emulsion, molding, and phase separation methods [228, 346-348]. For certain applications, it is important that the fabrication method used does not promote unfolding or aggregation of the encapsulated proteins, as

this may lead to a loss of their functional attributes or biological activity. Hydrogel beads fabricated from biopolymers (proteins and/or polysaccharides) are particularly suitable for the encapsulation of bioactive proteins because they often involve mild preparation conditions that do not alter protein properties, and can be prepared using food-grade ingredients [227-229]. The extrusion-gelation method is one of the most commonly used and effective methods of producing hydrogel beads [291]. In this method, a biopolymer solution containing the bioactive protein is injected into another ''hardening'' solution that promotes biopolymer gelation. This procedure results in the formation of hydrogel beads with bioactive proteins trapped inside a biopolymer matrix.

When designing a suitable hydrogel bead for this type of application it is important that it has good encapsulation, retention, and release properties [229, 270, 341]. There are a number of potential strategies to control the retention and release properties of hydrogel beads [270]. First, the pore size of the hydrogel matrix can be controlled by manipulating the amount of biopolymer and cross-linking agent used: larger pores typically lead to faster release. Second, the overall dimensions of the hydrogel beads can be controlled using different fabrication methods or preparation conditions: smaller beads typically lead to faster release. Third, specific interactions between the bioactive agents and biopolymer molecules in the hydrogel matrix can be utilized, *e.g.,* hydrophobic, hydrogen bonding, or electrostatic interactions. Fourth, the hydrogel beads can be designed to dissociate upon exposure to specific environmental conditions, thereby releasing their payload. Fifth, the hydrogel beads can be coated with layers of biopolymers or other materials to alter their permeability. The mechanism that is important for a particular delivery system depends on its composition and structure.

In the current study, we investigated the utilization of alginate as a building block for creating protein-loaded hydrogel beads that could release encapsulated proteins in response to pH changes. Alginate is a naturally occurring anionic polymer isolated from brown algae that has the ability to form strong hydrogels [349]. Protein-loaded alginate beads can be fabricated by extruding a solution of sodium alginate containing the bioactive protein into a divalent crosslinking solution, such as one containing Ca^{2+} ions [291]. Biopolymer gelation primarily occurs due to exchange of Na^{+} ions from carboxylic

acids on the sodium alginate molecules with Ca^{2+} ions from the crosslinking solution, which leads to the formation of cross-links with a characteristic "egg-box" structure [18-19, 21]. The internal environment of alginate hydrogels has been shown to have little impact on the functional properties of many globular proteins [291]. In addition, proteins can be retained within alginate beads that have sufficiently small pore sizes and/or specific attractive interactions between the proteins and alginate molecules [76] However, the proteins can be released when the system conditions are changed to increase the pore size and/or reduce the attractive interactions.

In the present study, whey protein was incorporated into hydrogel beads fabricated from calcium alginate using an automated extrusion device with a small vibrating nozzle. We hypothesized that the retention and release of the protein molecules would depend on their electrical characteristics because this would influence their interactions with the alginate molecules in the hydrogel matrix. The solution pH was therefore altered relative to the isoelectric point (pI) of the whey proteins so as to obtain highly positive (pH 3), approximately neutral (pH 5) and highly negative (pH 7) proteins. The influence of pH on the encapsulation, retention and release of the proteins was then measured. The information obtained from this study may be useful for the rational design of more effective delivery systems for bioactive proteins in the food and other industries.

6.1.2. Materials and methods

6.1.2.1 Materials

Whey protein isolate (WPI) was kindly provided by Davisco Foods International Inc. (Le Sueur MN). The company reported that the WPI contained 97.9 wt.% protein and 0.2 wt.% fat. Alginic acid (sodium salt), calcium chloride dihydrate ($CaCl_2 \cdot H_2O$) and fluorescein isothiocynate (FITC) isomer I was purchased from the Sigma Chemical Company (St. Louis, MO). Double distilled water was used to make all solutions.

6.1.2.2 Methods

6.1.2.2.1. ζ-potential measurements

ζ-potential *versus* pH profiles of WPI and alginate solutions was measured using a commercial micro-electrophoresis instrument (Zetasizer Nano ZA series, Malvern Instruments Ltd. Worcestershire, UK). Samples were diluted using 10 mM phosphate buffer (at the same pH as the sample) prior to analysis to keep the instrument attenuation value between 5 and 10.

6.1.2.2.2. Turbidity measurements

Turbidity *versus* pH profiles of WPI or WPI-alginate solutions was determined using a UV–visible spectrophotometer at 600 nm (Ultrospec 3000 pro, Biochrom Ltd., Cambridge, UK). The samples were contained within 1 cm path length optical cells, and phosphate buffer (PBS) was used as a control. Turbidity measurements were carried out on at least two freshly prepared samples.

6.1.2.2.3 Encapsulation of WPI in alginate beads

An aqueous alginate (2% w/v) solution was prepared by dissolving the powdered ingredient in distilled water, stirring at 60 ºC for an hour, and then reducing the temperature to 35 ºC. The WPI (2% w/v) and alginate (2% w/v) solutions were then mixed together (1:1 v/v) for 1 h with continuous stirring to form a uniform solution. And then the mixture solution was adjusted to different pH (3. 5 and 7) for the different hydrogel beads formation. WPI-loaded hydrogel beads were prepared using a commercial encapsulation unit (Encapsulator B-390, BUCHI, Switzerland) to inject the different WPI/alginate solutions into 10% corresponding pH calcium chloride solution with continuous stirring. The hydrogel beads were allowed to crosslink with Ca^{2+} for 1 h at ambient temperature. The hardened beads were then collected by filtration and subsequently washed with distilled water and buffer solution to remove any excess Ca^{2+} from their surfaces.

6.1.2.2.4 Particle size measurements

The mean particle diameter and particle size distribution of biopolymer mixtures (WPI and alginate) and hydrogel beads formed at different pH values (3, 5 and 7) were determined using static light scattering (Mastersizer 2000, Malvern Instruments, Worcestershire, United Kingdom). This instrument infers the size of the particles from measurements of their angular scattering pattern. Samples were diluted in 10 mM PBS buffer (pH 3, 5 and 7) by adding small aliquots into a measurement chamber.

6.1.2.2.5 Encapsulation efficiency and protein release

The ability of hydrogel beads formed at different pH values (pH 3, 5, and 7) to retain the protein was determined by immersing them within the corresponding phosphate buffer solutions (pH 3, 5 and 7) at room temperature. The concentration of protein in the surrounding aqueous phase was then measured at various time intervals by recording the absorbance at 280 nm using the UV-visible spectrophotometer. The encapsulation efficiency (%) was determined by dividing the amount of protein remaining in the beads by the initial protein in the beads. The amount of protein in the beads was taken to be he difference between the initial protein and that released into the phosphate buffer. In some cases, the amount of protein released was determined for protein-loaded hydrogel beads formed at pH 3, and then incubated in solutions at higher pH values for 10 min.

6.1.2.2.6 Microstructure analysis

The microstructure of hydrogel beads formed at different pH values (pH 3, 5 and 7) was recorded, as well as the impact of pH on protein release from alginate-based beads. The microstructure of the protein-loaded alginate beads was examined using confocal scanning laser microscopy with a 20 × objective lens (Nikon D-Eclipse C1 80i, Nikon, Melville, NY, U.S.). The proteins were dyed prior to hydrogel bead formed by adding 0.1 mL of FITC dye solution (1 mg FITC /mL dimethyl sulfoxide) to 2 mL of sample and then storing at 5 °C overnight. The excitation and emission wavelength used for FITC were 488 nm and 515 nm, respectively. Specially, a relatively high gain value was adjusted in the hydrogel beads (formed at different pH values) detection to facilitate the

observation of encapsulated protein. The microstructure images for confocal microscopy were analyzed using image analysis software (NIS-Elements, Nikon, Melville, NY).

6.1.2.3 Statistical analysis

All experiments were carried out in triplicate using freshly prepared samples. Means and standard deviations were calculated from a minimum of three measurements using Excel (Microsoft, Redmond, VA, USA).

6.1.3 Results and discussion

6.1.3.1 Electrical characteristics of biopolymer molecules

An encapsulated protein can electrically interact with the charged biopolymer molecules used to fabricate the hydrogel beads and thereby influence its encapsulation, retention, and release properties. For this reason, the pH dependence of the ζ-potential of WPI and alginate solutions was determined using an electrophoresis method. The ζ-potential of the WPI solution went from negative at pH 7.0 (≈ -26 mV) to positive at pH 2.0 (≈ +23 mV), with a point of zero charge around pH 4.7 (**Fig. 6.1**), which can be attributed to changes in the protonation of acid (-COOH) and basic ($-NH_2$) groups on the protein molecules with pH. The ζ-potential of the alginate solution remained negative across the whole pH range studied (from pH 2 to 7), changing from strongly negative (≈ -68 mV) at pH 7 to slightly negative (≈ -10 mV) at pH 2. The magnitude of the negative charge on the alginate molecules was lower under acidic conditions than neutral conditions due to partial protonation of the carboxylic acid groups on the mannuronic and guluronic acid groups: $-COO^- \Rightarrow$ -COOH (pK ≈ 3.5) [349]. The pH dependence of the ζ-potential of mixed WPI-alginate solutions was also measured by electrophoresis to obtain information about the interactions between the two biopolymers (**Fig. 6.1**). At relatively high pH values (pH > 5.5), the ζ-potential of the mixed system was between that of the two individual biopolymers, which suggests that both biopolymers contributed to the overall ζ-potential. At lower pH values, the ζ-potential of the mixed system tended towards that of the alginate molecules, which suggests that an electrostatic complex was

formed between the two biopolymers whose charge characteristics were dominated by the presence of the anionic alginate molecules.

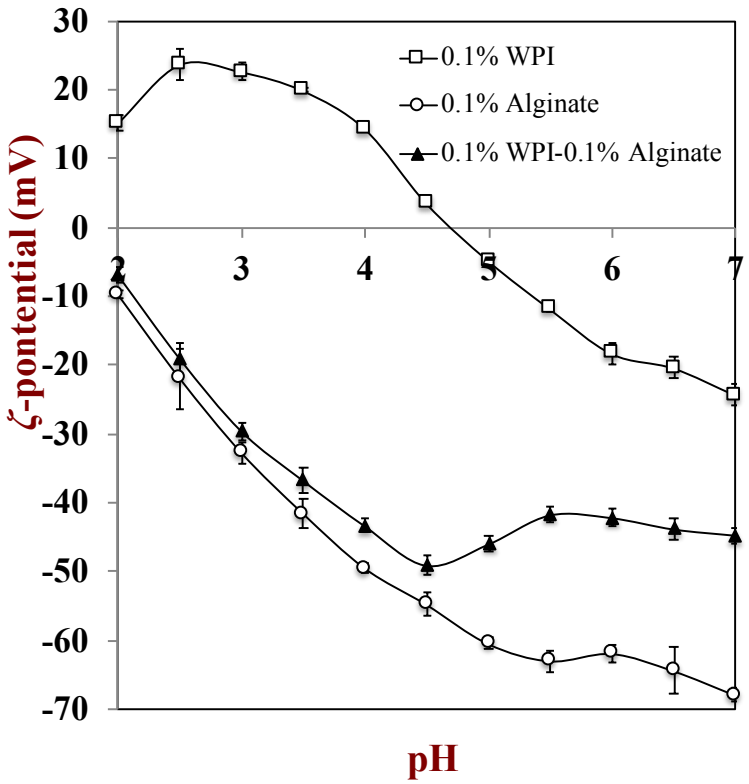

Figure 6. 1 Dependence of the ζ-potential on pH for 0.1 wt% WPI solution, 0.1 wt% sodium alginate solution, and 0.1% WPI + 0.1 wt% sodium alginate solution (10 mM phosphate buffer).

Based on the electrical characteristics of the two individual biopolymers (**Fig.6.1**), it would be expected that alginate and whey protein should be attracted to each other at low-to-intermediate pH (pH < 4.7) where they have opposite charges, but repel each other at high pH (pH > 4.7) where they have similar charges (negative charge). However, the ζ-potential and turbidity measurements on the mixed systems suggest that the two biopolymers become associated at higher pH values (pH 5.5) even though they have similar charges (**Figs. 6.1 and 6.2**), which can be attributed to the binding of anionic groups on the alginate molecules to cationic patches on the surfaces of the protein molecules [191]. Based on these measurements, we anticipate that whey proteins would be retained by the beads at relatively low pH values due to electrostatic attraction, but be released at high pH values due to electrostatic repulsion.

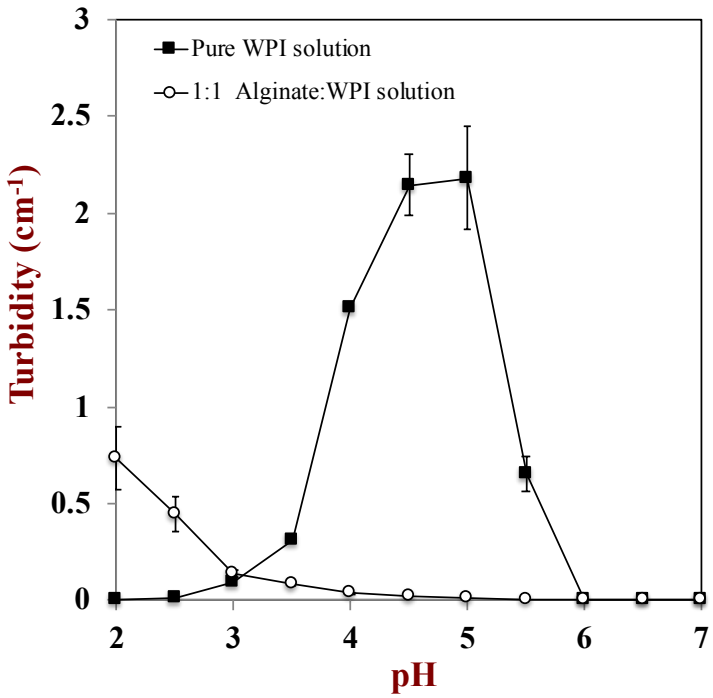

Figure 6. 2 Turbidity (at 600 nm) as a function of pH for aqueous solutions containing either 0.1% WPI and 0.1% sodium alginate or 0.1% WPI only.

6.1.3.2 Turbidity characterization of mixed biopolymer systems

The formation of electrostatic complexes in biopolymer solutions can simply be monitored using turbidity measurements [194]. In this section, the turbidity *versus* pH profiles of the alginate solution, WPI solution, and WPI-alginate mixture were measured as a function of pH using a spectrophotometric method. The alginate solution had a very low turbidity at all pH values (data not shown), indicating that the alginate molecules did not aggregate. As expected, there was a large increase in the turbidity of the WPI solution around the protein's isoelectric point (pI ≈ 4.5) due to protein aggregation associated with the low electrostatic repulsion between the whey protein molecules (**Fig. 6.2**). For the alginate-WPI mixtures, the solution turbidity was relatively low at high pH ($5 < pH < 7$) due to the high solubility of the individual protein and alginate molecules, and the fact that there would be a strong electrostatic repulsion between the two types of biopolymer in this pH range. When the pH was reduced further, there was a gradual increase in turbidity from pH 5 to 3, followed by a steep increase from pH 3 to a maximum value at pH 2. This result suggests that electrostatic complexes large enough

to scatter light strongly were formed at pH values below about 4. As mentioned earlier, small electrostatic complexes may also be formed under conditions (pH 4.0 to 5.5) where both the WPI and alginate molecules have net negative charges due to electrostatic attraction between anionic groups on the polysaccharide and cationic patches on the protein surfaces [166, 191, 350]. As reported in these studies, the presence of an anionic polysaccharide can suppress the aggregation of globular proteins that normally occurs around their isoelectric point. This effect can be attributed to the fact that the protein and polysaccharide molecules form an electrostatic complex, and there is a relatively strong electrostatic and steric repulsion between the complexes. In summary, these results have highlighted the fact that the alginate and whey protein molecules should bind strongly to each other at relatively low pH values due to electrostatic attraction.

6.1.3.3 Particle size characterization of polymer mixtures at different pH

Three different pH values were selected for further study based on the expected differences in the electrostatic interactions between the whey protein and alginate molecules: electrostatic repulsion at pH 7; soluble complex formation at pH 5; and, insoluble complex formation at pH 3. The particle size distributions of biopolymer mixtures containing alginate and WPI at a ratio of 1:1 (w/w) were measured at different pH values (**Fig. 6.3**). At pH 7, the biopolymer mixtures appeared optically transparent, which suggested that they did not contain particles large enough to scatter light appreciably, consequently reliable light scattering measurements could not be made. At pH 5, the particle size distribution of the biopolymer mixtures was bimodal, suggesting there was a wide range of different-sized colloidal particles present. These particles were presumably held together by a weak electrostatic attraction between the whey protein and alginate molecules. Visually, these samples had a turbid appearance, which again indicated the formation of relatively large complexes in these samples. At pH 3, there was a monomodal distribution of relatively large particles present ($d \approx 500$ μm), which formed due to the strong electrostatic attraction between the cationic whey protein and anionic alginate molecules. The colloidal dispersions formed in the mixed systems at pH 3 had a higher lightness (white color) than those formed at pH 5, which suggests that the former particles scattered light more strongly. This may have occurred because the

biopolymer molecules were packed more tightly together in the complexes at the lower pH value [191], which led to a higher refractive index contrast.

6.1.3.4 Hydrogel beads formed at different pH

Relatively large alginate beads (d > 1 mm) are typically formed using the most commonly used extrusion method, which involves simply injecting an alginate solution into a calcium bath using a syringe or pipette [252, 351-352]. This bead size is too large for many commercial applications since it adversely impacts the physicochemical or sensory properties of the products they are incorporated into. In this study, we therefore fabricated relatively small alginate beads (d < 500 μm) using a specially designed extrusion device (Encapsulator) that uses a vibrating 120-μm nozzle and a syringe pump. These smaller beads may have several advantages over larger ones in terms of their impact on product appearance, rheology, mouthfeel and stability. On the other hand, smaller beads may have lower retention and higher release rates than large ones because of the reduced diffusion path of the encapsulated agents through the hydrogel matrix [76]. It is therefore important to design alginate beads so that they satisfy the different

physicochemical requirements for each application.

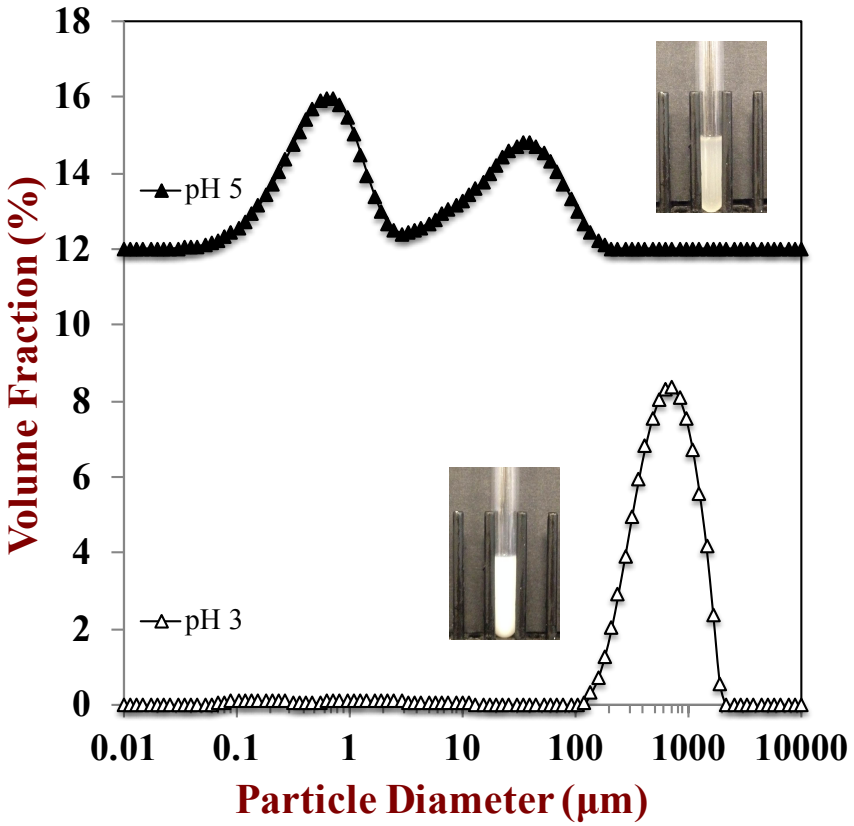

Figure 6. 3 Particle size distribution and appearance of biopolymer mixtures containing alginate and WPI (1:1 w/w) at pH 3 and 5. The solutions were transparent at pH 7, and therefore reliable particle size measurements could not be made.

The influence of fabrication pH on the properties of alginate beads was investigated by injecting WPI-alginate mixtures into Ca^{2+} solutions at pH 3, 5, and 7. As mentioned earlier, these three pH values were selected because they led to different electrostatic interactions between the protein and alginate molecules. The light scattering measurements indicated that the particle size distribution and mean diameter of the hydrogel beads was influenced by the fabrication pH: d_{43} = 288, 471, and 516 µm at pH 7, 5 and 3, respectively (**Fig. 6.4**). There are a number of factors that may contribute to the influence of pH on bead dimensions. First, the negative charge on the alginate molecules decreases with decreasing pH (**Fig. 6.1**), which may reduce the number of anionic groups on the alginate molecules that are available for cross-linking with calcium ions. Second, the charge on the protein molecules varied from negative to positive with decreasing pH

(**Fig. 6.1**), which will have altered any interactions between the protein and alginate molecules. Again, these interactions may also have interfered with the ability of the calcium ions to cross-link the alginate molecules. As a result of these effects, the kinetics of alginate gelation, as well as the nature of the gel network formed, may have been changed, which altered the dimensions of the beads formed.

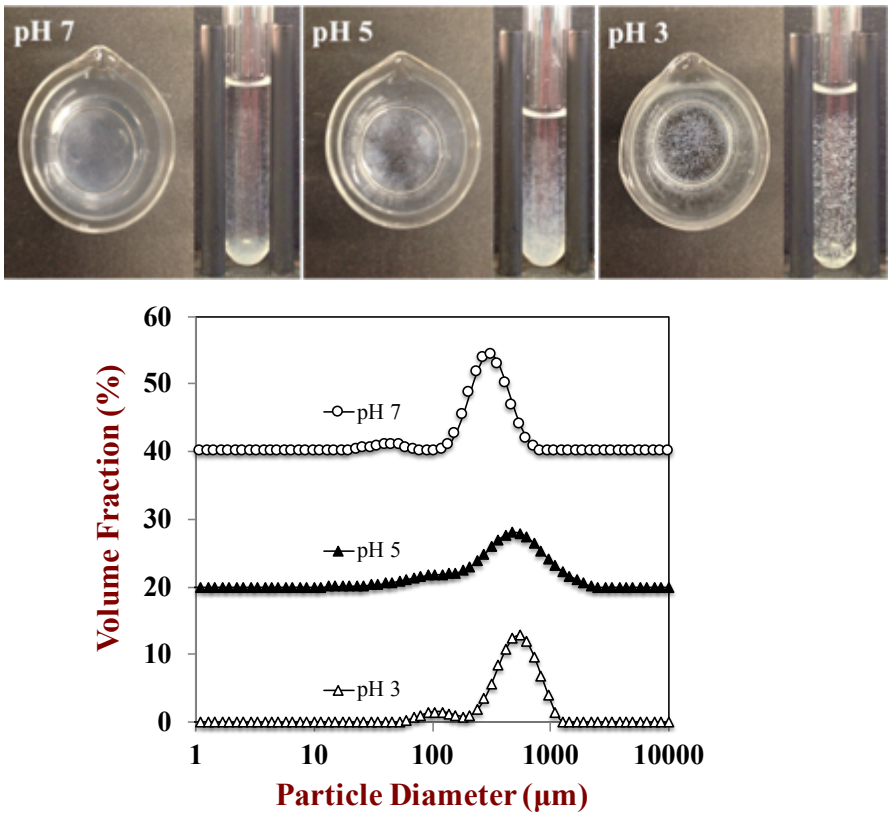

Figure 6. 4 Particle size distribution and appearance images of hydrogel beads formed at different pH (pH 3, 5 and 7).

The appearance of the suspensions of hydrogel beads changed from translucent to a whitish color when the fabrication pH was reduced from 7 to 3 (**Fig. 6.4**). In addition, there appeared to be some visible clumping of the particles at lower pH values. This result suggests that there may have been some aggregation of the protein-loaded alginate beads, which may have been due to a reduction in the electrostatic repulsion between the beads at lower pH values.

The protein encapsulation efficiency of the alginate beads depended on the pH used to fabricate them: pH 7 (11.6%) < pH 5 (19.1%) < pH 3 (58.6%) (**Fig. 6.5**). In addition, the confocal fluorescence microscopy images of the hydrogel beads indicated that the protein concentration (fluorescence intensity) within them was higher at the lowest fabrication pH (**Fig. 6.5**). This trend is related to the strength of the electrostatic interactions between the protein and alginate molecules. At pH 5 and 7, there will be a strong electrostatic repulsion between the anionic protein and anionic alginate molecules (**Fig. 6.1**), and therefore the protein molecules may not have been effectively trapped within the alginate beads during their formation. As mentioned earlier, at pH 5 alginate and protein molecules may bind together due to the attraction of anionic groups on the alginate molecules to cationic patches on the protein surfaces (even though both have a net negative charge). However, the attractive alginate-protein interactions may have been much weaker than the alginate-calcium interactions, and so the protein was released when the alginate solution was titrated into the calcium solution. At pH 3, there will have been a strong electrostatic attraction between the cationic protein and anionic alginate molecules (**Fig. 6.1**), and therefore the two biopolymers may be held together more strongly during the cross-linking process. Consequently, the protein molecules are retained within the alginate beads during their fabrication at low pH values. It should also be noted that the pores within the alginate beads must have been sufficiently large to allow the protein molecules to diffuse through them [291]. It is interesting to note that the particle size of beads observed from these confocal images was slightly inconsistent with the results of light scattering measurements (**Fig.6.4**). It may be because the beads fabricated in this study were not uniform sphere, and then the size characterization observed by the confocal microscope could be influenced by the viewing angle. Moreover, all the beads formed at different pH conditions showed the broad particle size distributions. The confocal images of these beads were taken by random, which cannot guarantee the obtaining of images of beads with the representative characterization (e.g., a mean diameter).

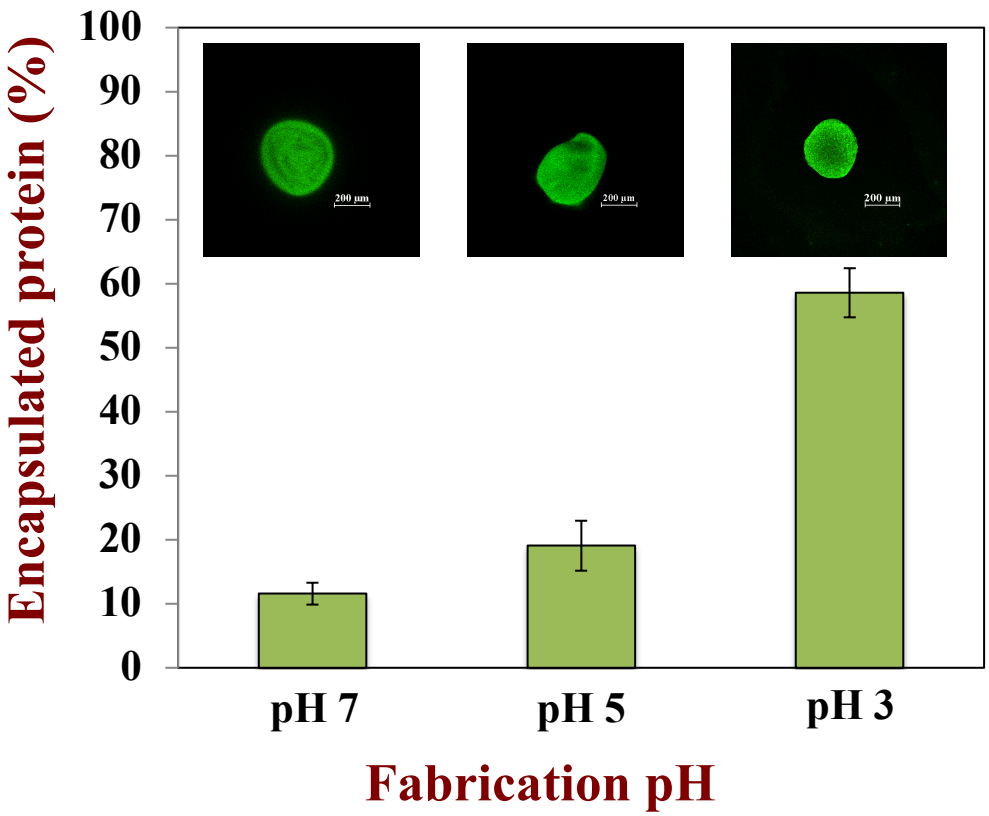

Figure 6. 5 Confocal images and protein encapsulation efficiency of hydrogel beads formed at different pH (pH 3, 5 and 7). The WPI (green) was stained with FITC.

6.1.3.5 Protein release during storage

In this section, the rate of protein release from the alginate beads formed at different fabrication pH values was compared. At pH 5 and 7, there was a relatively rapid release of protein during the first 30 min of storage, followed by a more gradual release at longer storage times (**Fig. 6.6**). On the other hand, at pH 3, the release of protein occurred relatively slowly throughout the 6-hour storage period. The final amount of protein released at the end of the incubation period depended strongly on pH: pH 3 (24%) < pH 5 (78.9%) < pH 7 (95.3%). As discussed in the previous section, this effect can be attributed to differences in the electrostatic interactions of the alginate and protein molecules at different pH values. At pH 3, the protein and alginate have opposite charges and are strongly attracted to each other, and so the protein is better retained within the hydrogel beads. Conversely, at pH 5 and 7 the protein and alginate have similar charges and therefore tend to electrostatically repel each other, so the protein tends to leach out of

the hydrogel beads. A similar effect has also been observed with electrically charged drugs trapped within alginate beads. For example, it has been reported that a cationic drug (chlorpheniramine maleate) showed a much slower release rate from alginate gels than an anionic drug (sodium salicylate) [353-354].

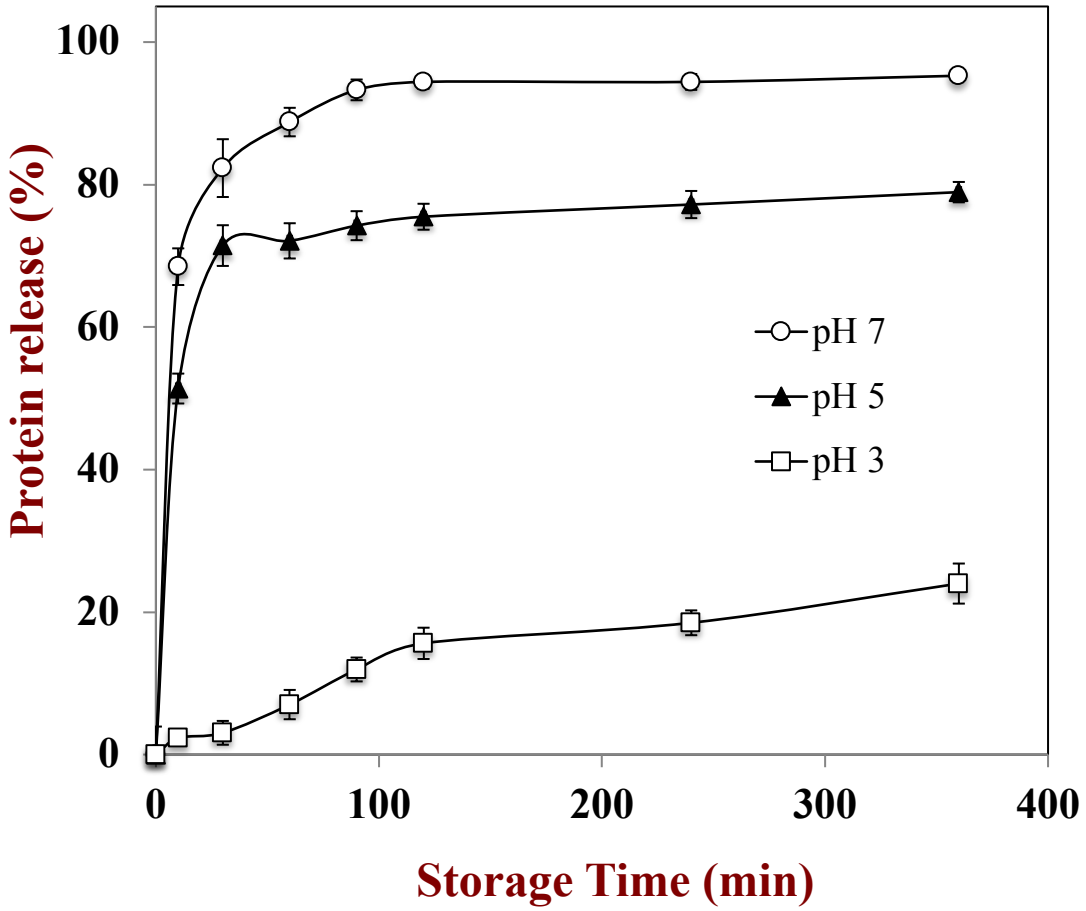

Figure 6. 6 Leakage of WPI from hydrogel beads formed at different pH as a function of incubation time. The beads were immersed into the according PBS buffer (pH 3, 5 and 7) at room temperature.

The pH dependence of the protein release rate may also depend on changes in the structure of the alginate beads under different solution conditions. It was reported that calcium alginate beads tend to shrink at low pH due to the loss of negative charge on the alginate molecules when the carboxyl groups become protonated (–COOH, p$K_a \approx 3.5$) [76]. Conversely, they tend to swell when placed in higher pH solutions due to the fact that the alginate molecules become highly charged and repel each other [270]. Thus, the faster release of the protein molecules at pH 5 and 7 may have been partly due to the fact that

the hydrogel network had larger pores at these higher pH values. Nevertheless, further work is required to measure the pore size of the alginate beads to confirm the importance of this mechanism, *e.g.,* using electron microscopy or size exclusion methods [291].

6.1.3.6 pH-triggered protein release from hydrogel beads

The change in the electrical properties of the alginate and protein molecules with pH means that protein-loaded alginate beads may be designed to release the proteins in response to a pH trigger [270]. In this section, protein-loaded alginate beads were initially fabricated at pH 3 since they had a high loading capacity and good retention properties (Sections 3.4 and 4.5). The protein release from these hydrogel beads was then measured after they were stored at different pH values for 10 min. The storage pH of the beads had a pronounced impact on the amount of protein released, with the amount released increasing with increasing pH (**Fig. 6.7b**). For example, around 11% protein was released from the hydrogel beads after incubation at pH 3.5, whereas around 90% protein was released when they were incubated at pH 7. These results were confirmed by confocal fluorescence microscopy images of the hydrogel beads, which showed that the fluorescence intensity (protein) of the hydrogel beads decreased with increasing pH (**Fig. 6.7a**), which suggests that some of the whey protein molecules had diffused out of the hydrogel beads at higher pH values. These results suggest that protein-loaded alginate beads could be fabricated at relatively low pH values (pH 3) to effectively retain the protein, and then the protein could be released by increasing the pH of the hydrogel beads environment. This type of pH-triggered hydrogel bead may be a useful tool for protection of proteins in the acidic environment of the stomach, and then releasing them in the neutral environment of the small intestine. If required, the initial hydrogel beads could be coated with extra layers of biopolymers (*e.g.*, chitosan or polylysine) using an electrostatic deposition approach to modulate their functional properties, such as stability, integrity, and permeability [291].

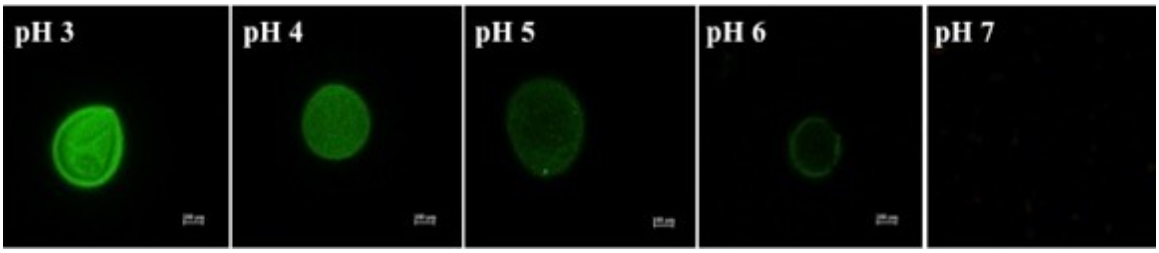

(a)

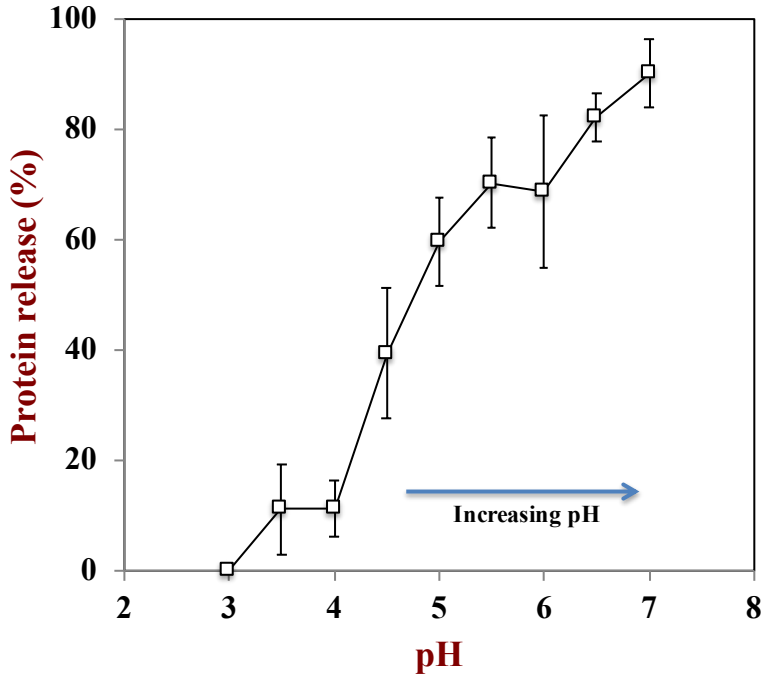

(b)

Figure 6. 7 Protein release characterization from the hydrogel beads by changing pH from the initial condition (pH 3): (a) confocal images of hydrogel beads at initial and final pH. (b) WPI release fraction (%) after changing pH condition.

6.1.4 Conclusions

The effect of pH on the encapsulation, retention and release of whey proteins from alginate-based hydrogel beads was studied. Different pH values (pH 3, 5 and 7) were chosen to fabricate the hydrogel beads based on differences in the nature of the

electrostatic interactions (attraction or repulsion) between the alginate and protein molecules. Protein-loaded hydrogel beads were successfully prepared using an encapsulation unit with a small vibrating nozzle to inject the whey protein/alginate mixture into a Ca^{2+} solution. The protein encapsulation efficiency and retention of the beads increased with decreasing fabrication pH (pH 7 < pH 5 < pH 3), which was attributed to the fact that there was a strong electrostatic attraction between the cationic protein and anionic alginate molecules at pH 3. Consequently, the protein molecules were held in the alginate beads more strongly. The hydrogel beads prepared in this study could be designed to release the protein molecules in response to a pH trigger. The amount of protein released increased as the pH of the surrounding solution was increased from pH 3 to pH 7, which was again attributed mainly to a weakening of the electrostatic attraction between the encapsulated protein molecules and the alginate hydrogel with increasing pH. These results have important implications for designing hydrogel beads to encapsulate, retain, and release of proteins in food products and within the gastrointestinal tract.

6.2 Fabrication of microgels to encapsulate the protein and control its digestion properties in GIT

6.2.1 Introduction

Proteins play a number of important roles as nutritional components within the human diet. They are a source of essential amino acids and bioactive peptides, provide energy, are potential allergens, and regulate hormonal responses, such as hunger, satiety and satiation [128, 133, 355-358]. The rate, extent, and location of protein hydrolysis within the human gastrointestinal tract (GIT) impacts many of these attributes. Protein hydrolysis is typically carried out by digestive enzymes within the stomach and small intestine [133, 359]. In humans, protein digestion begins in the stomach due to the presence of gastric pepsins that are activated under acidic conditions [360]. These enzymes breakdown peptide bonds within the protein molecule, which results in the formation of a mixture of polypeptides, oligopeptides, and amino acids. After leaving the stomach, any remaining proteins or peptides are further hydrolyzed by pancreatic enzymes (such as trypsin, chymotryosin, elastase and carboxypeptidases A and B) activated in the duodenum [361]. Eventually, the amino acids and small peptides resulting from protein digestion are absorbed by the epithelium cells and enter the systemic circulation. Protein digestion products impact various human functions regulated by hormones, including gastrointestinal motility, gastric emptying time, secretion of acid and pepsinogen, and total protein and energy intake [362-363]. It may therefore be possible to modulate these hormonal responses by controlling the rate and extent of protein digestion within the GIT.

Structural design of food matrices has been proposed as a method of controlling the digestion and release of macronutrients within the GIT, and therefore as a means to modulate their physiological effects [363-364]. In the current study, we examined the impact of encapsulating proteins inside biopolymer microgels on their gastrointestinal fate using an *in vitro* digestion model. Our previous studies showed that encapsulation of lipids inside biopolymer microgels retarded the rate and extent of lipid digestion under simulated GIT conditions, which was attributed to the ability of the biopolymer network to restrict interactions between the digestive enzymes and their substrates [76, 365]. Biopolymer microgels are normally fabricated from food-grade proteins and/or

polysaccharides [270, 366]. The substance to be encapsulated is typically mixed with a biopolymer solution, which is then gelled by adding an appropriate cross-linking agent (such as an ion, acid, base or enzyme) or by changing environmental conditions (such as temperature or pressure) [229, 270]. Numerous approaches can potentially be used to fabricate protein-loaded microgels, including injection, templating, and phase separation methods [367-368]. The injection-gelation method is one of the most commonly used approaches for encapsulating bioactive substances in biopolymer microgels because of its relative simplicity and low cost. In this approach, an aqueous solution containing the bioactive agent and a gelling biopolymer is injected into a ‘‘hardening’’ solution to promote particle formation and biopolymer cross-linking. This procedure results in the formation of biopolymer microgels with the bioactive agent trapped inside. The GIT fate of the bioactive agent can be modulated by changing the composition, dimensions, or pore size of the microgels [270].

In this study, we examined the possibility of control the digestion of proteins under simulated GIT conditions by encapsulating them inside biopolymer microgels fabricated from calcium alginate. Our previous studies have shown that native proteins can easily escape from biopolymer microgels under conditions where there is not a strong attraction between the biopolymer network and protein molecules, *i.e.,* at pH values above the isoelectric point of the protein [269]. This phenomenon was mainly attributed to the fact that the pore size of the microgels is appreciably greater than the dimensions of the native protein molecules. Consequently, the protein molecules can easily diffuse out of the microgels when there is no electrostatic attraction between them and the biopolymer network. For this reason, we examined the impact of using a thermal treatment to promote protein denaturation and aggregation inside the microgels on protein encapsulation and retention. The resulting protein-loaded microgels were passed through a simulated GIT that included mouth, stomach, and small intestinal phases. An *in vitro* pH-stat method was used to determine the degree of protein hydrolysis in the simulated stomach and small intestine phases. We hypothesized that the encapsulation of denatured protein inside the microgels would retard its digestion and release under simulated GIT conditions. The present work for the first time combined the alginate and WPI cross-linking through the calcium ions within one delivery system and then evaluated the

digestion fate of protein in this novel system. The information obtained in this study may be useful for the development of functional foods to regulate gastrointestinal responses, such as hunger, satiety, and satiation.

6.2.2 Materials and Methods

6.2.2.1 Materials

Whey protein isolate (WPI) was kindly provided by Davisco Foods International Inc. (Le Sueur MN). The following chemicals were purchased from the Sigma Chemical Company (St. Louis, MO): alginic acid (sodium salt); pepsin from porcine gastric mucosa; fluorescein isothiocynate (FITC) isomer I; calcium chloride dehydrate; porcine trypsin and bovine α-chymotrypsin. All chemicals used were analytical grade. Double distilled water was used to prepare all solutions. All concentrations are expressed as weight percentages (% w/w), unless otherwise stated.

6.2.2.2 Heated protein preparation

Protein solutions (10% WPI) were prepared by dissolving powdered whey protein isolate into phosphate buffer solution at pH 7 with continual stirring. In some cases, the dissolved protein solutions were heated at 80 °C for 15 min in a water-bath, then rapidly transferred to an ice-water bath for 10 min, and then stored at room temperature for 24 h.

6.2.2.3 Protein-loaded microgel preparation

For the heated WPI-loaded microgels, an aqueous alginate solution was first prepared by dissolving powdered sodium alginate (1.6%) in phosphate buffer with continual stirring until complete dissolution. The heated WPI and alginate solutions were then mixed together (1:1, v/v) for 1 h with continual stirring to form a uniform solution. The resulting mixture was then injected into a 10% calcium chloride solution using a commercial encapsulation unit with a 120 mm vibrating nozzle (Encapsulator B-390, BUCHI, Switzerland). The microgels formed by this process were then kept in the calcium chloride solution for 1 h at ambient temperature to promote cross-linking of the

alginate molecules. For digestion experiments, the calcium alginate beads were collected by filtration and then washed with phosphate buffer and distilled water to remove any excess ions from their surfaces. After determining the total weight of the dry beads, they were stored in a refrigerator for further measurements.

Two control samples were also fabricated to determine the impact of protein state on protein encapsulation and retention: native WPI-loaded microgels and heated native WPI-loaded microgels. The native WPI-loaded microgels were fabricated by encapsulation of unheated whey protein inside the microgels using the same procedure as described above. The heated native WPI-loaded microgels were prepared by firstly fabricating the native WPI-loaded microgels, and then heating them at 80 °C for 15 min in a water-bath. The resulting microgels were then cooled using an ice-water bath for 10 min, and then stored at room temperature for 24 h.

6.2.2.4 Gastrointestinal tract model

For the simulated GIT studies, four samples were prepared using the procedures described in the previous sections: native WPI; heated WPI; heated WPI-loaded beads; and, heated WPI with beads. The heated WPI with microgels samples were prepared by mixing a heated WPI solution with un-loaded microgels. All the samples were then diluted with buffer solution (5 mM phosphate buffer, pH 7) to obtain the same initial protein amount (0.375g). The diluted samples were then passed through a static GIT model that simulated the mouth, stomach, and small intestine phases.

Initial system. 7.5 g of the initial samples were preheated in an incubator shaker at a rotation speed of 100 rpm at 37 °C for 15 min (Innova Incubator Shaker, Model 4080, New Brunswick Scientc, Edison, NJ).

Mouth phase. 7.5 g of simulated saliva fluid (SSF) was preheated to 37 °C and then mixed with the initial samples with continual stirring. After being adjusted to pH 6.8, the mixture was incubated in an incubator shaker (37 °C) for 2 min to mimic agitation in the mouth.

Stomach phase. The potential gastric fate of the samples was monitored using a simulated stomach model based on previously reported standardized *in vitro* methods [253, 369-370], with some small modifications. Specifically, 15 g of sample solution resulting from the mouth phase was placed into a water bath at 37 °C and then adjusted to pH 3.0. 15 g of simulated gastric fluid (containing 0.0032 g/mL pepsin (≥ 250U/mg), preheated to 37 °C, at pH 3.0) was then added to the reaction vessel with constant stirring. An automatic titration unit (Metrohm, USA Inc.) was used to monitor the pH and maintain it at pH 3.0 by titrating 0.05 N HCl solution into the reaction vessel for 2 hours at 37 °C. The volume of acid added to the stomach phase was recorded over time and used to calculate the degree of hydrolysis (DH) of the proteins using the following equation [371] **(1, 2**):

$$DH = [(V_A \times N_A)/M_P] \times (1/P) \times F_{PH} \times 100\% \quad (1)$$

Here: V_A is the volume of acid (HCl) solution (mL) titrated into the reaction vessel, N_A is the normality of the acid (0.05 N), M_P is the mass of the protein (0.375 g), P is the total number of peptide bonds (8.75 mol/g for WPI) and F_{PH} is a correction factor (1.8) that takes into account that the peptides are only partially ionized at pH 3.0.

Small intestinal phase. Samples from the stomach phase were adjusted to pH 7.00 and then 1.5 mL of simulated intestinal fluid and 3.5 mL of bile salts (bile extract, porcine) solution was added to the reaction vessel with constant stirring. The resulting mixture was then adjusted back to pH 7.00 if required. 2 mL of 1.25 mg/mL trypsin (1000-2000U/mg) and 2 mL of 5 mg/mL α-chymotrypsin (≥ 40U/mg) were added to the reaction vessel. The quantity of enzymes used in this step based on previously published values [371-372]. The pH was maintained at 7.0 by titrating 0.1 N NaOH solution into the reaction vessel for 2 hours at 37 °C. The volume of alkali solution added to the small intestine phase was recorded over time and used to calculate the degree of protein hydrolysis using the following equation :

$$DH = [(V_B \times N_B)/M_P] \times (1/P) \times F_{PH} \times 100\% \quad (2)$$

Where: V_B is the volume of base (NaOH) solution (mL) titrated into the reaction vessel, N_B is the normality of the base solution (0.1 N), ($1/\alpha = 3.03$ at pH 7 at 37°C), M_P is the mass of the protein [$0.375g \times (1\text{-}DH_{stomach}\%)$], P is the total number of peptide bonds (8.75 mol/g for WPI), and F_{PH} is a correction factor (3.03) that takes into account that the peptides are only partially ionized at pH 7.0 [371].

6.2.2.5 Particle charge

The electrical characteristics (ζ-potential) of the samples were measured using an electrophoresis instrument (Zetasizer Nano ZA series, Malvern Instruments Ltd. Worcestershire, UK). Samples were diluted with appropriate pH-adjusted solutions prior to measurements to avoid multiple scattering effects. Phosphate buffer (5 mM, pH 7.0) was used to dilute the initial, mouth, and small intestine samples while acidified water (pH 3) was used for the dilution of stomach samples.

6.2.2.6 Particle size characterization

Particle size distributions of the samples were determined using static light scattering (Mastersizer 2000, Malvern Instruments Ltd., Malvern, Worcestershire, UK). Again, phosphate buffer (5 mM, pH 7.0) was used for the dilution of the initial, mouth and small intestine samples and acidified water (pH 3) was used to dilute the stomach samples to avoid multiple scattering effects. The average particle sizes are reported as the surface-weighted mean diameter (d_{43}).

6.2.2.7 Microstructure analysis

The microstructure of samples was analyzed using confocal scanning fluorescence laser microscopy with a 20 × objective lens (Nikon D-Eclipse C1 80i, Nikon, Melville, NY, U.S.). The proteins were dyed by adding 0.1 mL of FITC dye solution (1 mg FITC/mL dimethyl sulfoxide) to 2 mL of sample and then storing at 5 °C overnight. The excitation and emission wavelength used for FITC were 488 nm and 515 nm, respectively. The resulting confocal microstructure images were analyzed using image analysis software (NIS-Elements, Nikon, Melville, NY).

6.2.2.8 Statistical analysis

All experiments were performed on at least three freshly prepared samples. The results are reported as averages and standard deviations. These analyses were carried out using Excel (Microsoft, Redmond, VA, USA).

6.2.3 Results and discussion

6.2.3.1 Protein-loaded bead preparation and characterization

Three types of whey protein-loaded microgels were fabricated so as to determine the impact of protein state (native *versus* denatured) and time of denaturation (before or after protein loading) on microgel formation and protein retention. The three systems studied were: (i) native protein microgels (N-MGs); (ii) post-loading denatured protein microgels (post-D-MGs); and, (iii) pre-loading denatured protein microgels (pre-D-MGs). For system (ii), native whey proteins were first encapsulated inside microgels, and then the microgels were heated to denature the proteins. For system (iii), a solution of whey proteins was first heated to denature the proteins, and then the denatured proteins were encapsulated inside the microgels.

The visual appearance and confocal fluorescence images of these samples are shown in Figure 6.8. The microscopy images of the N-MGs showed that the proteins (stained green) were uniformly distributed throughout the continuous phase surrounding the microgels, rather than being located within the microgels (Fig. 6.8a). This result can be attributed to the low encapsulation efficiency of the native whey proteins in the microgels. Our previous studies have also shown that native proteins leaked out of alginate microgels when they are incubated in neutral buffer solutions [266, 269]. The reason for this phenomenon can be attributed to the relatively large pore size of the biopolymer network inside the microgels (tens to hundreds of nanometers) compared to the dimensions of the protein molecules (a few nanometers). In addition, the protein molecules and biopolymer network (alginate) are both negatively charged at neutral pH and so they tend to electrostatically repel each other. Fairly similar results were observed for the systems in which the proteins were denatured after they had been loaded into the

microgels, *i.e.,* post-D-MGs (Fig. 6.8b). Again, most of the proteins (stained green) were present in the continuous phase surrounding the microgels, rather than trapped inside them. There may have been a number of reasons for this phenomenon. First, the native proteins may have rapidly diffused out of the microgels prior to heating. Second, the protein molecules inside the microgels may have been resistant to thermal denaturation or aggregation, and so they were still small enough to rapidly diffuse out of the microgels. In contrast, almost all of the proteins appeared to remain trapped inside the microgels when the proteins were denatured before they were incorporated into the microgels, *i.e.,* pre-D-MGs (Fig. 6.8c). In addition, visual observations of these microgels indicated that they had a whitish color rather than the more translucent appearance of the other two samples. This effect was probably because the presence of the proteins inside the microgels increased their refractive index, which led to stronger light scattering [373]. These results suggest that the most effective means of ensuring a high retention of the proteins under neutral pH conditions is to pre-heat the proteins prior to forming the microgels.

Previous studies have reported that heating aqueous whey protein solutions above their thermal denaturation temperature at neutral pH leads to the formation of long filaments [374]. Moreover, studies have shown that these anionic protein filaments are cross-linked in the presence of Ca^{2+} ions at ambient temperature [375-377]. Consequently, the proteins may have remained within the microgels for the pre-D-MGs because they were present as large filaments that could not easily diffuse through the biopolymer network, and because they were cross-linked by the calcium ions during the alginate gelation process (**Fig. 6.9**). For this reason, the pre-D-MGs were selected to study the effect of bead encapsulation on the gastrointestinal fate of the whey proteins in the remainder of the study.

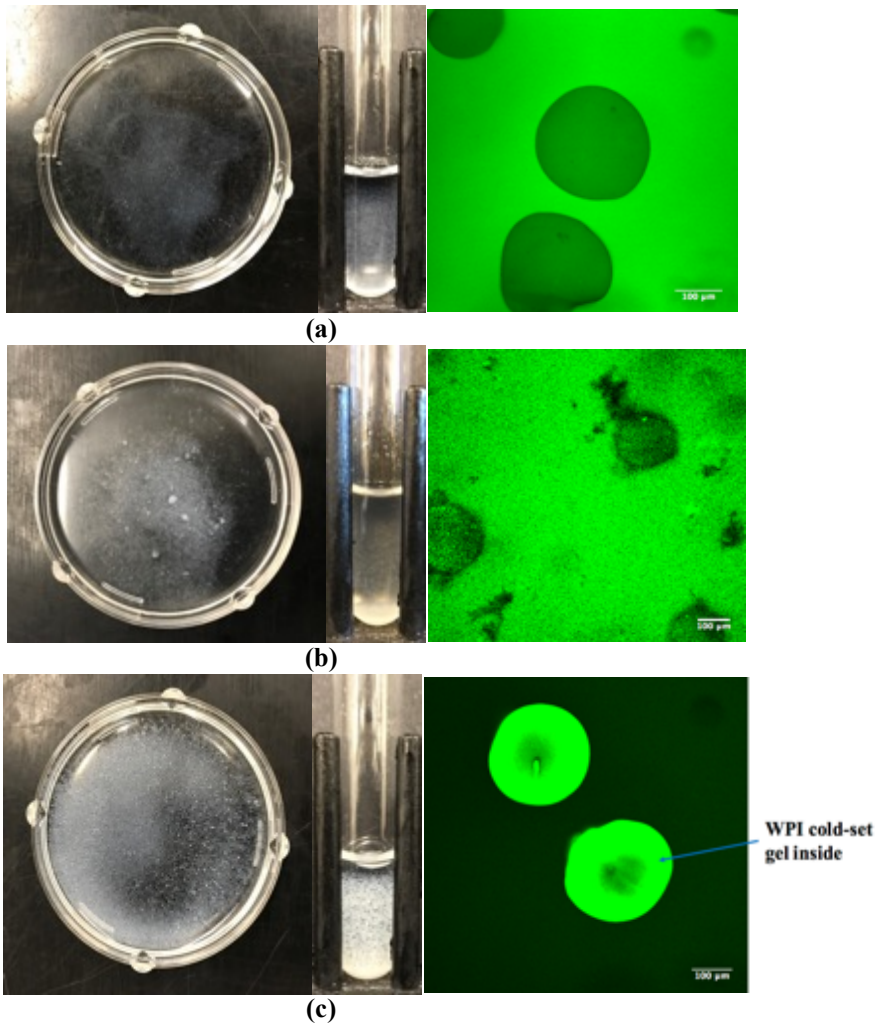

Figure 6. 8 Visual appearance and confocal images of (a) native protein microgels (N-MGs), (b) post-loading denatured protein microgels (post-D-MGs), and (c) pre-loading denatured protein microgels (pre-D-MGs) in the calcium chloride solution.

6.2.3.2 Impact of gastrointestinal passage on electrical characteristics

In this section, four different samples were studied to determine the impact of denaturation and encapsulation on the gastrointestinal fate of the proteins: native protein solutions (N-S); denatured protein solutions (D-S); pre-loading denatured protein microgels (pre-D-MGs); and, denatured protein solutions mixed with microgels (D-S+MGs). The electrical characteristics (ζ-potential) of these samples were measured as they passed through the various stages of the simulated GIT. The initial ζ-potential values of all the samples were highly negative: -19.9, -22.8, -26.7 and -21.9 mV for N-S, D-S, pre-D-MGs and D-S+MGs, respectively (**Figure 6.9**). The net negative charge of the

native and denatured protein solutions can be attributed to the fact that the pH was above the isoelectric point of the whey proteins. The negative charge on the protein-loaded microgels (pre-D-MGs) can be attributed to the presence of anionic carboxylic ($-COO^-$) groups on the mannuronic and guluronic acid monosaccharides that make up the alginate chains. As expected, the sample containing a mixture of denatured proteins and microgels (D-S+MGs) also had a negative charged because both the anionic proteins and the anionic microgels contributed to the overall electrophoretic signal [365].

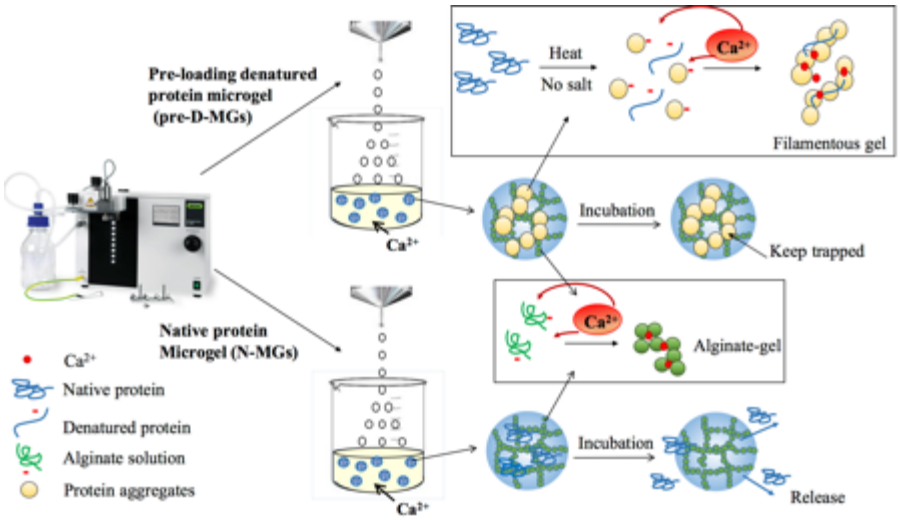

Figure 6. 9 The schematic of the fabrication and incubation properties of native protein microgels (N-MGs) and pre-loading denatured protein microgels (pre-D-MGs).

After passing through the simulated mouth phase, there was a slight decrease in the magnitude of the negative ζ-potential for all samples (Figure 6.9). This reduction may have occurred due to the presence of mineral ions in the simulated saliva, which decrease the magnitude of the ζ-potential due to ion binding and electrostatic screening effects [365]. A large reduction in the magnitude of the ζ-potential occurred on all the samples after incubation in the simulated stomach phase. Previous studies have attributed this effect to protonation of ionizable groups and electrostatic screening due to the low pH and high ionic strength of the simulated gastric fluids [230]. Under highly acidic pH conditions, the proteins should become positively charged, but this charge may have been partially neutralized by the presence of the anionic mucin molecules from the mouth. The microgels should also lose much of their negative charge under highly acidic conditions due to protonation of the carboxyl groups on the alginate chains. After exposure to the

simulated small intestine phase, all the samples again showed relatively high negative charges. Under these conditions both the digested proteins and the alginate molecules should have regained their negative charge since the pH was well above the pK_a values of the anionic carboxyl groups. Moreover, there will have been other types of anionic species present in the small intestine phase after digestion, such as bile salts, mucin, and digestive enzymes.

6.2.3.3 Impact of gastrointestinal passage on particle size and microstructure

In this section, the microstructure of the different systems was determined after exposure to each GIT stage. In addition, the particle size of the samples containing microgels was measured using static light scattering. The protein solutions could not be analyzed using light scattering because the particles were too small to detect using this instrument.

Protein solutions. The confocal microscopy images indicated that the microstructures of both protein solutions (native and denatured) were fairly similar throughout the GIT process (**Figure 6.11**). Initially, the proteins were uniformly dispersed throughout the samples. Previous studies have reported that heat denatured proteins tend to form homogenous fine stranded network structures at neutral pH [378]. After exposure to the mouth phase, the proteins were still fairly evenly dispersed throughout the system, but there did appear to be some evidence of clumping in the microscopy images. This may have been due to association of the protein molecules with mucin from the simulated saliva. A significant decrease in fluorescence intensity was observed when both protein solutions moved from the mouth to the stomach phase. This decrease can mainly be attributed to the fact that the intensity of the fluorescence probe used to stain the proteins (FITC) is reduced under highly acidic conditions due to quenching [275, 292]. After passing through the small intestine, some relatively large protein-rich particles were observed in the digesta by confocal microscopy, which were probably aggregated whey proteins, peptides, or digestive enzymes.

Microgel samples. The general shape of the particle size distributions of the microgel samples remained monomodal after passing through the different stages of the

GIT model (**Figure 6.10**). This suggested that the microgels were resistant to digestion and disintegration within the GIT, which was confirmed by the confocal microscopy images (**Figure 6.11**). These results were also in agreement with the finding in previous study (3). Nevertheless, appreciable changes in the average dimensions of the microgels were observed when they were exposed to different GIT phases. As has been reported in previous studies, the mean diameter of the alginate microgels was slightly smaller in the highly acidic gastric fluids than in the other phases [379]. This result can be attributed to the fact that the carboxyl groups on the alginate chains are highly charged at neutral pH, and so there is a relatively strong electrostatic repulsion between the chains that promotes swelling of the microgels. On the other hand, the carboxyl groups are partially protonated and so lose their negative charge in acid solutions (*i.e.,* stomach phase), which weakens the electrostatic repulsion between the chains and promotes shrinking of the microgels.

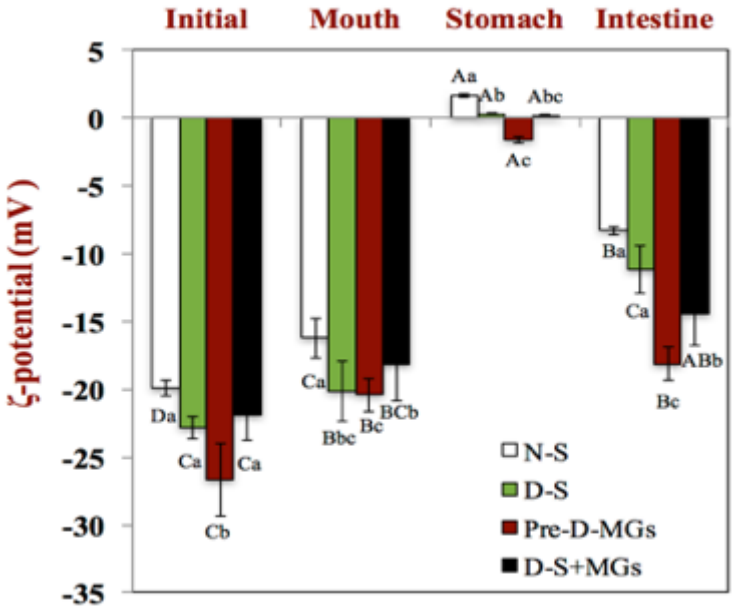

Figure 6. 10 Electrical properties of the different samples measured after exposure to different GIT stages. Samples designated with different capital letters (A, B, C and D) were significantly different (Duncan, $p < 0.05$) when compared between different GIT regions. Samples designated with different lower letters (a, b, c) were significantly different (Duncan, $p < 0.05$) when compared between different delivery systems. (N-S: native protein solutions; D-S: denatured protein solutions; pre-D-MGs: pre-loading denatured protein microgels; and, D-S+MGs: denatured protein solutions mixed with microgels).

The confocal microscopy images of the system that contained denatured proteins mixed with microgels (D-S+MGs) indicated that the proteins in the aqueous phase behaved in a fairly similar manner to those in the denatured protein solutions (D-S). Thus, the GIT fate of the denatured proteins did not appear to be significantly altered by the presence of the alginate microgels (**Figure 6.11**). The confocal microscopy images of the system that contained denatured proteins encapsulated within microgels (pre-D-MGs) indicated that the proteins remained trapped inside the microgels throughout the GIT.

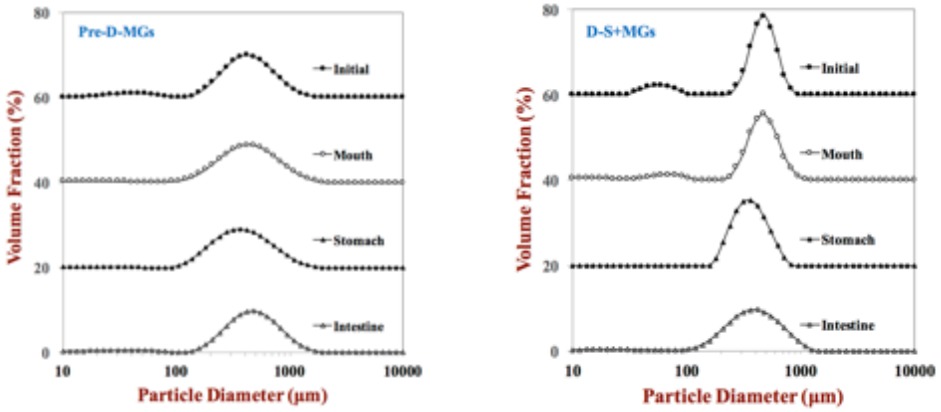

(a) **(b)**

Figure 6. 11 Particle size distributions of different samples after exposure to successive GIT stage: (a) heated WPI in beads (pre-D-MGs) and (b) heated WPI with beads (D-S+MGs).

6.2.3.4 Impact of encapsulation on protein digestion

In this series of experiments, an automatic titration (pH stat) method was used to evaluate the rate and extent of protein digestion in different delivery systems. The principle of this method is that protein hydrolysis causes a change in pH that depends on the number of peptide bonds cleaved, which can be determined by measuring the volume of acid or base solution required to keep the pH constant [371].

Under simulated stomach conditions, there was a rapid digestion of whey protein in all of the samples during the first 5 minutes, followed by a more gradual digestion throughout the rest of the incubation period (**Figure 6.12**). Nevertheless, there were some differences in the digestion rates between the different samples. For the proteins in

solution, the native protein (N-S) was digested more slowly than the denatured protein (D-S). Previous studies have also reported that native whey proteins are more resistant to gastric digestion than denatured ones [380-381], which was attributed to the fact that the peptide bonds in the native globular proteins are more difficult for the proteases to access. Heat treatment induces conformational changes in the protein molecules, which increases the exposure of peptic cleavage sites and thus increases their susceptibility to pepsin hydrolysis. The denatured proteins were digested at a similar rate in the protein solutions (D-S) and in the mixed systems (D-S+MGs), which suggested that the microgels did not alter their hydrolysis. On the other hand, encapsulation of the denatured proteins inside the microgels led to an appreciable decrease in their digestion under simulated gastric conditions (**Figure 6.12**). Presumably, the microgels were able to restrict the ability of the proteases from the aqueous phase to come into contact with the encapsulated protein molecules, thereby reducing their digestion**.**

Under small intestine conditions, the native protein solution (N-S) showed the fastest rate of protein hydrolysis, while all the samples containing denatured protein were digested at a similar slower rate (**Figure 6.13**). Previous studies have reported that the digestion of native proteins in the small intestine is facilitated after they pass through the stomach, which is probably due to partial denaturation of the proteins in the highly acidic gastric fluids [371]. The fact that encapsulation of the denatured proteins within the microgels did not appear to inhibit their digestion under small intestine conditions, despite the fact that the proteins appeared to be trapped within the microgels (**Figure 6.11**), suggests that the digestive enzymes may have been able to penetrate into the microgels under these conditions. These results suggest that the microgels may be able to inhibit protein digestion in the stomach phase, but not in the small intestine phase.

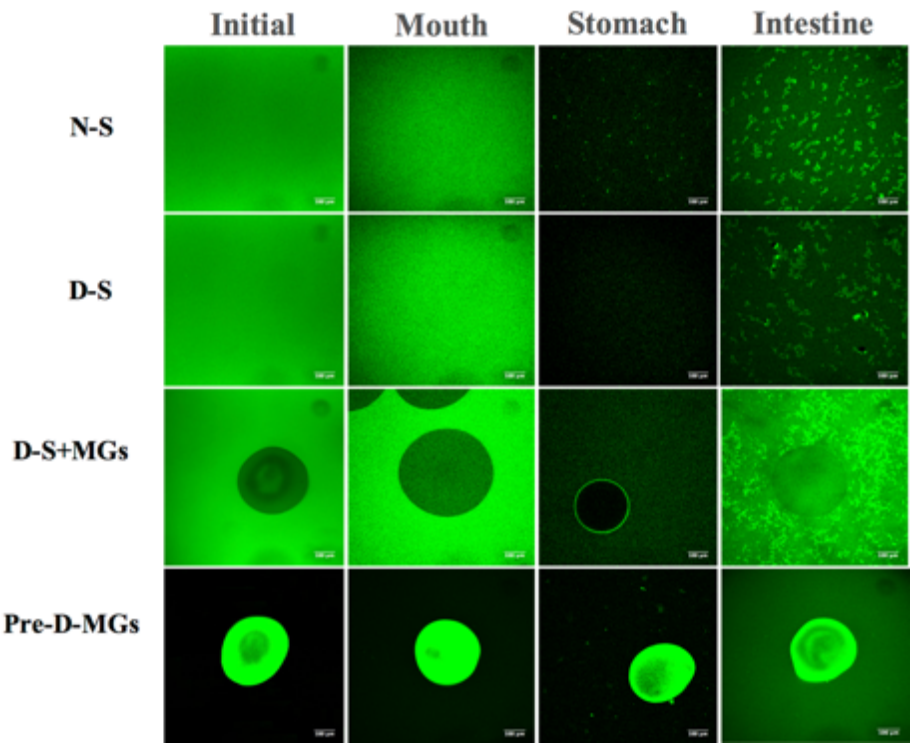

Figure 6. 12 Microstructures of different samples after exposing to different regions of the simulated GIT (Scale bar is 100 μm). (N-S: native protein solutions; D-S: denatured protein solutions; pre-D-MGs: pre-loading denatured protein microgels; and, D-S+MGs: denatured protein solutions mixed with microgels)

Overall, the relatively low extents of protein hydrolysis observed in our study (< 20%), are similar to those reported in other *in vitro* studies [371]. In reality, *in vitro* GIT models cannot reproduce the complex conditions that occur *in vivo* [370]. Therefore, animal and human studies are still needed to verify the impact of encapsulation on protein digestion in practice.

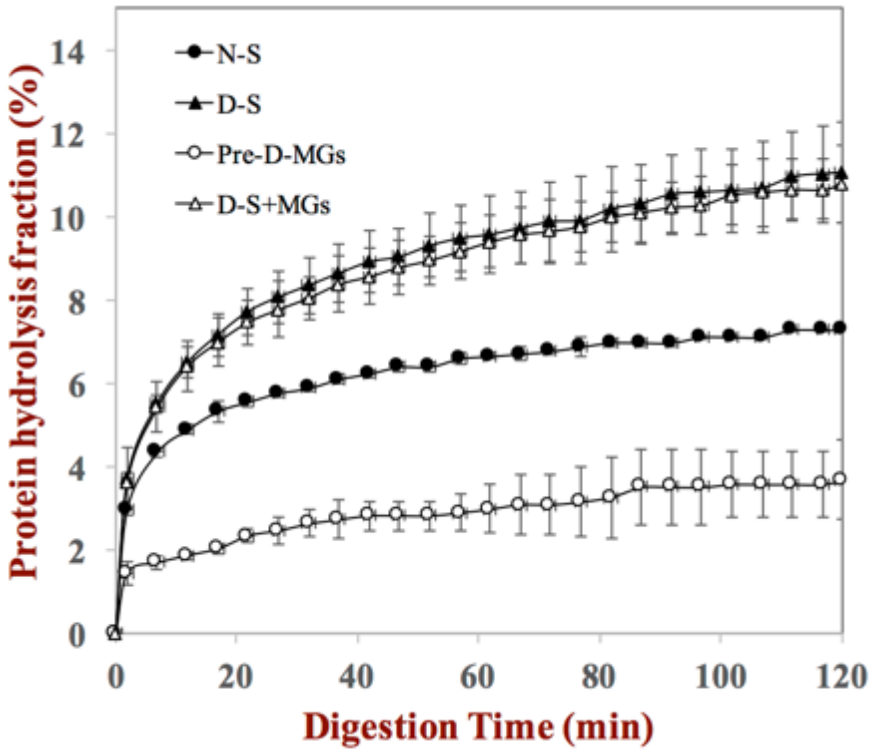

Figure 6. 13 The hydrolytic performance of WPI in different samples under simulated stomach digestion measured using a pH-stat *in vitro* digestion model. (N-S: native protein solutions; D-S: denatured protein solutions; pre-D-MGs: pre-loading denatured protein microgels; and, D-S+MGs: denatured protein solutions mixed with microgels)

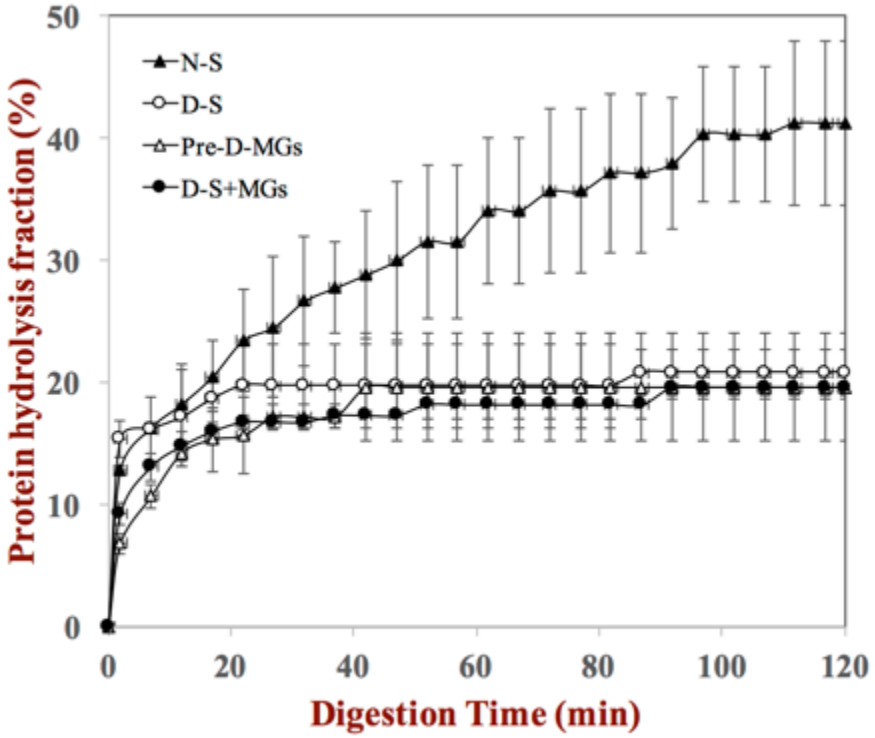

Figure 6. 14 The hydrolytic performance of WPI in different sample after simulated small intestine digestion measured using a pH-stat *in vitro* digestion model. (N-S: native protein solutions; D-S: denatured protein solutions; pre-D-MGs: pre-loading denatured protein microgels; and, D-S+MGs: denatured protein solutions mixed with microgels)

6.2.4 Conclusion

In the present study, it was shown that protein-loaded microgels could be fabricated by injecting a mixture heat-denatured whey protein and alginate molecules into a calcium solution. If the protein molecules were not denatured prior to incorporation into the microgels, they had a tendency to leach out, presumably because they were small enough to diffuse through the pores in the biopolymer network that makes up the interior of the microgels. A simulated GIT method suggested that encapsulation of the denatured proteins within the microgels inhibited their hydrolysis under stomach conditions, but not under small intestine conditions. These results suggest that protein encapsulation in biopolymer microgels may be useful for modulating protein digestion and peptide release within the gastrointestinal tract. However, animal and human studies are needed to confirm these findings in real GITs. Moreover, studies are needed to determine whether

modulating the rate and extent of protein digestion can impact hormonal responses such as hunger, satiety, and satiation.

CHAPTER 7

CONTROL THE RELEASE AND DIGESTION OF LIPIDS USING HYDROGEL BEADS

7.1 Introduction

Triacylglycerols are nutritionally important constituents of the human diet because they are a major supply of energy, a source of essential fatty acids, and carriers of lipophilic micronutrients and nutraceuticals [382]. The digestion of triacylglycerols within the human body is usually highly efficient [126, 383], which can be attributed to the fact that humans evolved in an environment where calories were often scarce. From a physicochemical point of view, lipid digestion is a highly complicated process involving various types of colloidal and interfacial processes throughout the gastrointestinal tract (GIT) [126, 384-385]. The triacylglycerols in ingested foods often exist as lipid droplets or they are converted into lipid droplets during mastication in the mouth or churning in the stomach [1, 385]. In humans, the process of triacylglycerol digestion begins in the stomach due to the presence of gastric lipase, but is mainly carried out in the small intestine due to the presence of pancreatic lipase [126, 238]. These lipases typically adsorb to the surfaces of the lipid droplets and convert the triacylglycerols (TGs) into diacylglycerols (DGs), monoacylglycerols (MGs), and free fatty acids (FFAs). The presence of lipid digestion products in the small intestine stimulates the release of hormones that regulate gastrointestinal motility, gastric emptying times, feelings of hunger/satiety/satiation, and total energy intake [386-388]. Consequently, controlling the rate and extent of triacylglycerol digestion within the GIT may lead to the creation of functional foods that can modulate food intake, and therefore aid in the fight against problems with overweight and obesity [389].

Structural design approaches can be used to create emulsion-based foods that can control lipid digestion within the GIT [62, 385, 390]. These approaches are used to change the size, composition, interfacial properties, aggregation state, or local environment of the lipid droplets in foods, thereby altering the way they are processed within the GIT [1]. Previous studies have shown that filled hydrogel beads are one of the most effective

means of retarding lipid digestion under simulated GIT conditions [76]. This type of delivery system consists of lipid droplets trapped within hydrogel beads. Filled hydrogel beads are typically fabricated using a two-step process: (i) a droplet-loaded biopolymer-rich particle is formed; (ii) the biopolymer molecules are cross-linked using a suitable physical or covalent method. A number of particle formation methods are available, including injection, coacervation, segregation, antisolvent precipitation, emulsion templating, and molding methods [270]. The injection-gelation method is one of the simplest and most widely used for encapsulating lipid droplets. An aqueous solution containing a mixture of lipid droplets and biopolymer is injected into a ‘‘hardening’’ solution that promotes cross-linking and gelation of the biopolymer molecules. This procedure results in the formation of a hydrogel bead with lipid droplets trapped inside. Changing the composition, dimensions, or pore size of the hydrogel beads can be used to modulate the GIT fate of the lipid droplets [76].

Magnetic resonance imaging (MRI) is a potentially powerful tool for the investigation of filled hydrogel beads in the GI tract as it is non-invasive and differentially sensitive to meal components without using ionising radiation. MRI can image fat and water components of model meals separately based on T_1 relaxation and chemical-shift properties. MRI have been previously used to directly visualize the lipids in alginate beads within the meal in the human GI tract, as well as in simulated GI conditions. Magnetic resonance spectroscopy (MRS) is a long established MR-based method and generally considered the clinical gold-standard technique to quantify the fat fraction in a sample or organ. The method is based on integrating the frequency spectrum peaks of water and the fat, which is obtained from a small, spatially localized volume of interest (voxel) within the region of interest.

In this study, we examined the possibility of modulating the rate and extent of lipid digestion under simulated GIT conditions by mixing together rapidly digesting and slowly digesting delivery systems. The rapidly digesting delivery systems were nanoemulsions containing free lipid droplets, whereas the slowly digesting delivery systems were lipid droplets encapsulated within hydrogel beads. It was hypothesized that mixing different ratios of free and encapsulated lipid droplets would lead to delivery systems with different lipid digestion profiles. Moreover, we examined the possibility of

utilizing MRI and MRS to determine the lipids release properties from hydrogel beads in simulated gastric conditions. The information obtained in this study may therefore lead to the development of functional foods that can control triacylglycerol blood levels, hunger/satiety/satiation responses, and calorie intake by controlling the rate and extent of lipid digestion. Furthermore, the results obtained from current study may also provide us the valuable evaluation of novel use of MR-based technology in emulsion based colloidal delivery system within GIT.

7.2 Materials and methods

7.2.1 Materials

Corn oil was purchased from a local supermarket and used without further purification. Carrageenan (κ-) was donated by FMC Biopolymer (Viscarin SD 389, Philadelphia, PA). Tween 80 and alginic acid (sodium salt, from brown algae, medium viscosity) were purchased from the Sigma Chemical Company (St. Louis, MO). All other chemicals were analytical grade. Double distilled water was obtained from a water-purification unit.

7.2.2. Preparation of nanoemulsions

The aqueous phase consisted of 4% (w/w) Tween 80 dispersed in buffer solution (5 mM phosphate buffer, pH 7.0), stirred for 2 hour at ambient temperature, and then stored overnight at 4 °C. The oil phase consisted of corn oil at ambient temperature.
Coarse emulsions were prepared by blending 40% (w/w) oil phase and 60% (w/w) aqueous phase using a high-shear mixer (Bamix, Biospec Products, Bartlesville, OK) for 2 min at ambient temperature. Nanoemulsions were prepared by passing the coarse emulsions through a dual-channel microfluidizer equipped with a Y- and Z-type interaction chamber (Microfluidics PureNano, Newton, MA, USA) three-times at 12 kpsi. The Y-type chamber was placed before the Z-type chamber, which facilitate the formation of small emulsion droplets with high lipid concentration. The resulting nanoemulsions were then diluted with buffer solution (5 mM phosphate, pH 7.0) to obtain samples with a range of lipid droplet levels.

7.2.3. Preparation of filled biopolymer microgels

Aqueous alginate and κ-carrageenan solutions were prepared by dissolving powdered polysaccharide ingredients in distilled water at evaluated temperature (60 °C), then reducing the temperature to 35 °C with continuous stirring until totally dissolved. Nanoemulsions were then mixed with polysaccharide solutions to create a final system containing 35% lipid droplets (w/w) and 0.5% polysaccharide (w/w). Filled alginate microgels were formed by using a simple hand-held syringe (BD Safety-Lok 10 mL Syringe with a 0.6 mm-diameter tip, Franklin Lakes, NJ) to drip nanoemulsion-alginate mixtures (2s per drop) into 20 mL 5% (w/w) calcium chloride (Ca^{2+}) solutions with continuous stirring. Similarly, filled carrageenan microgels were prepared by dripping nanoemulsion-κ-carrageenan mixtures into 5% (w/w) potassium chloride (K^{+}) solutions. The filled microgels formed were incubated in the cation (Ca^{2+} or K^{+}) solutions for 20 min at ambient temperature to promote crosslinking. They were then filtered by filtration paper (Fisher Science, P5) and washed with distilled water and phosphate buffer solution to remove any excess ions from their surfaces. The particle size of microgels were determined using a digital caliper (Fowler high Precision, Newton, MA, USA)

7.2.4. Simulated gastric conditions

The effect of simulated gastric conditions on the properties of the filled microgels was determined using a method described previously [318], with some slight modifications. Filled alginate or carrageenan microgels were added at a ratio of 1:1 (w/w) to simulated gastric fluids (SGF) that had been preheated to 37 °C and then adjusted to pH 2.5. The resulting mixture maintained at 37 °C with continual stirring for 2 h to mimic gastric peristalsis and digestion.

7.2.5. Turbidity measurements

The turbidity of the fluids surrounding the microgels was determined as an indication of the release of the lipid droplets. The beads were removed by filtration and the turbidities of residual solution were measured using a UV-visible spectrophotometer at 600 nm (Ultrospec 3000 pro, Biochrom Ltd., Cambridge, UK). Test samples were

contained within 1-cm path length optical cells and phosphate buffer was used as a control. Turbidity measurements were carried out on at least two freshly prepared samples. Changes in the appearance of the samples were also recorded throughout gastric digestion using a digital camera. A fraction of microgels were taken from the digestion phase to facilitate their detection.

7.2.6. MRI and MRS analysis

The release of the lipid droplets from the filled microgels during the simulated stomach digestion period were studied using a MRI instrument (3T, Siemens Skyra). Samples collected from the stomach phase were loaded into an glass tube with a screw-top. Any air bubbles were completely removed from the samples before sealing to eliminate deviation. MR imaging and spectroscopy were performed by placing the samples into the 3T MR instrument with a 15-ch knee RF coil. The tubes were positioned axially as a bundle of 7 tubes so that the tube axis was aligned with the magnet axis for the quantitation study in which the lipid content was measured. The tube bundle was also positioned vertically for the imaging of individual microgel. The tubes were scanned with a 3-dimensional T1-weighted sequence, i.e., T1 VIBE or water-selected T1 VIBE sequence, in an axial orientation with TR/TE = 10/4.92 ms, voxel size = 0.8×0.8×4 mm^3, and flip angle = 10 degree. The MR spectra were obtained using a stimulated echo acquisition mode (STEAM) sequence of a single voxel of 10×10×15 (F/H) mm^3, TR/TE=1200/20 ms, and water suppression [391-392].

7.2.7. Statistical analysis

All experiments were performed on at least two freshly prepared samples. The results are reported as averages and standard deviations. These analyses were carried out by T-tests using Excel (Microsoft, Redmond, VA, USA).

7.3. Results and Discussion

7.3.1. Influence of gastric conditions on characteristics of filled microgels

Filled microgels were prepared by injecting mixtures of lipid droplets and anionic biopolymers (carrageenan or alginate) into cationic mineral solutions (K^+ or Ca^{2+}). These constituents were selected as the formed microgels showed significantly different structure and properties. The carrageenan microgels produced had an irregular shape with rough surfaces, whereas the alginate microgels had spheroid shapes with smooth surfaces (Fig. 1). The diameter of the carrageenan microgels (≈ 3 mm) was slightly larger than that of the alginate ones (≈ 2.5 mm). These structural differences have previously been attributed to the different gelation mechanisms of the two polysaccharides. Carrageenan gelation is induced by crosslinking anionic sulfate groups in different polysaccharide chains with cationic potassium ions, whereas alginate gelation is the result of crosslinking of anionic carboxylic groups with cationic calcium ions [233]. Gelation of alginate would be expected to be stronger and faster than carrageenan because divalent calcium ions are more efficient crosslinking agents than monovalent potassium ions [393].

Initially, all of the lipid droplets were trapped inside the microgels, which could be deduced from the fact that the microgels looked white while the surrounding solution was optically clear (Figs. 1 and 2). Thus, both types of microgel could effectively trap the lipid droplets inside. Presumably, the dimensions of the lipid droplets were greater than those of the pore size of the biopolymer network inside the microgels, thereby inhibiting their movement [76].

After exposure to gastric conditions, visual observations showed there was a progressive reduction in the size and integrity of the carrageenan microgels, as well as an increase in the cloudiness of the surrounding aqueous phase (**Figure 7.1**). Indeed, almost all of the carrageenan microgels had fully dissociated after 120 min exposure to the simulated stomach phase. Conversely, the alginate microgels remained intact throughout the entire incubation period in the gastric fluids and there was only a slight increase in the cloudiness of the surrounding fluids. The turbidity of the solution surrounding the microgels increased steeply during incubation in the gastric fluids for the carrageenan system but only slightly for the alginate system (**Figure 7.2**). Taken together, these

results indicated that the carrageenan microgels were more unstable in simulated gastric conditions than the alginate microgels.

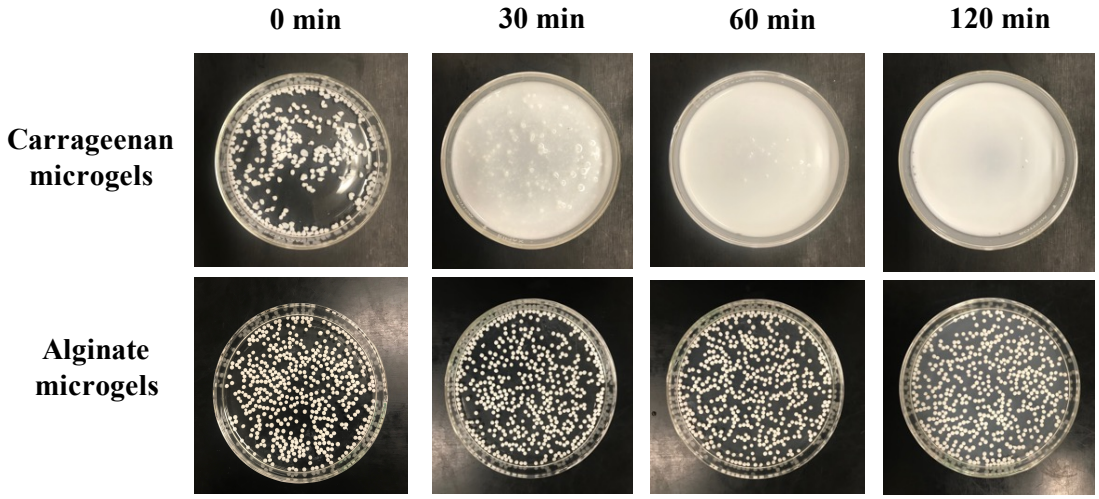

Figure 7. 1 The optical images of two types of microgels after different simulated stomach digestion period (a fraction of microgels were taken out from the simulated digestion phase to facilitate the observation).

The disintegration of carrageenan microgels under stomach conditions can be attributed to the strong acidity, high ionic strength, and mechanical agitation of the gastric fluids. Presumably, the crosslinks holding the carrageenan molecules together in the microgels are weaker than those holding the alginate molecules together. As a result, they are more likely to be disrupted at high ionic strengths because this weakens the electrostatic attraction between the polysaccharide molecules and the counter-ions. In particular, the sodium ions in the gastric fluids could displace the potassium ions that form the crosslinks between the carrageenan molecules, but not the calcium ions that form the crosslinks between the alginate molecules. Interestingly, the pK_a values of the sulfate groups in carrageenan (around pH 2) are considerably lower than those of the carboxyl groups in alginate (around pH 3.5). This suggests that deionization of the anionic groups on the polysaccharide molecules was not a major factor contributing to differences in their behavior in the acidic gastric fluids.

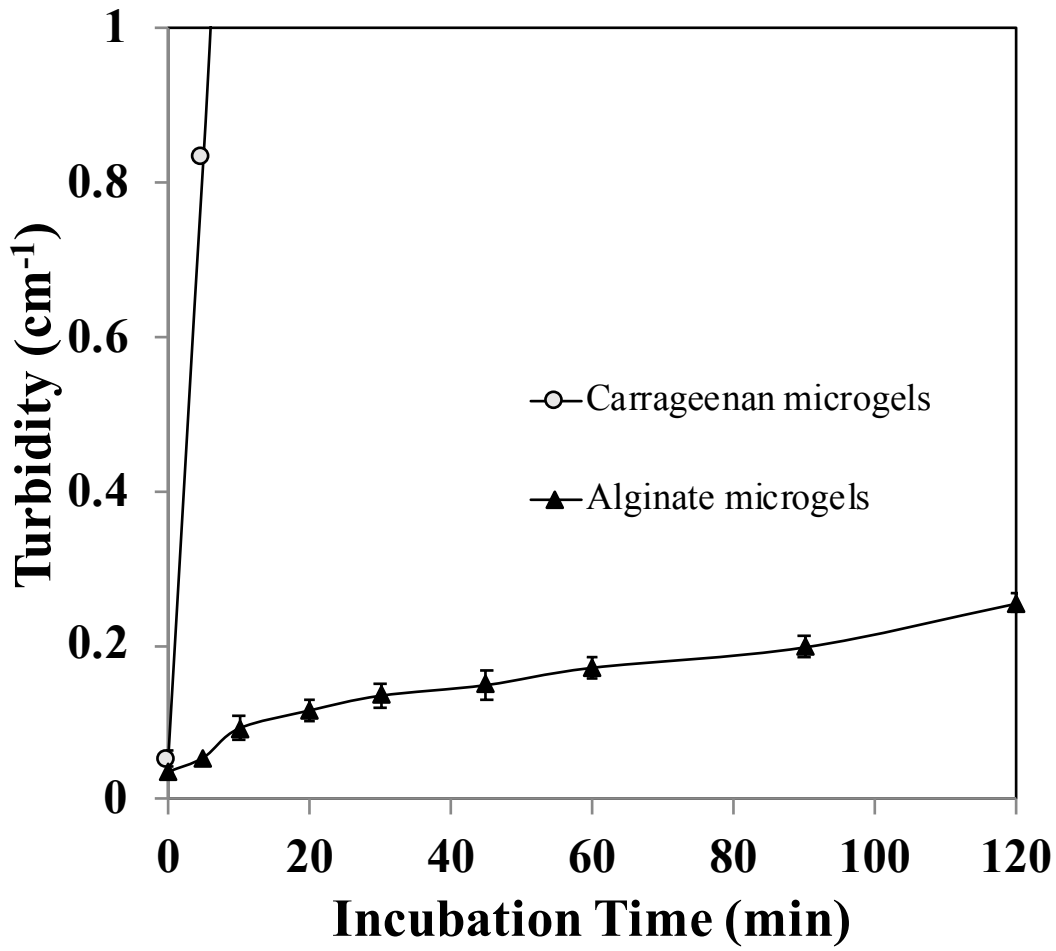

Figure 7. 2 The turbidity of residual solution in two types of microgels during different simulated stomach digestion period (0-120 min).

It has been reported that up to 30-40% of lipid digestion occurs within the human stomach [394]. Our previous study showed that free lipid droplets are digested much more rapidly than lipid droplets encapsulated within biopolymer microgels, which was attributed to the restricted diffusion of lipase molecules through the biopolymer matrix [76]. The early release of the lipid droplets from the carrageenan microgels might therefore be expected to lead to faster lipid digestion under gastrointestinal conditions, which has been reported in previous studies [395-396].

7.3.2. Development of standard curve for lipid quantification

A major goal of our research was to demonstrate the potential for magnetic resonance imaging and spectroscopy to non-invasively monitor the release of

encapsulated lipids from biopolymer microgels. Initially, it was therefore necessary to establish correlations between lipid droplets levels in the GIT fluids and measurable MRI parameters. We examined two different approaches for discriminating between the lipid and water in the samples, one based on measurements of relaxation times and the other based on chemical shift spectroscopy.

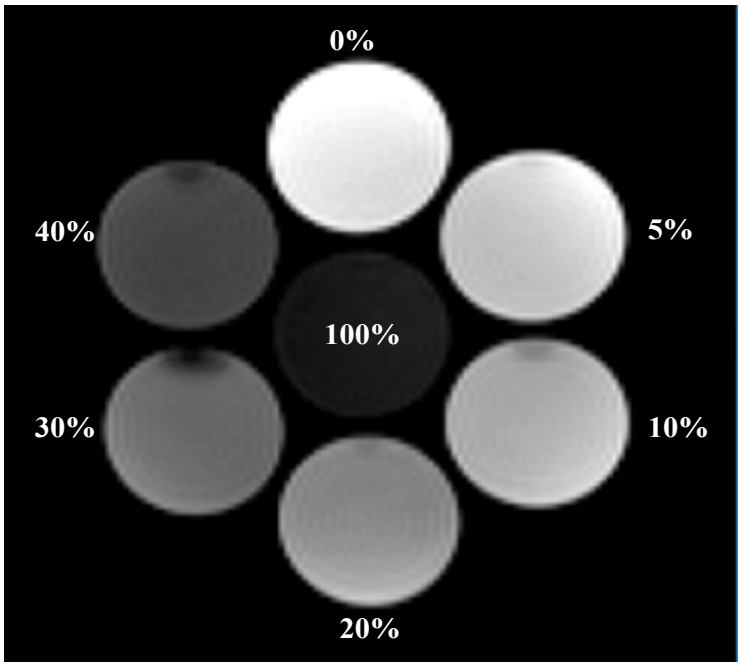

Figure 7. 3 A transaxial view of the 3-dimensional T_1-weighted water-selected images from tubes filled with emulsions with different lipid concentration. The lipid concentration of each tube is marked in percentage on or next to each tube. The tube axis was aligned with the magnet axis and thus the trapped air was seen as signal void on the top portion of some tubes.

A series of samples with different lipid levels (0-40%) was prepared by diluting the most concentrated nano emulsions produced by micro fluidization with buffer solutions. Water-selected T_1 weighted images and spectroscopy analysis of the samples were then carried out using the MRI instrument. The axis of the cylindrical phantom was aligned parallel to the static magnetic field and positioned in the center of the knee RF coil to improve magnetic homogeneity and obtain better water excitation images with high resolution.

Relaxation Measurements: Initially, we consider the use of relaxation measurements to determine the lipid content of the samples. A water-selected sequence was used to

discriminate the water phase from the lipid phase in the nanoemulsions [397]. Using this pulse sequence, the water is excited and produces a signal that appears as bright regions in the images. Conversely, the lipid remains in equilibrium, thereby producing no signal, which results in dark regions in the images.

Nanoemulsion samples with different lipid contents could clearly be distinguished using the T_1 water-selected images (**Figure 7.3**). As expected, the images became brighter as the lipid level decreased, *i.e.,* as the water level increased. For quantitative analyses, the signal intensity at identical positions within each sample was measured by selecting a target region of interest (ROI). The mean signal intensity over the ROI was used to represent the signal of each nanoemulsion sample. The signal intensity decreased linearly with increasing lipid concentration (**Figure 7.4a**), with a high negative correlation (R^2 = 0.9882). These results suggest that the MRI relaxation approach is suitable for determining the lipid content of samples.

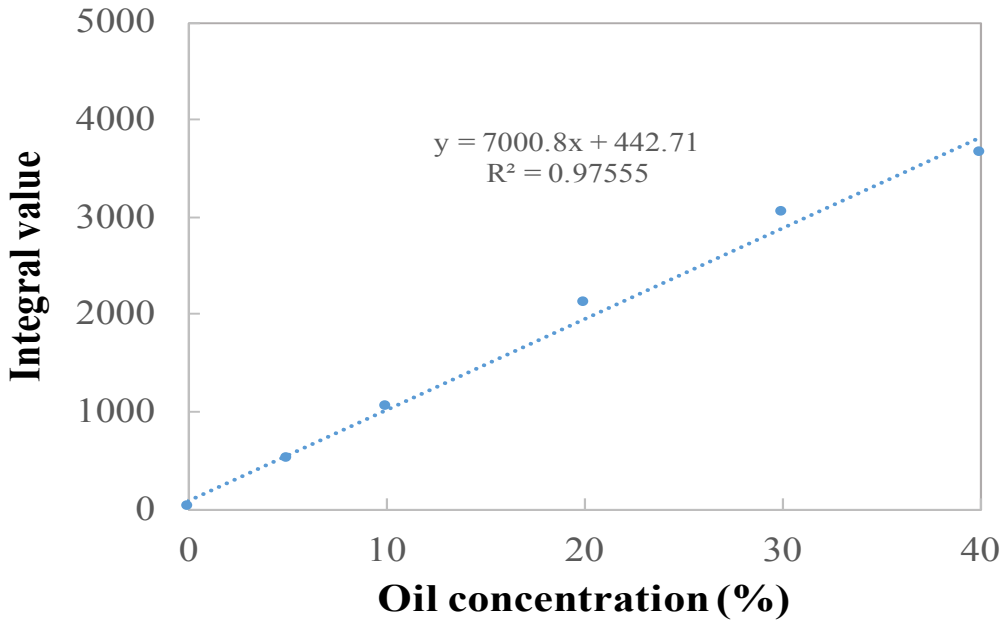

(a)

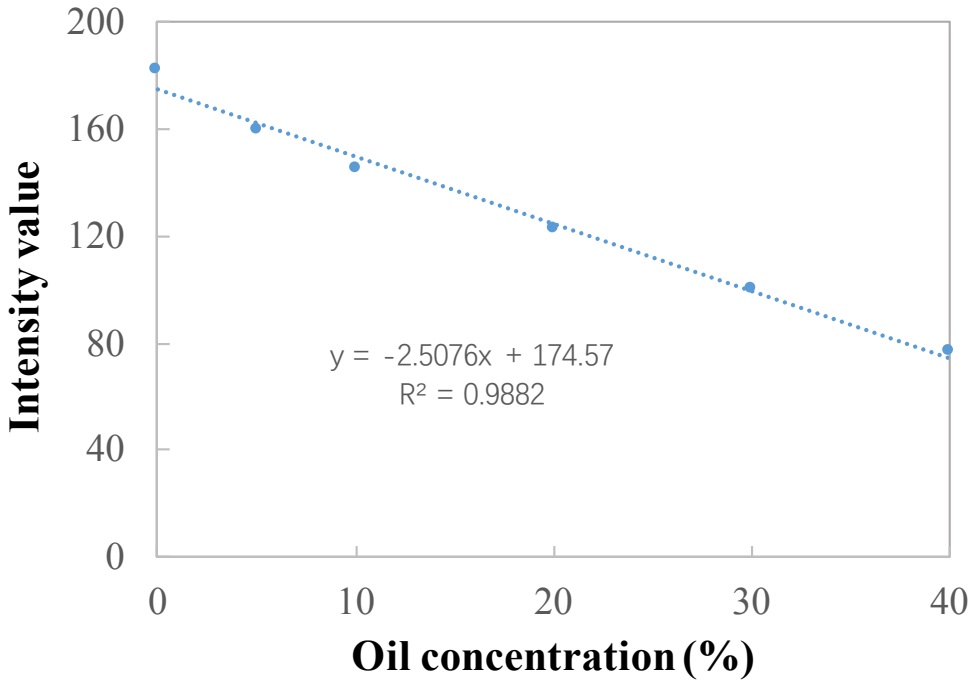

(b)

Figure 7. 4 Relationship of the lipid concentration with (a) T_1-weighted image intensity and (b) MR spectral peak amplitude. The dotted line in each graph indicates the linear regression with the equation denoted in each graph.

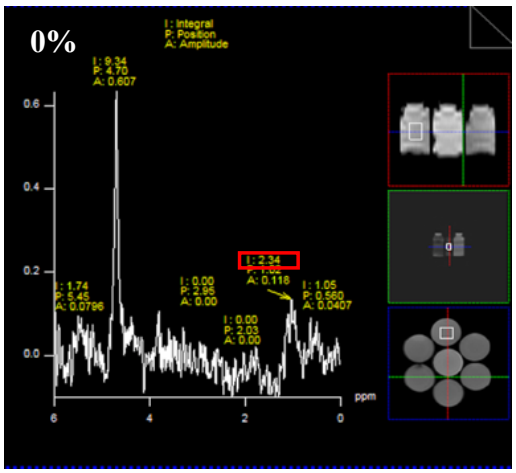

Integral value: 2.34

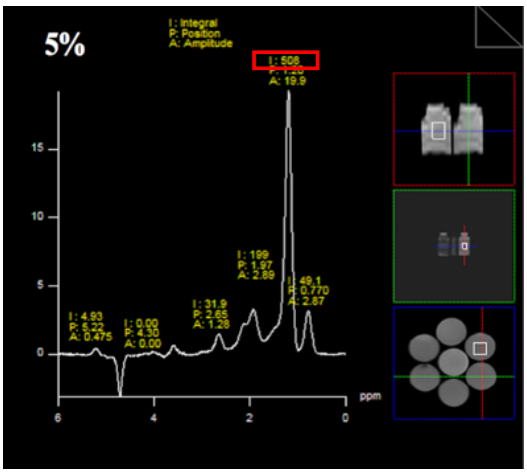

Integral value: 508

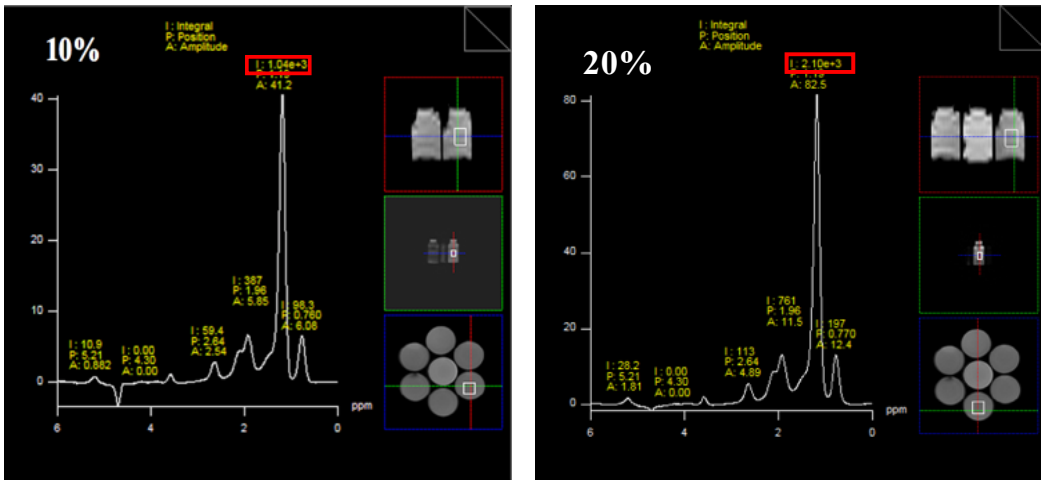

Integral value: 1040 **Integral value: 2100**

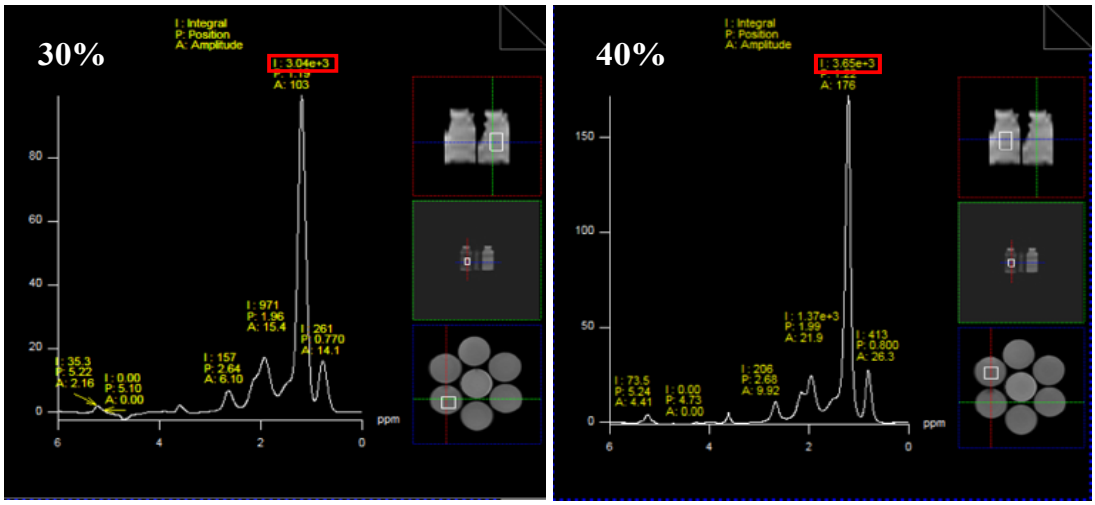

Integral value: 3040 **Integral value: 3650**

Figure 7. 5 MR spectra of emulsion samples with different lipid concentrations (0-40%). The peak integral value of the lipid peak is marked with a red rectangle.

Spectroscopy Measurements: A chemical spectroscopy method was also used to discriminate between the lipid and water phases in the samples (**Figure 7.5**). The peaks in the MRI frequency spectrum corresponding to the lipids and water were integrated from the ROI for each nanoemulsion sample. Previously, the main CH_2 (1.6 ppm) peak has been reported to be particularly useful for determining lipid contents in biological samples at clinical field strengths [398-399]. The area under the curve of the real part of the

frequency domain signal was used as the integrated signal amplitude to correlate to the lipid concentration. Our results indicated that the integral values increased linearly with lipid concentration in the nanoemulsion samples with a high positive correlation (R^2 = 0.9755) (**Figure 7.4b**, **Figure 7.5**). These results indicate that MR spectroscopy may also be used to determine the lipid content of samples.

7.3.3. Determination of the release properties of lipid droplets from microgels

In this section, filled carrageenan and alginate microgels were prepared for analysis using the two MR-based methods. T_1-weighted VIBE sequence images and T_1-weighted water-selected images of the microgel dispersions were then acquired after they were incubated in simulated gastric fluids for different period (0 to 120 min). The phantom configuration that was set vertically or aligned to the knee of coil to facilitate the observation or quantitation.

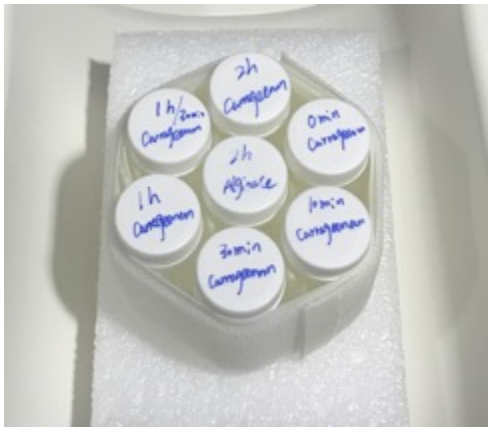

(a)

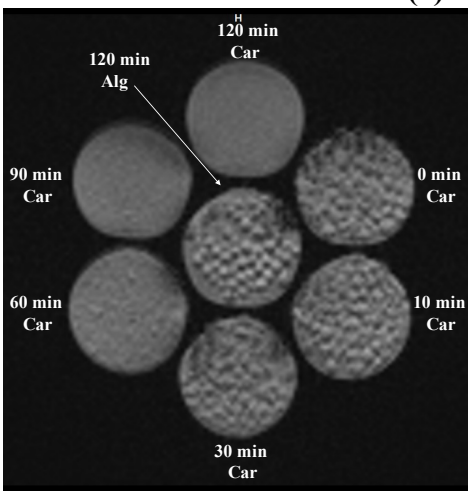

(b)

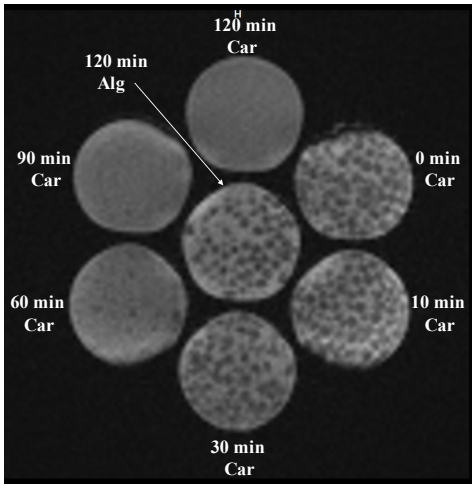

(c)

Figure 7. 6 Digestion periods of two types of microgels: (a) The phantom configuration that was set vertically inside the knee of coil, (b) T_1-weighted MRI and (c) water-selected T_1-weighted MRI. In each image, 'Car' and 'Alg' denote the carrageenan and alginate microgels, respectively. The digestion period of each tube is denoted next to each tube in minute.

For obtaining the T_1-weighted images, the tube bundle was positioned vertically inside the coil and a relatively small voxel size ($0.8\times0.8\times4$ mm^3) was used to visualize individual microgels. These images showed that the filled alginate microgels retained their spherical shape and integrity throughout the incubation period (**Figure 7.6b**). While the filled carrageenan microgels exhibited quite different behavior. They progressively disintegrated when they were dispersed in the gastric fluids, almost completely disappearing after 60 minutes of incubation (**Figure 7.6b**). These results agree with our previous studies, which showed that the digestion of lipid droplets was much slower when they were encapsulated in alginate microgels rather than carrageenan ones [400]. Again, these effects can be attributed to the fact that the crosslinks between the alginate molecules in the microgels are much stronger than those between the carrageenan molecules. As a result, the alginate microgels are more resistant to gastric conditions than the carrageenan molecules.

The phantom configuration was also set aligned to the knee of coil to improve magnetic homogeneity. We could observe that the lipid-loaded alginate microgels floated to the top of the simulated gastric fluids (**Figure 7.7b**). These results suggest that the encapsulation of the lipid droplets inside the alginate microgels could delay their gastric emptying, since they would tend to float on top of the gastric fluids and not easily pass through the pylorus sphincter [401]. This characteristic may be advantageous for certain applications of microgels in functional foods. For carrageenan microgels, most of them were dissolved in the simulated stomach phase after 60 minutes of incubation. However, they still floated to the top of the gastric fluids at shorter incubation times (**Figure 7.7b**).

We then determined the changes in the water-selected T_1-weighted images of the microgel samples over different simulated digestion time (**Figure 7.6c** and **7.7c**). The results obtained were very similar to those obtained from the T_1-weighted images. The alginate microgels remained intact throughout the digestion period, whereas the

carrageenan microgels progressively disintegrated. In addition, the microgels could again be seen to float to the top of the gastric fluids using this approach.

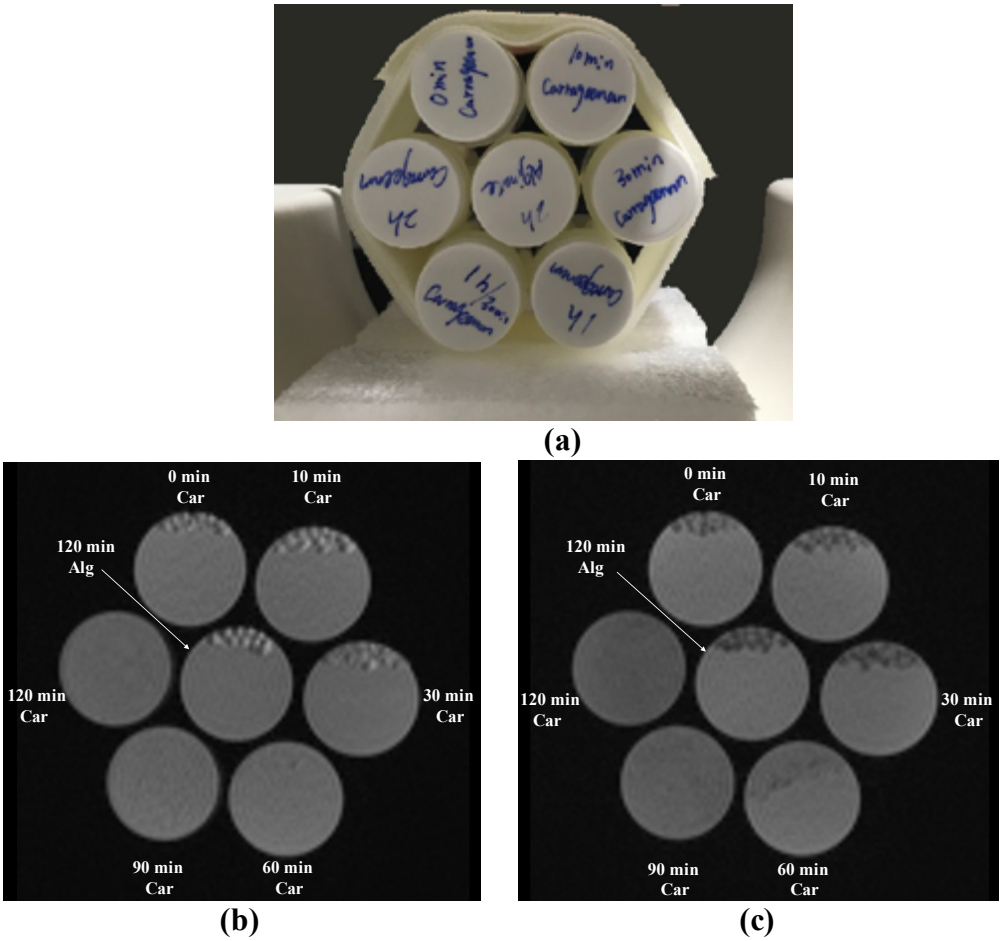

Figure 7. 7 Digestion periods of two types of microgels: (a) The phantom configuration that was set in the knee of coil, (b) T_1-weighted MRI and (c) water-selected T_1-weighted MRI. In each image, 'Car' and 'Alg' denote the carrageenan and alginate microgels, retrospectively. The digestion period of each tube is denoted next to each tube in minute. The tube axis was aligned with the magnet axis to improve magnetic homogeneity.

Quantification of Lipid Release: Finally, we compared the effectiveness of the relaxation and spectroscopy approaches for monitoring lipid droplet release from the microgels during incubation in the simulated gastric fluids (**Figure 7.8**, **Figure 7.9** and **7. 10**). The lipid release profiles were obtained using the standard curves of intensity *versus* lipid content (relaxation) or integral value *versus* lipid content (spectroscopy) described in the previous section. These measurements were carried out on the fluid phase

surrounding the microgels in the tubes settled aligned to the magnetic axis. Only the carrageenan microgels were analyzed in these experiments because there were so few lipid droplets released from the alginate microgels.

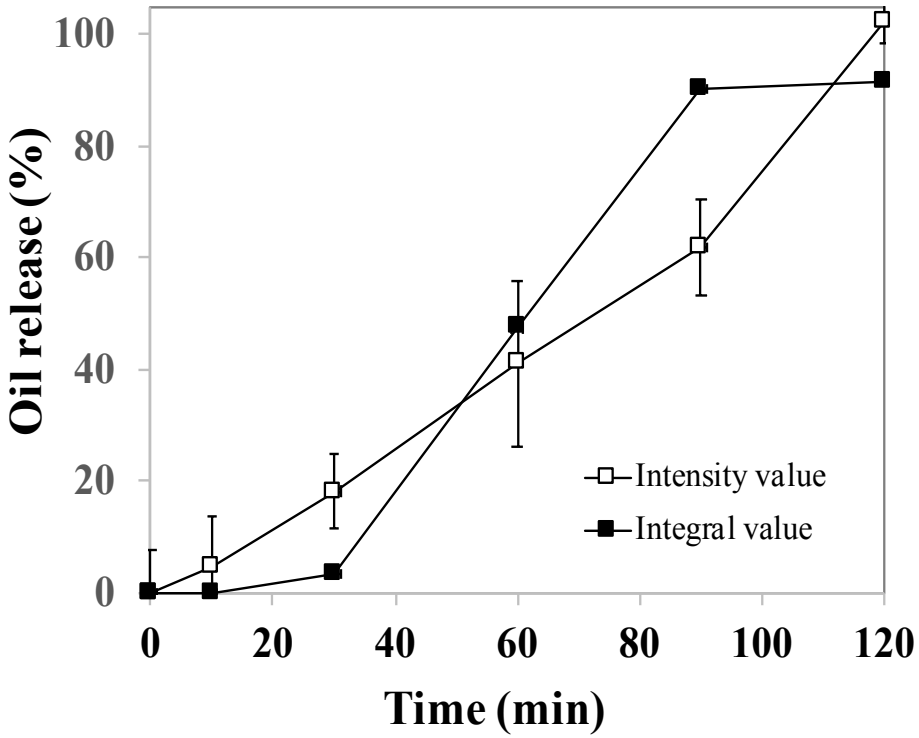

Figure 7. 8 The release profile of lipid from carrageenan microgels during 2h' simulated stomach digestion period. The lipid release fraction were calculated based on the intensity and integral value of carrageenan microgels samples obtained from T1 weighted MRI and the MR spectra.

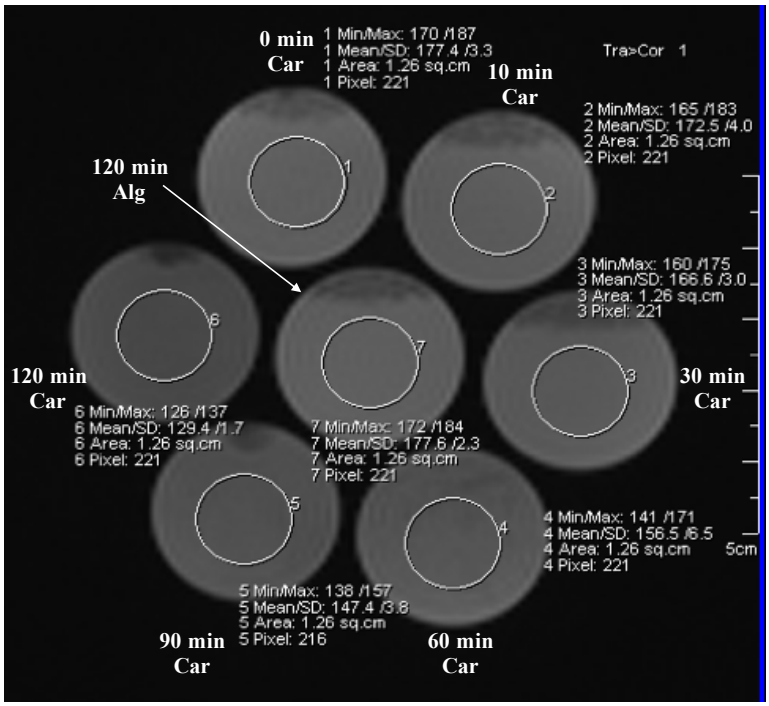

Figure 7. 9 Image intensities of two types of microgels obtained from the water-selected T_1-weighted MRI. 'Car' and 'Alg' denote the carrageenan and alginate microgels, respectively. The digestion period of each tube is denoted next to each tube in minute.

Our results suggest that the release of the lipid droplets from the carrageenan microgels occurred relatively slowly within the first 30 min, and then became faster after about 60 min's incubation (**Figure 7.8**). This effect can be attributed to the disintegration of the carrageenan microgels at around the same time, as seen in the MR images (**Figure 7.6** and **7.7**). The lipid release profiles obtained from intensity and integral values showed very similar trends, indicating both of these methods can be used to detect microgel integrity and lipid release *in situ*. Interestingly, the UV-visible spectroscopy measurements indicated that the turbidity of the carrageenan microgels increased immediately after they were incubated in gastric fluids (**Figure 7.2**). This may have been because only a very low concentration of lipid droplets is required to increase the turbidity of a solution, whereas a relatively high concentration is required to be detectable by MRI. The turbidity measurements are therefore not very useful for quantifying lipid droplet release at realistic food compositions. Moreover, turbidity measurements would be problematic in complex food systems that contained other types of particles that can scatter light.

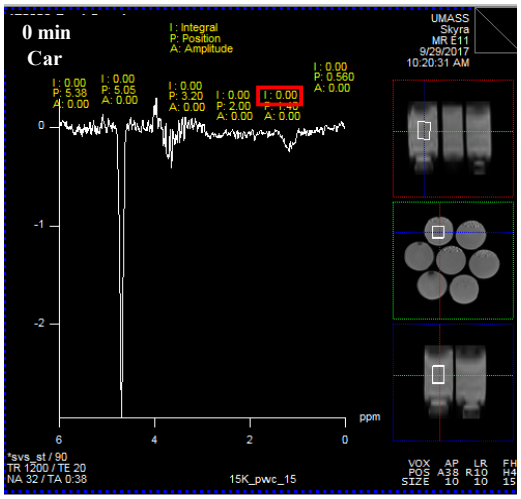

Integral value: 0

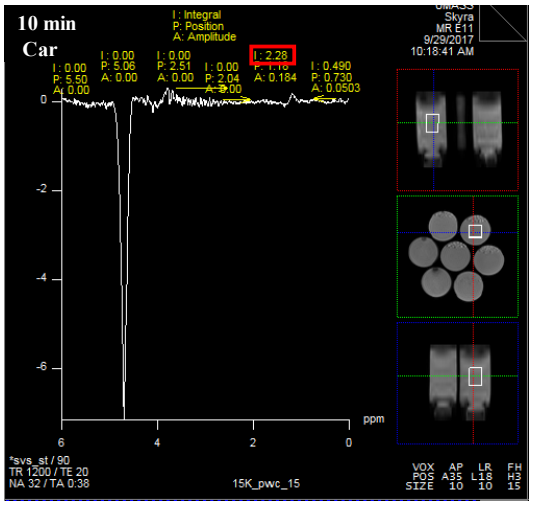

Integral value: 2.28

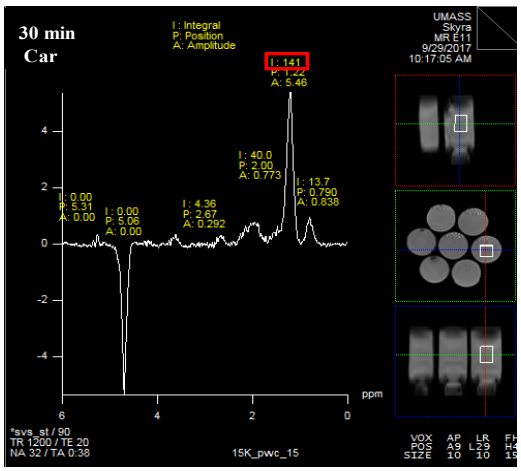

Integral value: 141

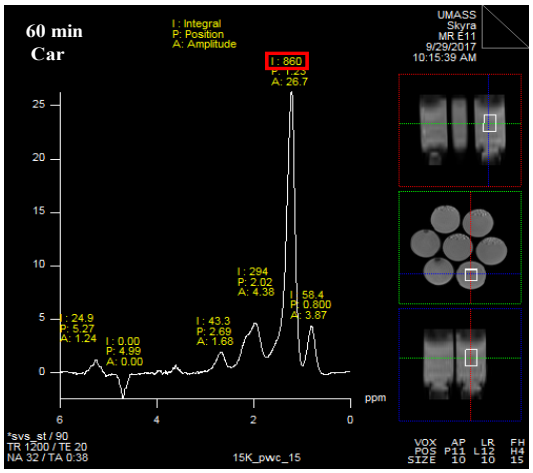

Integral value: 860

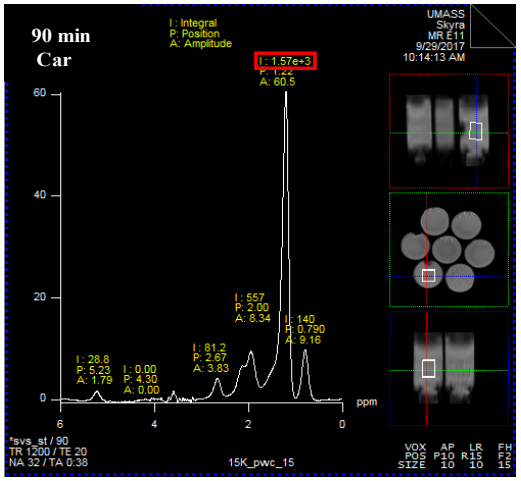

Integral value: 1570

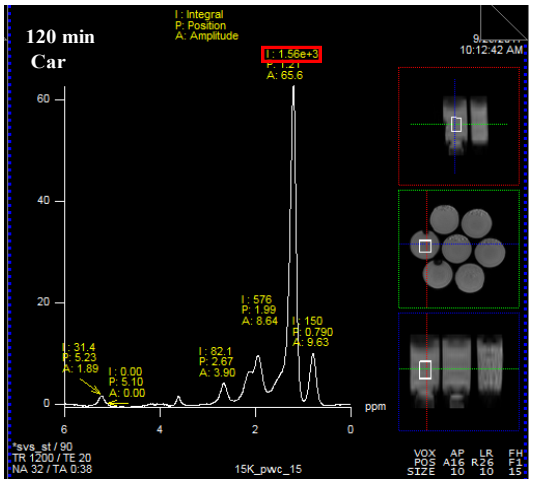

Integral value: 1560

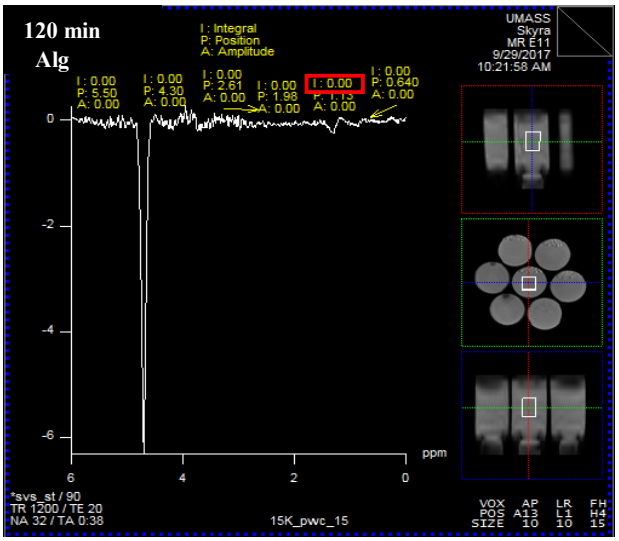

Integral value: 0

Figure 7. 10 MR spectra of two types of microgels after different simulated stomach digestion period. The integral value of the lipid peak is marked with a red rectangle. In each image, 'Car' and 'Alg' denote the carrageenan and alginate microgels, respectively.

7.4. Conclusion

This study demonstrates the feasibility of MRI-based approaches to non-invasively monitor microgel integrity and to quantify lipid droplet release under gastrointestinal conditions. The MRI techniques used clearly showed that alginate microgels are much more resistant to gastric conditions than carrageenan microgels. Carrageenan microgels broken down and released their lipid droplets, whereas alginate microgels stayed intact and retained their lipid droplets. This phenomenon may have important implications for the design of functional foods that control the release of bioactive agents within the human GIT. Carrageenan microgels could be used to slowly release bioactive agents in the stomach, whereas alginate microgels could be used to deliver them further down the gastrointestinal tract. One of the advantages of the MRI method is that 3-dimensional images of the samples can be obtained so it is possible to detect the location of the microgels over time. In this study, it was found that the lipid-loaded microgels tended to float on top of the gastric fluids, which would be expected to alter the gastrointestinal fate.

Previous studies have shown that MRI measurements can be carried out in humans to monitor the gastrointestinal of ingested microgels after a meal. The two signal

acquisition approaches developed in the current study may increase the power of MRI for obtaining detailed information about the behavior of lipids inside humans. These tools may facilitate the more rational design of functional foods that behave in a controlled fashion inside our bodies.

BIBLIOGRAPHY

1. McClements, D. J.; Li, Y., Structured emulsion-based delivery systems: Controlling the digestion and release of lipophilic food components. *Advances in colloid and interface science* **2010,** *159* (2), 213-228.

2. Gouin, S., Microencapsulation: industrial appraisal of existing technologies and trends. *Trends in food science & technology* **2004,** *15* (7), 330-347.

3. McClements, D. J.; Decker, E. A.; Weiss, J., Emulsion‐based delivery systems for lipophilic bioactive components. *Journal of Food Science* **2007,** *72* (8), R109-R124.

4. Hoare, T. R.; Kohane, D. S., Hydrogels in drug delivery: progress and challenges. *Polymer* **2008,** *49* (8), 1993-2007.

5. McClements, D. J., Emulsion Design to Improve the Delivery of Functional Lipophilic Components. In *Annual Review of Food Science and Technology, Vol 1*, 2010; Vol. 1, pp 241-269.

6. Coviello, T.; Matricardi, P.; Marianecci, C.; Alhaique, F., Polysaccharide hydrogels for modified release formulations. *Journal of Controlled Release* **2007,** *119* (1), 5-24.

7. Saha, D.; Bhattacharya, S., Hydrocolloids as thickening and gelling agents in food: a critical review. *Journal of food science and technology* **2010,** *47* (6), 587-597.

8. Hamman, J. H., Chitosan based polyelectrolyte complexes as potential carrier materials in drug delivery systems. *Marine Drugs* **2010,** *8* (4), 1305-1322.

9. Sungthongjeen, S.; Sriamornsak, P.; Pitaksuteepong, T.; Somsiri, A.; Puttipipatkhachorn, S., Effect of degree of esterification of pectin and calcium amount on drug release from pectin-based matrix tablets. *Aaps Pharmscitech* **2004,** *5* (1), 50-57.

10. Chourasia, M. K.; Jain, S. K., Pharmaceutical approaches to colon targeted drug delivery systems. *J Pharm Pharm Sci* **2003,** *6* (1), 33-66.

11. Nguyen, A. T.-B.; Winckler, P.; Loison, P.; Wache, Y.; Chambin, O., Physico-chemical state influences< i> in vitro</i> release profile of curcumin from pectin beads. *Colloids and Surfaces B: Biointerfaces* **2014,** *121*, 290-298.

12. Díaz-Rojas, E. I.; Pacheco-Aguilar, R.; Lizardi, J.; Argüelles-Monal, W.; Valdez, M. A.; Rinaudo, M.; Goycoolea, F. M., Linseed pectin: gelling properties and performance as an encapsulation matrix for shark liver oil. *Food hydrocolloids* **2004,** *18* (2), 293-304.

13. Kim, J. S.; Lee, J.-S.; Chang, P.-S.; Lee, H. G., Optimization,< i> in vitro</i> release and bioavailability of γ -oryzanol-loaded calcium pectinate microparticles reinforced with chitosan. *New biotechnology* **2010,** *27* (4), 368-373.

14. Dongowski, G., Influence of pectin structure on the interaction with bile acids under in vitro conditions. *Zeitschrift für Lebensmittel-Untersuchung und Forschung* **1995,** *201* (4), 390-398.

15. Hu, M.; Li, Y.; Decker, E. A.; McClements, D. J., Role of calcium and calcium-binding agents on the lipase digestibility of emulsified lipids using an< i> in vitro</i> digestion model. *Food Hydrocolloids* **2010,** *24* (8), 719-725.

16. Verrijssen, T. A. J.; Balduyck, L. G.; Christiaens, S.; Van Loey, A. M.; Van Buggenhout, S.; Hendrickx, M. E., The effect of pectin concentration and degree of methyl-esterification on the< i> in vitro</i> bioaccessibility of β -carotene-enriched emulsions. *Food Research International* **2014,** *57*, 71-78.

17. Sun-Waterhouse, D.; Wang, W.; Waterhouse, G. I. N., Canola oil encapsulated by alginate and its combinations with starches of low and high amylose content: effect of quercetin on oil stability. *Food and Bioprocess Technology* **2013**, 1-19.

18. Chan, E.-S., Preparation of Ca-alginate beads containing high oil content: Influence of process variables on encapsulation efficiency and bead properties. *Carbohydrate Polymers* **2011,** *84* (4), 1267-1275.

19. Ribeiro, A. J.; Neufeld, R. J.; Arnaud, P.; Chaumeil, J. C., Microencapsulation of lipophilic drugs in chitosan-coated alginate microspheres. *International journal of pharmaceutics* **1999,** *187* (1), 115-123.

20. Burey, P.; Bhandari, B. R.; Howes, T.; Gidley, M. J., Hydrocolloid gel particles: Formation, characterization, and application. *Crit. Rev. Food Sci. Nutr.* **2008,** *48* (5), 361-377.

21. Lertsutthiwong, P.; Noomun, K.; Jongaroonngamsang, N.; Rojsitthisak, P.; Nimmannit, U., Preparation of alginate nanocapsules containing turmeric oil. *Carbohydrate Polymers* **2008,** *74* (2), 209-214.

22. George, M.; Abraham, T. E., Polyionic hydrocolloids for the intestinal delivery of protein drugs: alginate and chitosan—a review. *Journal of controlled release* **2006,** *114* (1), 1-14.

23. Hari, P. R.; Chandy, T.; Sharma, C. P., Chitosan/calcium alginate microcapsules for intestinal delivery of nitrofurantoin. *Journal of microencapsulation* **1996,** *13* (3), 319-329.

24. Amsden, B.; Turner, N., Diffusion characteristics of calcium alginate gels. *Biotechnology and bioengineering* **1999,** *65* (5), 605-610.

25. Sato, A. C.; Perrechil, F.; Michelon, M.; Cunha, R. In *Biopolymeric microbeads for incorporation of lipophilic and hydrophilic compounds*, Book of Abstracts of the 1 st Congress on Food Structure Design, p 52.

26. Usov, A. I., Structural analysis of red seaweed galactans of agar and carrageenan groups. *Food Hydrocolloids* **1998,** *12* (3), 301-308.

27. Imeson, A. P.; Phillips, G. O.; Williams, P. A., Carrageenan. *Handbook of hydrocolloids* **2000**, 87-102.

28. Hezaveh, H.; Muhamad, I. I., The effect of nanoparticles on gastrointestinal release from modified κ -carrageenan nanocomposite hydrogels. *Carbohydrate polymers* **2012,** *89* (1), 138-145.

29. Piazza, L.; Benedetti, S., Investigation on the rheological properties of agar gels and their role on aroma release in agar/limonene solid emulsions. *Food research international* **2010,** *43* (1), 269-276.

30. Lahaye, M.; Rochas, C. In *Chemical structure and physico-chemical properties of agar*, International Workshop on Gelidium, Springer: 1991; pp 137-148.

31. Joye, I. J.; McClements, D. J., Biopolymer-based nanoparticles and microparticles: Fabrication, characterization, and application. *Current Opinion in Colloid & Interface Science* **2014**.

32. Meena, R.; Chaudhary, J. P.; Agarwal, P. K.; Maiti, P.; Chatterjee, S.; Raval, H. D.; Agarwal, P.; Siddhanta, A. K.; Prasad, K.; Ghosh, P. K., Surfactant-induced coagulation of agarose from aqueous extract of Gracilaria dura seaweed as an energy-efficient alternative to the conventional freeze–thaw process. *RSC Advances* **2014,** *4* (53), 28093-28098.

33. Shalviri, A.; Liu, Q.; Abdekhodaie, M. J.; Wu, X. Y., Novel modified starch–xanthan gum hydrogels for controlled drug delivery: Synthesis and characterization. *Carbohydrate Polymers* **2010,** *79* (4), 898-907.

34. Malone, M. E.; Appelqvist, I. A. M., Gelled emulsion particles for the controlled release of lipophilic volatiles during eating. *Journal of controlled release* **2003,** *90* (2), 227-241.

35. Mun, S.; Kim, Y.-R.; McClements, D. J., Control of β-carotene bioaccessibility using starch-based filled hydrogels. *Food chemistry* **2015,** *173*, 454-461.

36. Firoozmand, H.; Rousseau, D., Microstructure and elastic modulus of phase-separated gelatin–starch hydrogels containing dispersed oil droplets. *Food Hydrocolloids* **2013,** *30* (1), 333-342.

37. Zhang, L.-M.; Yang, C.; Yan, L., Perspectives on: strategies to fabricate starch-based hydrogels with potential biomedical applications. *Journal of bioactive and compatible polymers* **2005,** *20* (3), 297-314.

38. Paramera, E. I.; Konteles, S. J.; Karathanos, V. T., Stability and release properties of curcumin encapsulated in< i> Saccharomyces cerevisiae</i>, β-cyclodextrin and modified starch. *Food Chemistry* **2011,** *125* (3), 913-922.

39. Hejazi, R.; Amiji, M., Chitosan-based gastrointestinal delivery systems. *Journal of Controlled Release* **2003,** *89* (2), 151-165.

40. Luo, Y.; Zhang, B.; Whent, M.; Yu, L. L.; Wang, Q., Preparation and characterization of zein/chitosan complex for encapsulation of α-tocopherol, and its< i> in vitro</i> controlled release study. *Colloids and Surfaces B: Biointerfaces* **2011,** *85* (2), 145-152.

41. Abreu, F. O. M. S.; Oliveira, E. F.; Paula, H. C. B.; de Paula, R., Chitosan/cashew gum nanogels for essential oil encapsulation. *Carbohydrate polymers* **2012,** *89* (4), 1277-1282.

42. Nakagawa, K.; Sowasod, N.; Tanthapanichakoon, W.; Charinpanitkul, T., Hydrogel based oil encapsulation for controlled release of curcumin by using a ternary system of chitosan,< i> kappa-</i> carrageenan, and carboxymethylcellulose sodium salt. *LWT-Food Science and Technology* **2013,** *54* (2), 600-605.

43. Berger, J.; Reist, M.; Mayer, J. M.; Felt, O.; Peppas, N. A.; Gurny, R., Structure and interactions in covalently and ionically crosslinked chitosan hydrogels for biomedical applications. *European Journal of Pharmaceutics and Biopharmaceutics* **2004,** *57* (1), 19-34.

44. Dhawan, S.; Singla, A. K.; Sinha, V. R., Evaluation of mucoadhesive properties of chitosan microspheres prepared by different methods. *Aaps Pharmscitech* **2004,** *5* (4), 122-128.

45. Dhayal, S. K.; Gruppen, H.; de Vries, R.; Wierenga, P. A., Controlled formation of protein nanoparticles by enzymatic cross-linking of α-lactalbumin with horseradish peroxidase. *Food Hydrocolloids* **2014,** *36* (0), 53-59.

46. Soper, J. C.; Thomas, M. T., Enzymatically protein-encapsulating oil particles by complex coacervation. Google Patents: 2001.

47. Cho, Y. H.; Shim, H. K.; Park, J., Encapsulation of Fish Oil by an Enzymatic Gelation Process Using Transglutaminase Cross‐linked Proteins. *Journal of food science* **2003,** *68* (9), 2717-2723.

48. Gan, C.-Y.; Cheng, L.-H.; Easa, A. M., Evaluation of microbial transglutaminase and ribose cross-linked soy protein isolate-based microcapsules containing fish oil. *Innovative Food Science & Emerging Technologies* **2008,** *9* (4), 563-569.

49. Montero, P.; Fernández-Dıaz, M. D.; Gómez-Guillén, M. C., Characterization of gelatin gels induced by high pressure. *Food Hydrocolloids* **2002,** *16* (3), 197-205.

50. Chen, T.; Embree, H. D.; Brown, E. M.; Taylor, M. M.; Payne, G. F., Enzyme-catalyzed gel formation of gelatin and chitosan: potential for in situ applications. *Biomaterials* **2003,** *24* (17), 2831-2841.

51. Borkova, M.; Snaselova, J., Possibilities of different animal milk detection in milk and dairy products—a review. *Czech J. Food Sci* **2005,** *23* (2), 41-50.

52. Beaulieu, L.; Savoie, L.; Paquin, P.; Subirade, M., Elaboration and characterization of whey protein beads by an emulsification/cold gelation process: application for the protection of retinol. *Biomacromolecules* **2002,** *3* (2), 239-248.

53. Egan, T.; Jacquier, J.-C.; Rosenberg, Y.; Rosenberg, M., Cold-set whey protein microgels for the stable immobilization of lipids. *Food Hydrocolloids* **2013,** *31* (2), 317-324.

54. Veloso, A. C. A.; Teixeira, N.; Ferreira, I. M., Separation and quantification of the major casein fractions by reverse-phase high-performance liquid chromatography and urea–polyacrylamide gel electrophoresis: Detection of milk adulterations. *Journal of Chromatography A* **2002,** *967* (2), 209-218.

55. Benzaria, A.; Maresca, M.; Taieb, N.; Dumay, E., Interaction of curcumin with phosphocasein micelles processed or not by dynamic high-pressure. *Food Chemistry* **2013,** *138* (4), 2327-2337.

56. Saiz-Abajo, M. J.; Gonzalez-Ferrero, C.; Moreno-Ruiz, A.; Romo-Hualde, A.; Gonzalez-Navarro, C. J., Thermal protection of beta-carotene in re-assembled casein micelles during different processing technologies applied in food industry. *Food Chemistry* **2013,** *138* (2-3), 1581-1587.

57. Chevalier-Lucia, D.; Blayo, C.; Gracia-Julia, A.; Picart-Palmade, L.; Dumay, E., Processing of phosphocasein dispersions by dynamic high pressure: Effects on the dispersion physico-chemical characteristics and the binding of alpha-tocopherol acetate to casein micelles. *Innovative Food Science & Emerging Technologies* **2011,** *12* (4), 416-425.

58. Pan, K.; Zhong, Q.; Baek, S. J., Enhanced dispersibility and bioactivity of curcumin by encapsulation in casein nanocapsules. *Journal of agricultural and food chemistry* **2013,** *61* (25), 6036-6043.

59. Dickinson, E., Flocculation of protein-stabilized oil-in-water emulsions. *Colloids and Surfaces B-Biointerfaces* **2010,** *81* (1), 130-140.

60. Jones, O. G.; McClements, D. J., Functional biopolymer particles: design, fabrication, and applications. *Comprehensive Reviews in Food Science and Food Safety* **2010,** *9* (4), 374-397.

61. Hoffman, A. S., Hydrogels for biomedical applications. *Advanced drug delivery reviews* **2002,** *54* (1), 3-12.

62. Li, Y.; McClements, D. J., Controlling lipid digestion by encapsulation of protein-stabilized lipid droplets within alginate–chitosan complex coacervates. *Food Hydrocolloids* **2011,** *25* (5), 1025-1033.

63. Prata, A. S.; Zanin, M. H. A.; Ré, M. I.; Grosso, C. R. F., Release properties of chemical and enzymatic crosslinked gelatin-gum Arabic microparticles containing a fluorescent probe plus vetiver essential oil. *Colloids and Surfaces B: Biointerfaces* **2008,** *67* (2), 171-178.

64. Weinbreck, F.; Minor, M.; De Kruif, C. G., Microencapsulation of oils using whey protein/gum arabic coacervates. *Journal of microencapsulation* **2004,** *21* (6), 667-679.

65. Berger, J.; Reist, M.; Mayer, J. M.; Felt, O.; Gurny, R., Structure and interactions in chitosan hydrogels formed by complexation or aggregation for biomedical applications. *European Journal of Pharmaceutics and Biopharmaceutics* **2004,** *57* (1), 35-52.

66. Takahashi, T.; Takayama, K.; Machida, Y.; Nagai, T., Characteristics of polyion complexes of chitosan with sodium alginate and sodium polyacrylate. *International Journal of Pharmaceutics* **1990,** *61* (1), 35-41.

67. Chavasit, V.; Kienzle-Sterzer, C.; Torres, J. A., Formation and characterization of an insoluble polyelectrolyte complex: chitosan-polyacrylic acid. *Polymer Bulletin* **1988,** *19* (3), 223-230.

68. Argüelles-Monal, W.; Hechavarria, O. L.; Rodriguez, L.; Peniche, C., Swelling of membranes from the polyelectrolyte complex between chitosan and carboxymethyl cellulose. *Polymer Bulletin* **1993,** *31* (4), 471-478.

69. Lee, K. Y.; Park, W. H.; Ha, W. S., Polyelectrolyte complexes of sodium alginate with chitosan or its derivatives for microcapsules. *Journal of Applied Polymer Science* **1997,** *63* (4), 425-432.

70. Donato, L.; Schmitt, C.; Bovetto, L.; Rouvet, M., Mechanism of formation of stable heat-induced β-lactoglobulin microgels. *International Dairy Journal* **2009,** *19* (5), 295-306.

71. Yu, C.-Y.; Yin, B.-C.; Zhang, W.; Cheng, S.-X.; Zhang, X.-Z.; Zhuo, R.-X., Composite microparticle drug delivery systems based on chitosan, alginate and pectin with improved pH-sensitive drug release property. *Colloids and Surfaces B: Biointerfaces* **2009,** *68* (2), 245-249.

72. Mohanty, B.; Aswal, V. K.; Goyal, P. S.; Bohidar, H. B., Small-angle neutron and dynamic light scattering study of gelatin coacervates. *Pramana* **2004,** *63* (2), 271-276.

73. Matalanis, A.; Lesmes, U.; Decker, E. A.; McClements, D. J., Fabrication and characterization of filled hydrogel particles based on sequential segregative and aggregative biopolymer phase separation. *Food hydrocolloids* **2010,** *24* (8), 689-701.

74. Wu, B.-c.; Degner, B.; McClements, D. J., Soft matter strategies for controlling food texture: formation of hydrogel particles by biopolymer complex coacervation. *Journal of Physics: Condensed Matter* **2014,** *26* (46), 464104.

75. Zhang, Z.; Zhang, R.; Decker, E. A.; McClements, D. J., Development of food-grade filled hydrogels for oral delivery of lipophilic active ingredients: pH-triggered release. *Food Hydrocolloids* **2014**.

76. Li, Y.; Hu, M.; Du, Y.; Xiao, H.; McClements, D. J., Control of lipase digestibility of emulsified lipids by encapsulation within calcium alginate beads. *Food Hydrocolloids* **2011,** *25* (1), 122-130.

77. Bromley, E. H.; Krebs, M. R.; Donald, A. M., Mechanisms of structure formation in particulate gels of beta-lactoglobulin formed near the isoelectric point. *The European physical journal. E, Soft matter* **2006,** *21* (2), 145-52.

78. Jones, O. G.; McClements, D. J., Biopolymer Nanoparticles from Heat-Treated Electrostatic Protein-Polysaccharide Complexes: Factors Affecting Particle Characteristics. *Journal of Food Science* **2010,** *75* (2), N36-N43.

79. Matalanis, A.; Jones, O. G.; McClements, D. J., Structured biopolymer-based delivery systems for encapsulation, protection, and release of lipophilic compounds. *Food Hydrocolloids* **2011,** *25* (8), 1865-1880.

80. Schmitt, C.; Bovay, C.; Rouvet, M.; Shojaei-Rami, S.; Kolodziejczyk, E., Whey protein soluble aggregates from heating with NaCl: physicochemical, interfacial, and foaming properties. *Langmuir* **2007,** *23* (8), 4155-4166.

81. Krebs, M. R. H.; Devlin, G. L.; Donald, A. M., Protein particulates: another generic form of protein aggregation? *Biophysical journal* **2007,** *92* (4), 1336-1342.

82. Jones, O. G.; Decker, E. A.; McClements, D. J., Formation of biopolymer particles by thermal treatment of β-lactoglobulin – pectin complexes. *Food Hydrocolloids* **2009,** *23* (5), 1312-1321.

83. Yu, C.-Y.; Jia, L.-H.; Cheng, S.-X.; Zhang, X.-Z.; Zhuo, R.-X., Fabrication of microparticle protein delivery systems based on calcium alginate. *Journal of microencapsulation* **2010,** *27* (2), 171-177.

84. Albarghouthi, M.; Fara, D. A.; Saleem, M.; El-Thaher, T.; Matalka, K.; Badwan, A., Immobilization of antibodies on alginate-chitosan beads. *International journal of pharmaceutics* **2000,** *206* (1), 23-34.

85. González-Rodrıguez, M. L.; Holgado, M. A.; Sanchez-Lafuente, C.; Rabasco, A. M.; Fini, A., Alginate/chitosan particulate systems for sodium diclofenac release. *International Journal of Pharmaceutics* **2002,** *232* (1), 225-234.

86. Peniche, C.; Howland, I.; Carrillo, O.; Zaldívar, C.; Argüelles-Monal, W., Formation and stability of shark liver oil loaded chitosan/calcium alginate capsules. *Food hydrocolloids* **2004,** *18* (5), 865-871.

87. Pasparakis, G.; Bouropoulos, N., Swelling studies and in vitro release of verapamil from calcium alginate and calcium alginate–chitosan beads. *International journal of pharmaceutics* **2006,** *323* (1), 34-42.

88. Wittaya-areekul, S.; Kruenate, J.; Prahsarn, C., Preparation and in vitro evaluation of mucoadhesive properties of alginate/chitosan microparticles containing prednisolone. *International journal of pharmaceutics* **2006,** *312* (1), 113-118.

89. Wolf, B.; Frith, W. J.; Singleton, S.; Tassieri, M.; Norton, I. T., Shear behaviour of biopolymer suspensions with spheroidal and cylindrical particles. *Rheologica Acta* **2001,** *40* (3), 238-247.

90. Fernández Farrés, I.; Norton, I. T., Formation kinetics and rheology of alginate fluid gels produced by in-situ calcium release. *Food Hydrocolloids* **2014,** *40*, 76-84.

91. Gabriele, A.; Spyropoulos, F.; Norton, I. T., Kinetic study of fluid gel formation and viscoelastic response with kappa-carrageenan. *Food Hydrocolloids* **2009,** *23* (8), 2054-2061.

92. Mahdi, M. H.; Conway, B. R.; Smith, A. M., Evaluation of gellan gum fluid gels as modified release oral liquids. *International journal of pharmaceutics* **2014,** *475* (1), 335-343.

93. Oxley, J. D., Spray cooling and spray chilling for food ingredient and nutraceutical encapsulation. In *Encapsulation Technologies and Delivery Systems for Food Ingredients and Nutraceuticals*, Garti, N.; McClements, D. J., Eds. Woodhead Publishing: Oxford, U.K., 2012; pp 110-130.

94. Drusch, S.; Serfert, Y.; Scampicchio, M.; Schmidt-Hansberg, B.; Schwarz, K., Impact of physicochemical characteristics on the oxidative stability of fish oil microencapsulated by spray-drying. *Journal of agricultural and food chemistry* **2007,** *55* (26), 11044-11051.

95. Hamidi, M.; Azadi, A.; Rafiei, P., Hydrogel nanoparticles in drug delivery. *Advanced drug delivery reviews* **2008,** *60* (15), 1638-1649.

96. Salles, C.; Tarrega, A.; Mielle, P.; Maratray, J.; Gorria, P.; Liaboeuf, J.; Liodenot, J. J., Development of a chewing simulator for food breakdown and the analysis of< i> in vitro</i> flavor compound release in a mouth environment. *Journal of Food Engineering* **2007,** *82* (2), 189-198.

97. de Roos, K. B., Effect of texture and microstructure on flavour retention and release. *International Dairy Journal* **2003,** *13* (8), 593-605.

98. Hansson, A.; Giannouli, P.; van Ruth, S., The influence of gel strength on aroma release from pectin gels in a model mouth and in vivo, monitored with proton-transfer-reaction mass spectrometry. *Journal of agricultural and food chemistry* **2003,** *51* (16), 4732-4740.

99. Mills, T.; Spyropoulos, F.; Norton, I. T.; Bakalis, S., Development of an in-vitro mouth model to quantify salt release from gels. *Food hydrocolloids* **2011,** *25* (1), 107-113.

100. Lian, G.; Malone, M. E.; Homan, J. E.; Norton, I. T., A mathematical model of volatile release in mouth from the dispersion of gelled emulsion particles. *Journal of controlled release* **2004,** *98* (1), 139-155.

101. Malone, M. E.; Appelqvist, I. A. M.; Norton, I. T., Oral behaviour of food hydrocolloids and emulsions. Part 2. Taste and aroma release. *Food Hydrocolloids* **2003,** *17* (6), 775-784.

102. Kong, F.; Singh, R. P., A model stomach system to investigate disintegration kinetics of solid foods during gastric digestion. *Journal of food science* **2008,** *73* (5), E202-E210.

103. Guerra, A.; Etienne-Mesmin, L.; Livrelli, V.; Denis, S.; Blanquet-Diot, S.; Alric, M., Relevance and challenges in modeling human gastric and small intestinal digestion. *Trends in Biotechnology* **2012,** *30* (11), 591-600.

104. McClements, D. J., Edible lipid nanoparticles: Digestion, absorption, and potential toxicity. *Progress in lipid research* **2013,** *52* (4), 409-423.

105. McClements, D. J.; Decker, E. A.; Park, Y.; Weiss, J., Designing food structure to control stability, digestion, release and absorption of lipophilic food components. *Food Biophysics* **2008,** *3* (2), 219-228.

106. Murata, Y.; Sasaki, N.; Miyamoto, E.; Kawashima, S., Use of floating alginate gel beads for stomach-specific drug delivery. *European journal of pharmaceutics and biopharmaceutics* **2000,** *50* (2), 221-226.

107. Sriamornsak, P.; Thirawong, N.; Puttipipatkhachorn, S., Morphology and buoyancy of oil-entrapped calcium pectinate gel beads. *The AAPS journal* **2004,** *6* (3), 65-71.

108. Matalanis, A.; McClements, D. J., Impact of encapsulation within hydrogel microspheres on lipid digestion: an in vitro study. *Food biophysics* **2012,** *7* (2), 145-154.

109. Chen, L.; Hebrard, G.; Beyssac, E.; Denis, S.; Subirade, M., In Vitro Study of the Release Properties of Soy-Zein Protein Microspheres with a Dynamic Artificial Digestive System. *Journal of Agricultural and Food Chemistry* **2010,** *58* (17), 9861-9867.

110. McClements, D. J., *Understanding and controlling the microstructure of complex foods*. Elsevier: 2007.

111. Mun, S.; Kim, Y.-R.; McClements, D. J., Control of β-carotene bioaccessibility using starch-based filled hydrogels. *Food Chemistry* **2014**.

112. Wong, J. M. W.; de Souza, R.; Kendall, C. W. C.; Emam, A.; Jenkins, D. J. A., Colonic health: fermentation and short chain fatty acids. *Journal of clinical gastroenterology* **2006,** *40* (3), 235-243.

113. Yin, Y.; Yang, Y.; Xu, H., Swelling behavior of hydrogels for colon‐site drug delivery. *Journal of applied polymer science* **2002,** *83* (13), 2835-2842.

114. Das, S.; Ng, K.-Y., Colon-specific delivery of resveratrol: optimization of multi-particulate calcium-pectinate carrier. *International journal of pharmaceutics* **2010,** *385* (1), 20-28.

115. Xing, L.; Dawei, C.; Liping, X.; Rongqing, Z., Oral colon-specific drug delivery for bee venom peptide: development of a coated calcium alginate gel beads-entrapped liposome. *Journal of controlled release* **2003,** *93* (3), 293-300.

116. Hovgaard, L.; Brøndsted, H., Dextran hydrogels for colon-specific drug delivery. *Journal of Controlled Release* **1995,** *36* (1), 159-166.

117. Elias, E. J.; Anil, S.; Ahmad, S.; Daud, A., Colon targeted curcumin delivery using guar gum. *Natural product communications* **2010,** *5* (6), 915-918.

118. Bhattarai, N.; Gunn, J.; Zhang, M., Chitosan-based hydrogels for controlled, localized drug delivery. *Advanced drug delivery reviews* **2010,** *62* (1), 83-99.

119. Kolanowski, W.; Weissrodt, J., Sensory quality of dairy products fortified with fish oil. *International Dairy Journal* **2007,** *17* (10), 1248-1253.

120. Mao, Y. Y.; McClements, D. J., Modulation of emulsion rheology through electrostatic heteroaggregation of oppositely charged lipid droplets: Influence of particle size and emulsifier content. *Journal of Colloid and Interface Science* **2012,** *380*, 60-66.

121. Waraho, T.; McClements, D. J.; Decker, E. A., Mechanisms of lipid oxidation in food dispersions. *Trends in Food Science & Technology* **2011,** *22* (1), 3-13.

122. Jacobsen, C., Omega-3s in food emulsions: overview and case studies. *Agro Food Industry Hi-Tech* **2008,** *19* (5), 9-12.

123. Jacobsen, C.; Let, M. B.; Nielsen, N. S.; Meyer, A. S., Antioxidant strategies for preventing oxidative flavour deterioration of foods enriched with n-3 polyunsaturated lipids: a comparative evaluation. *Trends in Food Science & Technology* **2008,** *19* (2), 76-93.

124. Tikekar, R. V.; Nitin, N., Distribution of Encapsulated Materials in Colloidal Particles and Its Impact on Oxidative Stability of Encapsulated Materials. *Langmuir* **2012,** *28* (25), 9233-9243.

125. Drusch, S.; Benedetti, S.; Scampicchio, M.; Mannino, S., Stabilisation of omega-3 fatty acids by microencapsulation. *Agro Food Industry Hi-Tech* **2008,** *19* (4), 31-32.

126. Michalski, M. C.; Genot, C.; Gayet, C.; Lopez, C.; Fine, F.; Joffre, F.; Vendeuvre, J. L.; Bouvier, J.; Chardigny, J. M.; Raynal-Ljutovac, K.; Steering Comm, R. L., Multiscale structures of lipids in foods as parameters affecting fatty acid bioavailability and lipid metabolism. *Progress in Lipid Research* **2013,** *52* (4), 354-373.

127. Hernandez-Ledesma, B.; Contreras, M. D.; Recio, I., Antihypertensive peptides: Production, bioavailability and incorporation into foods. *Advances in Colloid and Interface Science* **2011,** *165* (1), 23-35.

128. Samaranayaka, A. G. P.; Li-Chan, E. C. Y., Food-derived peptidic antioxidants: A review of their production, assessment, and potential applications. *Journal of Functional Foods* **2011,** *3* (4), 229-254.

129. Sarmadi, B. H.; Ismail, A., Antioxidative peptides from food proteins: A review. *Peptides* **2010,** *31* (10), 1949-1956.

130. Udenigwe, C. C.; Aluko, R. E., Food Protein-Derived Bioactive Peptides: Production, Processing, and Potential Health Benefits. *Journal of Food Science* **2012,** *77* (1), R11-R24.

131. Hettiarachchy, N.; Sato, K.; Marshall, M.; Kannan, A., *Food Proteins and Peptides: Chemistry, Functionality, Interactions, and Commercialization*. CRC Press: Boca Raton, 2012.

132. Mohan, A.; Rajendran, S.; He, Q. S.; Bazinet, L.; Udenigwe, C. C., Encapsulation of food protein hydrolysates and peptides: a review. *Rsc Advances* **2015,** *5* (97), 79270-79278.

133. Moreno, F. J., Gastrointestinal digestion of food allergens: Effect on their allergenicity. *Biomedicine & Pharmacotherapy* **2007,** *61* (1), 50-60.

134. McClements, D. J., Nanoscale Nutrient Delivery Systems for Food Applications: Improving Bioactive Dispersibility, Stability, and Bioavailability. *Journal of Food Science* **2015,** *80* (7), N1602-N1611.

135. Gallaher, J. J.; Hollender, R.; Peterson, D. G.; Roberts, R. F.; Coupland, J. N., Effect of composition and antioxidants on the oxidative stability of fluid milk supplemented with an algae oil emulsion. *International Dairy Journal* **2005,** *15* (4), 333-341.

136. Porter, C. J. H.; Wasan, K. M., Lipid-based systems for the enhanced delivery of poorly water soluble drugs. *Advanced Drug Delivery Reviews* **2008,** *60* (6), 615-616.

137. Pouton, C. W., Formulation of poorly water-soluble drugs for oral administration: Physicochemical and physiological issues and the lipid formulation classification system. *European Journal of Pharmaceutical Sciences* **2006,** *29* (3-4), 278-287.

138. Huang, C. B.; George, B.; Ebersole, J. L., Antimicrobial activity of n-6, n-7 and n-9 fatty acids and their esters for oral microorganisms. *Arch. Oral Biol.* **2010,** *55* (8), 555-560.

139. Loesche, W. J., The antimicrobial treatment of periodontal disease: Changing the treatment paradigm. *Crit. Rev. Oral Biol. Med.* **1999,** *10* (3), 245-275.

140. Madene, A.; Jacquot, M.; Scher, J.; Desobry, S., Flavour encapsulation and controlled release - a review. *Int J Food Sci Tech* **2006,** *41* (1), 1-21.

141. van Ruth, S. M.; O'Connor, C. H.; Delahunty, C. M., Relationships between temporal release of aroma compounds in a model mouth system and their physico-chemical characteristics. *Food Chemistry* **2000,** *71* (3), 393-399.

142. McClements, D. J., *Nanoparticle- and Microparticle-based Delivery Systems: Encapsulation, Protection and Release of Active Compounds*. CRC Press: Boca Raton, FL, 2014; p 564.

143. Nakagawa, K.; Nagao, H., Microencapsulation of oil droplets using freezing-induced gelatin-acacia complex coacervation. *Colloids and Surfaces a-Physicochemical and Engineering Aspects* **2012,** *411*, 129-139.

144. Piacentini, E.; Giorno, L.; Dragosavac, M. M.; Vladisavljevic, G. T.; Holdich, R. G., Microencapsulation of oil droplets using cold water fish gelatine/gum arabic complex coacervation by membrane emulsification. *Food Research International* **2013,** *53* (1), 362-372.

145. Wang, B.; Adhikari, B.; Barrow, C. J., Optimisation of the microencapsulation of tuna oil in gelatin-sodium hexametaphosphate using complex coacervation. *Food chemistry* **2014,** *158*, 358-65.

146. Yang, Z.; Peng, Z.; Li, J.; Li, S.; Kong, L.; Li, P.; Wang, Q., Development and evaluation of novel flavour microcapsules containing vanilla oil using complex coacervation approach. *Food Chemistry* **2014,** *145*, 272-277.

147. Kayitmazer, A. B.; Seeman, D.; Minsky, B. B.; Dubin, P. L.; Xu, Y., Protein-polyelectrolyte interactions. *Soft Matter* **2013,** *9* (9), 2553-2583.

148. Kizilay, E.; Kayitmazer, A. B.; Dubin, P. L., Complexation and coacervation of polyelectrolytes with oppositely charged colloids. *Advances in Colloid and Interface Science* **2011,** *167* (1-2), 24-37.

149. Schmitt, C.; Kolodziejczyk, E., *Protein - polysaccharide complexes from basics to food applications*. 2010; p 211-222.

150. Schmitt, C.; Sanchez, C.; Desobry-Banon, S.; Hardy, J., Structure and technofunctional properties of protein-polysaccharide complexes: A review. *Crit. Rev. Food Sci. Nutr.* **1998,** *38* (8), 689-753.

151. Schmitt, C.; Turgeon, S. L., Protein/polysaccharide complexes and coacervates in food systems. *Advances in Colloid and Interface Science* **2011,** *167* (1-2), 63-70.

152. Turgeon, S. L.; Schmitt, C.; Sanchez, C., Protein-polysaccharide complexes and coacervates. *Current Opinion in Colloid & Interface Science* **2007,** *12* (4-5), 166-178.

153. Xiao, Z.; Liu, W.; Zhu, G.; Zhou, R.; Niu, Y., A review of the preparation and application of flavour and essential oils microcapsules based on complex coacervation technology. *Journal of the science of food and agriculture* **2014,** *94* (8), 1482-94.

154. Koupantsis, T.; Pavlidou, E.; Paraskevopoulou, A., Flavour encapsulation in milk proteins - CMC coacervate-type complexes. *Food Hydrocolloids* **2014,** *37*, 134-142.

155. Matalanis, A.; Decker, E. A.; McClements, D. J., Inhibition of lipid oxidation by encapsulation of emulsion droplets within hydrogel microspheres. *Food Chemistry* **2012,** *132* (2), 766-772.

156. Stieger, M.; van de Velde, F., Microstructure, texture and oral processing: New ways to reduce sugar and salt in foods. *Current Opinion in Colloid & Interface Science* **2013,** *18* (4), 334-348.

157. van Aken, G. A.; Vingerhoeds, M. H.; de Wijk, R. A., Textural perception of liquid emulsions: Role of oil content, oil viscosity and emulsion viscosity. *Food Hydrocolloids* **2011,** *25* (4), 789-796.

158. van Vliet, T.; van Aken, G. A.; de Jongh, H. H. J.; Hamer, R. J., Colloidal aspects of texture perception. *Advances in Colloid and Interface Science* **2009,** *150* (1), 27-40.

159. Buettner, A., Influence of human salivary enzymes on odorant concentration changes occurring in vivo. 1. Esters and thiols. *Journal of Agricultural and Food Chemistry* **2002,** *50* (11), 3283-3289.

160. Hansson, A.; Leufven, A.; Van Ruth, S., Partition and release of 21 aroma compounds during storage of a pectin gel system. *Journal of Agricultural and Food Chemistry* **2003,** *51* (7), 2000-2005.

161. van Ruth, S. M.; Grossmann, I.; Geary, M.; Delahunty, C. M., Interactions between artificial saliva and 20 aroma compounds in water and oil model systems. *Journal of Agricultural and Food Chemistry* **2001,** *49* (5), 2409-2413.

162. Sarkar, A.; Goh, K. K. T.; Singh, H., Colloidal stability and interactions of milk-protein-stabilized emulsions in an artificial saliva. *Food Hydrocolloids* **2009,** *23* (5), 1270-1278.

163. Kinsella, J. E., Milk-Proteins - Physicochemical and Functional-Properties. *Crc Critical Reviews in Food Science and Nutrition* **1984,** *21* (3), 197-262.

164. Klemmer, K. J.; Waldner, L.; Stone, A.; Low, N. H.; Nickerson, M. T., Complex coacervation of pea protein isolate and alginate polysaccharides. *Food Chemistry* **2012,** *130* (3), 710-715.

165. Barroso da Silva, F. L.; Joensson, B., Polyelectrolyte-protein complexation driven by charge regulation. *Soft Matter* **2009,** *5* (15), 2862-2868.

166. Chung, C.; Degner, B.; Decker, E. A.; McClements, D. J., Oil-filled hydrogel particles for reduced-fat food applications: Fabrication, characterization, and properties. *Innovative Food Science & Emerging Technologies* **2013,** *20*, 324-334.

167. Lv, Y.; Yang, F.; Li, X.; Zhang, X.; Abbas, S., Formation of heat-resistant nanocapsules of jasmine essential oil via gelatin/gum arabic based complex coacervation. *Food Hydrocolloids* **2014,** *35*, 305-314.

168. Girard, M.; Turgeon, S. L.; Gauthier, S. F., Interbiopolymer complexing between beta-lactoglobulin and low- and high-methylated pectin measured by potentiometric titration and ultrafiltration. *Food Hydrocolloids* **2002,** *16* (6), 585-591.

169. McClements, D. J.; Decker, E. A.; Park, Y., Controlling Lipid Bioavailability through Physicochemical and Structural Approaches. *Crit. Rev. Food Sci. Nutr.* **2009,** *49* (1), 48-67.

170. Singh, H.; Ye, A.; Horne, D., Structuring food emulsions in the gastrointestinal tract to modify lipid digestion. *Progress in Lipid Research* **2009,** *48* (2), 92-100.

171. Rediguieri, C. F.; de Freitas, O.; Lettinga, M. P.; Tuinier, R., Thermodynamic incompatibility and complex formation in pectin/caseinate mixtures. *Biomacromolecules* **2007,** *8* (11), 3345-3354.

172. Peng, X.-W.; Ren, J.-L.; Zhong, L.-X.; Peng, F.; Sun, R.-C., Xylan-rich Hemicelluloses-graft-Acrylic Acid Ionic Hydrogels with Rapid Responses to pH, Salt, and Organic Solvents. *Journal of Agricultural and Food Chemistry* **2011,** *59* (15), 8208-8215.

173. Matalanis, A.; McClements, D. J., Hydrogel microspheres for encapsulation of lipophilic components: Optimization of fabrication & performance. *Food Hydrocolloids* **2013,** *31* (1), 15-25.

174. McClements, D. J., Utilizing food effects to overcome challenges in delivery of lipophilic bioactives: structural design of medical and functional foods. *Expert Opinion on Drug Delivery* **2013,** *10* (12), 1621-1632.

175. Velikov, K. P.; Pelan, E., Colloidal delivery systems for micronutrients and nutraceuticals. *Soft Matter* **2008,** *4* (10), 1964-1980.

176. Augustin, M. A.; Hemar, Y., Nano- and micro-structured assemblies for encapsulation of food ingredients. *Chemical Society Reviews* **2009,** *38* (4), 902-912.

177. McClements, D. J.; Xiao, H., Excipient foods: designing food matrices that improve the oral bioavailability of pharmaceuticals and nutraceuticals. *Food & Function* **2014,** *5* (7), 1320-1333.

178. McClements, D. J., *Nanoparticle- and Microparticle-based Delivery Systems: Encapsulation, Protection and Release of Active Components*. CRC Press: Boca Raton, FL, 2014.

179. Pothakamury, U. R.; BarbosaCanovas, G. V., Fundamental aspects of controlled release in foods. *Trends in Food Science & Technology* **1995,** *6* (12), 397-406.

180. Sorensen, L. B.; Moller, P.; Flint, A.; Martens, M.; Raben, A., Effect of sensory perception of foods on appetite and food intake: a review of studies on humans. *International Journal of Obesity* **2003,** *27* (10), 1152-1166.

181. Doyennette, M.; Déléris, I.; Feron, G.; Guichard, E.; Souchon, I.; Trelea, I. C., Main individual and product characteristics influencing in-mouth flavour release during eating masticated food products with different textures: Mechanistic modelling and experimental validation. *Journal of theoretical biology* **2014,** *340*, 209-221.

182. Porter, C. J. H.; Wasan, K. M.; Constantinides, P., Lipid-based systems for the enhanced delivery of poorly water soluble drugs. *Advanced drug delivery reviews* **2008,** *60* (6), 615-616.

183. Pouton, C. W., Formulation of poorly water-soluble drugs for oral administration: physicochemical and physiological issues and the lipid formulation classification system. *European Journal of Pharmaceutical Sciences* **2006,** *29* (3), 278-287.

184. Gershkovich, P.; Wasan, K. M.; Barta, C. A., A review of the application of lipid-based systems in systemic, dermal/transdermal, and ocular drug delivery. *Critical Reviews™ in Therapeutic Drug Carrier Systems* **2008,** *25* (6).

185. Han, S.-f.; Yao, T.-t.; Zhang, X.-x.; Gan, L.; Zhu, C.; Yu, H.-z.; Gan, Y., Lipid-based formulations to enhance oral bioavailability of the poorly water-soluble drug anethol trithione: effects of lipid composition and formulation. *International journal of pharmaceutics* **2009,** *379* (1), 18-24.

186. Lee, J. H.; Jeong, J. S.; Park, S. W.; Kim, D. S.; Kim, W.; Ahn, S. I.; Park, J. H.; Kim, Y. T.; Shin, H.-S.; Rhee, J. M., Biopharmaceutical correlation of insoluble drugs using lipid-based formulations. *Tissue Engineering and Regenerative Medicine* **2008,** *5* (4-6), 750-757.

187. McClements, D. J., Emulsion design to improve the delivery of functional lipophilic components. *Annual review of food science and technology* **2010,** *1*, 241-269.

188. Nordly, P.; Madsen, H. B.; Nielsen, H. M.; Foged, C., Status and future prospects of lipid-based particulate delivery systems as vaccine adjuvants and their combination with immunostimulators. **2009**.

189. Semalty, A.; Semalty, M.; Rawat, B. S.; Singh, D.; Rawat, M. S. M., Pharmacosomes: the lipid-based new drug delivery system. **2009**.

190. Yao, M.; Xiao, H.; McClements, D. J., Delivery of Lipophilic Bioactives: Assembly, Disassembly, and Reassembly of Lipid Nanoparticles. *Annual Review of Food Science and Technology, Vol 5* **2014,** *5*, 53-81.

191. Kayitmazer, A. B.; Seeman, D.; Minsky, B. B.; Dubin, P. L.; Xu, Y., Protein–polyelectrolyte interactions. *Soft Matter* **2013,** *9* (9), 2553-2583.

192. Zhang, Z.; Decker, E. A.; McClements, D. J., Development of food-grade filled hydrogels for oral delivery of lipophilic active ingredients: pH-triggered release. *Food Hydrocolloids* **2014**.

193. Zhang, Z.; Decker, E. A.; McClements, D. J., Encapsulation, Protection, and Release of Polyunsaturated Lipids using Biopolymer-based Hydrogel Particles. *Food Research International* **2014**.

194. Tsuboi, A.; Izumi, T.; Hirata, M.; Xia, J.; Dubin, P. L.; Kokufuta, E., Complexation of proteins with a strong polyanion in an aqueous salt-free system. *Langmuir* **1996,** *12* (26), 6295-6303.

195. Bengoechea, C.; Jones, O. G.; Guerrero, A.; McClements, D. J., Formation and characterization of lactoferrin/pectin electrostatic complexes: Impact of composition, pH and thermal treatment. *Food Hydrocolloids* **2011,** *25* (5), 1227-1232.

196. Cooper, C. L.; Dubin, P. L.; Kayitmazer, A. B.; Turksen, S., Polyelectrolyte-protein complexes. *Current Opinion in Colloid & Interface Science* **2005,** *10* (1-2), 52-78.

197. Malay, Ö.; Bayraktar, O.; Batıgün, A., Complex coacervation of silk fibroin and hyaluronic acid. *International journal of biological macromolecules* **2007,** *40* (4), 387-393.

198. Karim, A. A.; Bhat, R., Gelatin alternatives for the food industry: recent developments, challenges and prospects. *Trends in food science & technology* **2008,** *19* (12), 644-656.

199. Jin, K.-M.; Kim, Y.-H., Injectable, thermo-reversible and complex coacervate combination gels for protein drug delivery. *Journal of Controlled Release* **2008,** *127* (3), 249-256.

200. Syed, H. K.; Liew, K. B.; Loh, G. O. K.; Peh, K. K., Stability indicating HPLC–UV method for detection of curcumin in Curcuma longa extract and emulsion formulation. *Food Chemistry* **2015,** *170*, 321-326.

201. Prasad, S.; Gupta, S. C.; Tyagi, A. K.; Aggarwal, B. B., Curcumin, a component of golden spice: From bedside to bench and back. *Biotechnology advances* **2014,** *32* (6), 1053-1064.

202. Heger, M.; van Golen, R. F.; Broekgaarden, M.; Michel, M. C., The molecular basis for the pharmacokinetics and pharmacodynamics of curcumin and its metabolites in relation to cancer. *Pharmacological reviews* **2014,** *66* (1), 222-307.

203. Wilken, R.; Veena, M. S.; Wang, M. B.; Srivatsan, E. S., Curcumin: A review of anti-cancer properties and therapeutic activity in head and neck squamous cell carcinoma. *Mol Cancer* **2011,** *10* (12), 1-19.

204. Sharma, R. A.; Gescher, A. J.; Steward, W. P., Curcumin: the story so far. *European Journal of Cancer* **2005,** *41* (13), 1955-1968.

205. Ringman, J. M.; Frautschy, S. A.; Cole, G. M.; Masterman, D. L.; Cummings, J. L., A potential role of the curry spice curcumin in Alzheimer's disease. *Current Alzheimer Research* **2005,** *2* (2), 131.

206. Anand, P.; Kunnumakkara, A. B.; Newman, R. A.; Aggarwal, B. B., Bioavailability of curcumin: Problems and promises. *Molecular Pharmaceutics* **2007,** *4* (6), 807-818.

207. Letchford, K.; Liggins, R.; Burt, H., Solubilization of hydrophobic drugs by methoxy poly (ethylene glycol) ‐ block ‐ polycaprolactone diblock copolymer micelles: Theoretical and experimental data and correlations. *Journal of Pharmaceutical Sciences* **2008,** *97* (3), 1179-1190.

208. Sharma, R. A.; Steward, W. P.; Gescher, A. J., Pharmacokinetics and pharmacodynamics of curcumin. In *The Molecular Targets and Therapeutic Uses Of Curcumin In Health And Disease*, Aggarwal, B. B.; Surh, Y.-J.; Shishodia, S., Eds. Springer: Berlin, Germany, 2007; pp 453-470.

209. Sahu, A.; Kasoju, N.; Bora, U., Fluorescence study of the curcumin− casein micelle complexation and its application as a drug nanocarrier to cancer cells. *Biomacromolecules* **2008,** *9* (10), 2905-2912.

210. Maiti, K.; Mukherjee, K.; Gantait, A.; Saha, B. P.; Mukherjee, P. K., Curcumin–phospholipid complex: preparation, therapeutic evaluation and pharmacokinetic study in rats. *International Journal of Pharmaceutics* **2007,** *330* (1), 155-163.

211. Tiyaboonchai, W.; Tungpradit, W.; Plianbangchang, P., Formulation and characterization of curcuminoids loaded solid lipid nanoparticles. *International Journal of Pharmaceutics* **2007,** *337* (1), 299-306.

212. Margulis, K.; Magdassi, S.; Lee, H. S.; Macosko, C. W., Formation of curcumin nanoparticles by flash nanoprecipitation from emulsions. *Journal of Colloid and Interface Science* **2014,** *434*, 65-70.

213. Yu, H.; Shi, K.; Liu, D.; Huang, Q., Development of a food-grade organogel with high bioaccessibility and loading of curcuminoids. *Food Chemistry* **2012,** *131* (1), 48-54.

214. Tapal, A.; Tiku, P. K., Complexation of curcumin with soy protein isolate and its implications on solubility and stability of curcumin. *Food Chemistry* **2012,** *130* (4), 960-965.

215. Zou, L.; Liu, W.; Liu, C.; Xiao, H.; McClements, D. J., Utilizing food matrix effects to enhance nutraceutical bioavailability: Increase of curcumin bioaccessibility using excipient emulsions. *Journal of Agricultural and Food Chemistry* **2015,** *63* (7), 2052-2062.

216. Zou, L.; Zheng, B.; Liu, W.; Liu, C.; Xiao, H.; McClements, D. J., Enhancing nutraceutical bioavailability using excipient emulsions: Influence of lipid droplet size on solubility and bioaccessibility of powdered curcumin. *Journal of Functional Foods* **2015,** *15*, 72-83.

217. Ahmed, K.; Li, Y.; McClements, D. J.; Xiao, H., Nanoemulsion-and emulsion-based delivery systems for curcumin: encapsulation and release properties. *Food Chemistry* **2012,** *132* (2), 799-807.

218. Ting, Y.; Jiang, Y.; Ho, C.-T.; Huang, Q., Common delivery systems for enhancing in vivo bioavailability and biological efficacy of nutraceuticals. *Journal of Functional Foods* **2014,** *7*, 112-128.

219. Anand, P.; Nair, H. B.; Sung, B.; Kunnumakkara, A. B.; Yadav, V. R.; Tekmal, R. R.; Aggarwal, B. B., Design of curcumin-loaded PLGA nanoparticles formulation with enhanced cellular uptake, and increased bioactivity in vitro and superior bioavailability in vivo. *Biochemical Pharmacology* **2010,** *79* (3), 330-338.

220. Patel, A. R.; Velikov, K. P., Colloidal delivery systems in foods: A general comparison with oral drug delivery. *Lwt-Food Science and Technology* **2011,** *44* (9), 1958-1964.

221. Sun, M.; Su, X.; Ding, B.; He, X.; Liu, X.; Yu, A.; Lou, H.; Zhai, G., Advances in nanotechnology-based delivery systems for curcumin. *Nanomedicine* **2012,** *7* (7), 1085-1100.

222. Yu, H.; Huang, Q., Improving the Oral Bioavailability of Curcumin Using Novel Organogel-Based Nanoemulsions. *Journal of Agricultural and Food Chemistry* **2012,** *60* (21), 5373-5379.

223. Zou, L.; Liu, W.; Liu, C.; Xiao, H.; McClements, D. J., Designing excipient emulsions to increase nutraceutical bioavailability: emulsifier type influences curcumin stability and bioaccessibility by altering gastrointestinal fate. *Food & Function* **2015,** *6* (8), 2475-2486.

224. Porter, C. J. H.; Pouton, C. W.; Cuine, J. F.; Charman, W. N., Enhancing intestinal drug solubilisation using lipid-based delivery systems. *Advanced Drug Delivery Reviews* **2008,** *60* (6), 673-691.

225. Yao, M.; Xiao, H.; McClements, D. J., Delivery of Lipophilic Bioactives: Assembly, Disassembly, and Reassembly of Lipid Nanoparticles. In *Annual Review of*

Food Science and Technology, Vol 5, Doyle, M. P.; Klaenhammer, T. R., Eds. 2014; Vol. 5, pp 53-81.

226. McClements, D. J., *Food Emulsions: Principles, Practice and Techniques*. Third Edition ed.; CRC Press: Boca Raton, FL, 2015.

227. Chen, L. Y.; Remondetto, G. E.; Subirade, M., Food protein-based materials as nutraceutical delivery systems. *Trends in Food Science & Technology* **2006,** *17* (5), 272-283.

228. Joye, I. J.; McClements, D. J., Biopolymer-based nanoparticles and microparticles: fabrication, characterization, and application. *Current Opinion in Colloid & Interface Science* **2014,** *19* (5), 417-427.

229. Shewan, H. M.; Stokes, J. R., Review of techniques to manufacture micro-hydrogel particles for the food industry and their applications. *Journal of Food Engineering* **2013,** *119* (4), 781-792.

230. Zhang, R.; Zhang, Z.; Zhang, H.; Decker, E. A.; McClements, D. J., Influence of emulsifier type on gastrointestinal fate of oil-in-water emulsions containing anionic dietary fiber (pectin). *Food Hydrocolloids* **2015,** *45*, 175-185.

231. Li, Y.; McClements, D. J., New mathematical model for interpreting pH-stat digestion profiles: Impact of lipid droplet characteristics on in vitro digestibility. *Journal of Agricultural and Food Chemistry* **2010,** *58* (13), 8085-8092.

232. Sikorski, P.; Mo, F.; Skjåk-Bræk, G.; Stokke, B. T., Evidence for egg-box-compatible interactions in calcium-alginate gels from fiber X-ray diffraction. *Biomacromolecules* **2007,** *8* (7), 2098-2103.

233. Ellis, A.; Jacquier, J. C., Manufacture of food grade κ -carrageenan microspheres. *Journal of Food Engineering* **2009,** *94* (3), 316-320.

234. Mayer, S.; Weiss, J.; McClements, D. J., Behavior of vitamin E acetate delivery systems under simulated gastrointestinal conditions: lipid digestion and bioaccessibility of low-energy nanoemulsions. *Journal of Colloid and Interface Science* **2013,** *404*, 215-222.

235. Zhang, R. J.; Zhang, Z. P.; Zhang, H.; Decker, E. A.; McClements, D. J., Influence of emulsifier type on gastrointestinal fate of oil-in-water emulsions containing anionic dietary fiber (pectin). *Food Hydrocolloids* **2015,** *45*, 175-185.

236. Vingerhoeds, M. H.; Blijdenstein, T. B. J.; Zoet, F. D.; van Aken, G. A., Emulsion flocculation induced by saliva and mucin. *Food Hydrocolloids* **2005,** *19* (5), 915-922.

237. Hebrard, G.; Hoffart, V.; Cardot, J. M.; Subirade, M.; Beyssac, E., Development and characterization of coated-microparticles based on whey protein/alginate using the Encapsulator device. *Drug Development and Industrial Pharmacy* **2013,** *39* (1), 128-137.

238. Reis, P.; Holmberg, K.; Watzke, H.; Leser, M. E.; Miller, R., Lipases at interfaces: a review. *Advances in colloid and interface science* **2009,** *147*, 237-250.

239. Chan, A. W.; Neufeld, R. J., Modeling the controllable pH-responsive swelling and pore size of networked alginate based biomaterials. *Biomaterials* **2009,** *30* (30), 6119-6129.

240. Bauer, E.; Jakob, S.; Mosenthin, R., Principles of physiology of lipid digestion. *Asian-Australasian Journal of Animal Sciences* **2005,** *18* (2), 282-295.

241. Dahan, A.; Hoffman, A., Rationalizing the selection of oral lipid based drug delivery systems by an in vitro dynamic lipolysis model for improved oral bioavailability of poorly water soluble drugs. *Journal of Controlled Release* **2008,** *129* (1), 1-10.

242. Devraj, R.; Williams, H. D.; Warren, D. B.; Mullertz, A.; Porter, C. J. H.; Pouton, C. W., In vitro digestion testing of lipid-based delivery systems: Calcium ions combine with fatty acids liberated from triglyceride rich lipid solutions to form soaps and reduce the solubilization capacity of colloidal digestion products. *International Journal of Pharmaceutics* **2013,** *441* (1-2), 323-333.

243. Yi, J.; Li, Y.; Zhong, F.; Yokoyama, W., The physicochemical stability and in vitro bioaccessibility of beta-carotene in oil-in-water sodium caseinate emulsions. *Food Hydrocolloids* **2014,** *35*, 19-27.

244. Qian, C.; Decker, E. A.; Xiao, H.; McClements, D. J., Nanoemulsion delivery systems: influence of carrier oil on β-carotene bioaccessibility. *Food chemistry* **2012,** *135* (3), 1440-1447.

245. Losso, J. N.; Khachatryan, A.; Ogawa, M.; Godber, J. S.; Shih, F., Random centroid optimization of phosphatidylglycerol stabilized lutein-enriched oil-in-water emulsions at acidic pH. *Food chemistry* **2005,** *92* (4), 737-744.

246. Boon, C. S.; McClements, D. J.; Weiss, J.; Decker, E. A., Role of iron and hydroperoxides in the degradation of lycopene in oil-in-water emulsions. *Journal of agricultural and food chemistry* **2009,** *57* (7), 2993-2998.

247. Qian, C.; Decker, E. A.; Xiao, H.; McClements, D. J., Inhibition of β-carotene degradation in oil-in-water nanoemulsions: Influence of oil-soluble and water-soluble antioxidants. *Food chemistry* **2012,** *135* (3), 1036-1043.

248. Silva, H. D.; Cerqueira, M. A.; Souza, B. W. S.; Ribeiro, C.; Avides, M. C.; Quintas, M. A. C.; Coimbra, J. S. R.; Carneiro-da-Cunha, M. G.; Vicente, A. A., Nanoemulsions of β-carotene using a high-energy emulsification–evaporation technique. *Journal of Food Engineering* **2011,** *102* (2), 130-135.

249. Ribeiro, H. S.; Guerrero, J. M. M.; Briviba, K.; Rechkemmer, G.; Schuchmann, H. P.; Schubert, H., Cellular uptake of carotenoid-loaded oil-in-water emulsions in colon carcinoma cells in vitro. *Journal of agricultural and food chemistry* **2006,** *54* (25), 9366-9369.

250. Gao, Y.; Kispert, L. D., Reaction of carotenoids and ferric chloride: Equilibria, isomerization, and products. *The Journal of Physical Chemistry B* **2003,** *107* (22), 5333-5338.

251. Krinsky, N. I., The Antioxidant and Biological Properties of the Carotenoidsa. *Annals of the New York Academy of Sciences* **1998,** *854* (1), 443-447.

252. Zeeb, B.; Saberi, A. H.; Weiss, J.; McClements, D. J., Retention and release of oil-in-water emulsions from filled hydrogel beads composed of calcium alginate: impact of emulsifier type and pH. *Soft matter* **2015,** *11* (11), 2228-2236.

253. Zhang, R.; Zhang, Z.; Zhang, H.; Decker, E. A.; McClements, D. J., Influence of lipid type on gastrointestinal fate of oil-in-water emulsions: In vitro digestion study. *Food Research International* **2015,** *75*, 71-78.

254. Salvia-Trujillo, L.; Qian, C.; Martín-Belloso, O.; McClements, D. J., Influence of particle size on lipid digestion and β-carotene bioaccessibility in emulsions and nanoemulsions. *Food chemistry* **2013,** *141* (2), 1472-1480.

255. Hébrard, G.; Hoffart, V.; Cardot, J.-M.; Subirade, M.; Beyssac, E., Development and characterization of coated-microparticles based on whey protein/alginate using the Encapsulator device. *Drug development and industrial pharmacy* **2013,** *39* (1), 128-137.

256. Zhang, Z.; Zhang, R.; Chen, L.; Tong, Q.; McClements, D. J., Designing hydrogel particles for controlled or targeted release of lipophilic bioactive agents in the gastrointestinal tract. *European Polymer Journal* **2015**.

257. Zhang, R.; Zhang, Z.; Zou, L.; Xiao, H.; Zhang, G.; Decker, E. A.; McClements, D. J., Enhancing nutraceutical bioavailability from raw and cooked vegetables using excipient emulsions: Influence of lipid type on carotenoid bioaccessibility from carrots. *Journal of Agricultural and Food Chemistry* **2015**.

258. Zhang, R.; Zhang, Z.; Zou, L.; Xiao, H.; Zhang, G.; Decker, E. A.; McClements, D. J., Impact of Lipid Content on the Ability of Excipient Emulsions to Increase Carotenoid Bioaccessibility from Natural Sources (Raw and Cooked Carrots). *Food Biophysics* **2015**, 1-10.

259. Salvia-Trujillo, L.; Qian, C.; Martín-Belloso, O.; McClements, D. J., Modulating β-carotene bioaccessibility by controlling oil composition and concentration in edible nanoemulsions. *Food chemistry* **2013,** *139* (1), 878-884.

260. Sikkens, E. C. M.; Cahen, D. L.; Kuipers, E. J.; Bruno, M. J., Pancreatic enzyme replacement therapy in chronic pancreatitis. *Best Practice & Research Clinical Gastroenterology* **2010,** *24* (3), 337-347.

261. Domínguez‐Muñoz, J. E., Pancreatic exocrine insufficiency: diagnosis and treatment. *Journal of gastroenterology and hepatology* **2011,** *26* (s2), 12-16.

262. Guarner, L.; Rodriguez, R.; Guarner, F.; Malagelada, J. R., Fate of oral enzymes in pancreatic insufficiency. *Gut* **1993,** *34* (5), 708-712.

263. Whitcomb, D. C.; Lowe, M. E., Human pancreatic digestive enzymes. *Digestive diseases and sciences* **2007,** *52* (1), 1-17.

264. Domínguez‐Muñoz, J. E.; Iglesias‐García, J.; Iglesias‐Rey, M.; Figueiras, A.; Vilariño‐Insua, M., Effect of the administration schedule on the therapeutic efficacy of oral pancreatic enzyme supplements in patients with exocrine pancreatic insufficiency: a randomized, three‐way crossover study. *Alimentary pharmacology & therapeutics* **2005,** *21* (8), 993-1000.

265. Layer, P.; Go, V. L.; DiMagno, E. P., Fate of pancreatic enzymes during small intestinal aboral transit in humans. *American Journal of Physiology-Gastrointestinal and Liver Physiology* **1986,** *251* (4), G475-G480.

266. Zhang, Z.; Zhang, R.; Chen, L.; McClements, D. J., Encapsulation of lactase (β-galactosidase) into κ-carrageenan-based hydrogel beads: Impact of environmental conditions on enzyme activity. *Food chemistry* **2016,** *200*, 69-75.

267. Betancor, L.; Luckarift, H. R.; Seo, J. H.; Brand, O.; Spain, J. C., Three‐dimensional immobilization of β‐galactosidase on a silicon surface. *Biotechnology and bioengineering* **2008,** *99* (2), 261-267.

268. Böyükbayram, A. E.; Kıralp, S.; Toppare, L.; Yağcı, Y., Preparation of biosensors by immobilization of polyphenol oxidase in conducting copolymers and their use in determination of phenolic compounds in red wine. *Bioelectrochemistry* **2006,** *69* (2), 164-171.

269. Zhang, Z.; Zhang, R.; Zou, L.; McClements, D. J., Protein encapsulation in alginate hydrogel beads: Effect of pH on microgel stability, protein retention and protein release. *Food Hydrocolloids* **2016,** *58*, 308-315.

270. Zhang, Z.; Zhang, R.; Chen, L.; Tong, Q.; McClements, D. J., Designing hydrogel particles for controlled or targeted release of lipophilic bioactive agents in the gastrointestinal tract. *European Polymer Journal* **2015,** *72*, 698-716.

271. Srivastava, R.; Brown, J. Q.; Zhu, H.; McShane, M. J., Stable encapsulation of active enzyme by application of multilayer nanofilm coatings to alginate microspheres. *Macromolecular bioscience* **2005,** *5* (8), 717-727.

272. Taqieddin, E.; Amiji, M., Enzyme immobilization in novel alginate–chitosan core-shell microcapsules. *Biomaterials* **2004,** *25* (10), 1937-1945.

273. Mei, L.; He, F.; Zhou, R.-Q.; Wu, C.-D.; Liang, R.; Xie, R.; Ju, X.-J.; Wang, W.; Chu, L.-Y., Novel intestinal-targeted Ca-alginate-based carrier for pH-responsive protection and release of lactic acid bacteria. *ACS applied materials & interfaces* **2014,** *6* (8), 5962-5970.

274. Zhu, G.; Mallery, S. R.; Schwendeman, S. P., Stabilization of proteins encapsulated in injectable poly (lactide-co-glycolide). *Nature biotechnology* **2000,** *18* (1), 52-57.

275. Deriy, L. V.; Gomez, E. A.; Zhang, G.; Beacham, D. W.; Hopson, J. A.; Gallan, A. J.; Shevchenko, P. D.; Bindokas, V. P.; Nelson, D. J., Disease-causing mutations in the cystic fibrosis transmembrane conductance regulator determine the functional responses of alveolar macrophages. *Journal of Biological Chemistry* **2009,** *284* (51), 35926-35938.

276. Chen, Y.; Arriaga, E. A., Individual acidic organelle pH measurements by capillary electrophoresis. *Analytical chemistry* **2006,** *78* (3), 820-826.

277. Cope, S. J.; Hibberd, S.; Whetstone, J.; MacRae, R. J.; Melia, C. D., Measurement and mapping of pH in hydrating pharmaceutical pellets using confocal laser scanning microscopy. *Pharmaceutical research* **2002,** *19* (10), 1554-1563.

278. Li, L.; Schwendeman, S. P., Mapping neutral microclimate pH in PLGA microspheres. *Journal of Controlled Release* **2005,** *101* (1), 163-173.

279. Liu, Y.; Schwendeman, S. P., Mapping microclimate pH distribution inside protein-encapsulated PLGA microspheres using confocal laser scanning microscopy. *Molecular pharmaceutics* **2012,** *9* (5), 1342-1350.

280. Invernizzi, G.; Casiraghi, L.; Grandori, R.; Lotti, M., Deactivation and unfolding are uncoupled in a bacterial lipase exposed to heat, low pH and organic solvents. *Journal of biotechnology* **2009,** *141* (1), 42-46.

281. Heyman, M. B., Lactose intolerance in infants, children, and adolescents. *Pediatrics* **2006,** *118* (3), 1279-86.

282. Vesa, T. H.; Marteau, P.; Korpela, R., Lactose intolerance. *Journal of the American College of Nutrition* **2000,** *19* (2), 165S-175S.

283. Lomer, M. C. E.; Parkes, G. C.; Sanderson, J. D., Review article: lactose intolerance in clinical practice–myths and realities. *Alimentary Pharmacology & Therapeutics* **2008,** *27* (2), 93-103.

284. Montalto, M.; Curigliano, V.; Santoro, L.; Vastola, M.; Cammarota, G.; Manna, R.; Gasbarrini, A.; Gasbarrini, G., Management and treatment of lactose malabsorption. *World Journal of Gastroenterology* **2006,** *12* (2), 187-191.

285. Nichele, V.; Signoretto, M.; Ghedini, E., β -Galactosidase entrapment in silica gel matrices for a more effective treatment of lactose intolerance. *Journal of Molecular Catalysis B: Enzymatic* **2011,** *71* (1), 10-15.

286. He, H. J.; Zhang, X. T.; Sheng, Y., Enteric-coated capsule containing beta-galactosidase-loaded polylactic acid nanocapsules: enzyme stability and milk lactose hydrolysis under simulated gastrointestinal conditions. *Journal of Dairy Research* **2014,** *81* (4), 479-484.

287. Kim, J.; Grate, J. W.; Wang, P., Nanostructures for enzyme stabilization. *Chemical Engineering Science* **2006,** *61* (3), 1017-1026.

288. Xu, S. W.; Zhang, J.; Yang, Z. P.; Cao, J. H.; Ma, X. L.; Jiang, Z. Y., Analyzing the effect of carrier on the microenvironment of encapsulated enzyme. *Progress in Chemistry* **2008,** *20* (1), 163-170.

289. Es, I.; Vieira, J. D.; Amaral, A. C., Principles, techniques, and applications of biocatalyst immobilization for industrial application. *Appl Microbiol Biotechnol* **2015,** *99* (5), 2065-82.

290. Onwulata, C., Encapsulation of New Active Ingredients*. *Annual review of food science and technology* **2012,** *3*, 183-202.

291. Gombotz, W. R.; Wee, S. F., Protein release from alginate matrices. *Advanced Drug Delivery Reviews* **2012,** *64*, 194-205.

292. Cook, M. T.; Saratoon, T.; Tzortzis, G.; Edwards, A.; Charalampopoulos, D.; Khutoryanskiy, V. V., CLSM method for the dynamic observation of pH change within polymer matrices for oral delivery. *Biomacromolecules* **2013,** *14* (2), 387-393.

293. Crank, J., *The mathematics of diffusion*. Oxford university press: 1979.

294. Thành, T. T.; Yasunaga, H.; Takano, R.; Urakawa, H.; Kajiwara, K., Molecular characteristics and gelling properties of carrageenan family 2. Tri-sulfated and tetra-sulfated carrageenans. *Polymer Bulletin* **2001,** *47* (3-4), 305-312.

295. Marcus, Y., Volumes of aqueous hydrogen and hydroxide ions at 0 to 200 C. *The Journal of chemical physics* **2012,** *137* (15), 154501.

296. Guariguata, L.; Whiting, D. R.; Hambleton, I.; Beagley, J.; Linnenkamp, U.; Shaw, J. E., Global estimates of diabetes prevalence for 2013 and projections for 2035. *Diabetes Research and Clinical Practice* **2014,** *103* (2), 137-149.

297. Li, R.; Zhang, P.; Barker, L. E.; Chowdhury, F. M.; Zhang, X. P., Cost-Effectiveness of Interventions to Prevent and Control Diabetes Mellitus: A Systematic Review. *Diabetes Care* **2010,** *33* (8), 1872-1894.

298. Asche, C.; LaFleur, J.; Conner, C., A Review of Diabetes Treatment Adherence and the Association with Clinical and Economic Outcomes. *Clinical Therapeutics* **2011,** *33* (1), 74-109.

299. Shah, R. B.; Patel, M.; Maahs, D. M.; Shah, V. N., Insulin delivery methods: Past, present and future. *International Journal of Pharmaceutical Investigation* **2016,** *6* (1), 1-9.

300. Atkinson, M. A.; Eisenbarth, G. S.; Michels, A. W., Type 1 diabetes. *Lancet* **2014,** *383* (9911), 69-82.

301. Van Belle, T. L.; Coppieters, K. T.; Von Herrath, M. G., Type 1 Diabetes: Etiology, Immunology, and Therapeutic Strategies. *Physiological Reviews* **2011,** *91* (1), 79-118.

302. Guo, X. H.; Wang, W., Challenges and recent advances in the subcutaneous delivery of insulin. *Expert Opinion on Drug Delivery* **2017,** *14* (6), 727-734.

303. Nawaz, M. S.; Shah, K. U.; Khan, T. M.; Rehman, A. U.; Rashid, H. U.; Mahmood, S.; Khan, S.; Farrukh, M. J., Evaluation of current trends and recent development in insulin therapy for management of diabetes mellitus. *Diabetes & Metabolic Syndrome-Clinical Research & Reviews* **2017,** *11*, S833-S839.

304. Silva, C. M.; Ribeiro, A. J.; Figueiredo, I. V.; Goncalves, A. R.; Veiga, F., Alginate microspheres prepared by internal gelation: development and effect on insulin stability. *Int J Pharm* **2006,** *311* (1-2), 1-10.

305. Wong, C. Y.; Martinez, J.; Dass, C. R., Oral delivery of insulin for treatment of diabetes: status quo, challenges and opportunities. *Journal of Pharmacy and Pharmacology* **2016,** *68* (9), 1093-1108.

306. Sood, A.; Panchagnula, R., Peroral route: an opportunity for protein and peptide drug delivery. *Chemical reviews* **2001,** *101* (11), 3275-303.

307. Cardenas-Bailon, F.; Osorio-Revilla, G.; Gallardo-Velazquez, T., Microencapsulation techniques to develop formulations of insulin for oral delivery: a review. *Journal of Microencapsulation* **2013,** *30* (5), 409-424.

308. He, H. N.; Ye, J. X.; Sheng, J. Y.; Wang, J. X.; Huang, Y. Z.; Chen, G. Y.; Wang, J. K.; Yang, V. C., Overcoming oral insulin delivery barriers: application of cell penetrating peptide and silica-based nanoporous composites. *Frontiers of Chemical Science and Engineering* **2013,** *7* (1), 9-19.

309. des Rieux, A.; Fievez, V.; Garinot, M.; Schneider, Y. J.; Preat, V., Nanoparticles as potential oral delivery systems of proteins and vaccines: A mechanistic approach. *Journal of Controlled Release* **2006,** *116* (1), 1-27.

310. Fonte, P.; Araujo, F.; Silva, C.; Pereira, C.; Reis, S.; Santos, H. A.; Sarmento, B., Polymer-based nanoparticles for oral insulin delivery: Revisited approaches. *Biotechnology Advances* **2015,** *33* (6), 1342-1354.

311. van de Weert, M.; Hennink, W. E.; Jiskoot, W., Protein instability in poly(lactic-co-glycolic acid) microparticles. *Pharm Res* **2000,** *17* (10), 1159-67.

312. Cui, J. H.; Goh, J. S.; Park, S. Y.; Kim, P. H.; Le, B. J., Preparation and physical characterization of alginate microparticles using air atomization method. *Drug Dev Ind Pharm* **2001,** *27* (4), 309-19.

313. Anal, A. K.; Stevens, W. F., Chitosan-alginate multilayer beads for controlled release of ampicillin. *Int J Pharm* **2005,** *290* (1-2), 45-54.

314. Hari, P. R.; Chandy, T.; Sharma, C. P., Chitosan/calcium-alginate beads for oral delivery of insulin. *Journal of Applied Polymer Science* **1996,** *59* (11), 1795-1801.

315. El-Kamel, A. H.; Al-Gohary, O. M.; Hosny, E. A., Alginate-diltiazem hydrochloride beads: optimization of formulation factors, in vitro and in vivo availability. *J Microencapsul* **2003,** *20* (2), 211-25.

316. Pillay, V.; Danckwerts, M. P.; Muhidinov, Z.; Fassihi, R., Novel modulation of drug delivery using binary zinc-alginate-pectinate polyspheres for zero-order kinetics over several days: experimental design strategy to elucidate the crosslinking mechanism. *Drug Dev Ind Pharm* **2005,** *31* (2), 191-207.

317. Murata, Y.; Tsumoto, K.; Kofuji, K.; Kawashima, S., Effects of natural polysaccharide addition on drug release from calcium-induced alginate gel beads. *Chemical & pharmaceutical bulletin* **2003,** *51* (2), 218-20.

318. Zhang, Z.; Zhang, R.; McClements, D. J., Lactase (β -galactosidase) encapsulation in hydrogel beads with controlled internal pH microenvironments: Impact of bead characteristics on enzyme activity. *Food Hydrocolloids* **2017,** *67*, 85-93.

319. Zhang, Z.; Chen, F.; Zhang, R.; Deng, Z.; McClements, D. J., Encapsulation of Pancreatic Lipase in Hydrogel Beads with Self-Regulating Internal pH Microenvironments: Retention of Lipase Activity after Exposure to Gastric Conditions. *J Agric Food Chem* **2016,** *64* (51), 9616-9623.

320. Tanaka, T.; Yada, R. Y., N-terminal portion acts as an initiator of the inactivation of pepsin at neutral pH. *Protein engineering* **2001,** *14* (9), 669-74.

321. Zhang, Z.; Zhang, R.; Sun, Q.; Park, Y.; McClements, D. J., Confocal fluorescence mapping of pH profile inside hydrogel beads (microgels) with controllable internal pH values. *Food Hydrocolloids* **2017,** *65* (Supplement C), 198-205.

322. Deriy, L. V.; Gomez, E. A.; Zhang, G.; Beacham, D. W.; Hopson, J. A.; Gallan, A. J.; Shevchenko, P. D.; Bindokas, V. P.; Nelson, D. J., Disease-causing mutations in the cystic fibrosis transmembrane conductance regulator determine the functional responses of alveolar macrophages. *The Journal of biological chemistry* **2009,** *284* (51), 35926-38.

323. Chen, Y.; Arriaga, E. A., Individual acidic organelle pH measurements by capillary electrophoresis. *Analytical chemistry* **2006,** *78* (3), 820-6.

324. Hwang, S.-L.; Yang, B.-K.; Lee, J.-Y.; Kim, J.-H.; Kim, B.-H.; Suh, K.-H.; Kim, D.-Y.; Kim, M. S.; Song, H.; Park, B.-S.; Huh, T.-L., Isodihydrocapsiate stimulates plasma glucose uptake by activation of AMP-activated protein kinase. *Biochemical and Biophysical Research Communications* **2008,** *371* (2), 289-293.

325. Brange, J.; Langkjaer, L., Chemical-stability of insulin .3. Influence of excipients, formulation, and pH. *Acta Pharmaceutica Nordica* **1992,** *4* (3), 149-158.

326. Reis, C. P.; Ribeiro, A. J.; Neufeld, R. J.; Veiga, F., Alginate microparticles as novel carrier for oral insulin delivery. *Biotechnol Bioeng* **2007,** *96* (5), 977-89.

327. Deat-Laine, E.; Hoffart, V.; Cardot, J. M.; Subirade, M.; Beyssac, E., Development and in vitro characterization of insulin loaded whey protein and alginate microparticles. *Int J Pharm* **2012,** *439* (1-2), 136-44.

328. Chong, A. S. C.; Hashim, R.; Chow-Yang, L.; Ali, A. B., Partial characterization and activities of proteases from the digestive tract of discus fish (Symphysodon aequifasciata). *Aquaculture* **2002,** *203* (3), 321-333.

329. Lopes, M. A.; Abrahim-Vieira, B.; Oliveira, C.; Fonte, P.; Souza, A. M. T.; Lira, T.; Sequeira, J. A. D.; Rodrigues, C. R.; Cabral, L. M.; Sarmento, B.; Seica, R.; Veiga, F.; Ribeiro, A. J., Probing insulin bioactivity in oral nanoparticles produced by ultrasonication-assisted emulsification/internal gelation. *International Journal of Nanomedicine* **2015,** *10*, 5865-5880.

330. Zhao, K.; Li, W.; Zhang, Y.; Wei, H. X.; Wang, X. H.; Hong, K.; Jin, Z.; Wang, W. F., Preparation, Characterization and Hypoglycaemic Effects of Orally Delivered Insulin-Loaded PLGA Nanoparticles in Diabetic Rats. *Science of Advanced Materials* **2015,** *7* (6), 1114-1124.

331. Zhang, Y. L.; Wei, W.; Lv, P. P.; Wang, L. Y.; Ma, G. H., Preparation and evaluation of alginate-chitosan microspheres for oral delivery of insulin. *European Journal of Pharmaceutics and Biopharmaceutics* **2011,** *77* (1), 11-19.

332. Chaturvedi, K.; Ganguly, K.; Nadagouda, M. N.; Aminabhavi, T. M., Polymeric hydrogels for oral insulin delivery. *Journal of Controlled Release* **2013,** *165* (2), 129-138.

333. Kamei, N.; Morishita, M.; Eda, Y.; Ida, N.; Nishio, R.; Takayama, K., Usefulness of cell-penetrating peptides to improve intestinal insulin absorption. *Journal of Controlled Release* **2008,** *132* (1), 21-25.

334. Sarmento, B.; Ribeiro, A.; Veiga, F.; Sampaio, P.; Neufeld, R.; Ferreira, D., Alginate/chitosan nanoparticles are effective for oral insulin delivery. *Pharm Res* **2007,** *24* (12), 2198-206.

335. Zhang, Z.; Zhang, R.; Zou, L.; McClements, D. J., Protein encapsulation in alginate hydrogel beads: Effect of pH on microgel stability, protein retention and protein release. *Food Hydrocolloids* **2016,** *58* (Supplement C), 308-315.

336. Sood, N.; Bhardwaj, A.; Mehta, S.; Mehta, A., Stimuli-responsive hydrogels in drug delivery and tissue engineering. *Drug Delivery* **2016,** *23* (3), 758-780.

337. McClements, D. J., Encapsulation, protection, and release of hydrophilic active components: Potential and limitations of colloidal delivery systems. *Advances in Colloid and Interface Science* **2015,** *219*, 27-53.

338. Oehlke, K.; Adamiuk, M.; Behsnilian, D.; Graf, V.; Mayer-Miebach, E.; Walz, E.; Greiner, R., Potential bioavailability enhancement of bioactive compounds using food-grade engineered nanomaterials: a review of the existing evidence. *Food & Function* **2014,** *5* (7), 1341-1359.

339. Kesisoglou, F.; Panmai, S.; Wu, Y. H., Nanosizing - Oral formulation development and biopharmaceutical evaluation. *Advanced Drug Delivery Reviews* **2007,** *59* (7), 631-644.

340. Moller, N. P.; Scholz-Ahrens, K. E.; Roos, N.; Schrezenmeir, J., Bioactive peptides and proteins from foods: indication for health effects. *European Journal of Nutrition* **2008,** *47* (4), 171-182.

341. Cheng, X.; Liu, R.; He, Y., A simple method for the preparation of monodisperse protein-loaded microspheres with high encapsulation efficiencies. *European Journal of Pharmaceutics and Biopharmaceutics* **2010,** *76* (3), 336-341.

342. Xie, J.; Ng, W. J.; Lee, L. Y.; Wang, C.-H., Encapsulation of protein drugs in biodegradable microparticles by co-axial electrospray. *Journal of Colloid and Interface Science* **2008,** *317* (2), 469-476.

343. Castellanos, I. J.; Flores, G.; Griebenow, K., Effect of cyclodextrins on α - chymotrypsin stability and loading in PLGA microspheres upon S/O/W encapsulation. *Journal of pharmaceutical sciences* **2006,** *95* (4), 849-858.

344. Chang, K. L. B.; Lin, J., Swelling behavior and the release of protein from chitosan–pectin composite particles. *Carbohydrate polymers* **2000,** *43* (2), 163-169.

345. Bhatia, R. B.; Brinker, C. J.; Gupta, A. K.; Singh, A. K., Aqueous sol-gel process for protein encapsulation. *Chemistry of Materials* **2000,** *12* (8), 2434-2441.

346. Kim, Y. D.; Morr, C. V., Microencapsulation properties of gum arabic and several food proteins: spray-dried orange oil emulsion particles. *Journal of Agricultural and Food Chemistry* **1996,** *44* (5), 1314-1320.

347. Castellanos, I. J.; Crespo, R.; Griebenow, K., Poly (ethylene glycol) as stabilizer and emulsifying agent: a novel stabilization approach preventing aggregation and inactivation of proteins upon encapsulation in bioerodible polyester microspheres. *Journal of Controlled Release* **2003,** *88* (1), 135-145.

348. Ribeiro, S.; Hussain, N.; Florence, A. T., Release of DNA from dendriplexes encapsulated in PLGA nanoparticles. *International journal of pharmaceutics* **2005,** *298* (2), 354-360.

349. Lee, K. Y.; Mooney, D. J., Alginate: Properties and biomedical applications. *Progress in Polymer Science* **2012,** *37* (1), 106-126.

350. da Silva, F. L. B.; Jönsson, B., Polyelectrolyte–protein complexation driven by charge regulation. *Soft Matter* **2009,** *5* (15), 2862-2868.

351. Elçin, Y. M., Encapsulation of urease enzyme in xanthan-alginate spheres. *Biomaterials* **1995,** *16* (15), 1157-1161.

352. Wee, S.; Gombotz, W. R. In *Controlled release of recombinant human tumor necrosis factor receptor from alginate beads*, Proc. Int. Symp. Control. Release Bioact. Mater, 1994; pp 730-731.

353. Mumper, R. J.; Huffman, A. S.; Puolakkainen, P. A.; Bouchard, L. S.; Gombotz, W. R., Calcium-alginate beads for the oral delivery of transforming growth factor-β 1 (TGF-β 1): stabilization of TGF-β 1 by the addition of polyacrylic acid within acid-treated beads. *Journal of Controlled Release* **1994,** *30* (3), 241-251.

354. Segi, N.; Yotsuyanagi, T.; Ikeda, K., Interaction of calcium-induced alginate gel beads with propranolol. *Chemical and pharmaceutical bulletin* **1989,** *37* (11), 3092-3095.

355. Bendtsen, L. Q.; Lorenzen, J. K.; Bendsen, N. T.; Rasmussen, C.; Astrup, A., Effect of Dairy Proteins on Appetite, Energy Expenditure, Body Weight, and Composition: a Review of the Evidence from Controlled Clinical Trials. *Advances in Nutrition* **2013,** *4* (4), 418-438.

356. Halford, J. C. G.; Harrold, J. A., Satiety-enhancing products for appetite control: science and regulation of functional foods for weight management. *Proceedings of the Nutrition Society* **2012,** *71* (2), 350-362.

357. Dangin, M.; Guillet, C.; Garcia‐Rodenas, C.; Gachon, P.; Bouteloup‐Demange, C.; Reiffers‐Magnani, K.; Fauquant, J.; Ballèvre, O.; Beaufrère, B., The rate of protein digestion affects protein gain differently during aging in humans. *The Journal of physiology* **2003,** *549* (2), 635-644.

358. Erdmann, K.; Cheung, B. W. Y.; Schroder, H., The possible roles of food-derived bioactive peptides in reducing the risk of cardiovascular disease. *Journal of Nutritional Biochemistry* **2008,** *19* (10), 643-654.

359. Picariello, G.; Mamone, G.; Nitride, C.; Addeo, F.; Ferranti, P., Protein digestomics: Integrated platforms to study food-protein digestion and derived functional and active peptides. *Trac-Trends in Analytical Chemistry* **2013,** *52*, 120-134.

360. Freeman, H. J.; Kim, Y. S., Digestion and absorption of protein. *Annual review of medicine* **1978,** *29* (1), 99-116.

361. Erickson, R. H.; Kim, Y. S., Digestion and absorption of dietary protein. *Annual review of medicine* **1990,** *41* (1), 133-139.

362. Caron, J.; Domenger, D.; Dhulster, P.; Ravallec, R.; Cudennec, B., Protein Digestion-Derived Peptides and the Peripheral Regulation of Food Intake. *Frontiers in Endocrinology* **2017,** *8*.

363. Sah, B. N. P.; McAinch, A. J.; Vasiljevic, T., Modulation of bovine whey protein digestion in gastrointestinal tract: A comprehensive review. *International Dairy Journal* **2016,** *62*, 10-18.

364. Norton, J. E.; Espinosa, Y. G.; Watson, R. L.; Spyropoulos, F.; Norton, I. T., Functional food microstructures for macronutrient release and delivery. *Food & Function* **2015,** *6* (3), 663-678.

365. Zhang, Z.; Zhang, R.; Zou, L.; McClements, D. J., Tailoring lipid digestion profiles using combined delivery systems: mixtures of nanoemulsions and filled hydrogel beads. *RSC Advances* **2016,** *6* (70), 65631-65637.

366. Chen, L.; Remondetto, G. E.; Subirade, M., Food protein-based materials as nutraceutical delivery systems. *Trends in Food Science & Technology* **2006,** *17* (5), 272-283.

367. McClements, D. J., Recent progress in hydrogel delivery systems for improving nutraceutical bioavailability. *Food Hydrocolloids* **2017,** *68*, 238-245.

368. McClements, D. J., Designing biopolymer microgels to encapsulate, protect and deliver bioactive components: Physicochemical aspects. *Advances in Colloid and Interface Science* **2017,** *240*, 31-59.

369. Sun, Y.; Xia, Z.; Zheng, J.; Qiu, P.; Zhang, L.; McClements, D. J.; Xiao, H., Nanoemulsion-based delivery systems for nutraceuticals: Influence of carrier oil type on bioavailability of pterostilbene. *Journal of Functional Foods* **2015,** *13*, 61-70.

370. Minekus, M.; Alminger, M.; Alvito, P.; Ballance, S.; Bohn, T.; Bourlieu, C.; Carriere, F.; Boutrou, R.; Corredig, M.; Dupont, D., A standardised static in vitro digestion method suitable for food–an international consensus. *Food & function* **2014,** *5* (6), 1113-1124.

371. Yasumaru, F.; Lemos, D., Species specific in vitro protein digestion (pH-stat) for fish: method development and application for juvenile rainbow trout (Oncorhynchus

mykiss), cobia (Rachycentron canadum), and Nile tilapia (Oreochromis niloticus). *Aquaculture* **2014,** *426*, 74-84.

372. Moreno, F. J.; Quintanilla-López, J. E.; Lebrón-Aguilar, R.; Olano, A.; Sanz, M. L., Mass spectrometric characterization of glycated β-lactoglobulin peptides derived from galacto-oligosaccharides surviving the in vitro gastrointestinal digestion. *Journal of the American Society for Mass Spectrometry* **2008,** *19* (7), 927-937.

373. McClements, D. J., Theoretical prediction of emulsion color. *Advances in Colloid and Interface Science* **2002,** *97* (1-3), 63-89.

374. Phan-Xuan, T.; Durand, D.; Nicolai, T.; Donato, L.; Schmitt, C.; Bovetto, L., Tuning the Structure of Protein Particles and Gels with Calcium or Sodium Ions. *Biomacromolecules* **2013,** *14* (6), 1980-1989.

375. Maltais, A.; Remondetto, G. E.; Gonzalez, R.; Subirade, M., Formation of soy protein isolate cold‐set gels: protein and salt effects. *Journal of Food Science* **2005,** *70* (1).

376. Marangoni, A. G.; Barbut, S.; McGauley, S. E.; Marcone, M.; Narine, S. S., On the structure of particulate gels—the case of salt-induced cold gelation of heat-denatured whey protein isolate. *Food hydrocolloids* **2000,** *14* (1), 61-74.

377. Ye, A.; Taylor, S., Characterization of cold-set gels produced from heated emulsions stabilized by whey protein. *International Dairy Journal* **2009,** *19* (12), 721-727.

378. Carbonaro, M.; Cappelloni, M.; Sabbadini, S.; Carnovale, E., Disulfide reactivity and in vitro protein digestibility of different thermal-treated milk samples and whey proteins. *Journal of agricultural and food chemistry* **1997,** *45* (1), 95-100.

379. Rayment, P.; Wright, P.; Hoad, C.; Ciampi, E.; Haydock, D.; Gowland, P.; Butler, M. F., Investigation of alginate beads for gastro-intestinal functionality, Part 1: In vitro characterisation. *Food Hydrocolloids* **2009,** *23* (3), 816-822.

380. Singh, T. K.; Oiseth, S. K.; Lundin, L.; Day, L., Influence of heat and shear induced protein aggregation on the in vitro digestion rate of whey proteins. *Food & Function* **2014,** *5* (11), 2686-2698.

381. Peram, M. R.; Loveday, S. M.; Ye, A. Q.; Singh, H., In vitro gastric digestion of heat-induced aggregates of beta-lactoglobulin. *Journal of Dairy Science* **2013,** *96* (1), 63-74.

382. Marze, S., Bioaccessibility of lipophilic micro-constituents from a lipid emulsion. *Food & Function* **2015,** *6* (10), 3218-3227.

383. Tso, P.; Crissinger, K., Digestion and absorption of lipids. *Biochemical and physiological aspects of human nutrition* **2000**, 125-141.

384. Wilde, P. J.; Chu, B. S., Interfacial & colloidal aspects of lipid digestion. *Advances in Colloid and Interface Science* **2011,** *165* (1), 14-22.

385. Singh, H.; Ye, A.; Ferrua, M. J., Aspects of food structures in the digestive tract. *Current Opinion in Food Science* **2015,** *3*, 85-93.

386. Feinle-Bisset, C.; Patterson, M.; Ghatei, M. A.; Bloom, S. R.; Horowitz, M., Fat digestion is required for suppression of ghrelin and stimulation of peptide YY and pancreatic polypeptide secretion by intraduodenal lipid. *American Journal of Physiology-Endocrinology and Metabolism* **2005,** *289* (6), E948-E953.

387. Lundin, L.; Golding, M.; Wooster, T. J., Understanding food structure and function in developing food for appetite control. *Nutrition & Dietetics* **2008,** *65*, S79-S85.

388. Maljaars, P. W. J.; Peters, H. P. F.; Mela, D. J.; Masclee, A. A. M., Ileal brake: a sensible food target for appetite control. A review. *Physiology & behavior* **2008,** *95* (3), 271-281.

389. McClements, D. J., Reduced-Fat Foods: The Complex Science of Developing Diet-Based Strategies for Tackling Overweight and Obesity. *Advances in Nutrition* **2015,** *6* (3), 338S-352S.

390. Mao, L.; Miao, S., Structuring Food Emulsions to Improve Nutrient Delivery During Digestion. *Food Engineering Reviews* **2015,** *7* (4), 439-451.

391. Granot, J., Selected volume excitation using stimulated echoes (VEST). Applications to spatially localized spectroscopy and imaging. *Journal of Magnetic Resonance (1969)* **1986,** *70* (3), 488-492.

392. Frahm, J.; Merboldt, K.-D.; Hänicke, W., Localized proton spectroscopy using stimulated echoes. *Journal of Magnetic Resonance (1969)* **1987,** *72* (3), 502-508.

393. Bryant, C. M.; McClements, D. J., Molecular basis of protein functionality with special consideration of cold-set gels derived from heat-denatured whey. *Trends in Food Science & Technology* **1998,** *9* (4), 143-151.

394. Pafumi, Y.; Lairon, D.; de la Porte, P. L.; Juhel, C.; Storch, J.; Hamosh, M.; Armand, M., Mechanisms of inhibition of triacylglycerol hydrolysis by human gastric lipase. *Journal of Biological Chemistry* **2002,** *277* (31), 28070-28079.

395. Chen, F.; Deng, Z.; Zhang, Z.; Zhang, R.; Xu, Q.; Fan, G.; Luo, T.; McClements, D. J., Controlling lipid digestion profiles using mixtures of different types of microgel: alginate beads and carrageenan beads. *Journal of Food Engineering* **2018**.

396. Ma, D.; Tu, Z.-C.; Wang, H.; Zhang, Z.; McClements, D. J., Microgel-in-Microgel Biopolymer Delivery Systems: Controlled Digestion of Encapsulated Lipid Droplets under Simulated Gastrointestinal Conditions. *Journal of agricultural and food chemistry* **2018,** *66* (15), 3930-3938.

397. Kornaat, P. R.; Doornbos, J.; van der Molen, A. J.; Kloppenburg, M.; Nelissen, R. G.; Hogendoorn, P. C. W.; Bloem, J. L., Magnetic resonance imaging of knee cartilage using a water selective balanced steady-state free precession sequence. *Journal of Magnetic Resonance Imaging: An Official Journal of the International Society for Magnetic Resonance in Medicine* **2004,** *20* (5), 850-856.

398. Hamilton, G.; Yokoo, T.; Bydder, M.; Cruite, I.; Schroeder, M. E.; Sirlin, C. B.; Middleton, M. S., In vivo characterization of the liver fat 1H MR spectrum. *NMR in biomedicine* **2011,** *24* (7), 784-790.

399. Fauhl, C.; Reniero, F.; Guillou, C., 1H NMR as a tool for the analysis of mixtures of virgin olive oil with oils of different botanical origin. *Magnetic Resonance in Chemistry* **2000,** *38* (6), 436-443.

400. Zhang, Z.; Zhang, R.; Zou, L.; Chen, L.; Ahmed, Y.; Al Bishri, W.; Balamash, K.; McClements, D. J., Encapsulation of curcumin in polysaccharide-based hydrogel beads: Impact of bead type on lipid digestion and curcumin bioaccessibility. *Food Hydrocolloids* **2016,** *58*, 160-170.

401. Hussein, M. O.; Hoad, C. L.; Wright, J.; Singh, G.; Stephenson, M. C.; Cox, E. F.; Placidi, E.; Pritchard, S. E.; Costigan, C.; Ribeiro, H., Fat Emulsion Intragastric Stability and Droplet Size Modulate Gastrointestinal Responses and Subsequent Food Intake in Young Adults–4. *The Journal of nutrition* **2015,** *145* (6), 1170-1177.